Université de Montréal

Etude électrochimique et spectro-électrochimique de nouveaux composés électrochromes

par Yohan Gautier

Département de Chimie, Université de Montréal
Faculté des Arts et des Sciences

Mémoire présenté
en vue de l'obtention du grade de Magister Scientiae (M. Sc.)
en Chimie

Août 2019

Résumé

La recherche intensive sur les matériaux conjugués durant les dernières décennies a permis de mettre en évidence la multitude de propriétés opto-électroniques qu'ils peuvent présenter. Leur compatibilité avec des applications dans divers dispositifs électroniques les rend évident comme alternative aux composés inorganiques, et le fait qu'ils ouvrent la porte sur l'électronique plastique assure que la recherche les concernant n'est pas prête de diminuer.

L'utilisation de liaisons azométhines en lieu et place des liaisons « tout-carbone » de type vinylène pour la conception de molécules conjuguées est une alternative intéressante aux méthodes conventionnelles pas très éco-responsables habituellement employées, de par la simplicité relative de leur synthèse et purification. En continuité d'études précédentes, ce mémoire a pour objectif l'analyse des propriétés électro- et spectroélectrochimiques de nouveaux oligomères azométhines fonctionnalisés par des amides, en particulier leur propriété d'électrochromisme. L'influence sur ces propriétés de différents groupements électro-donneurs et électro-attracteurs au centre, ainsi qu'aux extrémités est ainsi présentée. L'emphase est portée sur la pérennité de leur changement de couleur lors de multiples cycles d'oxydation-neutralisation.

Mots-clés : Synthèse, Matériaux conjugués, Azométhine, Electrochimie, Spectro-électrochimie Electrochromisme, Photophysique.

Abstract

Intensive research on conjugated materials over the past few decades has highlighted the plethora of opto-electronic properties that these can present. Their compatibility with various electronic devices make them alternatives to inorganic materials, and the fact that they open the path to plastic electronics assures that research about them is not about to diminish soon.

Use of azomethine links instead of “all-carbon” vinylene-type double bonds, for the design and conception of conjugated molecules, is a very interesting alternative to the conventional methods, not very eco-friendly, usually employed, mostly due to their relative simplicity in terms of synthesis and purification. Following on previous work, this thesis aim to analyze the electro and spectro-electrochemical properties of a series of new azomethine-oligomeres that are functionalized with amides. Particular emphasis is placed on their electrochromism.. The influence of various electro-donating and electro-attracting groups in the core of the molecules as well as at their termini on the optical and electrochemical properties is presented. The emphasis is placed on demonstrating their robustness and the durability of their color change when undergoing multiple oxidation-neutralization cycles.

Keywords : Synthesis, Conjugated Materials, Azométhine, Electrochemistry, Spectro-electrochemistry, Electrochromisme, Photophysics**.**

Table des matières

Résumé i

Abstract ii

Table des matières iii

Liste des figures et tableaux (charts, tables) vi

Liste des sigles et abbréviations xvii

Remerciements xx

Introduction

- Les matériaux conjugués 2
- Problématique et objectifs 10
- Partie expérimentale : caractérisation des matériaux conjugués 18
  - Propriétés électrochimiques 18
  - Spectro-électrochimie et électrochromisme 22
  - Chromaticité et colorimétrie 25
  - Dispositifs électrochromiques 27
  - Déposition et immobilisation sur substrat 29
- Bibliographie 30

Chapitre 1

- Résumé 36
- Extending the duty cycle of azomethine electrochromes by structural modification 37
  - Abstract 38
  - Introduction 39
  - Results and Discussion 41

Conclusion 60

Experimental 60

References 68

SUPPORTING INFORMATION I ELECTROCHEMICAL AND SPECTROSCOPIC DATA 71

SUPPORTING INFORMATION II NMR SPECTRA 92

SUPPORTING INFORMATION III THEORETICALLY CALCULATED GEOMETRY COORDINATES 144

SUPPORTING INFORMATION IV X-RAY CRYSTALLOGRAPHIC DATA 199

Chapitre 2

Résumé 209

Crystal structure and DFT calculation of tetraethyl 5,5'-(((1*E*,1'*E*)-thiophene-2,5-diylbis(methanylylidene))bis(azanylylidene))bis(2-(4-(di-p-tolylamino)benzamido)thiophene-3,4-dicarboxylate) 210

Abstract and keywords 211

Chemical context 212

Structural commentary 213

Supramolecular features 215

DFT Calculations 215

Database survey 216

Synthesis and crystallization 217

Refinement 217

Acknowledgements 219

Funding information 220

References 220

Supporting information 222

Computing details 222

Conclusion……...236

Liste des figures et tableaux (charts, tables)

Figure 0-1 Représentation classique simplifiée des niveaux énergétiques des orbitales frontières d'une molécule conjuguée (a), ou dans un polymère conjugué (b) (inspiré de [4]). 3

Figure 0-2 Effet (a) de l'ajout de groupements électro-actifs, (b) de l'allongement de la conjugaison, sur la E_g d'une molécule conjuguée (inspiré de [5]). 4

Figure 0-3 Diagramme de Perrin-Jablonski – Phénomènes subséquents à l'excitation d'une molécule par absorption d'énergie (inspiré de [6-7]). 5

Figure 0-4 Représentation simplifiée du principe de fonctionnement d'une OLED (A) et d'une OPV (B). 7

Figure 0-5 Représentation schématique des états polaroniques d'une molécule conjuguée oxydée ou réduite (inspiré de [11]). 8

Figure 0-6 Exemple de types de polymères conjugués utilisés en électronique organique. 11

Figure 0-7 Exemples non exhaustifs de réactions et couplages conventionnels utilisés pour l'obtention de molécules conjuguées. 12

Figure 0-8 Représentation schématique de la condensation d'une amine et d'un aldéhyde pour former une azométhine. 13

Figure 0-9 Amino-thiophènes utilisés au laboratoire. 14

Figure 0-10 Exemple non exhaustifs de dimères et trimères antécédent investigués. 14

Figure 0-11 Exemples de trimères investigués par le passé 15

Figure 0-12 Exemples de polyazométhines précédement étudiées 15

Figure 0-13 Trimères présentés dans les travaux de ce mémoire 18

Figure 0-14 Voltampérogramme cyclique idéal d'un couple électrochimiquement réversible. 22

Figure 0-15 Schéma du montage spectro-électrochimique utilisé au laboratoire. 24

Figure 0-16 Diagramme de chromaticité LUV (CIE 1976 UCS). 26

Figure 0-17 Représentation schématique simplifiée d'un dispositif électrochromique actif. ... 28

Chart 1-1 Amido-azomethine precursors and the triads prepared for electrochemical and spectroelectrochemical evaluation and their previously reported amine end-terminated counterpart (**4**). 41

Figure 1-1 A) The atom-numbering diagram of **1D**. C, N, O and S atoms are drawn as displacement ellipsoids having a 50% probability. The hydrogens atoms are shown as spheres having an arbitrary radius. The cocrystallized chloroform solvent molecule was removed for clarity. 43

Figure 1-2 A) Packing of **1D** in the crystallographic unit cell shown along the *a*-axis. The main molecule is colored while the others are faded to highlight the adopted "Y"-like configuration. The hydrogens are removed for clarity. B) The intra- and intermolecular hydrogen bonds that are formed by **1D** in the solid state are drawn as blue lines. 43

Table 1-1 Inter- and intramolecular supramolecular bonding of **1D** in the crystal state. 43

Figure 1-3 A) Cyclic voltammogram of the electropolymerized film of **2** on the Pt working electrode measured in 0.1 M $TBAPF_6$ in dichloromethane at 100 mV/s with 10^{-3} M ferrocene. The reversible redox couple of ferrocene is shown as the dotted line. B) Cyclic voltammogram of the anodically prepared film of **2A** adsorbed on the Pt working electrode with ferrocene as the internal reference, measured in 0.1 M $TBAPF_6$ in dichloromethane at 100 mV/s initially (■) and after immersing the electrode in a mixture of TFA/THF/HCl (●) overnight. 45

Table 1-2 Electrochemical and spectroelectrochemical properties of the precursors and triad azomethines. 46

Figure 1-4 Anodic cyclic voltammograms (from bottom to top) of **1** (—), **3** (—), **1C** (—), **1D** (—), **3D** (—), **3A** (—), and **3B** (—) measured in degassed dichloromethane with 0.1 M $TBAPF_6$ at 100 mV/s. Arrows indicate the scan direction of the voltammograms. 49

Figure 1-5 A) Corrected change in percent transmittance of **3B** with applied potential of 1.0 and -0.2 V vs. Ag^o in dichloromethane and 0.1 M $TBAPF_6$ switched at 30 sec. intervals and monitored at 709 nm. Baseline corrected for drift in the 100% transmission over time. Inset: Inset: change in percent transmittance with applied potential of 1.1 V vs Ag^o monitored at 508 (—) and 637 nm (—) (left). Zoom between 99 and 103 min. with switching of applied

potential at 30 sec. intervals (right). B) Change in percent transmittance of **3B** with applied potential of 1.1 and -0.2 V vs. Ag^o in dichloromethane and 0.1 M $TBAPF_6$ switched at 5 min. oxidation and 2 min. neutralization intervals and monitored at 637 nm. Inset: photographs of the 19-well gold working honeycomb electrode of the neutral (middle), electrochemically oxidized (right), and electrochemically reduced (left) states of **3B**. 52

Figure 1-6 CIE (1976 UCS) chromaticity coordinates of the neutral (●), electrochemically oxidized (■) and reduced states (▲) of **3** (—), **1A** (—), **1C** (—), **1D** (—), **3A** (—), **3B** (—), and **3D** (—). 54

Figure 1-7 A) Top-down (left) and side-on (right) views of the optimized geometry of **2B** calculated by CAM-B3LYP DFT with the 6-311+G(d,p) basis set. The hydrogens were removed from the side-on view for clarity (right). B) The calculated spin density of the radical cation (left) and the triplet dication (right) **2B**. C) The calculated MM charge distribution (left) of **2B** from -1.1 (red) to +1.1 (green) and the calculated spin density of the radical cation (middle) and triplet dication (right) of **2**. D) The calculated spin density of the radical cation (left) and triplet dication (right) of **2A**. E) The calculated spin density of the radical cation (left) and triplet dication (right) of **1B**. F) Calculated NTOs of the α–HOMO (top left), β–HOMO (bottom left), α–LUMO (top right), and β–LUMO (bottom right) Frontier orbitals of the radical cation of **2B** that are principally involved in the excitation transition at 706 nm. 56

Figure S1-8Anodic cyclic voltammograms of the dyads **1** (squares), **2** (circles), and **3** (triangles) measured in degassed and anhydrous dichloromethane at 100 mV/s with 0.1 M $TBAPF_6$. 72

Figure S1-9 Cathodic cyclic voltammograms of **1A** (black),[1] **1C** (red), **1D** (blue). **3A** (pink), **3D** (green) measured in 0.1 M $TBAPF_6$ in degassed and anhydrous dichloromethane at 100 mV/s. 72

Figure S1-10 Absorption spectra of **2** (squares), **2A** (circles), **2D** (triangles) measured in dichloromethane. 73

Figure S1-11 Anodic cyclic voltammograms of the **1A** (■),[1] **1C** (●), and **1D** (▲) measured in degassed and anhydrous dichloromethane at 100 mV/s with 10^{-3} M ferrocene as an internal reference and with 0.1 M $TBAPF_6$ between -0.5 and ca 1.2 V vs. Fc/Fc^+. 73

Figure S1-12 Multiple anodic cyclic voltammograms of **2** measured in 0.1 M $TBAPF_6$ in degassed and anhydrous dichloromethane at 100 mV/s. 74

Figure S1-13 Change in absorption spectra of **3** with applied potential measured between 60 and 90 sec after the applying the potential in degassed and anhydrous dichloromethane. Inset: Photographs of the honeycomb gold electrode of the neutral (left) and electrochemically oxidized (right) states. 74

Figure S1-14 Uncorrected change in percent transmittance of **3** when switching the applied potential between 0.8 V and -0.2 V at 30 second intervals monitored at 705 nm during for 6 hours. 75

Figure S1-15 Differential pulse voltammogram of **1A** measured in degassed and anhydrous dichloromethane with 0.1 M $TBAPF_6$. 75

Figure S1-16 Absorption spectra of the neutral (■), electrochemically oxidized (●, ▲), and electrochemically reduced (▼) states of **1C** with applied potentials of 1.05, 1.3, and -1.8 V vs Ag^o, respectively. Inset: Photographs of the honeycomb gold electrode of the reduced, neutral, first oxidized, and second oxidized (from left to right) states. 76

Figure S1-17 Change in absorption spectra of **1D** with applied positive potential measured in anhydrous and degassed dichloromethane with 0.1 M $TBAPF_6$ at 100 mV/s. 76

Figure S1-18 Change in absorption spectra of **1D** with applied negative potential measured in anhydrous and degassed dichloromethane with 0.1 M $TBAPF_6$ at 100 mV/s. 77

Figure S1-19 Absorption spectra of the neutral (■), electrochemically oxidized (●), and electrochemically reduced (▲) states of **1D**. Inset: Photographs of the honeycomb gold electrode of the reduced, neutral, and oxidized (from left to right) states. 77

Figure S1-20 Anodic cyclic voltammograms of **3A** measured in degassed and anhydrous dichloromethane with 0.1 M $TBAPF_6$ at 100 mV/s without (black squares and blue triangles) and with 10^{-3} M ferrocene (red circles). 78

Figure S1-21 Anodic cyclic voltammograms of **3A** measured at different scan speeds (10 to 750 mV/s) in 0.1 M $TBAPF_6$ in in degassed and anhydrous dichloromethane. 78

Figure S1-22 Change in absorption spectra of **3A** with applied positive potential. 79

Figure S1-23 Change in absorption spectra of **3A** with applied negative potential. 79

Figure S1-24 Absorption spectra of the neutral (■), electrochemically oxidized (●), and electrochemically reduced (▲) states of **3A**. Inset: Photographs of the honeycomb gold electrode of the electrochemically reduced (left), neutral (middle), and electrochemically oxidized (right) states. 80

Figure S1-25 Change in percent transmittance of **3A** monitored at 708 nm with switching the applied potential between 1.15 and -0.1 V vs. Ag^o at 30 sec intervals over a 2 hour time range corrected for baseline drift over time at 100% transmittance. 80

Figure S1-26 Multiple anodic cyclic voltammograms of **2A** measured in 0.1 M $TBAPF_6$ in degassed and anhydrous dichloromethane at 100 mV/s. 81

Figure S1-27 Multiple (50) anodic cyclic voltammograms of **2A** leading to its electropolymerization measured in 0.1 M $TBAPF_6$ in in degassed and anhydrous dichloromethane at 100 mV/s. 81

Figure S1-28 Cyclic voltammograms of the resulting electropolymerized film of **2A** on an ITO electrode measured at different scan speeds in 0.1 M $TBAPF_6$ in degassed and anhydrous dichloromethane. 82

Figure S1-29 Anodic cyclic voltammogram of **3B** measured in 0.1 M $TBAPF_6$ in degassed and anhydrous dichloromethane at 100 mV/s without (red) and with 10^{-3} M ferrocene. 82

Figure S1-30 Anodic square wave voltammogram of **3B** measured in dichloromethane with 0.1 M $TBAPF_6$. 83

Figure S1-31 Anodic differential pulse voltammogram of **3B** measured in dichloromethane with 0.1 M $TBAPF_6$. 83

Figure S1-32 Absorption spectra of **3B** with applied potential: 0 V (—), after 15 min. at 1.1 V (—), and return to 0 V (—). Dotted lines are the mathematical deconvolution of the oxidized state at 1.1 V into the corresponding three spectral components: neutral (—), oxidized core (—), and oxidized end groups (—). 84

Figure S1-33 Change in absorption spectra of **3B** with applied negative potential..... 84

Figure S1-34 Change in absorption spectra of **3B** with applied positive potential. 85

Figure S1-35 Absorption spectra of the neutral (■), electrochemically oxidized (●), and electrochemically reduced (▲) states of **3B**. Inset: Photographs of the honeycomb gold electrode of the electrochemically reduced (left), neutral (middle), and electrochemically oxidized (right) states. 85

Figure S1-36 Anodic cyclic voltammogram of **2D** measured in 0.1 M $TBAPF_6$ in degassed and anhydrous dichloromethane at 100 mV/s. 86

Figure S1-37 Multiple (20) anodic cyclic voltammogram of **2D** measured in 0.1 M $TBAPF_6$ in degassed and anhydrous dichloromethane at 100 mV/s leading to its electropolymerization. 86

Figure S1-38 Anodic cyclic voltammograms of **3D** measured in 0.1 M $TBAPF_6$ in degassed and anhydrous dichloromethane at 100 mV/s with 10^{-3} M ferrocene as internal reference (red circles). 87

Figure S1-39 Anodic cyclic voltammograms of **3D** at different scan rates: 10mV/s (**–**), 25 mV/s (**–**) and 100 mV/s (**–**), measured in 0.1 M $TBAPF_6$ in degassed and anhydrous dichloromethane. 87

Figure S1-40 Squarewave voltammograms of **3D** contingent on different scan parameters. .. 88

Figure S1-41 Change in absorption spectra of **3D** with switching the applied potential. Inset: Photographs of the honeycomb gold electrode showing the change in color of **3D** contingent on applied potential. 88

Figure S1-42 Change in absorption spectra of **3D** with switching the applied potential up to 1 V max. 89

Figure S1-43 Change in percent transmittance of **3D** monitored at 709 nm with applied potentials switched between 1.1 V and -0.3 V vs Ag^o at 30 sec intervals over 6 hours corrected for the baseline drift overtime at 100% transmittance. 89

Figure S1-44 Calculated absorption spectra of **2B** via TD-DFT with CAM-B3LYP/6-311+g(d,p) in dichloromethane as the continuum solvent of the neutral singlet (**—**), radical

cation (▬), dication (▬), and triplet dication (▬). The vertical lines are the discrete calculated transitions for the given multiplicity and charge. 90

Figure S1-45 Calculated NTOs of the α–HOMO (top left), β–HOMO (bottom left), α–LUMO (top right), and β–LUMO (bottom right) Frontier orbitals of the radical cation of **2A** that are principally involved in the excitation transition at 706 nm..... 90

Figure S1-46. ^{1}H NMR spectrum of **1** in deuterated chloroform. 93

Figure S1-47. ^{13}C NMR spectrum of **1** in deuterated chloroform. 94

Figure S1-48. DEPT-135 NMR spectrum of **1** in deuterated chloroform. 95

Figure S1-49. COSY ^{1}H-^{1}H correlation NMR spectrum of **1** in deuterated chloroform. 96

Figure S1-50. HSQC ^{13}C- ^{1}H correlation NMR spectrum of **1** in deuterated chloroform. 97

Figure S1-51. ^{1}H NMR spectrum of **2** in deuterated chloroform. 98

Figure S1-52. ^{13}C NMR spectrum of **2** in deuterated chloroform. 99

Figure S1-53. HMBC ^{13}C-^{1}H correlation NMR spectrum of **2** in deuterated chloroform..... 100

Figure S1-54. ^{1}H NMR spectrum of **3** in deuterated chloroform. 101

Figure S1-55. ^{13}C NMR spectrum of **3** in deuterated chloroform. 102

Figure S1-56. HSQC ^{13}C-^{1}H correlation NMR spectrum of **3** in deuterated chloroform..... 103

Figure S1-57. HMBC ^{13}C-^{1}H correlation NMR spectrum of **3** in deuterated chloroform..... 104

Figure S1-58. High resolution mass spectrum of **3**..... 105

Figure S1-59. ^{1}H NMR spectrum of **1A** in deuterated chloroform..... 106

Figure S1-60. ^{13}C NMR spectrum of **1A** in deuterated chloroform. 107

Figure S1-61. DEPT-135 NMR spectrum of **1A** in deuterated chloroform. 108

Figure S1-62. HSQC ^{13}C-^{1}H correlation NMR spectrum of **1A** in deuterated chloroform.... 109

Figure S1-63. High resolution mass spectrum of **1A**..... 110

Figure S1-64. ^{1}H NMR spectrum of **1C** in deuterated chloroform..... 111

Figure S1-65. ^{13}C NMR spectrum of **1C** in deuterated chloroform. 112

Figure S1-66. DEPT-135 NMR spectrum of **1C** in deuterated chloroform. 113

Figure S1-67. High resolution mass spectrum of **1C**..... 114

Figure S1-68. ^{1}H NMR spectrum of **1D** in deuterated chloroform..... 115

Figure S1-69. ^{13}C NMR spectrum of **1D** in deuterated chloroform. 116

Figure S1-70. DEPT-135 NMR spectrum of **1D** in deuterated chloroform. 117

Figure S1-71. High resolution mass spectrum of **1D**..... 118

Figure S1-72. ^{1}H NMR spectrum of **2A** in deuterated chloroform..... 119

Figure S1-73. ^{13}C NMR spectrum of **2A** in deuterated chloroform. 120

Figure S1-74. DEPT-135 NMR spectrum of **2A** in deuterated chloroform. 121

Figure S1-75. COSY ^{1}H-^{1}H correlation NMR spectrum of **2A** in deuterated chloroform. 122

Figure S1-76. High resolution mass spectrum of **2A**..... 122

Figure S1-77. ^{1}H NMR spectrum of **2D** in deuterated chloroform..... 123

Figure S1-78. ^{13}C NMR spectrum of **2D** in deuterated chloroform. 124

Figure S1-79. DEPT NMR spectrum of **2D** in deuterated chloroform..... 125

Figure S1-80. HSQC ^{13}C-^{1}H correlation NMR spectrum of **2D** in deuterated chloroform. ... 126

Figure S1-81. High resolution mass spectrum of **2D**..... 127

Figure S1-82. ^{1}H NMR spectrum of **3A** in deuterated chloroform..... 128

Figure S1-83. ^{13}C NMR spectrum of **3A** in deuterated chloroform. 129

Figure S1-84. DEPT-135 NMR spectrum of **3A** in deuterated chloroform. 130

Figure S1-85. HSQC ^{13}C-^{1}H correlation NMR spectrum of **3A** in deuterated chloroform. ... 131

Figure S1-86. High resolution mass spectrum of **3A**..... 132

Figure S1-87. ^{1}H NMR spectrum of **3B** in deuterated chloroform..... 133

Figure S1-88. ^{13}C NMR spectrum of **3B** in deuterated chloroform..... 134

Figure S1-89. DEPT-135 NMR spectrum of **3B** in deuterated chloroform. 135

Figure S1-90. HSQC ^{13}C-^{1}H correlation NMR spectrum of **3B** in deuterated chloroform. ... 136

Figure S1-91. High resolution mass spectrum of **3B**. 137

Figure S1-92. ^{1}H NMR spectrum of **3D** in deuterated chloroform. 138

Figure S1-93. ^{13}C NMR spectrum of **3D** in deuterated chloroform. 139

Figure S1-94. DEPT-135 NMR spectrum of **3D** in deuterated chloroform. 140

Figure S1-95. HSQC ^{13}C-^{1}H correlation NMR spectrum of **3D** in deuterated chloroform. ... 141

Figure S1-96. HMBC ^{13}C-^{1}H correlation NMR spectrum of **3D** in deuterated chloroform. .. 142

Figure S1-97. High resolution mass spectrum of **3D**. 143

Table 1-3 Atomic coordinates of the neutral singlet of **2B** calculated by CAM-B3LYP/6-311+g(d,p). 145

Table 1-4 Atomic coordinates of the radical cation of **2B** calculated by CAM-B3LYP/6-311+g(d,p). 149

Table 1-5 Atomic coordinates of the singlet dication of **2B** calculated by CAM-B3LYP/6-311+g(d,p). 155

Table 1-6 Atomic coordinates of the triplet dication of **2B** calculated by CAM-B3LYP/6-311+g(d,p). 159

Table 1-7 Atomic coordinates of the radical cation of **2A** calculated by CAM-B3LYP/6-311+g(d,p). 164

Table 1-8 Atomic coordinates of the triplet dication of **2A** calculated by CAM-B3LYP/6-311+g(d,p). 169

Table 1-9 Atomic coordinates of the neutral singlet of **1B** calculated by CAM-B3LYP/6-311+g(d,p). 174

Table 1-10 Atomic coordinates of the radical cation of **1B** calculated by CAM-B3LYP/6-311+g(d,p). 177

Table 1-11 . Atomic coordinates of the triplet dication of **1B** calculated by CAM-B3LYP/6-311+g(d,p). 181

Table 1-12. Atomic coordinates of the neutral singlet of **2** calculated by CAM-B3LYP/6-311+g(d,p). 184

Table 1-13 Atomic coordinates of the radical cation of **2** calculated by CAM-B3LYP/6-311+g(d,p). 187

Table 1-14 Atomic coordinates of the triplet dication of **2** calculated by CAM-B3LYP/6-311+g(d,p). 189

Table 1-15 Excitation energies and oscillator strengths (f) of the neutral singlet of **2B**. Total energy E(TD-HF/TD-DFT)= -4973.7019 Hartrees. 191

Table 1-16 Excitation energies and oscillator strengths (f) of the radical cation of **2B**. Total energy E(TD-HF/TD-DFT)= -4973.55739 Hartrees. 193

Table 1-17 Excitation energies and oscillator strengths (f) of the dication of **2B**. Total energy E(TD-HF/TD-DFT)= -4973.319834 Hartrees. 196

Table 1-18 Excitation energies and oscillator strengths of the triplet dication of **2B**. Total energy E(TD-HF/TD-DFT)= -4973.33810045 Hartrees. 197

Table 1-19 Crystal data and structure refinement for **1C**. 200

Table 1-20 Fractional atomic coordinates ($\times 10^4$) and equivalent isotropic displacement parameters ($Å^2 \times 10^3$) for **1C**. 201

Table 1-21 Anisotropic displacement parameters ($Å^2 \times 10^3$) for **1C**. 203

Table 1-22 Bond lengths for **1C**. 204

Table 1-23 Bond angles for **1C**.Table 1-24. Hydrogen bonds for **1C**. 205

Table 1-25 Torsion Angles for **1C**. 205

Table 1-26 Hydrogen atom coordinates ($Å \times 10^4$) and isotropic displacement parameters ($Å^2 \times 10^3$) for **1C**. 206

Table 1-27 Atomic Occupancy for **1C**. 207

Figure 2-1 A) The atom-numbering diagram of **I**. C, N, O and S atoms are shown as displacement ellipsoids at the 50% probability level and H atoms are shown as spheres of arbitrary radius. B) Crystal lattice of **I** showing the intermolecular contacts (blue lines). 213

Figure 2-2 Top-down (top), side-on (middles), and *c*-axis views of the resolved X-ray crystallographic structure (A) and optimized geometry by DFT-B3LYP calculations with 6-31+g(d,p) basis set (B) **I**..... 214

Figure 2-3 Experimental (black) and calculated (red) absorption spectra of I in dichloromethane (top). HOMO (A) and LUMO (B) Frontier orbitals of **I** (bottom) calculated by DFT-B3LP. 216

Table 2-1 Experimental details 218

Table 2-2 Hydrogen-bond geometry (Å, º) for (yohan1)..... 219

Table 2-3 Comparison of selected bond lengths and angles of the title compound and literature counter parts. 219

Liste des sigles et abbréviations

CHAT :	2-amino-3-cyano-4-5[b]-cyclohexylaminothiophène
CI :	Conversion Interne
CIE :	Commision Internationale de l'Eclairage
CIS :	Croisement Inter-Système
DAT :	2,5-diaminothiophène-3,4-dicarboxylique acide diéthyléther
EDOT :	3,4-(éthylènedioxy)thiophène
E_g :	Energy gap/ Énergie de la bande interdite
E_{pa} :	Potentiel d'oxydation
E_{pc} :	Potentiel de réduction
HOMO :	Highest Occupied Molecular Orbital / Orbitale moléculaire occupée de plus haute énergie
Hυ :	Lumière
i_{pa} :	Courant au pic d'oxydation
i_{pc} :	Courant au pic de réduction
IUPAC :	International Union of Pure and Applied Chemistry
IR :	Infrarouge
ITO :	Indium Tin Oxide
LUMO :	Lowest Unoccupied Molecular Orbital / Orbitale moléculaire vacante de plus basse énergie
MAT :	éthyle-2-amiothiophène-3-carboxylate
MS :	Mass Spectrometry/ Spectrométrie de masse
NMR :	Nuclear Magnetic Resonnance/ Résonnance Magnétique Nucélaire (RMN)
OFET :	Organic Field-Effect Transistor / Transistor Organique à Effet de Champ
OLED :	Organic Light-Emitting Diode/ Diode organique électroluminescente
OPV :	Organic Photo-Voltaic / Cellules solaires organiques
$TBAPF_6$:	Tétrabutylammonium hexafluorophosphate
TPA :	Triphénylamine
UV :	Ultra-Violet

VC : Voltampérométrie Cyclique

XRD : X-Ray Diffraction/ Diffraction des rayons-X

ΔOD : Différence en absorbance

Digui nananou nanouna wo. – J. Starr

Remerciements

Remerciements au Professeur Will Skene pour m'avoir supervisé pendant ces plusieurs années.

Remerciements à Andréanne Bolduc, pour m'avoir passé la main quand j'ai commencé et à Antoine Leliège pour m'avoir conseillé et encadré pendant ma 1ère année au labo, J.-R. Bullet pour son aide et ses conseils précieux en synthèse organique, et bien entendu Maxime romain pour la même chose, pour ses muffins, et pour être revenu (mais pas pour être allé s'installer à Longueuil avec son chien et notre amie).

Merci au personnel technique, Pierre Ménard-Tremblay et Sylvain Essiembre, ainsi que les gars de l'atelier mécanique et électronique et électronique qui font ou faisaient tous un travail impressionnant.

Merci à Denis Deschenes, pour son professionnalisme et son attention en toutes circonstances, ainsi qu'à tous les techniciens de laboratoire que j'ai rencontrés ou côtoyés.

Enfin spécial dédicace à Michou, partenaire de tous les vins et fromages. Son arrivée aura ravivé pour un temps les braises mourantes d'un feu voué à l'étouffement. Une pensée pour les raclées que tu prends désormais à Mario Kart, à défaut du squash.

Dédicace à Chengzhang, who will wonder all his life why he made that terrible decision.

Abdel, bon courage et bonne chance, Inch'Allah.

Et pour finir, un immense merci à Heather, pour m'avoir soutenu à travers ces années, dans le meilleur et dans le pire.

Introduction

Les matériaux conjugués

Depuis un peu plus de quarante ans, un nouveau domaine s'est grandement développé au sein de la chimie organique moléculaire, après la découverte dans les années 70 des propriétés semi-conductrices de certains polymères conjugués par les 3 futurs prix Nobel Heeger, McDiarmid, et Shirakawa.[1-2] Ainsi est née l'électronique organique, donnant encore aujourd'hui lieu à d'intenses recherches, tant au niveau académique qu'industriel, sur différents sous-domaines.

La conjugaison, dans les composés organiques, est un phénomène par lequel une (ou plusieurs) liaison(s) peu(ven)t être délocalisée(s) entre plus de deux atomes. Elle apparait lorsque l'on est en présence d'électrons π impliqués dans une ou plusieurs liaison(s). La molécule peut alors présenter plusieurs formes de relative stabilité, selon les possibilités de délocalisation. Ainsi, en fonction de l'alternance des électrons π avec des électrons de liaison σ, ou de doublets non-liants, ou des électrons non appariés, ces composés possèdent un nuage électronique délocalisable et peuvent présenter différentes symétries, avec différentes propriétés optiques linéaire ainsi que non-linéaires.[3]

Les doubles liaisons se forment lorsque des atomes de carbone se lient par des orbitales moléculaires hybridées sp^2, configuration qui produit trois liaisons covalentes σ dans le même plan, et laisse la dernière orbitale non hybridée p_z perpendiculaire hors du plan. Le chevauchement d'orbitales p_z sur des carbones voisins peut alors créer une deuxième liaison, formée par une paire d'orbitales π (p_z), qui sont considérablement délocalisée le long du chemin de conjugaison de la molécule ou sur des segments de la chaine du polymère.

Cette facilité de délocalisation induit que l'écart (ou bande interdite, communément appelée E_g) entre les orbitales moléculaires frontières de la molécule est réduit (Figure 0-1). Ainsi, les électrons présents sur l'orbitale moléculaire occupée la plus éloignée (en anglais Highest Occupied Molecular Orbital : HOMO), se trouvent rapprochés de la prochaine orbitale moléculaire disponible, non occupée (en anglais Lowest Unoccupied Molecular Orbital : LUMO). Cette conséquence est cruciale. En effet, on peut alors moduler l'écart HOMO-LUMO de ces composés conjugués et affiner leurs propriétés selon leur structure.

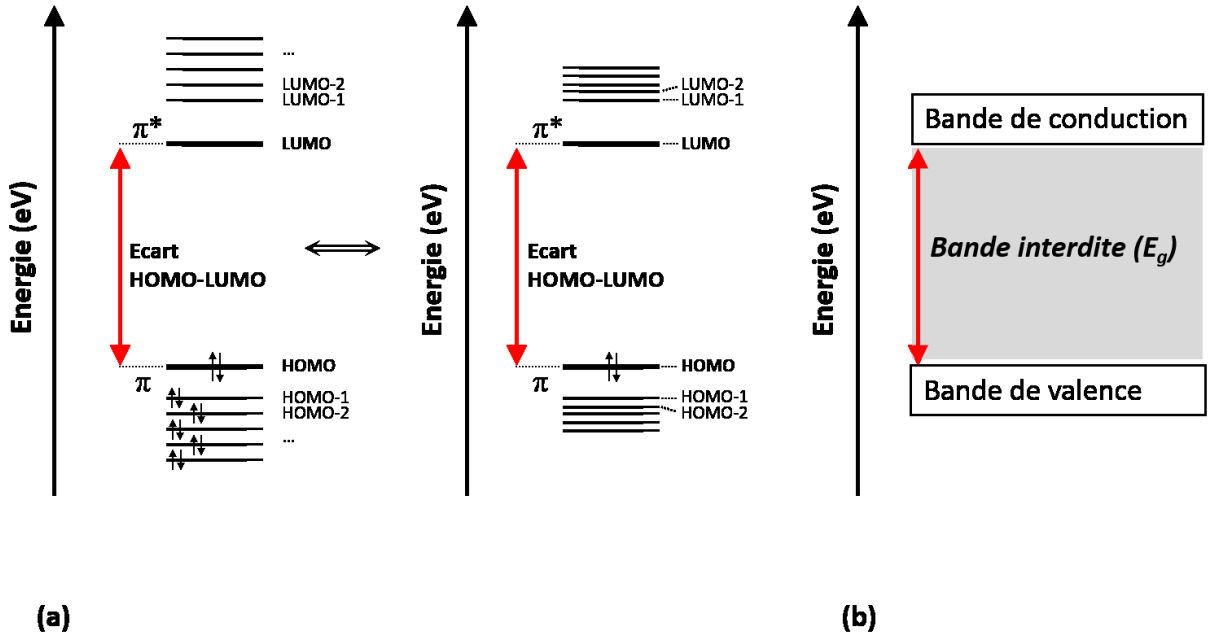

Figure 0-1 Représentation classique simplifiée des niveaux énergétiques des orbitales frontières d'une molécule conjuguée (a), ou dans un polymère conjugué (b) (inspiré de [4]).

L'utilisation de composés organiques permet de pouvoir moduler assez « simplement » les propriétés de ce genre de composés. Alors que l'allongement de la conjugaison, via des unités aromatiques, ou simplement par des groupements insaturés, permet de réduire l'écart HOMO-LUMO, l'introduction de groupements ou substituants électro-donneurs ou électro-attracteurs, c'est-à-dire riches ou pauvre en électrons, dans des composés conjugués dont on connait déjà les propriétés opto-electroniques, permet de faire varier les niveaux d'énergie des orbitales frontières (Figure 0-2). Un groupement ou un substituant donneur, riche en électrons, aura tendance à élever l'énergie de la HOMO alors qu'un groupement ou substituant accepteur, pauvre en électrons, aura tendance à abaisser l'énergie de la LUMO. En combinant habilement ces deux effets au choix de la structure des composés étudiés (unités aromatiques, longueur et degré de conjugaison), il est alors possible de réduire l'écart énergétique HOMO-LUMO de la molécule obtenue, par rapport à celui de la molécule analogue sans ces groupements ou substituants.

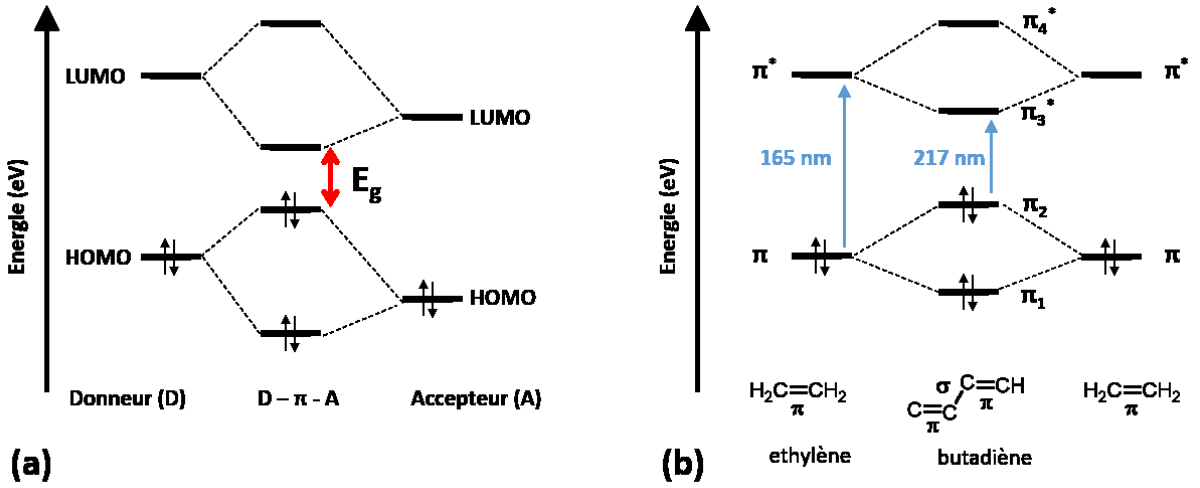

Figure 0-2 Effet (a) de l'ajout de groupements électro-actifs, (b) de l'allongement de la conjugaison, sur la E_g d'une molécule conjuguée (inspiré de [5]).

Le but recherché est de moduler la bande interdite, permettant à la molécule d'absorber ou d'émettre de la lumière dans le visible (400-800 nm), voire dans l'infra-rouge (IR), ou si plus élevée dans l'ultra-violet (UV), dépendamment de l'application souhaitée. En effet, la E_g est directement liée aux propriétés opto-électroniques des matériaux conjugués. Cet écart d'énergie, relativement faible dans ceux-ci, entre les électrons de la couche électronique externe de la molécule et les prochaines orbitales vacantes, leur permet d'absorber les photons des ondes électromagnétiques d'énergie similaire à cet écart. En effet, la relation de Planck-Einstein permet de quantifier l'énergie d'un photon en fonction de sa longueur d'onde :

$$\mathrm{E} = h\upsilon = \frac{hc}{\lambda},$$

avec *h* la constante de Planck, c la célérité de la lumière, υ la fréquence du rayonnement, et λ sa longueur d'onde. Les énergies de bande interdite de quelques électron-volts (eV) rencontrées dans les matériaux conjugués correspondent aux longueurs d'onde du spectre visible des ondes électromagnétiques (380-800 nm). L'absorption d'un photon par un électron promeut celui-ci sur une orbitale vacante. Ce faisant, la molécule passe de son état fondamental (S_0) à un état excité (S_1, ou S_2, S_3…) dû à l'excès momentané d'énergie qu'elle contient (Figure 0-3). C'est ce qui est responsable de la coloration observée dans beaucoup de ces composés, les longueurs d'onde absorbées n'étant plus réfléchies, on observe leurs couleurs complémentaires. Ceci

n'étant pas son état énergétique le plus bas possible, et donc le plus stable, la molécule va chercher à libérer cet excès d'énergie. L'absorption d'un photon se fait toujours à partir de l'état vibrationnel le plus bas de l'état fondamental, mais la molécule peut se retrouver sur des états vibrationnels énergétiques supérieurs de l'état excité. Il y a donc souvent une première perte d'énergie par relaxation vibrationnelle, modifiant la géométrie de la molécule. La molécule se stabilise sur son niveau vibrationnel le plus bas, par dissipation de son énergie vers ses voisines ou le solvant (chocs), ou dans le milieu par chaleur.

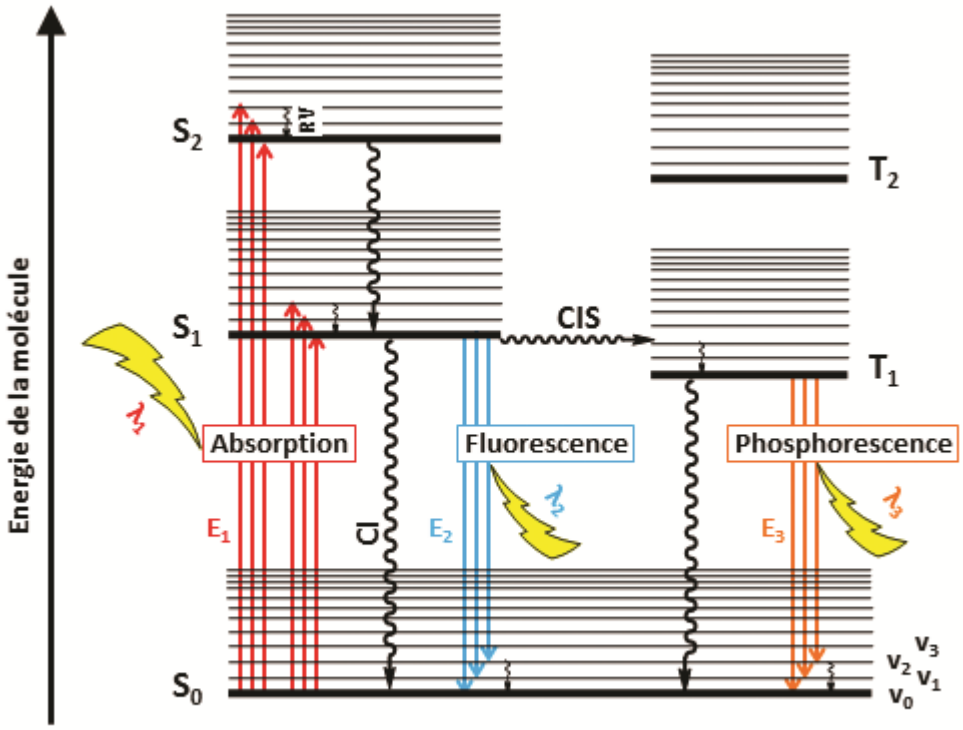

Figure 0-3 Diagramme de Perrin-Jablonski – Phénomènes subséquents à l'excitation d'une molécule par absorption d'énergie (inspiré de [6-7]).

A partir de là, plusieurs processus peuvent alors rentrer en compétition. Généralement, le phénomène de conversion interne (CI), non radiatif, l'emporte. Il s'agit du couplage d'un niveau vibrationnel de l'état excité avec un niveau vibrationnel de l'état fondamental de même énergie, puis de relaxation vibrationnelle. L'énergie est convertie en chaleur est dissipée dans le milieu. Mais, si, pour différentes raisons, comme la structure, l'encombrement stérique, le π-

stacking, la conversion interne est empêchée, ou ralentie, la molécule peut se désexciter par voir radiative. L'émission d'un photon permet alors à la molécule de passer de l'état S_1 aux différents niveaux vibrationnels de S_0, puis la relaxation vibrationnelle amène la molécule dans son état vibrationnel fondamental le plus stable. Suivant la configuration des états électroniques de la molécule, ainsi que, comme précédemment mentionné, la structure, etc… de la molécule, un dernier phénomène peut entrer en compétition avec la CI ou la fluorescence : le croisement inter-système (CIS). Si il y a suffisamment de temps, si c'est la seule voie de désexcitation ou si elle est facilitée, il peut y avoir inversion de spin de l'électron excité, et croisement (recouvrement) de deux niveaux vibrationnels des états excités singulet et triplet. Le cas échéant, une fois la relaxation vibrationnelle possible passée, la conversion interne se retrouve une nouvelle fois en compétition avec une voie radiative : la phosphorescence, i.e. la luminescence d'un état triplet à un état singulet. L'intervalle de temps entre l'absorption et la restitution d'énergie est appelé «durée de vie» de l'état excité. Il s'agit de temps très courts (10^{-12} s pour l'état vibrationnel excité, 10^{-8} à 10^{-9} s pour l'état électronique excité).

De nombreux sous-domaines se sont rapidement développés dans l'électronique et le photonique organique. On peut citer les diodes électroluminescentes organiques (OLED, de l'anglais *Organic Light-Emitting Diode*), l'absorption à deux photons et l'optique non-linéaire en général, les lasers, le photovoltaïque (OPV, de l'anglais *Organic Photo-Voltaic*), les transistors à effet de champ (OFET, de l'anglais *Organic Field-Effect Transistor*) ainsi que l'électrochromisme. Avec la découverte et le développement, peu après la confirmation du caractère semi-conducteur de certains composés organiques, de l'électroluminescence au sein de ceux-ci, la recherche sur les matériaux conjugués a connu un véritable essor.

Ainsi, de façon simplifiée, l'excitation d'un des électrons occupant la HOMO (Figure 4), par voie électrique, permet le phénomène de luminescence lors du retour de cet électron à son état fondamental, principe des OLEDs.[8]

De même, l'absorption par l'un de ces électrons d'un rayonnement lumineux correspondant énergétiquement à la E_g permet, en empêchant cet électron de retourner à l'état fondamental, de le faire se déplacer, amorçant alors un courant électrique, principe de fonctionnement des cellules photovoltaïques organiques (OPV).[9]

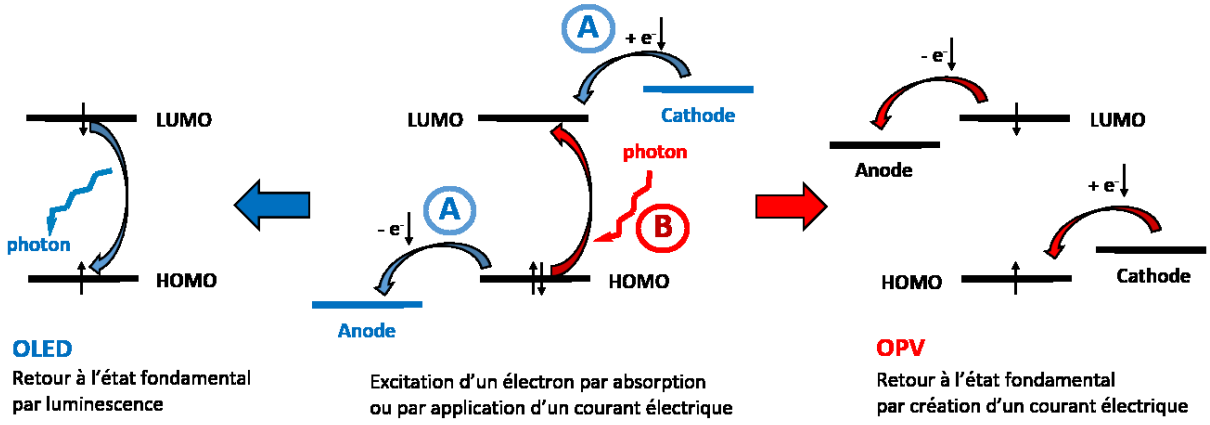

Figure 0-4 Représentation simplifiée du principe de fonctionnement d'une OLED (A) et d'une OPV (B).

La possibilité, pour les molécules conjuguées, une fois excitées, de délocaliser le(s) électron(s) concerné(s) permet aussi, dans certains cas, d'obtenir d'excellents candidats quant au semi-conducteur organique employé pour servir de canal entre la source et le drain des OFETs. Un changement de conformation, avec l'apparition de charges localisées, permet d'obtenir des interrupteurs, alors que le maintien de la localisation des charges sous certains stimuli peut en fait des mémoires organiques.

De façon générale, un matériau capable d'avoir un déficit de charges négatives (oxydé) est dit de type *p*, tandis qu'un matériau capable d'en avoir en excès (réduit) est dit de type *n*. On parle aussi de matériaux *n*- ou *p*-dopés, plus particulièrement pour les polymères.

Enfin, une autre propriété découlant de la conjugaison au sein des molécules organiques et qui nous intéresse particulièrement ici, est l'électrochromisme. C'est le changement de couleur, de façon idéalement réversible, d'un matériau suivant l'application d'un potentiel électrique. La réaction d'oxydoréduction modifie la E_g du matériau, en créant une nouvelle configuration électronique qui provoque le changement de couleur.[10] Ce phénomène est expliqué par la théorie du polaron. L'ionisation d'une molécule conjuguée (ou polymère) provoque une modification géométrique, pouvant passer d'une structure aromatique à une structure quinoïdale, pour une meilleure répartition du déséquilibre de charge créé. Cela

provoque des changements significatifs dans les orbitales frontières. Que l'on ait affaire à une oxydation (un électron de la HOMO en moins) ou une réduction (un électron en plus, sur la LUMO), on obtient un cation ou anion radicalaire respectivement (Figure 0-5). Les états électroniques du polaron résultant se retrouvent augmentés en énergie pour la HOMO, tandis que la LUMO est diminuée.[11-12] La E_g s'en trouve modifiée, pouvant mener à un changement de couleur de l'espèce ionisée, dans le cas d'électrochromisme. Une ionisation plus poussée peut conduire à un bipolaron (dication ou dianion), les deux nouveaux états électroniques se retrouvant davantage rapprochés.

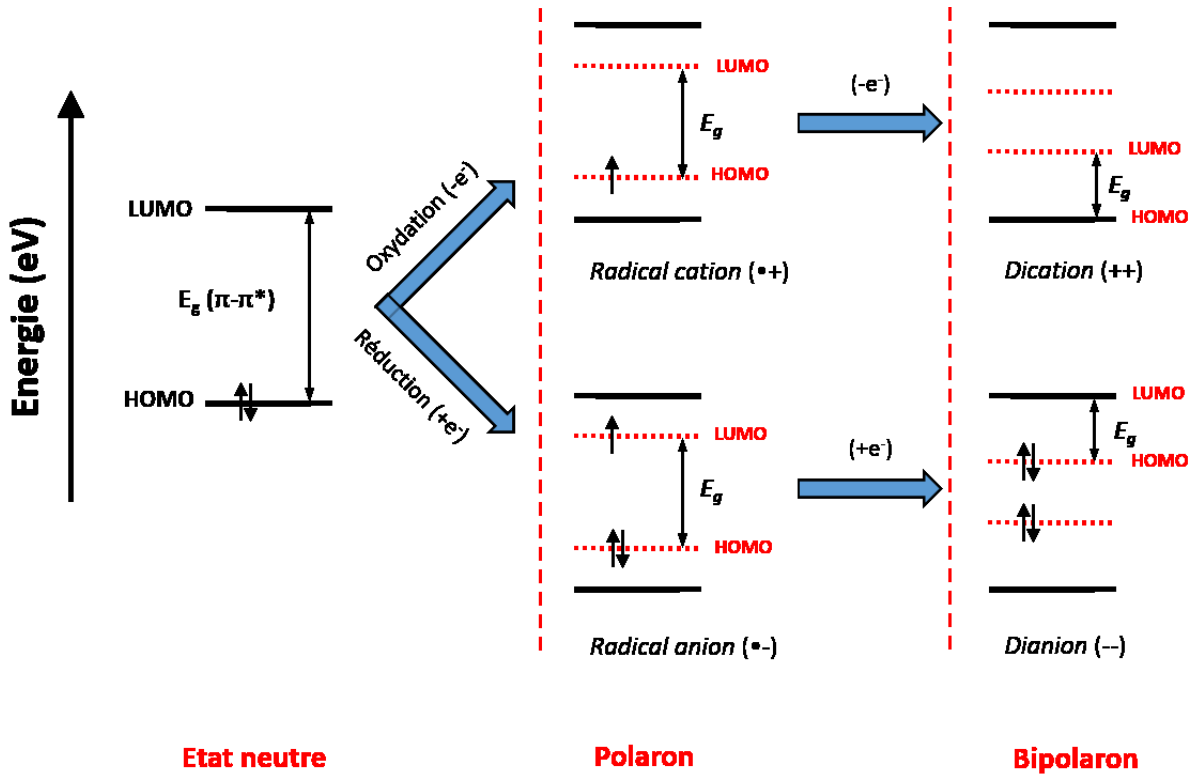

Figure 0-5 Représentation schématique des états polaroniques d'une molécule conjuguée oxydée ou réduite (inspiré de [11]).

Le phénomène d'électrochromisme n'est pas nouveau. Il a été pour la première fois décrit dans les années 1960, par Deb, lors de l'observation du changement de couleur induit électriquement de films fins d'oxyde de tungstène (WO_3).[13] Une grande attention s'est alors portée vers les oxydes de métaux de transition, tels que le V, Mo, Nb, Ti, Ni, Co, Ir, et

particulièrement le W, jusqu'à de nos jours. Des applications telles que les vitres intelligentes ont rapidement émergé et ont contribué à maintenir un engouement pour le sujet. En parallèle, comme mentionné précédemment, la recherche sur les matériaux conjugués, aussi en plein essor, a mis en évidence les propriétés électrochromes de certaines classes de molécules conjuguées comme par exemple le viologène ou les oligomères de thiophène, pour les molécules de faible masse molaire, ou comme les dérivés de poly(aniline), de poly(thiophène), ou de poly(pyroles) pour les polymères.[14]

La recherche actuelle sur les matériaux conjugués semi-conducteurs ne connait pas de désintérêt, car ceux-ci prouvent être une alternative toujours potentiellement compétitive aux matériaux inorganiques, actuellement encore majoritairement utilisés dans les dispositifs électroniques et applications commerciales, tels que les OPVs, les OLEDs, OFETs et autres.

En effet, les matériaux inorganiques, composés de métaux et éléments lourds du tableau périodique donnent d'excellents résultats, dû à leur bonne conduction, mais ils restent néanmoins chers à produire.[15] Leur mise en œuvre peut être effectuée par évaporation thermique, ablation à laser pulsé, pulvérisation pyrolytique déposition chimique en phase vapeur, etc… Ces procédés, relativement coûteux, les rendent peu compétitifs en termes de rapport coût-efficacité. De plus, ils sont en général lourds et cassants, puisque déposés principalement en films minces.

Les matériaux conjugués, et particulièrement les polymères conjugués, offrent, quant à eux, de nombreux avantages en termes de mise en œuvre d'applications. D'une part, après des années de recherches, une pléthore de familles de composés a déjà été synthétisée et étudiée. La facilité d'optimisation, avec précision, de leurs propriétés opto-électroniques avec de simples modifications synthétiques, est un des aspects attractifs des matériaux conjugués.[16-17] De par leur solubilité dans des solvants organiques communs, leur mise en œuvre est plus simple et son coût est moindre. La fabrication de films minces pour des dispositifs de grandes dimensions est facilement réalisable par évaporation/déposition sous vide, sublimation, pulvérisation, *spray-coating*, *spin-coating*, trempage, impression (*roll-to-roll*); une multitude de techniques a été développée pour répondre aux contraintes imposées par la structure et l'état à la température ambiante des différents composés imaginables tout en prenant en compte le besoin de reproductivité et de fabrication à grande échelle.[18] Enfin, d'autre part, contrairement aux

matériaux inorganiques, ils ouvrent la voie à l'électronique organique plastique, car via ces procédés, ils peuvent en effet être mis en œuvre sur des substrats flexibles en plus d'être peu coûteux.[19]

Concernant l'électrochromisme, de nombreuses applications sont actuellement commercialisées, et le sujet fait toujours l'état de recherches aujourd'hui. En plus des fenêtres intelligentes nommées précédemment (*smart windows*), dont la transmittance va changer, s'opacifiant, s'éclaircissant, filtrant certains rayonnements en fonction de la luminosité extérieure,[15, 20] on peut nommer les visières de casque de moto, les rétroviseurs « anti-reflet » de véhicules (miroirs anti-éblouissement) s'opacifiant pour atténuer le reflet des phares de voiture, le papier électronique (*e-paper*).[10, 21-24] L'industrie se tourne aussi maintenant vers les textiles, grâce à l'essor de l'électronique organique plastique.[25-27] Les matériaux conjugués sont considérés par beaucoup comme étant la prochaine génération de dispositifs opto-électroniques.

Dans le domaine des matériaux conjugués, la recherche porte tout autant sur les polymères que sur les petites molécules organiques (de faible masse molaire) et les oligomères (c'est le cas du travail présenté dans ce mémoire). Les polymères conjugués offrent certains avantages comme le fait de pouvoir être mis en œuvre aisément, un bas coût de production à grande échelle, un poids beaucoup plus léger que les matériaux inorganiques, une certaine flexibilité ainsi qu'une modulation facile de leurs propriétés par l'introduction de substituants.[18, 28] Les seconds permettent d'étudier rapidement les relations structures-propriétés au sein des différentes molécules, pour ensuite pouvoir prédire le comportement, anticiper sur des propriétés intéressantes de classes de matériaux similaires, ou de polymères à base d'unités similaires.

Problématique et objectifs

Les matériaux conjugués ayant donné lieu à d'intenses recherches dans le monde entier, de nombreuses stratégies ont été mises en place, afin de moduler la largeur de la E_g, ou pour obtenir des valeurs de HOMO ou LUMO souhaitables. Une possibilité est d'allonger la conjugaison des molécules. Pour cela, il est possible d'incorporer des éléments conjugués, tels que des liaisons doubles ou triples carbone-carbone, ou encore des cycles aromatiques ou des

hétérocycles. Ainsi ont vu le jour les polymères dérivés du poly(thiophène), poly(pyrole), poly(phénylène), poly(fluorène), poly(acéthylène) ou encore de la poly(aniline), pour n'en citer que quelques-uns. [29-30]

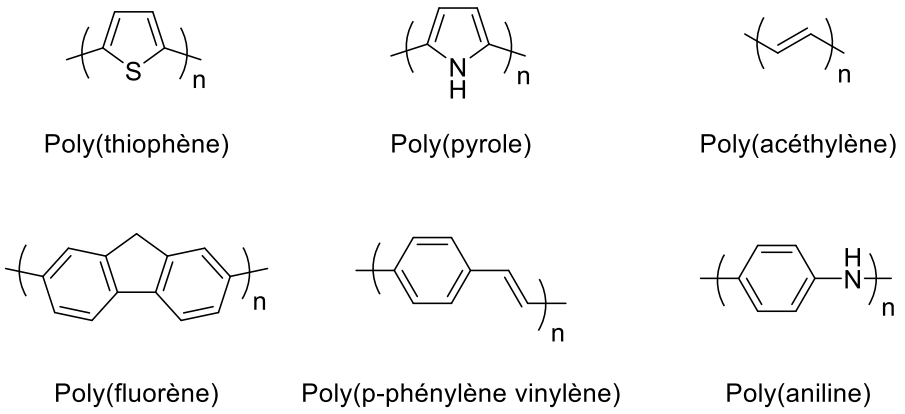

Figure 0-6 Exemple de types de polymères conjugués utilisés en électronique organique.

Les unités constituants les matériaux sont déjà conjugués, certaines absorbant dans le domaine du visible. En créant des oligomères voire des polymères à partir d'entre eux, de façon appropriée, la conjugaison augmente, et ainsi la délocalisation des électrons π, diminuant du coup la E_g. Le design, l'optimisation et l'étude approfondie des relations structure-propriétés de nombreux polymères conjugués a eu lieu durant les dernières décennies, en fonction des caractéristiques requises pour chaque type d'application recherchée.[31-33]

Les dérivés du thiophène, en tant qu'unités de base de polymères conjugués, ont particulièrement été étudiés. Ils sont facilement fonctionnalisables, possèdent une bonne stabilité chimique et thermique, en plus de propriétés optiques et électroniques déjà établies et intéressantes pour l'électronique organique.[30, 32, 34-36] Ils possèdent en plus un potentiel d'oxydation naturellement bas, qui leur permet ainsi d'être électro-polymérisés facilement.[28]

La majeure partie de la recherche sur les matériaux conjugués passée et actuelle porte sur des composés dont la conjugaison est assurée par une combinaison d'unités aromatiques, de double liaisons (groupements vinylènes) et/ou triple liaisons (groupements acétylèniques) carbone-carbone et/ou de doublets non liants d'atomes. Les méthodes conventionnelles

employées pour les obtenir font très souvent appel à des couplages et réactions catalysés par des métaux de transition lourds (Figure 0-7), difficiles à totalement éliminer ensuite, et nécessitant une purification intensive.[37-39] Le développement de la chimie verte, la nécessité d'avoir des composés exempts de toutes impuretés, l'impact environnemental lié à leur traitement et recyclage commencent à être vus comme des contre-parties négatives par rapport à la simplicité et l'innovation qu'apportaient ces méthodes de synthèses.

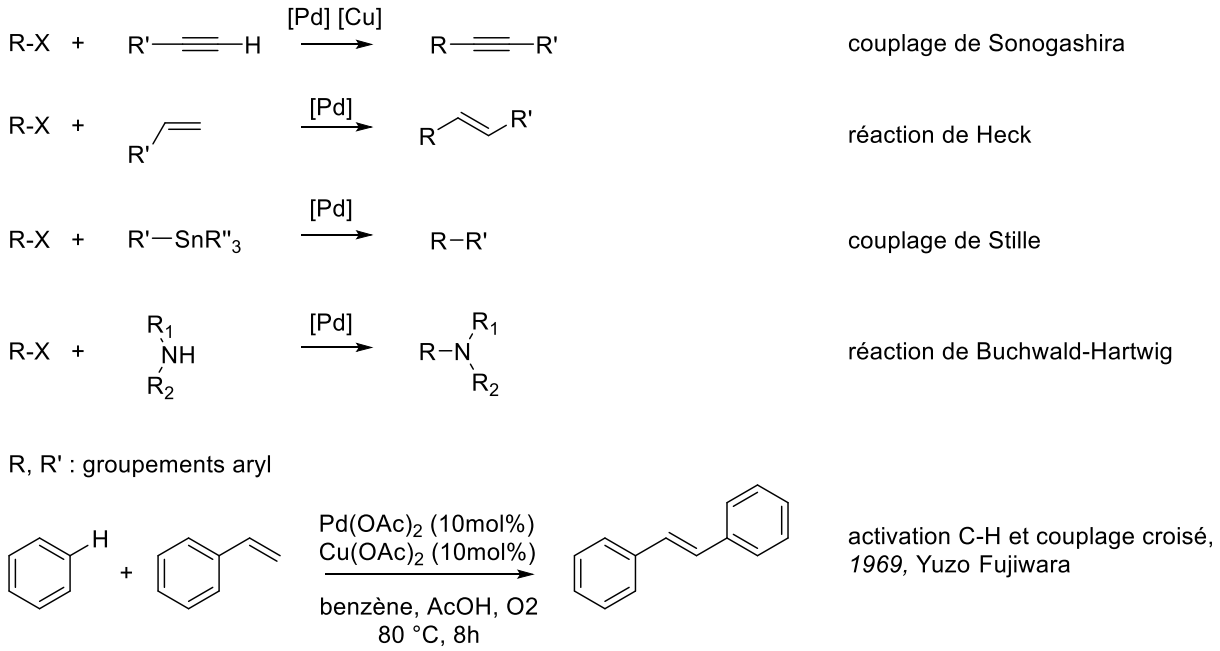

Figure 0-7 Exemples non exhaustifs de réactions et couplages conventionnels utilisés pour l'obtention de molécules conjuguées.

Un des axes majeurs de recherche dans le groupe du Pr. Skene porte sur l'étude de composés azométhines conjugués (Figure 0-8). En effet, en partie dû au fait que les imines sont généralement facilement hydrolysables, les azométhines ont longtemps été considérées comme peu intéressantes puisque perçues comme ayant un faible intérêt en termes de stabilité. Pourtant, ces imines, substituées sur l'azote et une fois sur le carbone, sont isoélectroniques avec leurs analogues carbonnés.[40-41] L'utilisation de ces doubles liaisons carbone-azote (C=N) dans des combinaisons avec des unités aromatiques se concentrait surtout sur des molécules à noyaux benzéniques substitués.[40-44] Les précurseurs aminés comme la para-phénylènediamine,

disponibles commercialement, sont plus stables à l'air et électrochimiquement que leurs analogues thiophéniques aminés, eux trop riches en électrons, et s'oxydant donc facilement. De façon générale, les azométhines sont le résultat de la condensation d'un aldéhyde et d'une amine primaire, typiquement dans un solvant « vert » comme l'éthanol, avec comme coproduit de l'eau (Figure 0-8), même si l'obtention de certaines azométhines peut aussi nécessiter l'emploi de conditions plus drastiques. En termes d'éco-responsabilité, elles présentent donc aussi un fort intérêt. Les recherches du groupe Skene se sont intéressées à l'exploration d'une famille de composés en particulier, les dérivés thiophéniques azométhines, comme de bons potentiels candidats en tant que matériaux conjugués.

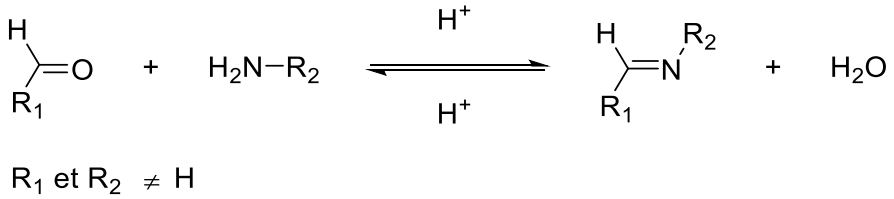

Figure 0-8 Représentation schématique de la condensation d'une amine et d'un aldéhyde pour former une azométhine.

Les diamino-thiophènes non-substitués n'étant pas stables à l'air, contrairement à leurs analogues aldéhydes, une première étape a consisté à trouver des amino-thiophènes stables à l'air et moins facilement oxydables. Cela fut atteint à l'aide de différents composés déjà reportés, mais peu utilisés dans cet optique, sur lesquels l'introduction de groupements attracteurs permet de stabiliser la charge électronique et les rend stables à l'air.. Ainsi le CHAT (cyclohexane-aminothiophène), le MAT (méthyl-aminothiophène) et le DAT (2,5-diaminothiophène)[45-47] ouvrent la voie à la mono- et di-condensation d'aldéhydes pour former des azométhines conjuguées à partir de précurseurs thiophèniques (Figure 0-9).

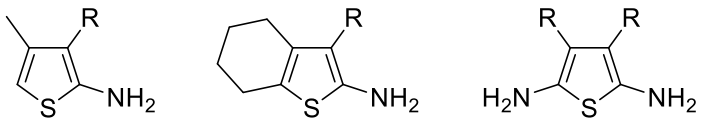

R = CN, COOEt

Figure 0-9 Amino-thiophènes utilisés au laboratoire.

En travaillant d'abord sur des petites molécules de faible masse molaire, le groupe Skene s'est intéressé à l'étude des relations structure-propriétés[48-51] de différents dérivés thiophéniques mono-azométhines, tout en leur robustesse i.e. leur résistance face à l'hydrolyse, ainsi que face à la réduction électrochimique. L'introduction de substituants et groupements avec différents effets inductifs permet d'observer les changements de propriétés en découlant (Figure 0-10). Cela permet de comprendre les propriétés électrochimiques et spectroscopiques de ces azométhines conjuguées, pour ensuite anticiper sur celles des composés à venir.

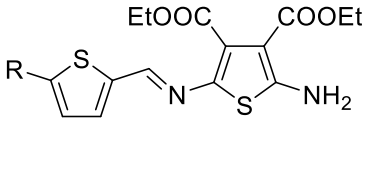

R = H, Me, NO_2, NEt_2, 2-thiophène

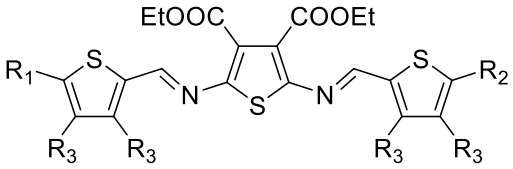

R_3 =H

R_1 = R_2 = H, Me, NO_2, NEt_2, 2-thiophène
R_1 = H ; R_2 = NO_2, 2-thiophène
R_1 = NEt_2 ; R_2 = NO_2

R_3 = $C_{10}H_{21}$; R_1 =R_2 =H

Figure 0-10 Exemple non exhaustifs de dimères et trimères antécédent investigués.

Au fur et à mesure, différentes mono-azométhines, di-azométhines, puis des oligomères et des poly-azométhines ont ensuite vus le jour. Dans les trimères, le placement du DAT au centre ou aux extrémités, l'ajout ou non de chaines alkyles sur les précurseurs thiophéniques, le remplacement du thiophène par l'EDOT (3,4-éthylène-dioxythiophène), plus riche en électron,

sont tous des paramètres qui ont été étudiés (Figure 0-11).[52-56] De même, plusieurs polyazométhines ont été synthétisées et examinées (Figure 0-12).[52, 57-58] Il a ainsi été observé, de façon générale, que les oligomères comportant des noyaux thiophéniques terminaux non α-substitués présentaient une irréversibilité de leur oxydation, ceux-ci s'électro-polymérisant par homo-couplage anodique.

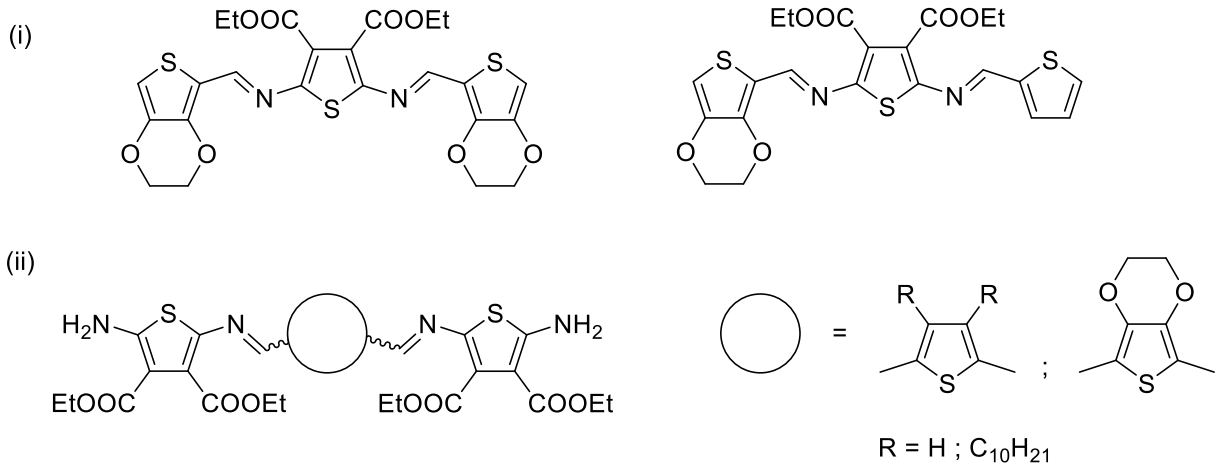

Figure 0-11 Exemples de trimères investigués par le passé

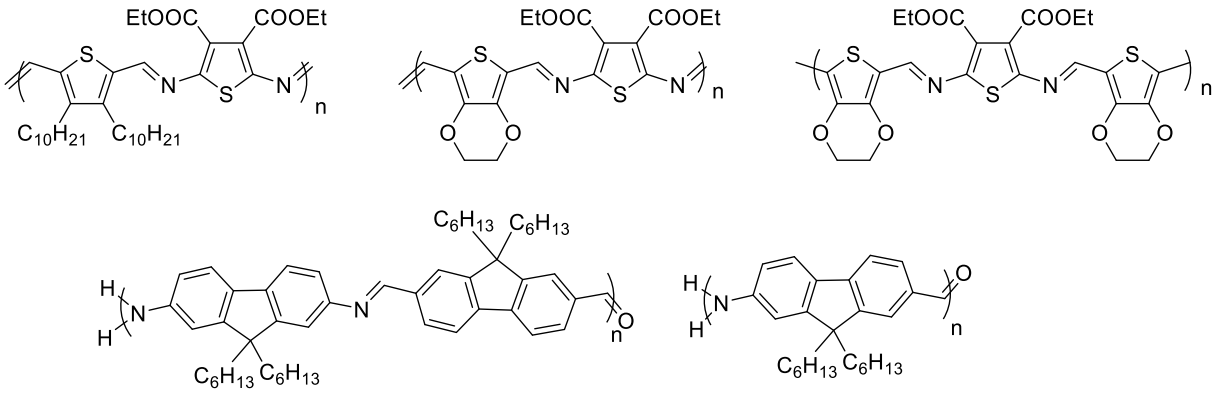

Figure 0-12 Exemples de polyazométhines précédement étudiées

Autre que leur fluorescence dans certains cas, une propriété attendue des azométhines conjuguées était leur électrochromisme. En effet, constituées de noyaux thiophéniques et de divers chromophores, leurs structures conjuguées laisse prédire l'absorption de rayonnement lumineux du domaine du visible lors de leur transition π-π*. Différents changements de couleur ont ainsi été observés, en faisant varier les unités thiophéniques ainsi que les différents substituants et autres chromophores. Ainsi, en particulier, le motif trimérique composé d'un thiophène central, substitué ou non, connecté par une azométhine à une unité de DAT de chaque côté (Figure 0-11,ii) montre une réversibilité, de par les extrémités amines (-NH_2) qui empêche l'homo-couplage lors de l'oxydation, ainsi qu'un changement de couleur de rouge (neutre) à vert (oxydé).[52]

L'étude de l'effet d'autres substituants sur les propriétés observées avait jusqu'ici peu été approfondie. De même, le choix de l'unité au centre des deux azométhines s'est souvent limité à des dérivés thiophéniques (Alkyl-thiophène, EDOT) ou à d'autres hétérocycles à 5 chainons. Un travail préliminaire portant sur le remplacement des amines terminales par des amides primaires monosubstituées par un groupement phényl a déjà été effectué. Les amides sont des groupements au caractère électro-attracteur, qui renforce celui des liaisons azométhines déjà présentes. Il était attendu que celles-ci rendent atteignable la réduction des molécules ainsi conçues. Ce travail a permis de confirmer que ces dérivés amides-azométhines peuvent être oxydés aussi bien que réduits, et que chacun de ces processus présente des changements de couleur remarquables i.e. de jaune ou orange (neutre) à incolore (oxydé) et à bleu (réduit).[59] Par contre, ces dérivés ne permettaient pas une utilisation optimale dans le temps, leur couleur se dégradant après seulement quelques cycles dans les dispositifs électrochromiques, et la réversibilité n'étant que légèrement présente, seulement pour l'oxydation.

À côté de cela, de précédents travaux du groupe se sont déjà intéressés à l'étude des propriétés électrochromes de composés azométhines incorporant des dérivés de la triphénylamine (TPA).[60-62] Cette triarylamine est connue pour avoir des propriétés opto-électroniques intéressantes, absorbant les photons proches de la région Ultra-Violet (UV), de par ses transitions π-π* et n-π* (doublet non-liant de l'azote). Dû à son caractère donneur d'électrons et transporteur de trous, elle est souvent utilisée dans des systèmes *push-pull*, où l'alternance de groupements donneur/accepteurs d'électrons dans la conjugaison permet de

générer des transferts de charges intra-moléculaires. Electrochimiquement, elle possède un faible potentiel d'oxydation associé à une réversibilité électrochimique lorsque les positions *para* des phényls sont substitués.[63] Elle a déjà été incorporée dans des matériaux conjugués destinés aux OLEDS,[64-65] aux OPV,[36, 66-67] entre autres, ainsi qu'aux dispositifs électrochromes.[68-69] La TPA était donc un une molécule de choix à intégrer dans les azométhines conjuguées, et particulièrement sur ce motif.

Dans le travail présenté ci-après, nous nous sommes intéressés à la synthèse, la caractérisation et l'étude des propriétés électrochimiques et spectro-électrochimiques de nouveaux composés azométhines conjugués (Figure 0-13). Composés d'un cœur di-azométhine, les amines terminales des DAT sont remplacées par des amides conjuguées, permettant de varier le substituant conjugué suivant. Trois substituants ont été étudiés, le phényl, la triphénylamine (TPA) et l'équivalent de celle-ci di-méthylé en position *para* sur les cycles terminaux. Au centre, l'effet du thiophène, de l'EDOT, et de la TPA sur les propriétés observées a aussi été étudié. L'objectif de l'étude de ces composés est de savoir si il est possible d'atteindre une réversibilité de l'oxydation et un meilleur accès à leur réduction, en parallèle d'observer quelles couleurs seraient mises en jeu dans ces processus, et si il est possible d'augmenter la performance de ces azométhines face au stress imposé par une répétition prolongée de ceux-ci (expérience de *switching*, *vide infra*).

Les composés cibles étaient initialement les diazométhines, appelés trimères (*triads*, dans le chapitre suivant) car composés de trois unités séparées par des liaisons azométhines. La stratégie de synthèse, expliquée dans le chapitre suivant, nous a amenés à synthétiser d'abord les composés amides-aldéhydes, pour ensuite les connecter au cœur des trimères via les liaisons azométhines. Par abus de langage, les amides sont appelées dimères (*dyads*) car composés de deux unités aromatiques séparées par une liaison amide.

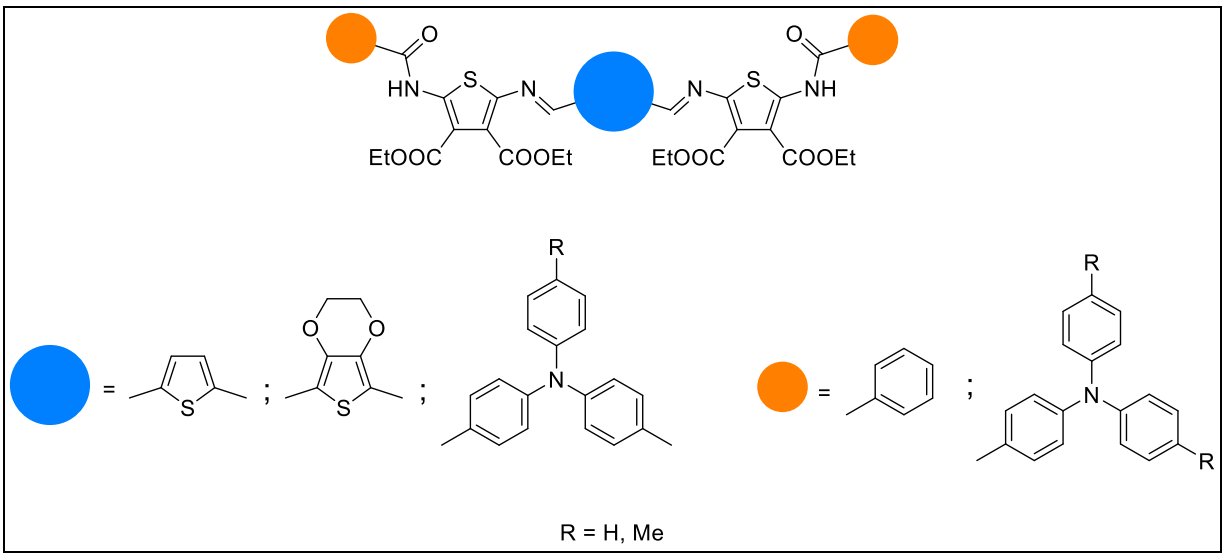

Figure 0-13 Trimères présentés dans les travaux de ce mémoire

Le chapitre 1 traitera de la synthèse et de la caractérisation de ces nouveaux composés azométhine-amide conjuguées. La stratégie de synthèse ainsi que les différentes analyses structurales y sont présentées, suivi des analyses électrochimiques, spectro-électrochimiques, ainsi que leur performances électrochromiques. Des calculs théoriques de DFT (Théorie de la Fonctionnelle de la Densité) viennent appuyer ces analyses, pour permettre de mieux comprendre les phénomènes électroniques mis en jeu.

Le second chapitre décrit les caractéristiques structurales d'un monocristal obtenues par diffraction des rayons-X. Cela permet de corroborer les hypothèses structurales de la DFT et permet aussi de comparer les données structurales telles que les longueurs de liaisons avec des composés relativement similaires déjà présents dans les bases de données.

Partie expérimentale : caractérisation des matériaux conjugués

Propriétés électrochimiques

Les niveaux d'énergie HOMO et LUMO d'une molécule peuvent être caractérisés selon différentes méthodes. Ainsi, on peut s'intéresser aux potentiels d'oxydation et de réduction de la molécule. En effet, lors de l'oxydation, un électron est arraché de l'orbitale moléculaire occupée de plus haute énergie (HOMO), alors que pour la réduction, il s'agit de l'introduction

d’un électron supplémentaire sur l’orbitale moléculaire inoccupée la plus basse en énergie (LUMO). En déterminant ces potentiels d’oxydation et de réduction de la molécule en solution, on peut alors remonter aux énergies des niveaux HOMO/LUMO mis en jeu.

Une des méthodes les plus courantes pour ce faire est la voltampérométrie cyclique (VC). Cela consiste à mesurer le courant électrique circulant entre une électrode de travail et une électrode auxiliaire, lorsque que l’on fait varier linéairement le potentiel entre l’électrode de travail et un électrode de référence, de façon cyclique. Un électrolyte support est ajouté à la solution de l’analyte dans un solvant afin d'assurer une conductivité suffisante. Cette technique permet d’observer rapidement le comportement redox d’une molécule sur une large plage de potentiel. En effet, elle est capable de générer un nouvel état redox pendant le balayage aller, et de sonder son devenir sur le balayage retour, en seulement quelques secondes. En plus de permettre d’accéder aux potentiels électrochimiques, la VC peut aussi donner accès à d’autres informations, tels que la réversibilité électrochimique du processus étudié ou le nombre d’électrons échangés au cours des processus observés.

L’électrode de référence sert à calibrer les potentiels pour pouvoir les comparer entre eux, et maintient un potentiel pratiquement invariant dans les conditions de la mesure électrochimique. Il en existe différentes sortes, selon que la VC est effectuée en milieu aqueux ou organique. En milieu organique, on peut utiliser des électrodes de type $Ag/AgNO_3$, Ag/AgCl, dans lesquelles un fil d’argent trempe dans une solution contenant le contre-ion de l’argent oxydé, séparée du milieu expérimental par un fritté poreux, ne permettant pas aux différents ions de passer à travers. Pour des raisons pratiques, on peut aussi utiliser un fil d’argent directement, on parle dans ce cas de quasi-référence, le potentiel d’oxydation de celui-ci pouvant varier quelque peu selon le milieu et les conditions, d’une mesure à l’autre. Il est alors d’usage d’introduire, pendant la mesure ou à la fin, un couple redox dont le potentiel est connu par rapport à d’autres systèmes de référence, typiquement le ferrocène, qui s’oxyde en ion ferrocinium. On peut alors recalibrer les potentiels obtenus grâce au potentiel du couple ferrocène/ferrocinium versus une référence connue, ou versus le potentiel de demi-vague du ferrocène placé à 0V. Il est ensuite possible, le cas échéant, de remonter jusqu’aux valeurs des niveaux d’énergie HOMO/LUMO via une conversion mathématique.

La notion de réversibilité doit être différenciée selon que l'on parle de réversibilité chimique ou électrochimique. Un système réversible chimiquement signifie que lors de l'oxydation (ou la réduction) d'une espèce, la nouvelle espèce obtenue est stable, ne subissant pas de réaction secondaire (décomposition, homo-couplage, réaction subséquente avec une autre espèce présente) et peut, suivant l'application du potentiel adéquat, subir le processus inverse pour redonner l'espèce initiale. Cette stabilité est relative à l'échelle de temps de la mesure et au milieu expérimental. Un système réversible électrochimiquement fait référence au taux de transfert d'électrons à l'interface électrode-solution, autrement dit à la constante de vitesse électrochimique. Dans le cas d'un couple redox réversible électrochimiquement, les deux espèces échangent rapidement des électrons avec l'électrode de travail. Le potentiel formel du processus examiné est alors défini comme :

$$E_{\frac{1}{2}} = E'_0 = \frac{(E_{pa}+E_{pc})}{2}$$

Découlant de l'équation de Nernst, pour des conditions expérimentales à température ambiante (398.15 K), le nombre d'électrons échangés avec l'électrode (n) peut être déterminé expérimentalement à partir de la séparation des 2 pics :

$$\Delta E_p = E_{pa} - E_{pc} \approx \frac{0.059\,V}{n}$$

De plus, les valeurs des courants de pics maximum i_{pa} et i_{pc} sont normalement égales, signifiant que la quantité de matière oxydée puis réduite, ou vice-versa, est la même. Une méthode pour la détermination graphique du courant de pic maximum du balayage retour implique une extrapolation de la ligne de base du courant (Figure 0-14), qui n'est pas toujours évidente lorsque plusieurs processus se suivent de près.

Enfin, le maximum du pic de courant du balayage aller, pour un système réversible, est décrit par l'équation de Randles-Sevcik (valable pour la CV en solution, impliquant un processus diffusionnel):

$$I_p = (2.69*10^5)n^{3/2}AD^{1/2}C\upsilon^{1/2},$$

où i_p est le maximum du pic de courant (en A), n le nombre d'électron échangés avec l'électrode, A la surface de l'électrode (cm^2), D le coefficient de diffusion (cm^2/s), C la concentration de l'espèce étudiée (mol/cm^3) et υ la vitesse de balayage (V/s).

Lorsque le transfert d'électrons avec l'électrode est trop lent, la séparation des pics est supérieure à 59 mV, et les trois équations sus-mentionnées ne s'appliquent plus. Le processus est alors électrochimiquement « irréversible ».

Dans le cas d'une absence de pic de retour, le processus est chimiquement irréversible, dans l'échelle de temps de la mesure.

La Figure 0-14 décrit le voltampérogramme obtenu avec un couple réversible. La convention utilisée ici et dans le prochain chapitre pour décrire les courbes courant-potentiel suit les recommandations de l'IUPAC (*International Union of Pure and Applied Chemistry*), i.e. les potentiels négatifs (réducteurs) à gauche de l'axe (0 V)) et ceux positifs (oxydants) à droite, et les courants anodiques (oxydation) positifs, au-dessus de l'axe (0 A), les courants cathodiques (réduction) négatifs en dessous. Le sens de balayage, pour plus de clarté, est indiqué par une flèche. Lorsque l'expérience décrite Figure 0-14 commence, le potentiel appliqué n'est pas assez élevé pour oxyder l'espèce en solution. Au point A, ce n'est plus le cas. L'oxydation commence, et le courant augmente rapidement jusqu'à ce que la concentration en espèce à oxyder, à la surface de l'électrode, commence à diminuer de façon substantielle. Le courant commence alors à augmenter moins rapidement, jusqu'au pic (point B), où il commence à diminuer, la concentration d'espèce à oxyder diminuant de plus en plus à la surface de l'électrode. Au point C, le balayage est inversé, le potentiel appliqué commence à diminuer linéairement. Étant toujours assez élevé pour oxyder l'espèce initiale, le courant anodique continue sa progression. Au point D, le potentiel atteint une valeur appropriée pour commencer à réduire l'espèce oxydée, qui s'est accumulée autour de l'électrode. Le courant, maintenant cathodique augmente rapidement, jusqu'au point E, où, comme précédemment, la concentration de l'espèce oxydée à la surface de l'électrode est suffisamment diminuée. Le courant commence alors à diminuer, alors que l'espèce oxydée à réduire se fait rare autour de l'électrode, jusqu'à ce que le potentiel soit trop faible pour continuer à réduire.

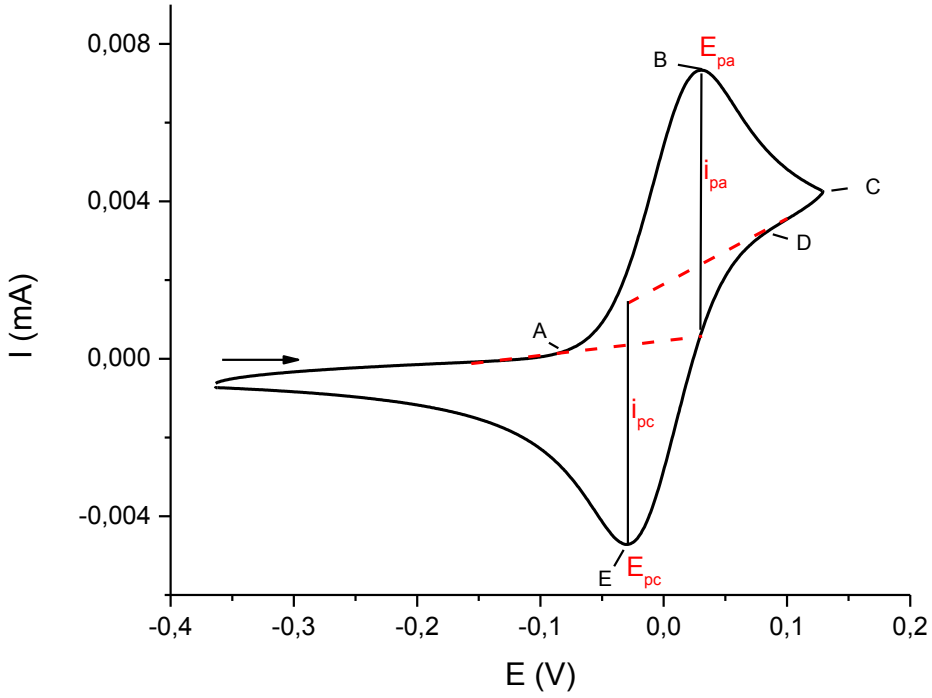

Figure 0-14 Voltampérogramme cyclique idéal d'un couple électrochimiquement réversible.

Pour des composés subissant des processus électrochimiquement réversibles, on cherche à déterminer les potentiels de demi-vagues, qui sont réellement caractéristiques du couple redox en jeu. Cependant, lorsque l'on veut comparer entre eux des composés qui ne présentent pas tous des processus réversibles, il est plus pratique de comparer les potentiels de vagues entre eux, soit les différents E_{pa} ou E_{pc} déterminés, comme c'est le cas dans le chapitre suivant.

Spectro-électrochimie et électrochromisme

De façon générale, un matériau électrochrome est un matériau ayant la propriété de changer de couleur lors de l'application d'un potentiel électrique. Plus spécifiquement, c'est un matériau dont l'absorbance (et donc la couleur), ou la transmission, change de façon réversible en fonction de sa charge électrique. La réversibilité est la cible recherchée lorsque l'on étudie cette propriété. Le changement peut avoir lieu entre différentes couleurs, ou entre un état « transparent » et un état coloré. Ainsi, un matériau électrochrome possède au moins un état

dont la largeur de la bande interdite E_g permet l'absorption de la lumière dans le domaine du visible.

Les matériaux organiques conjugués sont particulièrement intéressants pour étudier cette propriété. En effet, leur transition π- π^* est souvent responsable de leur absorption dans l'ultra-violet (UV), le visible et l'infra-rouge (IR). Cette transition, typique des matériaux conjugués, et dont l'énergie correspond souvent à des longueurs d'onde du rayonnement du domaine du visible, en fait donc potentiellement tous des électrochromes, et permet aussi une plus grande variabilité dans la couleur comparé aux composés inorganiques. Au laboratoire, plusieurs méthodes sont employées pour étudier les propriétés électrochromes d'une molécule. En effet, on peut coupler la caractérisation électrochimique avec la caractérisation spectrométrique. Tout d'abord, la VC du composé doit montrer au moins une réversibilité électrochimique, en oxydation et/ou en réduction, pour un intérêt potentiel. L'analyse spectro-électrochimique en solution est alors de mise. Il s'agit de mesurer la variation de l'absorbance du composé en fonction du potentiel électrique appliqué. Une mesure d'absorbance est effectuée pour chaque valeur de potentiel appliqué. Lors de cette mesure, on voit habituellement le pic d'absorbance du composé neutre diminuer puis disparaitre, et si l'espèce créée (radical cation ou anion, dication, ou dianion) absorbe dans la gamme de l'UV, visible, ou le proche IR, l'apparition du pic d'absorbance lui correspondant. Il est habituel de voir, au fil des mesures, un point isobestique dans le spectre d'absorbance. Il confirme la seule présence des deux espèces en jeu, soient l'espèce neutre et l'espèce oxydée ou réduite, suivant le phénomène étudié, et montre aussi leur inter-dépendance. Sans celui-ci, il est alors probable que la nouvelle espèce créée subisse soit une dégradation, par manque de stabilité, soit une réaction subséquente entre les différentes espèces présentes. Si plusieurs changements de couleur sont observables, il est aussi possible de déterminer quel changement est imputable à quel état d'oxydation.

Cette première analyse, en solution, permet ainsi d'observer si la molécule étudiée présente des changements de couleurs désirés, ainsi que les longueurs d'ondes impliquées et d'avoir une idée des potentiels requis pour observer ces changements.

Elle nécessite un montage particulier (Figure 0-15), permettant de coupler ces deux techniques d'analyse. Le montage électrochimique doit être inséré dans une cuvette spectroscopique. Comme prérequis, l'électrode de travail doit pouvoir laisser passer le

rayonnement lumineux. Il en existe différentes sortes. Ainsi, une électrode de platine en forme de grille peut être utilisée. Depuis plusieurs années, un autre type d'électrode a été adopté au laboratoire, de source commerciale.

Il s'agit d'une électrode « honeycomb », c'est-à-dire ayant une structure alvéolaire. Fabriquée en céramique, un revêtement métallique (or ou platine) permet d'y imprimer l'électrode de travail ainsi que l'électrode auxiliaire. L'électrode de travail est de plus composée de dix-neuf trous (disposés en forme alvéolaire), dont la surface interne est aussi revêtue du métal. La cuvette spectroscopique utilisée est elle aussi spécifique, son épaisseur au niveau des trous étant pratiquement réduite à l'épaisseur de l'électrode. Le chemin optique, très mince, traverse ainsi alors uniquement au niveau des trous, au niveau de l'espèce électrochimiquement générée. Cette disposition permet aussi de minimiser la diffusion des molécules au niveau de l'électrode de travail et assure que la réaction redox étudiée est complète dans la fenêtre d'analyse. L'électrode « honeycomb » et celle de référence sont finalement connectées au potentiostat.

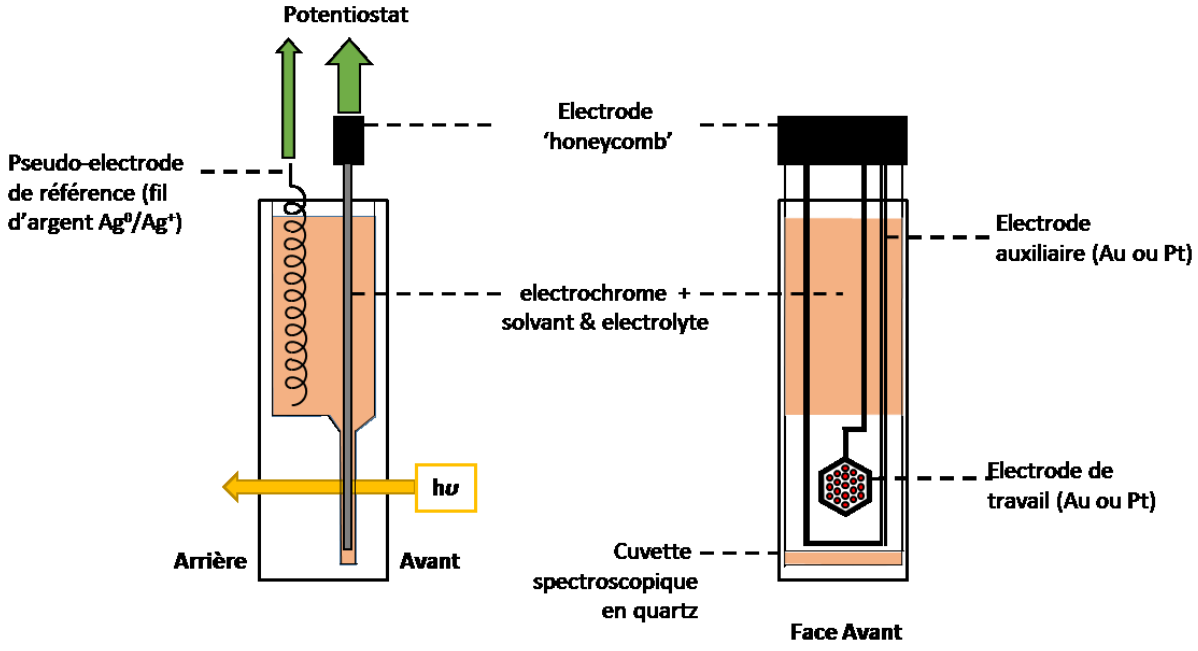

Figure 0-15 Schéma du montage spectro-électrochimique utilisé au laboratoire.

Une fois cette analyse préliminaire effectuée, si elle est concluante, il est possible de mesurer l'efficacité de coloration du composé, ainsi que de vérifier la stabilité de l'espèce électrochimiquement créée.

Pour cela, on utilise le même type de montage, en changeant l'expérience électrochimique. Il s'agit alors d'appliquer en alternance un potentiel oxydatif et réducteur, sur des périodes de temps prédéterminées, pour une durée totale pouvant être de plusieurs heures, et de regarder le changement en transmittance de la solution contenant le composé. Typiquement, on alterne le potentiel toutes les 30 secondes pour avoir suffisamment de variation de la transmittance sans sur-oxyder/réduire le composé. Une régularité dans la différence de transmittance observée indiquera que le composé réagit bien au stress imposé.

L'efficacité de coloration est donnée par :

$$\mathrm{EC} = \frac{\Delta \mathrm{OD}}{\Delta \mathrm{Q}} = \frac{\log\left(\frac{\mathrm{T_b}}{\mathrm{T_c}}\right)}{\Delta \mathrm{Q}} , \qquad \text{où } \Delta \mathrm{Q} = \frac{\mathrm{Q}}{\mathrm{A}} ,$$

avec ΔOD la différence de densité optique (absorbance) entre l'état initial et final, Q la charge coulomique échangée pendant cette transition (C), T_b et T_c les valeurs initiale et finale de transmission du milieu et A la surface de l'électrode (cm^2). Cela représente la « quantité de couleur » formée par la charge consommée. C'est une valeur caractéristique de l'électrochrome, seul ou dans un dispositif.

Chromaticité et colorimétrie

L'œil humain perçoit les couleurs grâce à trois types de récepteurs photosensibles, appelés cônes. Il en découle que toute couleur discernable par l'œil humain est caractérisée par un point dans un espace à trois dimensions. Ces valeurs « mesurées » par les trois types de cônes représentent essentiellement les intensités du rouge, du vert et du bleu, ce qui permet, en autre, de définir l'espace RVB à partir de ces trois couleurs primaires. La perception des couleurs étant propre à chacun, il est nécessaire de pouvoir décrire les couleurs de manière objective, afin d'être en mesure de reproduire une même couleur sans aucun doute. Différents espaces de couleur ont été développés à cette fin, depuis plus d'une centaine d'années, leur objectif étant de décrire une couleur de la façon la plus proche de la perception visuelle humaine. Ces espaces,

basés sur des modèles mathématiques ont été améliorés et modifiés avec le temps. La CIE (Commission Internationale de l'Eclairage) est en charge de définir et normaliser ces espaces. Le système colorimétrique CIE 1976 LUV est issu de l'amélioration de plusieurs autres espaces avant lui et tente de quantifier de façon plus uniforme la perception des différences des couleurs par la vision humaine. Il est spécifiquement utilisé pour la caractérisation des écrans et affichages. Il permet de représenter sur un diagramme de chromaticité les coordonnées de chaque couleur définies par cet espace (Figure 0-16). Ses trois coordonnées sont la clarté (L*), et les deux coordonnées chromatiques u' et v'. Elles peuvent être calculées, par ordinateur, à partir du spectre d'absorption d'un composé. En plus de caractériser une couleur de manière la plus objective possible, ce système permet, dans notre cas, de comparer entre eux différents composés présentant des couleurs similaires ou totalement opposées.

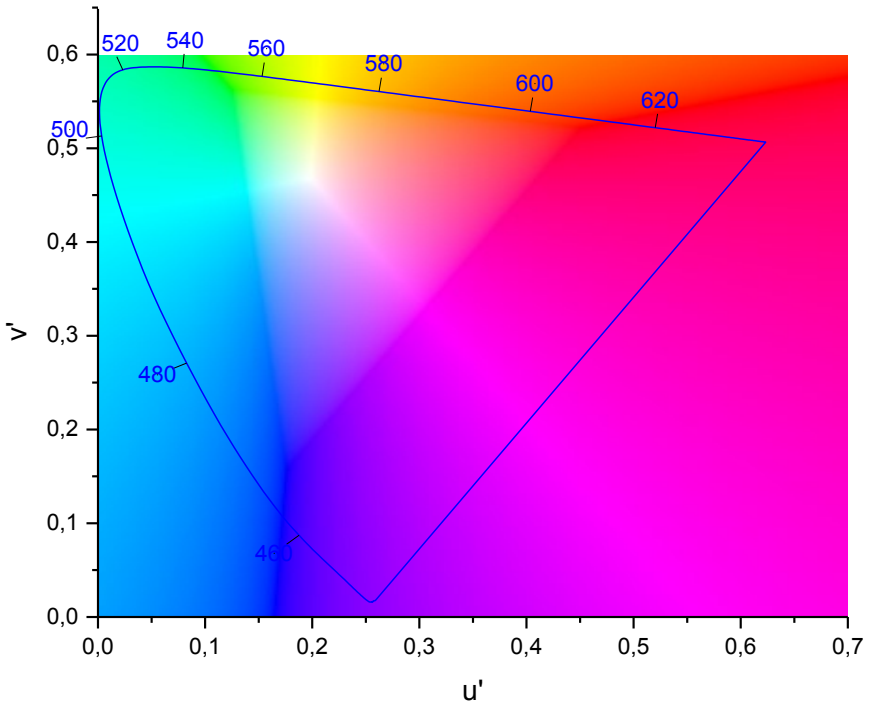

Figure 0-16 Diagramme de chromaticité LUV (CIE 1976 UCS).

Dispositifs électrochromiques

La réalisation d'un dispositif électrochromique est le but final, lors de l'étude de nouveaux composés électrochromes. Elle sert de preuve de concept. En effet, il est important de savoir si les composés en question ont une application potentielle. Pour cela on réalise des dispositifs simplifiés répliquant le fonctionnement des dispositifs existant dans l'industrie. L'idéal est un dispositif passif (ou dispositif à contre-électrode complémentaire),[70] c'est-à-dire avec deux composés électrochromes complémentaires d'un point de vue électrochimiques. Le concept est plus facile à imaginer avec des polymères, chacun immobilisé sur une des électrodes. L'un est oxydé à l'état au repos, l'autre réduit. Ainsi, lorsque le premier est réduit, le second est oxydé, et le gel électrolytique permet de balancer le nouvel équilibre de charges. De cette façon, les deux polymères se comportent comme un couple redox. Une condition évidente est qu'ils doivent présenter des transitions électrochromiques se complétant sous des conditions redox opposées, c.-à-d. avoir un état coloré lorsque l'autre est dans un état incolore. Cela nécessite aussi que les deux matériaux complémentaires soient suffisamment stables dans leur forme dopée, afin que l'application d'un potentiel électrique ne soit pas nécessaire en permanence. Au laboratoire, on réalise des dispositifs actifs. N'intégrant qu'un composé électrochrome, seulement sur une des électrodes, ils nécessitent un potentiel électrique extérieur permanent pour alterner entre leurs couleurs (Figure 0-17).

Les différentes composantes du dispositif se doivent d'être un maximum transparentes, afin que les changements de couleurs étudiés soient facilement observables mais aussi que celles-ci n'interfèrent pas avec le rayonnement lumineux nécessaire à l'absorbance du composé électrochrome. La structure générale d'un dispositif électrochrome est représentée sur la Figure 0-17. Il est d'usage d'utiliser des plaques d'oxyde d'indium et d'étain (ITO, pour *Indium Tin Oxide*, en anglais) comme électrodes. Elles sont constituées d'une plaque de verre sur laquelle se trouve une fine couche d'ITO, conductrice et transparente dans le domaine du visible (>360 nm). L'ITO de source commerciale est habituellement transmissif à plus de 80%. Elles peuvent servir d'anode et de cathode. Pour un composé dont on étudie l'oxydation, on le déposera sur la plaque d'ITO jouant le rôle d'anode. On ajoute ensuite une couche de gel électrolytique, composé d'une matrice liquide ou solide (polymère) et d'un électrolyte (sel ionique). Celui-ci permet le passage du courant ionique entre les deux électrodes. Il permet le déplacement des

ions pour contre-balancer les charges crées, préservant ainsi l'électro-neutralité du dispositif. Enfin la deuxième plaque d'ITO est ajoutée pour clore le dispositif. Pour assurer un bon contact entre le dispositif fabriqué et l'appareillage électrique sans abimer les couches d'ITO, on peut utiliser du ruban adhésif de cuivre, que l'on colle sur une partie des plaques d'ITO nues. Enfin, pour assurer la bonne étanchéité du dispositif et éviter des fuites de gel ou que les électrodes ne se séparent lors de l'utilisation, on peut sceller le tout avec de la colle époxy.

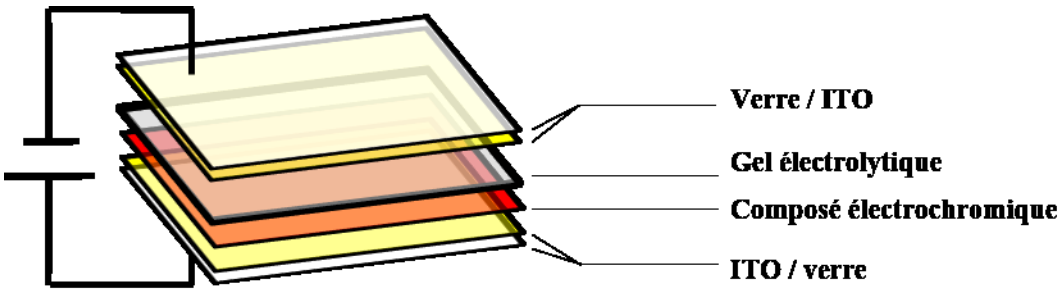

Figure 0-17 Représentation schématique simplifiée d'un dispositif électrochromique actif.

Le choix du gel électrolytique est d'importance. Plusieurs paramètres rentrent en compte. Ses composants doivent aussi être transmissifs, pour que les changements de couleur soient visibles, ou tout du moins minimalement impactés, et ne doivent donc idéalement pas absorber dans le domaine du visible, ou tout du moins interférer avec les longueurs d'onde des transitions des composés étudiés. Différents sels électrolytes sont disponibles, dont parmi les plus fréquents l'hexafuorophosphate de tétrabutylammonium ($TBAPF_6$) ou le perchlorate de lithium ($LiClO_4$). La taille des contre-ions du gel peut affecter leur migration dans celui-ci, De plus, la conductivité du gel dépend directement de leur mobilité, et de leur quantité dans celui-ci. Pour obtenir un simili-gel, il est d'usage d'utiliser un polymère, parfois solubilisé initialement avec l'électrolyte dans un solvant qu'on laisse s'évaporer, ou dans le carbonate de propylène, utilisé comme solvant et plastifiant. Utilisé comme matrice, il est en quantité excessive. Un des gels utilisés au laboratoire permet, par l'ajout d'un initiateur photochimique, de faire réticuler le polymère sous lumière UV, donnant une consistance beaucoup plus solide au gel. Dans certains cas, il peut nuire au dispositif en interagissant avec le composé électrochrome. Enfin, la stratégie de choix

du gel peut différer en fonction du type de molécules électrochromes étudiées. En effet, les petites molécules de faible masse molaire ont tendance à se solubiliser dans le gel, compromettant l'efficacité du dispositif. L'étude de polymères ou oligomères insolubles est souvent facilitée concernant ce dernier point.

Déposition et immobilisation sur substrat

Lorsque vient la nécessité de déposer un composé sur un substrat, plusieurs techniques sont possibles. Parmi elles, le *spray-coating* est relativement simple à éxécuter. Le composé est dissout dans un solvant volatil, puis pulvérisé sous pression. Le *spin-coating* est une méthode alternative. Le composé, toujours dissout dans un solvant plus ou moins volatil, est déposé sur le substrat, lui-même sur un support permettant de faire tourner l'ensemble à une vitesse choisie, ce qui a pour effet, par force centrifuge, d'étaler le système solvant-composé en une couche plus ou moins homogène. Dans ces deux techniques, l'évaporation postérieure du solvant permet d'obtenir une couche d'une épaisseur donnée du composé sur le substrat. Le *drop-casting*, une technique plus simpliste, consiste à déposer directement le soluté et le solvant sur le substrat puis de laisser s'évaporer le solvant. Chacune de ces techniques présentent des avantages et des inconvénients, en fonction des molécules étudiées. Le *drop-casting* ne permet aucun contrôle précis de l'épaisseur du film obtenu, et peut donner des films non homogènes. Le *spray-coating*, avec un matériel adapté, et après calibration, permet le contrôle de l'épaisseur et de l'homogénéité du film. Avec du matériel plus simpliste, du genre aérographe, cela donne des résultats non homogènes et peu reproductibles d'un échantillon à l'autre. Enfin, le *spin-coating* permet aussi, par calibration, de contrôler l'épaisseur du film et permet d'atteindre la reproductibilité. Il nécessite par contre le choix d'un solvant adapté à cette technique (solubilité, viscosité, volatilité,…)

Bibliographie

(1) Chiang, C. K.; Fincher, C. R.; Park, Y. W.; Heeger, A. J.; Shirakawa, H.; Louis, E. J.; Gau, S. C.; MacDiarmid, A. G., Electrical Conductivity in Doped Polyacetylene. *Phys. Rev. Lett.* **1977,** *39* (17), 1098-1101.

(2) Chiang, C. K.; Druy, M. A.; Gau, S. C.; Heeger, A. J.; Louis, E. J.; MacDiarmid, A. G.; Park, Y. W.; Shirakawa, H., Synthesis of highly conducting films of derivatives of polyacetylene, (CH)x. *J. Am. Chem. Soc.* **1978,** *100* (3), 1013-1015.

(3) Patil, A. O.; Heeger, A. J.; Wudl, F., Optical properties of conducting polymers. *Chem. Rev.* **1988,** *88* (1), 183-200.

(4) Rehahn, M., Elektrisch leitfähige Kunststoffe: Der Weg zu einer neuen Materialklasse. *Chem. unserer Zeit* **2003,** *37* (1), 18-30.

(5) Tsuneda, T.; Singh, R. K.; Chattaraj, P. K., Diagrams for comprehensive molecular orbital-based chemical reaction analyses: reactive orbital energy diagrams. *PCCP* **2018,** *20* (20), 14211-14222.

(6) Thompson, R. B.; Scarlata, S., Fluorescence Made Easier: Fluorescence Techniques for the Novice. Episode 1: The Basics. In *Reviews in Fluorescence 2016*, Geddes, C. D., Ed. Springer International Publishing: Cham, 2017; pp 1-8.

(7) Introduction to Fluorescence. In *Principles of Fluorescence Spectroscopy*, Lakowicz, J. R., Ed. Springer US: Boston, MA, 2006; pp 1-26.

(8) Ingram, G. L.; Lu, Z.-H., Design principles for highly efficient organic light-emitting diodes. *J. Photonics Energy* **2014,** *4*, 18.

(9) Markvart, T.; Castañer, L., Chapter IA-1 - Principles of Solar Cell Operation. In *Practical Handbook of Photovoltaics (Second Edition)*, McEvoy, A.; Markvart, T.; Castañer, L., Eds. Academic Press: Boston, 2012; pp 7-31.

(10) Mortimer, R. J.; Dyer, A. L.; Reynolds, J. R., Electrochromic organic and polymeric materials for display applications. *Displays* **2006,** *27* (1), 2-18.

(11) Bredas, J. L.; Street, G. B., Polarons, bipolarons, and solitons in conducting polymers. *Acc. Chem. Res.* **1985,** *18* (10), 309-315.

(12) Steinmüller, D.; Ramsey, M. G.; Netzer, F. P., Polaron and bipolaronlike states in n-doped bithiophene. *Phys. Rev. B* **1993,** *47* (20), 13323-13329.

(13) Deb, S. K., A Novel Electrophotographic System. *Appl. Opt.* **1969,** *8* (S1), 192-195.

(14) Mortimer, R. J., Organic electrochromic materials. *Electrochim. Acta* **1999,** *44* (18), 2971-2981.

(15) Heuer, H. W.; Wehrmann, R.; Kirchmeyer, S., Electrochromic Window Based on Conducting Poly(3,4-ethylenedioxythiophene)–Poly(styrene sulfonate). *Adv. Funct. Mater.* **2002,** *12* (2), 89-94.

(16) Walczak, R. M.; Reynolds, J. R., Poly(3,4-alkylenedioxypyrroles): The PXDOPs as Versatile Yet Underutilized Electroactive and Conducting Polymers. *Adv. Mater.* **2006,** *18* (9), 1121-1131.

(17) Mortimer, R. J., Electrochromic materials. *Chem. Soc. Rev.* **1997,** *26* (3), 147-156.

(18) Günes, S.; Neugebauer, H.; Sariciftci, N. S., Conjugated Polymer-Based Organic Solar Cells. *Chem. Rev.* **2007,** *107* (4), 1324-1338.

(19) Berggren, M.; Nilsson, D.; Robinson, N. D., Organic materials for printed electronics. *Nat. Mater.* **2007,** *6*, 3.

(20) Sbar, N. L.; Podbelski, L.; Yang, H. M.; Pease, B., Electrochromic dynamic windows for office buildings. *Int. J. Sustainable Built Environ.* **2012,** *1* (1), 125-139.

(21) Bach, U.; Corr, D.; Lupo, D.; Pichot, F.; Ryan, M., Nanomaterials-Based Electrochromics for Paper-Quality Displays. *Adv. Mater.* **2002,** *14* (11), 845-848.

(22) Rosseinsky, D. R.; Mortimer, R. J., Electrochromic Systems and the Prospects for Devices. *Adv. Mater.* **2001,** *13* (11), 783-793.

(23) Gillaspie, D. T.; Tenent, R. C.; Dillon, A. C., Metal-oxide films for electrochromic applications: present technology and future directions. *J. Mater. Chem.* **2010,** *20* (43), 9585-9592.

(24) Lampert, C. M., Chromogenic smart materials. *Mater. Today* **2004,** *7* (3), 28-35.

(25) Donovan, S. M.; Hartford, S. D.; Kvernmo, M. L.; Owings, A. A.; Wilkins, B. W. Article of footwear with color change portion and method of changing color. US 20130033378, 2013.

(26) Martin, P. J.; Di Pasquale, M. Flexible electrochromic devices US 6456418, 2002.

(27) Kline, W. M.; Lorenzini, R. G.; Sotzing, G. A., A review of organic electrochromic fabric devices. *Color. Technol.* **2014,** *130* (2), 73-80.

(28) Roncali, J., Conjugated poly(thiophenes): synthesis, functionalization, and applications. *Chem. Rev.* **1992,** *92* (4), 711-738.

(29) He, X.; Baumgartner, T., Conjugated main-group polymers for optoelectronics. *RSC Adv.* **2013,** *3* (29), 11334-11350.

(30) Feast, W. J.; Tsibouklis, J.; Pouwer, K. L.; Groenendaal, L.; Meijer, E. W., Synthesis, processing and material properties of conjugated polymers. *Polymer* **1996,** *37* (22), 5017-5047.

(31) Beaujuge, P. M.; Amb, C. M.; Reynolds, J. R., Spectral Engineering in π-Conjugated Polymers with Intramolecular Donor−Acceptor Interactions. *Acc. Chem. Res.* **2010,** *43* (11), 1396-1407.

(32) Guo, X.; Baumgarten, M.; Müllen, K., Designing π-conjugated polymers for organic electronics. *Prog. Polym. Sci.* **2013,** *38* (12), 1832-1908.

(33) Meier, H., Conjugated Oligomers with Terminal Donor–Acceptor Substitution. *Angew. Chem. Int. Ed.* **2005,** *44* (17), 2482-2506.

(34) Perepichka, I. F.; Perepichka, D. F.; Meng, H.; Wudl, F., Light-Emitting Polythiophenes. *Adv. Mater.* **2005,** *17* (19), 2281-2305.

(35) Kim, J.; You, J.; Kim, B.; Park, T.; Kim, E., 1) Solution Processable and Patternable Poly(3,4-alkylenedioxythiophene)s for Large-Area Electrochromic Films. *Adv. Mater.* **2011,** *23* (36), 4168-4173.

(36) Cravino, A.; Roquet, S.; Alévêque, O.; Leriche, P.; Frère, P.; Roncali, J., Triphenylamine−Oligothiophene Conjugated Systems as Organic Semiconductors for Opto-Electronics. *Chem. Mater.* **2006,** *18* (10), 2584-2590.

(37) Kraft, A.; Grimsdale, A. C.; Holmes, A. B., Electroluminescent Conjugated Polymers—Seeing Polymers in a New Light. *Angew. Chem. Int. Ed.* **1998,** *37* (4), 402-428.

(38) Leclerc, M., Polyfluorenes: Twenty years of progress. *J. Polym. Sci., Part A: Polym. Chem.* **2001,** *39* (17), 2867-2873.

(39) Lavastre, O.; Illitchev, I.; Jegou, G.; Dixneuf, P. H., Discovery of New Fluorescent Materials from Fast Synthesis and Screening of Conjugated Polymers. *J. Am. Chem. Soc.* **2002,** *124* (19), 5278-5279.

(40) Yang, C. J.; Jenekhe, S. A., Conjugated aromatic poly(azomethines). 1. Characterization of structure, electronic spectra, and processing of thin films from soluble complexes. *Chem. Mater.* **1991,** *3* (5), 878-887.

(41) Wang, C.; Shieh, S.; LeGoff, E.; Kanatzidis, M. G., Synthesis and Characterization of A New Conjugated Aromatic Poly(azomethine) Derivative Based on the 3‘,4‘-Dibutyl-α-Terthiophene Building Block. *Macromolecules* **1996,** *29* (9), 3147-3156.

(42) Thomas, O.; Inganäs, O.; Andersson, M. R., Synthesis and Properties of a Soluble Conjugated Poly(azomethine) with High Molecular Weight. *Macromolecules* **1998,** *31* (8), 2676-2678.

(43) Ng, S. C.; Chan, H. S. O.; Wong, P. M. L.; Tan, K. L.; Tan, B. T. G., Novel heteroarylene polyazomethines: their syntheses and characterizations. *Polymer* **1998,** *39* (20), 4963-4968.

(44) Yang, C.-J.; Jenekhe, S. A., Conjugated Aromatic Polyimines. 2. Synthesis, Structure, and Properties of New Aromatic Polyazomethines. *Macromolecules* **1995,** *28* (4), 1180-1196.

(45) Harlmann, H.; Mayer, R., Aminothiophene aus N,N-disubstituierten Thioamiden. *Zeitschrift für Chemie* **1966,** *6* (1), 28-28.

(46) Gewald, K.; Kleinert, M.; Thiele, B.; Hentschel, M., Zur basenkatalysierten Reaktion von methylenaktiven Nitrilen mit Schwefel. *J. Prakt. Chem.* **1972,** *314* (2), 303-314.

(47) Gewald, K., Methods for the synthesis of 2-aminothiophenes and their reactions (review). *Chem. Heterocycl. Compd.* **1976,** *12* (10), 1077-1090.

(48) Bourgeaux, M.; Guarìn, S. A. P.; Skene, W. G., Photophysical, crystallographic, and electrochemical characterization of novel conjugated thiopheno azomethines. *J. Mater. Chem.* **2007,** *17* (10), 972-979.

(49) Bourgeaux, M.; Skene, W. G., A Highly Conjugated p- and n-Type Polythiophenoazomethine: Synthesis, Spectroscopic, and Electrochemical Investigation. *Macromolecules* **2007,** *40* (6), 1792-1795.

(50) Bourgeaux, M.; Skene, W. G., Photophysics and Electrochemistry of Conjugated Oligothiophenes Prepared by Using Azomethine Connections. *J. Org. Chem.* **2007,** *72* (23), 8882-8892.

(51) Dufresne, S.; Bourgeaux, M.; Skene, W. G., Tunable spectroscopic and electrochemical properties of conjugated push–push, push–pull and pull–pull thiopheno azomethines. *J. Mater. Chem.* **2007,** *17* (12), 1166-1177.

(52) Bolduc, A.; Dufresne, S.; Skene, W. G., Chemical doping of EDOT azomethine derivatives: insight into the oxidative and hydrolytic stability. *J. Mater. Chem.* **2012,** *22* (11), 5053-5064.

(53) Bolduc, A.; Dufresne, S.; Skene, W. G., EDOT-containing azomethine: an easily prepared electrochromically active material with tuneable colours. *J. Mater. Chem.* **2010,** *20* (23), 4820-4826.

(54) Bolduc, A.; Rivier, L.; Dufresne, S.; Skene, W. G., Spectral investigation of conjugated azomethines: A large palette of colors possible with acid and oxidant doping. *Mater. Chem. Phys.* **2012,** *132* (2), 722-728.

(55) Dufresne, S.; Bolduc, A.; Skene, W. G., Towards materials with reversible oxidation and tuneable colours using heterocyclic conjugated azomethines. *J. Mater. Chem.* **2010,** *20* (23), 4861-4866.

(56) Dufresne, S.; Perez Guarin, S. A.; Bolduc, A.; Bourque, A. N.; Skene, W. G., Conjugated fluorene-thiophenes prepared from azomethine connections Part I. The effect of electronic and aryl groups on the spectroscopic and electrochemical properties. *Photochem. Photobiol. Sci.* **2009,** *8* (6), 796-804.

(57) Bolduc, A.; Barik, S.; Lenze, M. R.; Meerholz, K.; Skene, W. G., Polythiophenoazomethines - alternate photoactive materials for organic photovoltaics. *J. Mater. Chem. A* **2014,** *2* (37), 15620-15626.

(58) Bolduc, A.; Skene, W. G., Direct preparation of electroactive polymers on electrodes and their use in electrochromic devices. *Polym. Chem.* **2014,** *5* (4), 1119-1123.

(59) Mulholland, M. E.; Navarathne, D.; Khedri, S.; Skene, W. G., Towards multichromatic electrochromes from ambipolar conjugated azomethines. *New J. Chem.* **2014,** *38* (4), 1668-1674.

(60) Tremblay, M.-H.; Gellé, A.; Skene, W. G., Ambipolar azomethines as potential cathodic color switching materials. *New J. Chem.* **2017,** *41* (6), 2287-2295.

(61) Sicard, L.; Navarathne, D.; Skalski, T.; Skene, W. G., On-Substrate Preparation of an Electroactive Conjugated Polyazomethine from Solution-Processable Monomers and its Application in Electrochromic Devices. *Adv. Funct. Mater.* **2013,** *23* (28), 3549-3559.

(62) Tremblay, M.-H.; Skalski, T.; Gautier, Y.; Pianezzola, G.; Skene, W. G., Investigation of Triphenylamine–Thiophene–Azomethine Derivatives: Toward Understanding Their Electrochromic Behavior. *J. Phys. Chem. C* **2016,** *120* (17), 9081-9087.

(63) Seo, E. T.; Nelson, R. F.; Fritsch, J. M.; Marcoux, L. S.; Leedy, D. W.; Adams, R. N., Anodic Oxidation Pathways of Aromatic Amines. Electrochemical and Electron Paramagnetic Resonance Studies. *J. Am. Chem. Soc.* **1966,** *88* (15), 3498-3503.

(64) Ge, Z.; Hayakawa, T.; Ando, S.; Ueda, M.; Akiike, T.; Miyamoto, H.; Kajita, T.; Kakimoto, M.-a., Novel Bipolar Bathophenanthroline Containing Hosts for Highly Efficient Phosphorescent OLEDs. *Org. Lett.* **2008,** *10* (3), 421-424.

(65) Tao, Y.; Wang, Q.; Ao, L.; Zhong, C.; Yang, C.; Qin, J.; Ma, D., Highly Efficient Phosphorescent Organic Light-Emitting Diodes Hosted by 1,2,4-Triazole-Cored Triphenylamine Derivatives: Relationship between Structure and Optoelectronic Properties. *J. Phys. Chem. C* **2010,** *114* (1), 601-609.

(66) Roncali, J., Molecular Bulk Heterojunctions: An Emerging Approach to Organic Solar Cells. *Acc. Chem. Res.* **2009,** *42* (11), 1719-1730.

(67) Wu, G.; Zhao, G.; He, C.; Zhang, J.; He, Q.; Chen, X.; Li, Y., Synthesis and photovoltaic properties of a star-shaped molecule with triphenylamine as core and benzo[1,2,5]thiadiazol vinylene as arms. *Sol. Energy Mater. Sol. Cells* **2009,** *93* (1), 108-113.

(68) Yen, H.-J.; Guo, S.-M.; Liou, G.-S., Synthesis and unexpected electrochemical behavior of the triphenylamine-based aramids with ortho- and para-trimethyl-protective substituents. *J. Polym. Sci., Part A: Polym. Chem.* **2010,** *48* (23), 5271-5281.

(69) Beaupré, S.; Dumas, J.; Leclerc, M., Toward the Development of New Textile/Plastic Electrochromic Cells Using Triphenylamine-Based Copolymers. *Chem. Mater.* **2006,** *18* (17), 4011-4018.

(70) Gazotti Jr., W. A.; Casalbore-Miceli, G.; Geri, A.; de Paoli, M.-A., A Solid-State Electrochromic Device Based on Two Optically Complementary Conducting Polymers. *Adv. Mater.* **1998,** *10* (1), 60-64.

Chapitre 1

Résumé

Ce chapitre présente de façon détaillée la synthèse des différentes molécules étudiées dans ce mémoire ainsi que les analyses structurales par RMN et spectrométrie de masse. Il met en perspective le choix des molécules étudiées ainsi que la stratégie de synthèse retenue pour y parvenir. Une résolution de structure cristallographique d'un des oligomères obtenus est aussi incluse, afin de confirmer la structure attendue et de donner plus de détails sur la configuration interne de la molécule au sein du mono-cristal.

S'en suit une analyse de l'effet des différents substituants sur les propriétés électrochimiques des composés obtenus, tels que les potentiels d'oxydation et de réduction, ainsi que sur la réversibilité potentielle de ces processus. L'étude de leurs propriétés spectro-électrochimiques permet d'assigner les contributions électroniques des différents groupements, ainsi que de confirmer leur intérêt comme matériaux électrochromes. Cela est facilité par des calculs théoriques de DFT, permettant de spéculer sur les configurations électroniques engendrées par les processus d'oxydo-réduction.

Ma contribution à ces travaux a été la synthèse, la purification et la caractérisation structurale des différents composés présentés, leur caractérisation électrochimique et spectro-électrochimique, ainsi que l'obtention des mono-cristaux appropriés à la diffraction des rayons X, et, en partie, leur montage sur le diffractomètre et la résolution de la structure à partir des données obtenues.

Extending the duty cycle of azomethine electrochromes by structural modification

Yohan Gautier and W. G. Skene*

Département de Chimie, Université de Montréal

CP 6128, Centre-ville Montreal, QC, H3C 3J7, Canada

w. skene@umontreal.ca

Submitted to *Journal of Materials Chemistry C*

Received June 21th 2019 (correction process)

Abstract

Towards understanding the structural requirements for extended anodic duty cycle, a series of conjugated azomethine triads end-capped with amides were prepared. The effect of a phenyl and two triphenylamine end-capping groups on the oxidation potential, electrochemical reversibility, and color were assessed. The core aromatic of the conjugated framework was also varied to include thiophene, EDOT, and two triphenylamines derivatives. With the amide end group, the anodic potential increased by 270 mV relative to the amine termini counterpart. An irreversible anodic process was observed with the unsubstituted triphenylamine end group, resulting in an electroactive film deposited on the working electrode. In contrast, desired reversible oxidation was possible with an 4,4′-dimethyltriphenylamine end-capping group. The anodically induced reversible perceived color change was from orange to violet when the central aromatic was a triphenylamine. The absorption of the oxidized intermediate was contingent on the capping-group and the central aromatic and it was upwards of 220 nm red-shifted from the neutral state. Similar spectral shifts were found with the EDOT and thiophene cores. In these cases, the red color of the intrinsic chromophore bleached upon oxidation and it was replaced with a blue color with a broad absorption at ca. 650 nm. Extended duty cycles consisting of constant difference in transmittance with repeated oxidation/neutralization cycles were possible upwards of 6 hours when end-capping with the 4,4′-dimethyltriphenylamine, regardless of the aromatic core.

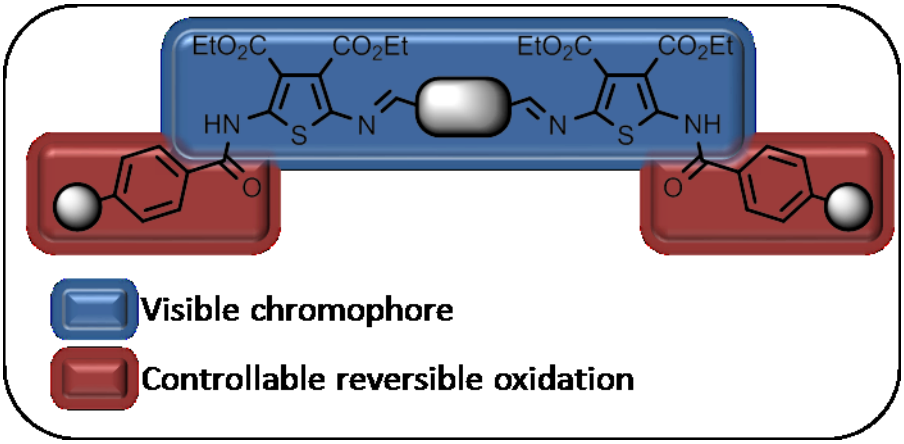

Introduction

Azomethines have found many uses as protecting groups[1] in organic synthesis and as dynamic materials.[2-4] They have also been exploited for a wide range of practical applications, including sensors,[5] probes,[6] magnetic storage materials,[7] and functional organic materials in plastic devices.[8-10] An interesting property of azomethines is their visible color. The absorption of these conjugated materials can be tailored depending on the aryl amines and aldehydes used for their preparation.[11,12] The oxidation potential and the electrochemical reversibility of azomethines can also be modulated contingent on structure. The collective visible colors and electrochemical properties make azomethines suitable for use in electrochromics,[13,14] being the reversible color changes with applied potential.[15-17] Azomethines are also interesting from an environmental perspective given their preparation produces an equivalent amount of benign water and they can be prepared from innocuous solvents.

Despite the synthetic and environmental advantages of azomethines, their properties lag behind those of their all-carbon counterparts. In fact, their color consistency with repeated electrochemical switching remains elusive. Overcoming this limitation would make azomethines truly suitable as electroactive layers for use in electrochromic devices. Ultimately, the ecological synthesis of electrochromic azomethines would contribute to reducing the environmental footprint of electrochromic devices. Understanding the underlying principles that impact the reversible electrochemical behavior and color would be beneficial for designing and preparing azomethines that have enhanced electrochromic properties. Such knowledge can be derived from structure-property studies.

In light of the known electrochromic properties of azomethine triads such a **4** (Chart 1-1),[18] including tunable absorption and moderate oxidation potentials, this framework was investigated. This was to investigate the effect of structural modification on both the electrochemical performance and the color consistency with repeated redox cycles, towards achieving truly electrochromic functional materials. The terminal amines are ideal sites for modifying the azomethine without disrupting the conjugation of the core that is otherwise responsible for the material's color in the visible region. Modifying the terminal group for adjusting the properties of heterocyclic azomethines is relatively underexplored. Within this context, the amines were converted to amides to assess the impact of this structural modification

on a key property that is required for electrochromic use: reversible color switching over multiple electrochemical oxidation/neutralization cycles. Amides were chosen because they resist both the imination reactions used to prepare the conjugated azomethines and repeated electrochemical oxidation at potentials required to induce visible color changes. The added benefit of the amide is that it electronically isolates the end group from the conjugated core. Therefore, various end groups can be used without affecting the color and the redox potentials of the electrochromic azomethine core.

Triphenylamines are of particular interest for use as end groups. This is owing to their reversible oxidation and visible color switching that are ideally suited for use in electrochromics.[19,20] In fact, their amide derivatives have been extensively employed as the color switching materials for electrochromic applications.[21-31] Incorporating triphenylamines as end groups into conjugated azomethines should enhance the duty cycle of the electrochromic materials. The colored materials should therefore be capable of reversible color changes when switching between their neutral and oxidized states in addition to sustaining this performance over extended periods of time. Towards understanding the structural requirements for such extended duty cycle,[32] conjugated azomethine triads were end-capped with phenyl and triphenylamines amides (Chart 1-1). Different aromatics, including thiophene, EDOT and triphenylamine were incorporated into the core to evaluate their impact on the color of the neutral and oxidized states when end-capped with the different amides. The structural dependency of the electrochromic properties, notably the reversible oxidation and color stability with extended electrochemical switching are herein presented towards achieving the overarching goal of enhancing the azomethine electrochemical stability for their ultimate use as active layers in electrochromics.

Results and Discussion

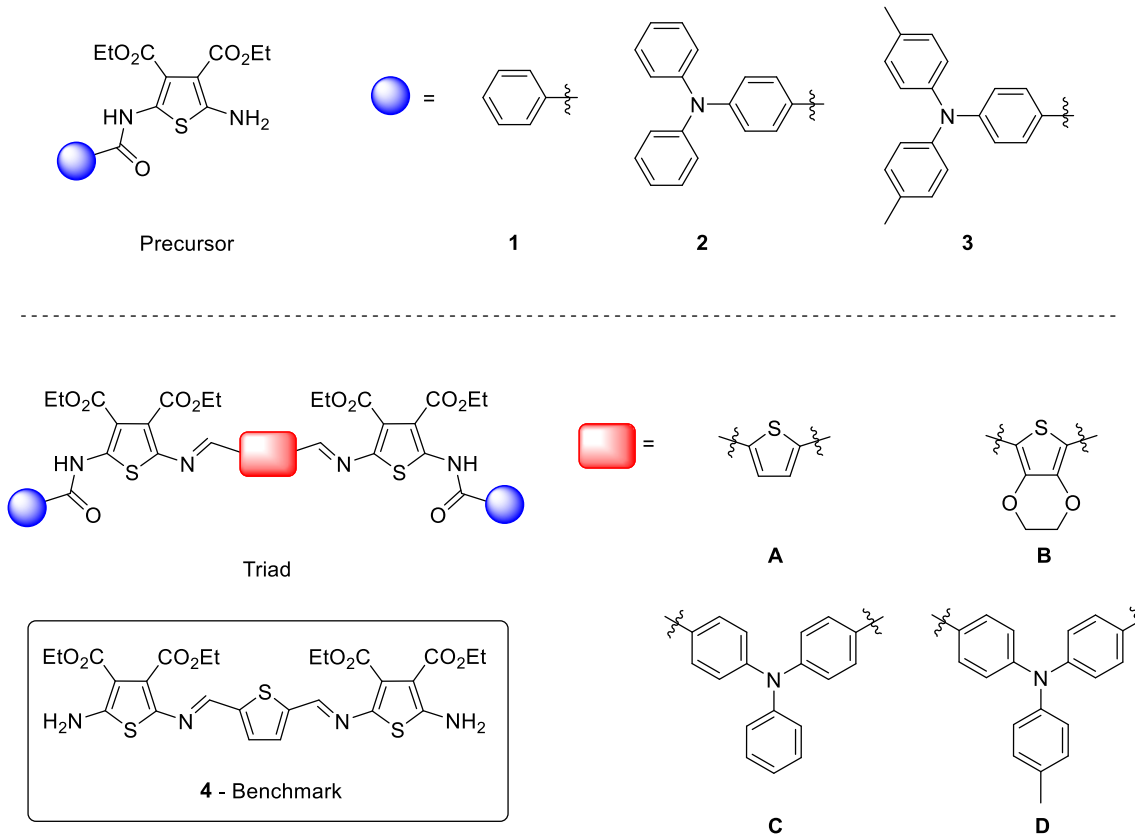

Chart 1-1 Amido-azomethine precursors and the triads prepared for electrochemical and spectroelectrochemical evaluation and their previously reported amine end-terminated counterpart (**4**).

While a divergent approach starting from the diamino triad core of **4** would be ideal for rapidly generating a library of compounds to assess the impact of substitution on the electrochemical and spectroscopic properties, a convergent route was adopted. This was to avoid any unwanted hydrolysis of the azomethine bond that could potentially occur at any step during the preparation and purification. This route was further selected so that the dyads could be characterized to confirm their identity during each step of the preparation of the targeted azomethines in Chart 1-1 . This is of interest given the challenge of accurately identifying the final products, especially the isomer of the heteroatomic bond by ^{1}H-NMR spectroscopy. A benefit of isolating the triad precursors (**1-3**) is their electrochemistry and absorption can be evaluated for benchmarking the properties of the corresponding triads (**A-D**).

Crystals of **1D** that were suitable for X-ray crystallography were obtained by the slow evaporation of chloroform. The X-ray ray structure was used to unambiguously confirm the identity of the compound along with the configuration of the conjugated heteroatomic bond. The resolved structure is represented in the ORETEP diagram in Figure 1-1, where the *E* configuration of the azomethine bonds is apparent. The double bond character of the azomethine is confirmed by its short bond length of 1.275(2) Å. The N2-C11 bond is 0.09 Å shorter than the N3-C16 bond, which is a single bond having a length of 1.365(2) Å. An interesting feature of the resolved compound is the coplanarity of the phenyl of the triphenylamine that is bonded to the amide and the thiophene. In fact, the planes described by these two aromatics are twisted by only 1.09(8)°. In contrast, the plane of the terminal phenyl is twisted by 20.83(10)°. This configuration leads to an electronic *push-pull* arm that is conjugated with the electron donating central amine and the collective electron withdrawn effect of the azomethine bond and the terminal amide. The two phenyl-thiophene-phenyl arms are electronically isolated from each other as a result of a "Y" configuration that can be seen in Figure 1-2. The torsion angle between the planes of the two arms is 64.22(4)°. The overall structure is consistent with its azomethine counterpart prepared azomethine from 2-amino-3-carbonitrile.[33]

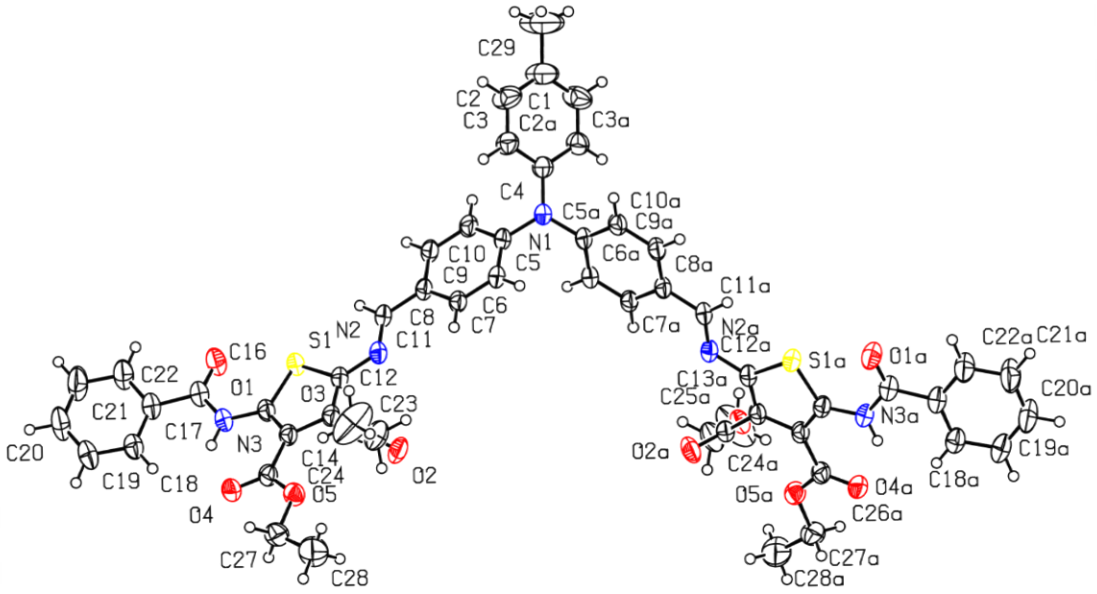

Figure 1-1 A) The atom-numbering diagram of **1D**. C, N, O and S atoms are drawn as displacement ellipsoids having a 50% probability. The hydrogens atoms are shown as spheres having an arbitrary radius. The cocrystallized chloroform solvent molecule was removed for clarity.

2-Amino,3-ester thiophene derivatives are known to form an intramolecular hydrogen bond between the carbonyl acceptor and either the primary or the secondary amine donor.[34-37] In fact, the nitrogens of the amine and amide of **3** formed both intra- and intermolecular bonds, resulting in a head-to-head supramolecular dimer.[38] **1D** also formed hydrogen bonds (Figure 1-2 and Table 1-1). In this case, a hydrogen bond takes place between the N3 donor and the O4 acceptor. An intermolecular hydrogen bond was also found between the carbonyl acceptor and the weak CH donor in the *ortho* position of the central phenyl (C3···O4). The collective intermolecular effects result in an organized packing as per Figure 1-2A.

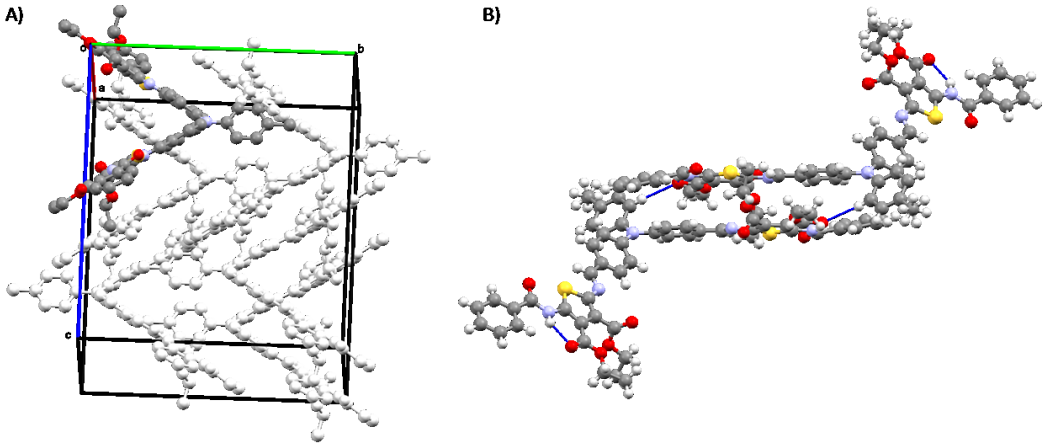

Figure 1-2 A) Packing of **1D** in the crystallographic unit cell shown along the *a*-axis. The main molecule is colored while the others are faded to highlight the adopted "Y"-like configuration. The hydrogens are removed for clarity. B) The intra- and intermolecular hydrogen bonds that are formed by **1D** in the solid state are drawn as blue lines.

Table 1-1 Inter- and intramolecular supramolecular bonding of **1D** in the crystal state.

D-H···*A*	*D*-H	H···*A*	*D*···*A*	*D*-H···*A*
N3-H3···O4	0.88	2.03	2.691 (2)	131.0
C3-H3A···O4^{i}	0.95	2.54	3.441 (2)	158.9

Symmetry codes: (i) $-x+½, y-½, -z+3/2$.The electrochemical properties, notably the redox potentials and the anodic reversibility of the targeted compounds were of particular interest. To

better understand the effect of structure on both the electrochemical reversibility and the oxidation potentials, the redox properties of the dyads were used as a benchmark. **1** was an ideal model for assessing the electrochemical properties. The electron donating effect of its amine should contribute to lowering the oxidation potential. This effect in turn would be offset by the intrinsic electron withdrawing effect of the amide. The oxidation potential was nonetheless expected to occur within the operating window of dichloromethane, the solvent used for the electrochemical measurements. The amide should also disrupt the degree conjugation between the colored core and the terminus. The three amides were found to undergo two oxidation processes. The first process was nearly irreversible, while the second was pseudo-reversible. These behaviors are based on the asymmetric peak current for the forward and reverse anodic scans. As per Table 1-2, the first oxidation process (E_{ox}^{1}) of **2** and **3** is less positive than the benchmark **1**. This was expected owing to the electron donating property of the triarylamine. The E_{ox}^{1} of **3** was 10 mV less positive than **2** because of the weak donating effect of the methyl groups. The irreversible behavior of **3** was surprising as the 4,4′-dimethylsubstitution of the triphenylamine is understood to promote reversibility of the radical cation by limiting its homo coupling. Its unexpected irreversible behavior suggests that the intermediate formed from the first oxidation is located on the thiophene. This aside, both multiple anodic cycling and chronoamperometry of **2** deposited an electroactive film on the working electrode. This is consistent with the behavior of its reported azomethine counterpart.[39] Adsorption of the electrochemically produced product was confirmed by the overlapping forward and reverse waves in the anodic cyclic voltammogram (Figure 1-3). Moreover, the immobilized product consisted of two reversible oxidation processes. The processes were nearly overlapping when measured at 100 mV/sec. Given that no product was deposited under similar conditions with the methylated derivative **3**, the product of **2** is assumed to proceed by radical cation cross-coupling involving the triphenylamine. It is worthy to note that no electrochemical reduction was observed for the triad precursors within the cathodic working limit of the solvent.

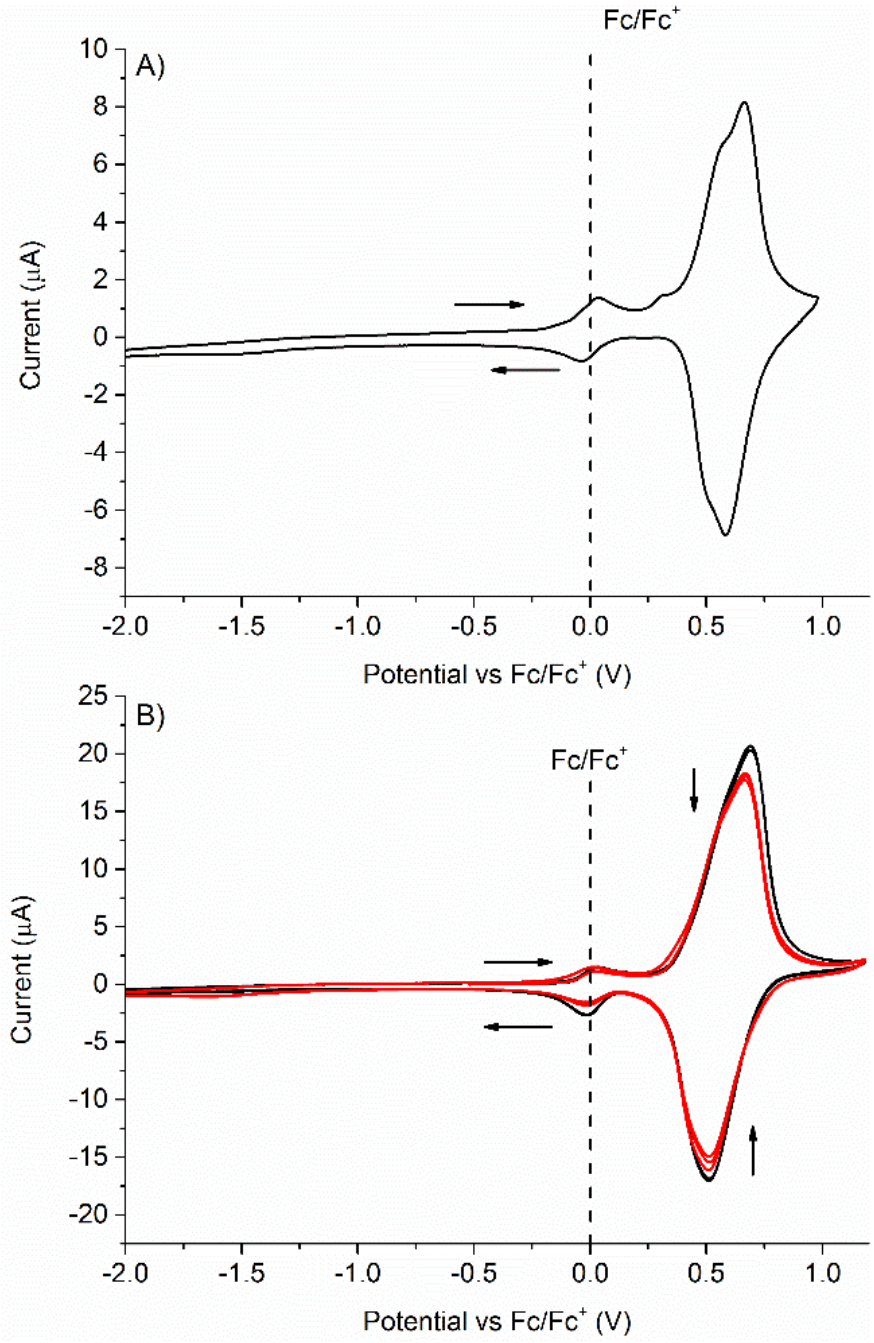

Figure 1-3 A) Cyclic voltammogram of the electropolymerized film of **2** on the Pt working electrode measured in 0.1 M $TBAPF_6$ in dichloromethane at 100 mV/s with 10^{-3} M ferrocene. The reversible redox couple of ferrocene is shown as the dotted line. B) Cyclic voltammogram of the anodically prepared film of **2A** adsorbed on the Pt working electrode with ferrocene as the internal reference, measured in 0.1 M $TBAPF_6$ in dichloromethane at 100 mV/s initially (■) and after immersing the electrode in a mixture of TFA/THF/HCl (●) overnight.

Table 1-2 Electrochemical and spectroelectrochemical properties of the precursors and triad azomethines.

	Compound	Abs (nm)[a]	Abs^{ox} (nm)[b]	Abs^{red} (nm)[c]	E_{ox} (mV)[d]	E_{red} (mV)[d]
Precursors	**1**	-[e]	-[e]	-[e]	520, 880	-[e]
	2	375	-[h]	-[i]	460, 720, 865	-[i]
	3	377	710	-[i]	450, 625, 745	-[i]
Triads	**1A**[f]	480	425	620	795	-1640
	2A[g]	490	-[h]	-[h]	1220, 1430	-1200
	3A	490	708	581	695, 975, 1140	-1695, -1835
	3B	508	645, 709	598	690	-2035
	1C	458	553, 680	486, 510	665, 925, 1175	-2085
	1D	470	560	517	530, 840, 1035, 1130	-2205
	2D[f]	455	-[h]	-[h]	1070, 1315	-1 700
	3D	455	556, 705-710	-[i]	520,[k] 6701 260	-[i]

[a] Absorbance maximum measured in dichloromethane. [b] Maximum absorbance observed with applied anodic potential equal to the E_{ox} measured by cyclic voltammetry. [c] Maximum absorbance observed with applied cathodic potential equal to the E_{red} measured by cyclic voltammetry. [d] Maximum electrochemical peak (ox=anodic forward scan; red=cathodic forward scan) measured in 0.1 M $TBAPF_6$ in degassed and anhydrous dichloromethane. Values vs. Fc/Fc^+. [e] Not determined. [f] Literature values.[40] [g] Potentials vs. Ag^o. [h] Electrodeposited on working electrode. [i] No observed reduction within the working window of the solvent. [k] Overlapping peak.

The first oxidation potential of the triads was more positive than their corresponding triad precusor. The increased E_{ox} is as result of the electron-withdrawing character of the two terminal amides and the two azomethines. The collective effect of the electron withdrawn groups

offsets the stabilization gained from the conjugated core, consisting of three aromatics and two azomethines. The triad oxidation potential was contingent on both the end group and the central aromatics (Figure 1-4). Of interest is the reversible electrochemical oxidation of **3A**, **3B**, and **3C**. In contrast, the oxidation process of the phenylamides (**1A**, **1C**, **1D**) was not reversible. This behavior was assigned by the peak current of the reverse anodic wave being less intense than the peak current for the forward wave. The non-reversible behavior is consistent with what was previously reported for **1A**.[40] An irreversible behavior was also observed for **2A**. In fact, similar to its precursor counterpart, the anodic cycling between the oxidized and neutral states of **2A** resulted in the immobilization of an electroactive film on the working electrode (Figures Figure S1-26-Figure S1-28). Electropolymerization was also observed for azomethine triads of reduced degrees of conjugation.[39] The electroactive film illustrates the tolerance of azomethines towards anodic polymerization. The anodic behavior of the resulting adsorbed layer was reversible. Immersing the film in aqueous THF with catalytic amounts of trifluoroacetic acid did not alter the cyclic voltammogram (Figure 1-3). Such conditions would otherwise hydrolyze the azomethine bond and should shift the oxidation potential to more positive potentials owing to a decrease in degree of conjugation. The absence of electrochemical change under known hydrolysis conditions illustrates the robustness of the immobilized layer and its resistance to hydrolysis.

The first oxidation process of the other triads was mostly reversible and it corresponded to a one-electron transfer process. This was assessed according to the similar peak current intensities of the equimolar internal reference of ferrocene and the given azomethine (Figures Figure S1-11, Figure S1-20, Figure S1-29, and Figure S1-38). It should be noted that this is only an approximation, as exact ferrocene/triad stoichiometry could not be achieved owing to the small amounts used for electrochemical analyses. Nonetheless, the oxidation process of the triads was ca. 270 mV was more positive than their diamine end-capped counterpart **4** as a result of the electron withdrawn effect of the amide end-groups. Moreover, the similar oxidation potential of **1C** with its 2-imino-3-nitrile derivative illustrates that the oxidation potential is modulated by the terminal azomethine and its electronic groups.[18,33] The reversible behavior was contingent on the structure of the triads and not from a decrease in the robustness of the azomethine bond towards electrochemical oxidation. Among the azomethines studied, **3B** was

the only compound that exhibited a unique anodic process. In contrast, the other compounds underwent either 2 or 3 oxidations (Table 1-2 and Figure 1-4). Squarewave (Figure S1-30) and differential pulse (Figure S1-31) voltammetry provided evidence for only one electrochemical processes of **3B** within the limit of the solvent used for the measurements. The unique electrochemical oxidation was assigned to a one-electron process.

The effect of structure on the oxidation potential can further be assessed by comparing the anodic voltammograms of the various azomethines. For example, the triphenylamine oxidized at 520 mV when it was part of conjugated core. Its oxidation potential increased by 150 mV when the arylamine was the end-capping group. The oxidation potential of the triads **3A**, **3B**, and **3D** were approximately the same. This suggests that the central aromatic does not significantly impact the oxidation potential. In all the cases, an irreversible cathodic process was observed. The collective cyclic voltammetric data confirm that reversible oxidation of azomethines is indeed possible through structural modification. Notably, including the 4,4′-dimethyltriphenyl amine, whether in the terminal position (**3A**, **3B** and **3D**) or as the core (**3D**), contributes to stabilizing the oxidized intermediate, resulting in desired reversible oxidation.

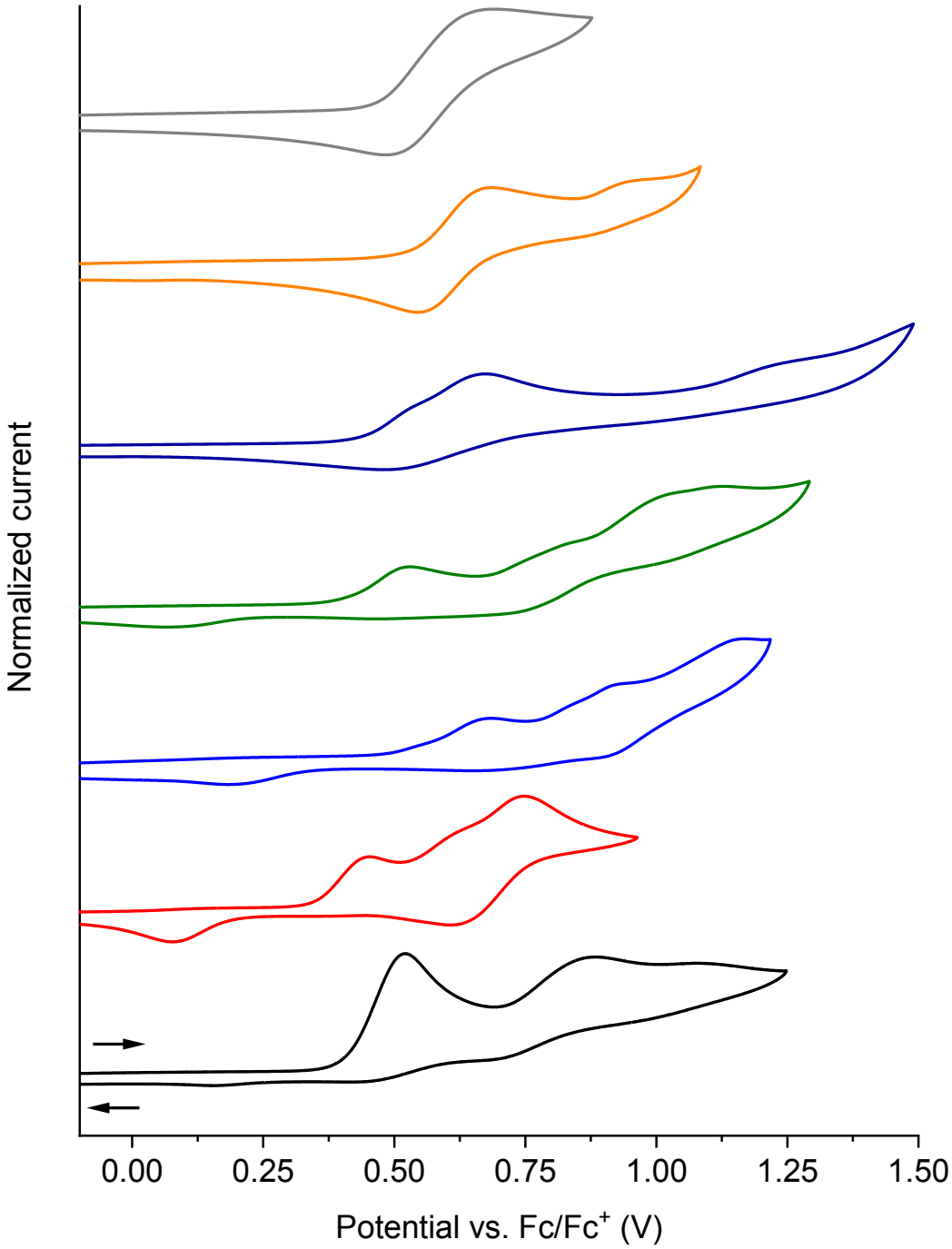

Figure 1-4 Anodic cyclic voltammograms (from bottom to top) of **1** (—), **3** (—), **1C** (—), **1D** (—), **3D** (—), **3A** (—), and **3B** (—) measured in degassed dichloromethane with 0.1 M $TBAPF_6$ at 100 mV/s. Arrows indicate the scan direction of the voltammograms.

The spectroelectrochemistry of the azomethines was assessed in light of their confirmed electroactivity. This was to evaluate their electrochemically mediated color switching

capacities. Focus was placed on the visible region because accurate spectral scans could be done within the time response of the detector to match the rapid changes with applied potential. Covering a wide spectral range from the UV to NIR would not result in accurate and consistent spectra, owing to the slow instrument scanning speed. Significant changes in the visible region were expected given the α-α'-diamino counterparts of the triads such as **4** are known to undergo color changes from red in the neutral state to green when electrochemically oxidized. The color switching was done by applying potentials slightly greater than the E_{ox} that was observed by cyclic voltammetry and measuring the resulting absorption spectrum after a given period of time. An arbitrary wait time between 30 sec and 1 min was chosen before measuring the spectra after applying the potential. This was to ensure that sufficient amounts of the original state were converted to the intermediate state for their spectroscopic detection. The spectroelectrochemistry of the azomethine precursor **3** was first examined. This was to benchmark the change in absorption with applied potential and to frame the impact of varying the end group and the central aromatic on the spectrum.

Given the known absorption of the oxidized triphenylamine,[18,41,42] the effect of the amide group on the absorption could be assessed from **3**. It was further expected that the 4,4′-dimethyl triphenylamine intermediate would be anodically stable and it would not couple to produce electrochemically mediated products (vide supra). The absorption spectra of **3** should therefore consist exclusively of the neutral and oxidized states. An absorption at 705 nm occurred when **3** was oxidized (Figure 1-6). A small shoulder at 578 nm also formed at potentials >1.05 V vs. Ag^{o}. Its absorption at 395 nm additionally decreased and it was blue shifted when oxidized. Its triad counterpart **3A** similarly absorbed at 715 nm when oxidized (Figure S1-23). In fact, only the red-shifted absorption was observed and no other peak was observed in the absorption spectrum. Only a small shoulder was observed at 640 nm with oxidation. From the collective spectral data, the blue color that is formed without complete bleaching of the neutral absorption at 490 nm implies that the anodic intermediate is localized on the triphenylamine. Meanwhile, the shoulder at 640 nm was assigned to the oxidized intermediate being located on the core. This was in part based on the visible absorbance of the neutral core bleaching with applied potential with the concurrent formation of the red-shifted absorption. The neutral state of **3B** also bleached upon oxidation with the concurrent formation of a new broad absorption at ca. 650 nm

(Figure 1-5 A). These confirm that the electrochemically mediated color change is from the core being oxidized. In fact, the red-shifted absorbance consisted for three species: the neutral, the oxidized core, and the oxidized triphenylamine. This was based on the mathematical deconvolution of the spectrum using the absorption maximum of the three discrete chromophores. The oxidized and neutral states of the azomethine core contributed 70% and 0.5% per area, respectively, to the absorption spectrum, while the triphenylamine contribution was 29%, by peak deconvolution (Figure S1-32). The broad red-shifted absorption coalesced into the characteristic narrow absorption of the triphenylamine segment at ca. 710 nm when the oxidation potential was increased to 1.2 V for **3B** (Figure S1-34). The absorption spectrum of **3D** similarly underwent more than one color change with applied potential. Its neutral state at 455 nm bleached with the concurrent formation of a new broad absorption at 570 nm along with a new blue-shifted absorption at 365 nm with an applied positive potential (Figure S1-41). A small shoulder at 715 nm, ascribed to the oxidized triphenylamine located at the termini, also appeared. The long wavelength absorption dominated when the applied potential was increased by 100 mV relative to the first color change, with the absorption at 570 nm persistently contributing to the spectrum, albeit in in decreasing amount with increasing potential. The central conjugated framework therefore can be oxidized with both the core and triphenylamine end groups contributing to the electrochemically mediated red-shifted absorption.

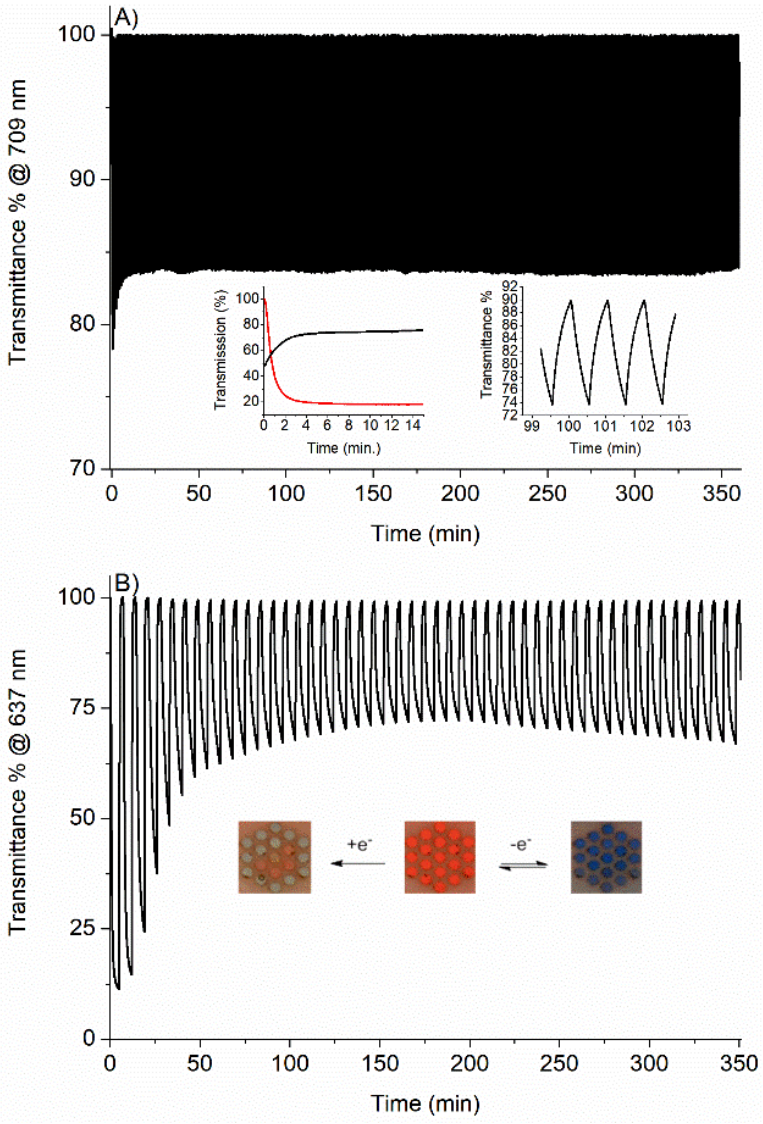

Figure 1-5 A) Corrected change in percent transmittance of **3B** with applied potential of 1.0 and -0.2 V vs. Ag^o in dichloromethane and 0.1 M $TBAPF_6$ switched at 30 sec. intervals and monitored at 709 nm. Baseline corrected for drift in the 100% transmission over time. Inset: Inset: change in percent transmittance with applied potential of 1.1 V vs Ag^o monitored at 508 (▬) and 637 nm (▬) (left). Zoom between 99 and 103 min. with switching of applied potential at 30 sec. intervals (right). B) Change in percent transmittance of **3B** with applied potential of 1.1 and -0.2 V vs. Ag^o in dichloromethane and 0.1 M $TBAPF_6$ switched at 5 min. oxidation and 2 min. neutralization intervals and monitored at 637 nm. Inset: photographs of the 19-well gold working honeycomb electrode of the neutral (middle), electrochemically oxidized (right), and electrochemically reduced (left) states of **3B**.

The absorption spectra of **3A**, **3B**, and **3D** can be unraveled in part by assessing the spectroelectrochemistry of the corresponding phenyl-capped triads **1A**, **1C**, **1D**. Given the conjugated core is exclusively responsible for the absorption of the neutral state in the visible

spectrum, any anodically induced change in the visible color is a result of the central chromophore being oxidized. A red-shifted peak formed with both **1C** and **1D** when the applied potential was equal to their first E_{ox} that was measured by cyclic voltammetry (Figures Figure S1-16 and Figure S1-17). The absorption occurred at 550 nm for **1C** and 558 nm for **1D**. The red-shifted absorption of **1D** relative to **1C** is a result of the weak donating effect of the 4,4′-dimethyl substitution. Meanwhile, a broad absorption occurred at 682 nm for **1C** when the potential applied was equal to that of the second oxidation potential that was measured by cyclic voltammetry. In contrast to **1C** and **1D**, no red-shifted peak occurred with the oxidation of **1A**. Rather, its absorption was blue-shifted to 425 nm when the first oxidation state was formed. The spectroelectrochemistry confirms that the central aromatic of the phenyl amides is oxidized. These results, taken together with those of the triphenylamine end-capped triads, confirm that both the conjugated framework and the end group modulate the absorption spectrum, and hence, the color when oxidized. In fact, the absorption spectrum and the perceived colors of **3B** can be tuned from red to blue with applied potential. The collective perceived colors of the azomethines evaluated upon both electrochemical oxidation and reduction are summarized in the uniform color space (UCS) diagram in Figure 1-6.[43] The spectroelectrochemistry confirm that the intrinsic color of the azomethine framework can also be reversibly bleached, especially with the triads **3A**-**C**.

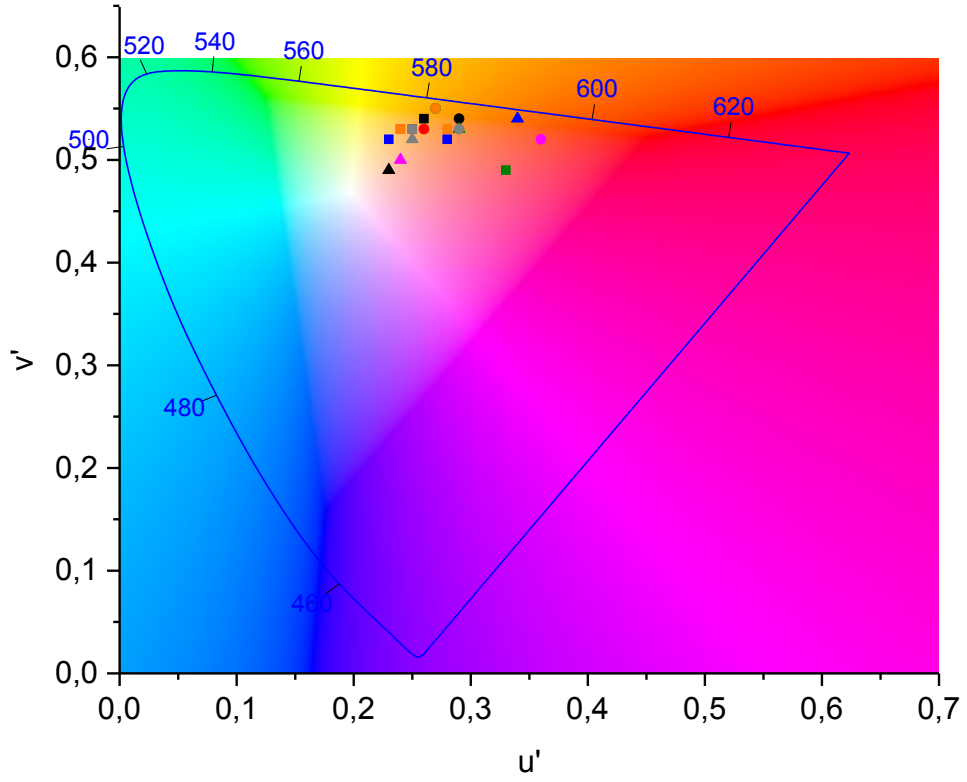

Figure 1-6 CIE (1976 UCS) chromaticity coordinates of the neutral (●), electrochemically oxidized (■) and reduced states (▲) of **3** (—), **1A** (—), **1C** (—), **1D** (—), **3A** (—), **3B** (—), and **3D** (—).

Theoretical calculations were additionally done on **2B** to better understand the electrochemically mediated absorption changes. To accelerate the calculation time, **2B** was calculated rather **3B**. CAM-B3LYP DFT was used to optimize the geometry of the triad.[44] To mimic the experimental conditions as close as possible, dichloromethane was used as the solvent continuum for calculating both the optimized geometries and the absorption spectra of the neutral and the different oxidation states. The optimized geometries that were calculated included the doublet cation, singlet dication, triplet dication, and the neutral singlet, corresponding to the radical cation, dication, bis(radical cation), and neutral states, respectively. The singly occupied molecular orbital (SOMO) of the doublets were also calculated. These spin density calculations were expected to provide insight on the location of the oxidation of the electrochrome, whether it be on the conjugated core or on the end-cap. The bis(radical dication)

was also calculated since it could potentially be formed indirectly by the disproportionation of two radical cations. It could also be potentially formed by either i) two sequential one-electron oxidations or ii) simultaneous two one-electron oxidations. These processes cannot be dismissed from the experimental electrochemical data. The optimized structures were subsequently used to calculate the charge distribution, and the spin delocalization. It should be noted that the absolute thermodynamic parameters and the electronic spectra cannot be accurately calculated. Calculation errors are systematic and the relative values between a series of similar compounds can nonetheless be reliably calculated.

The salient features of the optimized structure of the neutral **2B** are the following. The C=N bond lengths were calculated to be 1.279 Å and these were consistent with those found in the X-ray crystal structure of **1C**. The calculated thiophene-N bond length (1.375 Å) was also similar to the resolved X-ray structure. Of interest is the orientation of the thiophenes and their planarity with respect to each other. The thiophenes adopted an anti-planar configuration, as per Figure 1-7A. The near coplanarity of the thiophenes is also apparent from the figure. In fact, the terminal thiophenes are twisted by 0.95 and 3.23^{o} from the plane described by the central thiophene and its two connected azomethines. This near planar configuration leads to an extended degree of conjugation, confirmed by its experimentally measured red color. It should be noted that the calculated dihedral angle of the central thiophenes is consistent with the experimental values. Indeed, the torsion angles of similar planes measured from previously reported X-ray crystallographic data for **4** that was substituted with decyl chains in the central thiophene's 3,4-positions are 1.6^{o} and 6.2^{o}. In contrast, the planes of the terminal thiophenes of a counterpart of **4** with a central EDOT were greater. In this case, two molecules were found in the unit cell and the terminal aromatics were twisted 8.59^{o}/6.54^{o} and 23.53^{o}/4.63^{o} form the central EDOT. The calculated optimized structure of the neutral ground state and its resulting bond lengths and configuration are consistent with the experimentally derived X-ray crystal structure. Theoretical properties can therefore be calculated with a degree of confidence based on the similar structural geometries between the calculated structure and reported X-ray data.

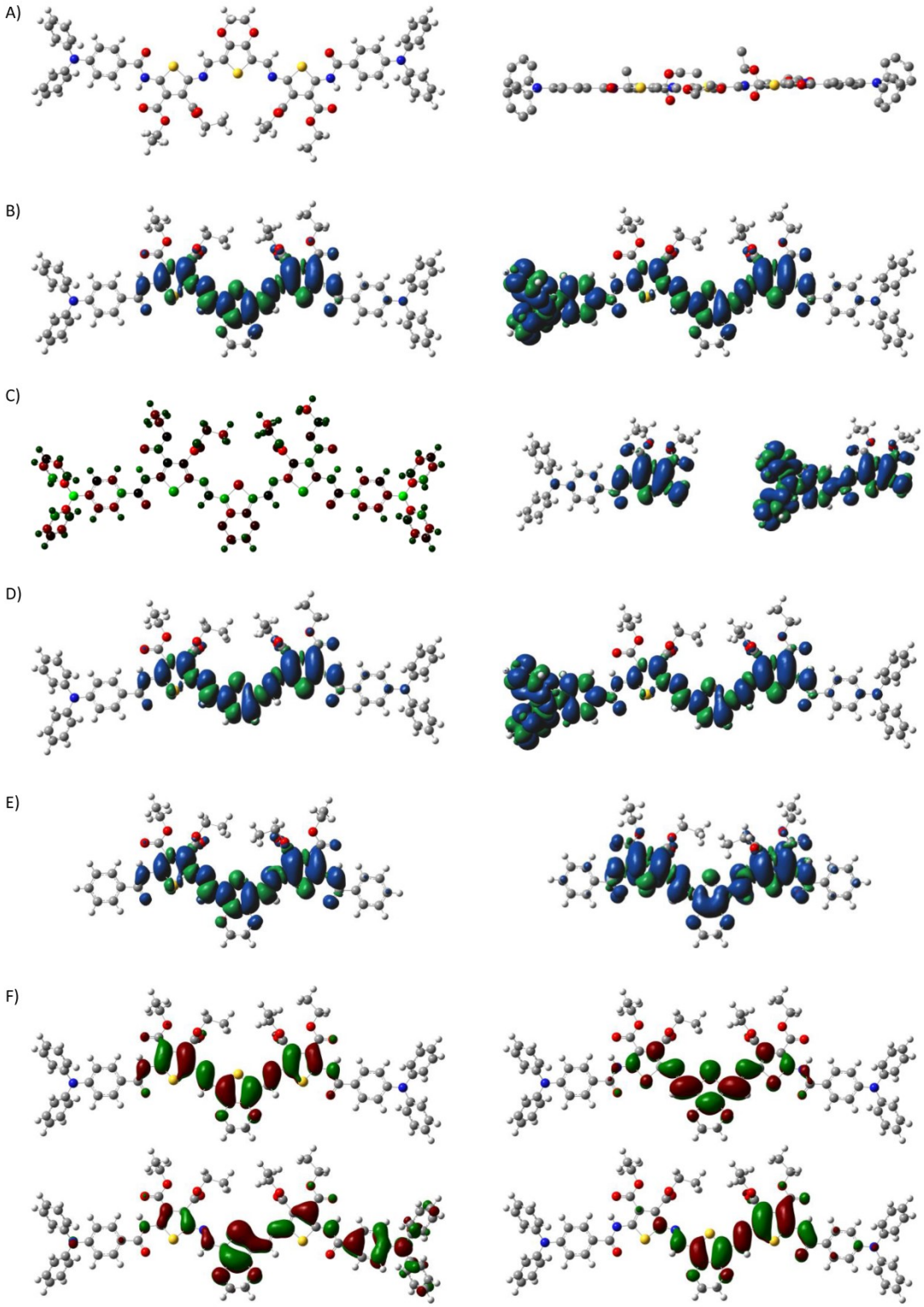

Figure 1-7 A) Top-down (left) and side-on (right) views of the optimized geometry of **2B** calculated by CAM-B3LYP DFT with the 6-311+G(d,p) basis set. The hydrogens were removed from the side-on view for clarity (right). B) The calculated spin density of the

radical cation (left) and the triplet dication (right) **2B**. C) The calculated MM charge distribution (left) of **2B** from -1.1 (red) to +1.1 (green) and the calculated spin density of the radical cation (middle) and triplet dication (right) of **2**. D) The calculated spin density of the radical cation (left) and triplet dication (right) of **2A**. E) The calculated spin density of the radical cation (left) and triplet dication (right) of **1B**. F) Calculated NTOs of the α–HOMO (top left), β–HOMO (bottom left), α–LUMO (top right), and β–LUMO (bottom right) Frontier orbitals of the radical cation of **2B** that are principally involved in the excitation transition at 706 nm.

The optimized geometry and resulting spin distribution of both the radical cation and the bis(radical cation) of **2** were also calculated to benchmark the calculations of **2B**. In the case of the radical cation of **2**, the spin density was localized on the thiophene and not the triphenylamine. Meanwhile, the spin of the bis(radical cation) was distributed over both the thiophene and the triphenylamine (Figure 1-7C). The collective electrochemical results of **3** and the calculations of its analogue **2** imply that both the thiophene radical cation intermediate and the triphenylamine are involved in the electrodeposition of **2** on the electrode. This aside, the spin of the radical cation of **2B** was also localized mainly on the conjugated framework. Only a small spin contribution was located on the end-capped triphenylamines (Figure 1-7B). In contrast, the positive charge of the cation intermediate was located on the nitrogen of the terminal groups (Figure 1-7C left panel). The spin of the bis(radical cation) of **2B** was distributed over the central aromatic and one of the triphenylamine end groups. The calculations show that the central framework is preferentially oxidized over the terminal triphenylamine. In fact, the radical is distributed across the entire core, whether it be a radical cation or two discrete radical cations, as in the case of the bis(radical cation). Both **2A** and **1B** were also calculated to frame the spin density calculations of **2B**. In both cases, the spin of the radical cation was similarly distributed over the conjugated core. Taking the electrochemical, spectroelectrochemical, and theoretical results together, the conjugated core of **3B** is oxidized during the one-electron anodic process, rather the triphenylamine end group.

The collective results point towards the azomethine core being responsible for the broad red-shifted absorption that occurs upon oxidation. This can be confirmed from the theoretically calculated absorption spectra. Three main absorptions in the visible region were calculated for the radical cation of **2B**. The principle excitations in the visible region occurred at 707, 659, and 623 nm (Figure S1-45). These concurred with the absorption spectrum that was measured upon

oxidizing **3B**. While many HOMO and LUMO levels are involved in the given transition, these can be condensed to the principle orbitals by the natural transition orbitals (NTO) analysis. The principle orbitals involved in the transition at 707 nm were the α–HOMO→ α-LUMO and β–HOMO→β–LUMO transitions. This is based on their oscillator strengths of 1.53 and 0.22, respectively for the α–HOMO→ α-LUMO and β–HOMO→β–LUMO transitions. As can be seen in Figure 1-7F, the β-HOMO is located on the core and it extends out to one of the triphenylamine termini, while the β-LUMO is located on the conjugated core. The triphenylamine terminus therefore contributes to the color of the radical cation. The same behavior was calculated for the NTOs of **2A** with the β-HOMO localized on one of the termini and the β-LUMO concentrated on the conjugated core. In contrast to **2B**, the β–HOMO→β–LUMO of **2A** involving the interaction between the end and central segment was the major transition compared to the α–HOMO→ α-LUMO transition, with the respective harmonic oscillator strengths of 1.2 and 0.64 (Figure S1-45). The calculated absorption of the dication also had a main absorption in the visible region at 820 nm. Meanwhile, the neutral **2B** was calculated to absorb at 457 nm. While the exact absorption spectra cannot be truly calculated, the theoretically transitions are consistent with the experimental results. They further demonstrate that both the end group and the core contribute to the visible color, especially when **3B** undergoes a one-electron oxidation, even though the conjugated framework is electronically disconnected from the termini.

The ultimate end use of the azomethines is in functioning electrochromic devices. They therefore must be able to sustain repeated switching between their neutral and oxidized states with consistent color change. Any variation in the conjugated azomethine that can occur by degradation or hydrolysis can be detected by a decrease in percent transmittance of both the oxidized and neutral states with applied potential over time. The performance and stability of the azomethines were evaluated over extended periods by monitoring the oxidized state. Monitoring this intermediate was preferred because any formation of the oxidized state, whether it is minute, can be measured. In contrast, depleting sufficient amount of the strongly absorbing neutral state for its accurate measurement requires extended monitoring times. Given that any degradation of the original neutral state would decrease the amount of oxidized generated, the stability of the given compound towards multiple switching cycles over an extended period of

time can be assessed by monitoring the transmission difference when reversibly generating the oxidized state.

Preliminary stability results were investigated with **3B** by monitoring the change in transmittance with an applied potential. The oxidized intermediate absorbing at 637 nm was observed because of its dependence on the neutral colored state of the azomethine that was determined by spectroelectrochemistry. As seen in the inset of Figure 1-5, this state is stable for more than 14 min. with applied potential, based on the consistent transmittance of 20% upon oxidization. Similarly, the bleaching of the neutral state upon oxidation is maintained over the same time frame. Indeed, the absorption of the neutral state at 500 nm was bleached, resulting in a ca. 30% change in transmittance. Reducing the oxidized intermediate to the neutral state regenerates the initial absorption (Figure 1-5A). The collective spectroscopic data demonstrate that the color of **3B** can be reversibly oxidized. Prolonged switching tests were also done by monitoring the reversible formation of the oxidized state for up to 6 hours. Given the two spectroscopically overlapping states that are simultaneously formed when **3B** was oxidized, they were monitored separately. The variation in transmittance of the triphenylamine end group was monitored at 705 nm. The difference in transmittance between the neutral and oxidized states when electrochemical switched was ca. 17%. As per Figure 1-5B, no change in the transmittance percent difference was observed when switching between the oxidized and neutral states at 30 sec intervals for 360 complete redox cycles during 6 hours.

The same trend of consistent transmittance difference was also observed when monitoring the electrochemically oxidized azomethine core at 637 nm. In this case, the oxidation and neutralizing times were 2 and 5 min, respectively. These time intervals were selected as they gave the maximum change in transmittance with applied potential, as per the inset of Figure 1-5A. While an 88% difference in transmittance was originally observed at 637 nm when switching between the initial and oxidized states, the value gradually dropped after 8 complete cycles. The value remained consistent after 42 min. of switches with the observed value being approximately the same difference in transmittance that was seen with the intermediate at 705 nm. Similar reversible switching behavior without significant change in the transmittance difference at ca. 705 nm was also observed for **3A** and **3D** (Figures Figure S1-25 and Figure S1-43). The consistent data observed when switching at both 637 and 705 nm for **3B**, provide

sound evidence that the triad can sustain multiple electrochemical oxidation/neutralization cycles. The collective switching data further demonstrate that the azomethines meet the switching performance requirements for use in electrochromic devices, being reversible color changes with extended periods of 6 hrs. The collective spectroelectrochemical and the switching data also demonstrate that the reversible color switching over extended periods is possible by incorporating the triphenylamine into the conjugated azomethine.

Conclusion

Conjugated azomethines that exhibit visible color changes upon both electrochemical oxidation and reduction are possible. While converting the terminal amines to amides increases the oxidation potential of the azomethines, this functionalization provides a handle to adjust the reversible oxidation behavior and modulate the color of the azomethines. In fact, extended electrochemical oxidation/neutralization cycles are possible by covalently attaching electroactive end groups to the colored azomethine core via amides. Electrochemically robust functional materials are achieved when end-functionalizing with 4′4′-dimethyltriphenylamines. These conjugated azomethine derivatives can be electrochemically switched between their neutral and oxidized states over 360 times during 6 hours. Electrochemically robust azomethines having desired extended electrochromic switching cycles are therefore possible. The remaining challenges that must be overcome are to use the extended duty cycle azomethines in functioning electrochromic devices and to expand their palette of colors to cover the entire visible spectrum.

Experimental

All reagents and solvents used were from commercial sources unless otherwise stated. Anhydrous solvents were obtained from a commercially available dry-solve alumina column system.

Electrochemical measurements were done with a platinum button working electrode, silver pseudo-reference electrode, and platinum counter electrode. The electrolyte was 0.1 tetrabutylammonium hexafluorophosphate ($TBAPF_6$) in anhydrous dichloromethane. The concentration of the azomethine of study was ca. 1 mM in the electrolyte solution. The solution was bubbled with nitrogen for at least 20 minutes. Afterwards, either a blanket of nitrogen was

maintained over the solution during electrochemical measurements. The electrochemical measurements were done with a conventional potentiostat. Ferrocene (ca. 1 mM) in equimolar to the azomethine was added after the cyclic voltammetry studies to serve as an internal reference. The oxidation potentials were calibrated to the reversible Fc/Fc^+ couple by taking the average of the forward and reverse waves of the anodic scan of ferrocene. E_{ox} refers to the peak maximum for the forward anodic scan, whereas E_{red} refers to the peak maximum for the forward cathodic scan.

Spectroelectrochemical measurements were done with a quartz cuvette having a reduced optical path length. A commercially available ceramic honeycomb 19-well gold working electrode was used along with the silver wire pseudo-reference electrode. A platinum wire was the counter electrode that was embedded in the ceramic electrode. The sample was bubbled with nitrogen and the cuvette was sealed with parafilm to prevent both oxygen diffusion and solvent evaporation. The absorption spectrum was measured in a UV-visible spectrophotometer and the electrodes were connected to a potentiostat. The change in transmittance overtime with applied potential was measured and plotted as is. In certain cases, the baseline of the instrument drifted during the prolonged measurements. The baseline was mathematically corrected by adjusted it to 100% transmittance for the cases were baseline the drift was observed over time. This mathematical transformation adjusted only esthetically the resulting plot without changing the absolute transmittance difference between the neutral and oxidized states. It is stated in the corresponding switching graphs when the baseline correction was applied to the data. Long term switching analyses were done similar to the spectroelectrochemical measurements. For the long time measurements, parafilm was tightly wrapped around the cuvette to minimize solvent evaporation during the time measurements. The gold coated 19-well honeycomb working electrode was used along with a silver pseudo-reference. The instrument was zeroed against air. For the spectroelectrochemical measurements, the baseline was reference against the solvent with the electrolyte.

Theoretical calculations were done with the Gaussian 16, Revision B.01 software.[45] The optimized geometries along with the spin densities and charge locations were calculated from the optimized states for the corresponding neutral and oxidized states with CAM-B3LYP[44,46,47] by DFT[48] means with the 6-311+G(d,p) basis set for **1B**, **2**, **2A**, and **2B** . The connectivity of the

geometry was specified for the calculations, the orbitals were biorthogonalized, and the ESP charges were saved. The absorption spectra of the neutral, dication, radical cation, and triplet dication of **2B** were calculated by time-dependent DFT (TD-DFT)[49] means from the corresponding optimized ground state geometry. The natural transitions orbitals (NTO)[50] were calculated from the second transition of the singlet transition having an absorption in the visible region for **2B** from the TD-DFT calculations.

Diethyl 2-amino-5-benzamidothiophene-3,4-dicarboxylate (**1**).

Prepared according to previously reported method.[40] ^{1}H-NMR (400 MHz, $CDCl_3$): δ (ppm) = 11.45 (s, 2H), 7.95 (dt, *J* = 3.5, 2.3 Hz, 2H), 7.62 – 7.56 (m, 1H), 7.55 – 7.49 (m, 2H), 5.51 (2H), 4.35 (q, *J* = 7.2 Hz, 2H), 4.29 (q, *J* = 7.2 Hz, 2H), 1.36 (t, *J* = 7.2 Hz, 3H), 1.33 (t, *J* = 7.2 Hz, 3H). ^{13}C-NMR **(**100 MHz, $CDCl_3$): δ (ppm) = 166.2, 165.4, 163.8, 154.6, 135.6, 132.8, 132.1, 129.1, 127.5, 110.2, 102.1, 61.2, 60.3, 14.6, 14.3.

Diethyl 2-amino-5-(4-(diphenylamino)benzamido)thiophene-3,4-dicarboxylate (**2**). To 4-(diphenylamino)benzoic acid (1.11 g, 3.8 mmol, 1 eq) in anhydrous dichloromethane (30 mL) was added oxalyl chloride (0.4 mL, 4.6 mmol, 1.2 eq) along with a drop anhydrous DMF. The mixture was stirred for 16 h under nitrogen at room temperature. The solvent was then removed under reduced pressure and the resulting 4-(diphenylamino)benzoyl chloride was taken up in anhydrous THF (30 mL). The mixture was added dropwise to a solution of diethyl 2,5-diaminothiophene-3,4-dicarboxylate (1.39 g, 5.4 mmol, 1.4 eq) and triethylamine (0.75 mL, 5.4 mmol, 1.4 eq) in anhydrous THF (20 mL). The resulting mixture was stirred for 6 h under nitrogen atmosphere at room temperature. Afterwards, the solvent was removed under reduced pressure and the title compound was isolated as a yellow solid (1.23 g, 61%) after purification by silica gel column chromatography (hexanes:ethyl acetate/3:2). ^{1}H-NMR (400 MHz, $CDCl_3$): δ (ppm) = 11.34 (s, 1H), 7.76 (d, *J* = 8.9 Hz, 2H), 7.34-7.30 (m, 4H), 7.17-7.12 (m, 6H), 7.05 (d, *J* = 8.9 Hz, 1H), 5.49 (s, 2H), 4.34-4.25 (m, 4H), 1.36-1.31 (m, 6H). ^{13}C-NMR (100 MHz,

$CDCl_3$): δ (ppm) = 166.2, 165.5, 163.4, 154.4, 152.0, 146.6, 136.3, 129.8, 128.8, 126.1. HRMS (m/z): $[M+H]^+$ calcd for $C_{29}H_{28}N_3O_5S$, 530.1744; found, 530.1737.

Diethyl 2-amino-5-(4-(di-*p*-tolylamino)benzamido)thiophene-3,4-dicarboxylate (**3**). With a similar protocol to **3**, 4-(di-*p*-tolylamino)benzoic acid (668 mg, 1.7 mmol, 1 eq) with added oxalyl chloride (0.21 mL, 2.3 mmol, 1.8 eq). The resulting acid chloride was added dropwise to a solution of diethyl 2,5-diaminothiophene-3,4-dicarboxylate (594 mg, 2.3 mmol, 1.1 eq) and triethylamine (0.32 mL, 2.3 mmol, 1.1 eq) in anhydrous THF (5 mL). The title compound was obtained as a yellow solid (589 mg, 62%) after purification by silica gel column chromatography (hexanes:ethyl acetate/2:1). ^{1}H NMR (400 MHz, $CDCl_3$): δ (ppm) = 11.31 (s, 1H), 7.72 (d, ^3J = 8.9 Hz, 2H), 7.13 (d, ^3J = 8.2 Hz, 4H), 7.05 (d, ^3J = 8.2 Hz, 4H), 6.97 (d, ^3J = 8.9 Hz, 2H), 5.67 (s, 2H), 4.29 (m, 4H), 2.34 (s, 6H), 1.34 (t, ^3J = 7.12 Hz, 3H), 1.32 (t, ^3J = 7.1 Hz, 3H). ^{13}C NMR (100 MHz, $CDCl_3$): δ (ppm) = 166.2, 165.5, 163.4, 154.6, 152.3, 143.9, 136.4, 134.6, 130.4, 128.7, 126.2, 122.5, 119.0, 109.2, 101.8, 61.0, 60.2, 21.0, 14.5, 14.3. HRMS (m/z): $[M+H]^+$ calcd for $C_{31}H_{32}N_3O_5S$, 558.2062; found, 558.2057.

General procedure for the preparation of the triads

The given amide precursor (**1**, **2**, or **3**) and the corresponding dialdehyde (1 eq) were dissolved in a minimum amount of acetone (dichloromethane for **1C**). The mixture was heated at 45°C (40°C for **1C**) until the solids disappeared. Then, a catalytic amount of trifluoroacetic acid (0.05 eq) was added and the reaction mixture was stirred under reflux overnight. The resulting precipitate was filtered and washed with acetone. **3A** and **2A**, were further purified by re-precipitation in a mixture of dichloromethane/hexanes.

Tetraethyl 5,5'-(((1*E*,1'*E*)-thiophene-2,5-diylbis(methanylylidene))bis(azanylylidene))bis(2-benzamidothiophene-3,4-dicarboxylate) (1A).Prepared according to previously reported method.[40] ^{1}H NMR (400 MHz,

$CDCl_3$): δ (ppm) = 12.25 (s, 2H), 8.49 (s, 2H), 8.02 (d, *J* = 7.4 Hz, 4H), 7.63 (t, *J* = 7.3 Hz, 2H), 7.55 (t, *J* = 7.5 Hz, 4H), 7.43 (s, 2H), 4.46 (d, *J* = 7.2 Hz, 4H), 4.38 (d, *J* = 7.2 Hz, 4H), 1.49 (t, *J* = 7.1 Hz, 6H), 1.39 (t, *J* = 7.1 Hz, 6H). ^{13}C NMR (100 MHz, $CDCl_3$): δ (ppm) = 165.4, 165.2, 164.1, 148.8, 146.5, 146.2, 142.1, 133.3, 132.7, 131.7, 129.3, 128.1, 127.8, 110.1, 61.9, 61.7, 14.6, 14.1. HRMS (*m/z*): $[M+H]^+$ calcd for $C_{40}H_{37}N_4O_{10}S_3$, 829.1697; found, 829.1666.

Tetraethyl 5,5'-(((1*E*,1'*E*)-((phenylazanediyl)bis(4,1-phenylene))bis(methanylylidene))bis(azanylylidene))bis(2-benzamidothiophene-3,4-dicarboxylate) (1C). 1 (217 mg, 0.59 mmol, 3 eq) and 4,4'-(phenylazanediyl)dibenzaldehyde (60 mg, 0.19 mmol, 1 eq). The title compound was isolated as a yellow solid (142 mg, 75 %). ^{1}H NMR (400 MHz, $CDCl_3$): δ (ppm) = 12.23 (s, 2H), 8.40 (s, 2H), 8.03 (d, *J* = 7.2 Hz, 4H), 7.72 (d, *J* = 8.7 Hz, 4H), 7.63 (t, *J* = 7.3 Hz, 2H), 7.56 (t, *J* = 7.4 Hz, 4H), 7.36 (t, *J* = 7.8 Hz, 2H), 7.23-7.08 (m, 7H), 4.47-4.34 (m, 8H), 1.41 (dt, *J* = 20.0, 7.1 Hz, 12H). ^{13}C NMR (100 MHz, $CDCl_3$): δ (ppm) = 165.8, 165.3, 164.12, 155.9, 150.1, 145.5, 143.4, 131.2, 132.0, 130.4, 130.3, 130.0, 129.3, 127.7, 126.6, 125.4, 123.3, 110.0, 61.7, 61.6, 14.6, 14.2 (two overlapping signals). HRMS (*m/z*): $[M+H]^+$ calcd for $C_{54}H_{48}N_5O_{10}S_2$, 990.2872; found, 990.2837.

Tetraethyl 5,5'-(((1*E*,1'*E*)-((p-tolylazanediyl)bis(4,1-phenylene))bis(methanylylidene))bis(azanylylidene))bis(2-benzamidothiophene-3,4-dicarboxylate) (1D). 1 (286 mg, 0.79 mmol, 2.0 eq) and 4,4'-(*p*-tolylazanediyl)dibenzaldehyde (126 mg, 0.40 mmol, 1 eq). The title compound was isolated as an orange solid, (281 mg, 70 %). ^{1}H NMR (400 MHz, $CDCl_3$): δ (ppm) = 12.22 (s, 2H), 8.39 (s, 2H), 8.07-7.98 (m, 4H), 7.70 (d, *J* = 8.8 Hz, 4H), 7.65-7.59 (m, 2H), 7.55 (t, *J* = 7.4 Hz, 4H), 7.19-7.05 (m, 8H), 4.40 (2 q, *J* = 18 Hz, 2x4H), 2.37 (s, 3H), 1.43 (t, *J* = 7.1 Hz, 6H), 1.38 (t, *J* = 7.1 Hz, 6H). ^{13}C NMR (100 MHz, $CDCl_3$): δ (ppm) = 165.8, 165.3, 164.1, 156.0, 150.2, 145.4, 143.6, 143.4, 135.5, 133.2, 131.9, 130.7, 130.3, 130.1, 129.2, 127.7, 126.8, 126.2, 122.9, 109.9, 61.7, 61.6, 21.1, 14.6, 14.20. HRMS (*m/z*): $[M+H]^+$ calcd for $C_{55}H_{50}N_5O_{10}S_2$, 1004.3018; found, 1004.2994.

Tetraethyl 5,5'-(((1*E*,1'*E*)-thiophene-2,5-diylbis(methanylylidene))bis(azanylylidene))bis(2-(4-(diphenylamino)benzamido)thiophene-3,4-dicarboxylate) (2A). 2 (262 mg, 0.49 mmol, 3 eq) and 2,5-thiophenedicarboxaldehyde (24 mg, 0.17 mmol, 1 eq). The resulting red product was dissolved in dichloromethane. It was then precipitated by adding hexane, filtered, and washed with acetone to afford an orange/red solid (121 mg, 61%). ^{1}H NMR (400 MHz, $CDCl_3$): δ (ppm) = 12.12 (s, 2H), 8.46 (s, 2H), 7.83 (d, *J* = 8.9 Hz, 4H), 7.40 (s, 2H), 7.37 – 7.29 (m, 8H), 7.21-7.11 (m, 12H), 7.06 (d, *J* = 8.9 Hz, 4H), 4.44 (q, *J* = 7.1 Hz, 4H), 4.34 (q, *J* = 7.2 Hz, 4H), 1.48 (t, *J* = 7.1 Hz, 6H), 1.36 (t, *J* = 7.2 Hz, 6H). ^{13}C NMR (100 MHz, $CDCl_3$): δ (ppm) = 165.5, 165.2, 163.6, 152.4, 148.4, 146.9, 146.5, 146.4, 141.7, 132.5, 129.8, 129.1, 128.1, 126.2, 125.0, 123.0, 120.1, 109.4, 61.9, 61.6, 14.6, 14.2. HRMS (*m/z*): $[M+H]^+$ calcd for $C_{64}H_{55}N_6O_{10}S_3$, 1163.315; found, 1163.3142.

Tetraethyl 5,5'-(((1*E*,1'*E*)-((*p*-tolylazanediyl)bis(4,1-phenylene))bis(methanylylidene))bis(azanylylidene))bis(2-(4-(diphenylamino)benzamido)thiophene-3,4-dicarboxylate) (2D). 2 (231 mg, 0.44 mmol, 3 eq) and 4,4'-(*p*-tolylazanediyl)dibenzaldehyde (47 mg, 0.15 mmol, 1 eq). The title compound was isolated as a yellow solid (154 mg, 77 %). ^{1}H NMR (400 MHz, $CDCl_3$): δ (ppm) = 12.10 (s, 2H), 8.36 (s, 2H), 7.84 (d, *J* = 8.7 Hz, 4H), 7.69 (d, *J* = 8.6 Hz, 4H), 7.33 (t, *J* = 7.8 Hz, 8H), 7.22-7.01 (m, 24H), 4.42 (q, *J* = 7.0 Hz, 4H), 4.34 (q, *J* = 7.1 Hz, 4H), 2.37 (s, 1H), 1.43 (t, *J* = 7.1 Hz, 6H), 1.36 (t, *J* = 7.1 Hz, 6H). ^{13}C NMR (100MHz, $CDCl_3$): δ (ppm) = 165.9, 165.3, 163.6, 155.7, 152.3, 150.1, 146.5, 146.0, 143.6, 143.0, 135.4, 130.6, 130.2, 130.2, 129.8, 129.1, 126.8, 126.2, 126.2, 124.9, 123.3, 122.9, 120.2, 109.3, 61.7, 61.4, 21.1, 14.6, 14.2. HRMS (*m/z*): $[M+H]^+$ calcd for $C_{79}H_{68}N_7O_{10}S_2$, 1338.4514; found, 1338.4469.

Tetraethyl 5,5'-(((1*E*,1'*E*)-thiophene-2,5-diylbis(methanylylidene))bis(azanylylidene))bis(2-(4-(di-*p*-tolylamino)benzamido)thiophene-3,4-dicarboxylate) (3A). 3 (265 mg, 0.48 mmol, 2.9 eq) and 2,5-thiophenedicarboxaldehyde (23 mg, 0.16, 1 eq). The product was isolated as a red solid

(129 mg, 64%). ^{1}H NMR (400 MHz, $CDCl_3$): δ (ppm) = 12.10 (s, 2H), 8.45 (s, 2H), 7.79 (d, *J* = 9.0 Hz, 4H), 7.39 (s, 2H), 7.14 (d, *J* = 8.2 Hz, 8H), 7.07 (d, *J* = 8.4 Hz), 6.99 (d, *J* = 8.9 Hz, 4H), 4.44 (q, *J* = 7.1 Hz, 4H), 4.34 (q, *J* = 7.1 Hz, 4H), 1.48 (t, *J* = 7.1 Hz, 6H), 1.36 (t, *J* = 7.1 Hz, 6H). ^{13}C NMR (100 MHz, $CDCl_3$): δ (ppm) = 165.5, 165.2, 163.6, 152.7, 148.4, 146.9, 146.5, 143.8, 141.7, 134.9, 132.5, 130.4, 129.1, 128.0, 126.3, 122.0, 118.9, 109.3, 61.8, 61.5, 21.1, 14.6, 14.2. HRMS (*m/z*): $[M+H]^+$ calcd for $C_{68}H_{63}N_6O_{10}S_3$, 1219.3791; found, 1219.3762.

Tetraethyl 5,5'-(((1*E*,1'*E*)-(2,3-dihydrothieno[3,4-b][1,4]dioxine-5,7-diyl) bis(methanylylidene)) bis(azanylylidene))bis(2-(4-(di-*p*-tolylamino)benzamido)thiophene-3,4-dicarboxylate) (3B). 3 (193 mg, 0.35 mmol, 2.2 eq) and 2,3-dihydrothieno[3,4-b][1,4]dioxine-5,7-dicarbaldehyde (31 mg, 0.16 mmol, 1 eq). The resulting precipitate was washed several times with ether afford a dark red solid (98 mg, 49%). ^{1}H NMR (400 MHz, $CDCl_3$): δ = 12.08 (s, 2H), 8.51 (s, 2H), 8.51 (s, 2H), 7.79 (d, ^{3}J = 8.9 Hz, 4H), 7.14 (d, ^{3}J = 8.2 Hz, 8H), 7.06 (d, ^{3}J = 8.4 Hz, 8H), 6.99 (d, ^{3}J = 8.9 Hz, 4H), 4.42 (q, ^{3}J = 7.1 Hz, 4H), 4.36 (s, 4H), 4.32 (q, ^{3}J = 7.1 Hz, 4H), 2.35 (s, 12H), 1.47 (t, ^{3}J = 7.1 Hz, 6H), 1.35 (t, ^{3}J = 7.1 Hz, 6H). ^{13}C NMR (100 MHz, $CDCl_3$): δ (ppm) = 165.6, 165.2, 163.6, 152.7, 146.6, 145.3, 144.4, 143.8, 142.7, 134.8, 130.4, 129.0, 127.1, 126.3, 122.2, 121.9, 119.0, 109.3, 65.3, 61.7, 61.5, 21.1, 14.6, 14.1. HRMS (*m/z*): $[M+H]^+$ calcd for $C_{70}H_{65}N_6O_{12}S_3$, 1277.3817; found, 1277.3817.

Tetraethyl 5,5'-(((1*E*,1'*E*)-((*p*-tolylazanediyl)bis(4,1-phenylene))bis(methanylylidene)) bis(azanylylidene)) bis(2-(4-(di-p-tolylamino)benzamido)thiophene-3,4-dicarboxylate) (3D). 3 (175 mg, 0.31 mmol, 2.2 eq) and 4,4'-(*p*-tolylazanediyl)dibenzaldehyde (45 mg, 0.14 mmol, 1 eq). The product was isolated as a dark yellow solid (147 mg, 74 %). ^{1}H NMR (400 MHz, $CDCl_3$): δ (ppm) = 12.08 (s, 2H), 8.37 (s, 2H), 7.81 (d, *J* = 8.8 Hz, 2H), 7.69 (d, *J* = 8.6 Hz, 2H), 7.22-7.04 (m, 13H), 7.00 (d, *J* = 8.8 Hz, 2H), 4.42 (q, *J* = 7.1 Hz, 2H), 4.34 (q, *J* = 7.1 Hz, 2H), 2.38 (s, 2H), 2.36 (s, 6H), 1.43 (t, *J* = 7.1 Hz, 3H), 1.36 (t, *J* = 7.1 Hz, 4H). ^{13}C NMR (100 MHz, $CDCl_3$): δ (ppm) = 165.9, 165.3, 163.7, 155.6, 152.6, 150.1, 146.2, 143.9, 143.7, 142.9, 135.4, 134.8, 130.6, 130.4, 130.2, 129.0, 126.8, 126.3, 126.2, 122.9, 122.3, 118.9, 109.1,

61.7, 61.4, 21.1, 21.1, 14.6, 14.2 (two overlapping signals). HRMS (*m/z*): $[M+H]^+$ calcd for $C_{83}H_{76}N_7O_{10}S_2$, 1394.5017; found, 1394.5102.

Conflicts of interest

There are no conflicts to declare.

Acknowledgements

Both NSERC Canada and the Canada Foundation for Innovation are acknowledged for Discovery and infrastructure grants, respectively, that enabled this work. Compute Canada (www.computecanada.ca) and their partners, Compute Ontario (computeontario.ca) and WestGrid (www.westgrid.ca), are also thanked for access to both computational resources and software for theoretical calculations. Mr. S. Bonus and Dr. T. Maris are also thanked for the preliminary contributions for developing compounds **2A-C** and for assistance in resolving the X-ray diffraction structure of compound **1C**, respectively.

References

1) P. G. M. Wuts and T. W. Greene, *Greene's Protective Groups in Organic Synthesis*, Wiley-Interscience, 4th edn., 2007.

2) R. D. Mukhopadhyay, Y. Kim, J. Koo and K. Kim, *Acc. Chem. Res.*, 2018, **51**, 2730-2738.

3) M. E. Belowich and J. F. Stoddart, *Chem. Soc. Rev.*, 2012, **41**, 2003-2024.

4) R. Bui and M. A. Brook, *Polymer*, 2019, **160**, 282-290.

5) A. Kundu and S. P. Anthony, *Spectrochim. Acta A*, 2018, **189**, 342-348.

6) L. Wang, S. Wu, H. Tang, H. Meier and D. Cao, *Sens. Actuators, B*, 2018, **273**, 1085-1090.

7) I. I. Ebralidze, G. Leitus, L. J. W. Shimon, Y. Wang, S. Shaik and R. Neumann, *Inorg. Chim. Acta*, 2009, **362**, 4713-4720.

8) N. Khalid, A. Bibi, K. Akhtar, K. Mustafa, M. Khan and N. Saeed, *Polym. Plast. Technol. Eng.*, 2019, **58**, 419-426.

9) J. Wojtkiewicz, A. Iwan, M. Pilch, B. Boharewicz, K. Wójcik, I. Tazbir and M. Kaminska, *Spectrochim. Acta A*, 2017, **181**, 208-217.

10) X. Zheng, W. Zhu, C. Zhang, Y. Zhang, C. Zhong, H. Li, G. Xie, X. Wang and C. Yang, *J. Am. Chem. Soc.*, 2019, **141**, 4704-4710.

11) S. Liu, T. Wu, Q. Zhu, J. Pu, G. Chen, W. Zhang and Z. Li, *RSC Adv.*, 2018, **8**, 12779-12784.

12) S. Dufresne and W. G. Skene, *J. Phys. Org. Chem.*, 2012, **25**, 211-221.

13) L.-C. Yeh, T.-C. Huang, F.-Y. Lai, G.-H. Lai, A.-Y. Lo, S.-C. Hsu, T.-I. Yang and J.-M. Yeh, *Surf. Coat. Technol.*, 2016, **303**, 154-161.

14) M. Wałęsa-Chorab, M.-H. Tremblay and W. G. Skene, *Chem. Eur. J.*, 2016, **22**, 11382-11393.

15) M. H. Chua, Q. Zhu, K. W. Shah and J. Xu, 2019, **11**, 98.

16) X. Ma, Y. Wu, H. Wen, H. Niu, C. Wang, C. Qin, X. Bai, L. Lei and W. Wang, *RSC Adv.*, 2016, **6**, 4564-4575.

17) Y. Dong, D. Navarathne, A. Bolduc, N. McGregor and W. G. Skene, *J. Org. Chem.*, 2012, **77**, 5429-5433.

18) M. Bourgeaux and W. G. Skene, *J. Org. Chem.*, 2007, **72**, 8882-8892.

19) H.-J. Yen and G.-S. Liou, *Polym. Chem.*, 2018, **9**, 3001-3018.

20) H.-J. Yen and G.-S. Liou, *Prog. Polym. Sci.*, 2019, **89**, 250-287.

21) F. Liu, Y. Zhang, G. Yu, Y. Hou and H. Niu, *J. Appl. Polym. Sci.*, 2019, **136**, 47264.

22) S.-H. Hsiao and H.-Y. Lu, *J. Electrochem. Soc.*, 2018, **165**, H638-H645.

23) S.-H. Hsiao and Y.-P. Huang, *Dyes Pigm.*, 2018, **158**, 368-381.

24) S.-H. Hsiao and J.-S. Han, *Eur. Polym. J.*, 2017, **90**, 122-135.

25) S.-H. Hsiao and Y.-Z. Chen, *Eur. Polym. J.*, 2018, **99**, 422-436.

26) S.-H. Hsiao and H.-Y. Lu, *Polymers*, 2017, **9**, 708.

27) S.-H. Hsiao and C.-N. Wu, *J. Electroanal. Chem.*, 2016, **776**, 139-147.

28) Y.-J. Wang, X.-L. Liu, Z.-Z. Huang, J.-W. Jiang and S.-R. Sheng, *J. Macromol. Sci. A*, 2017, **54**, 534-542.

29) F. Feng, N. Sun, D. Wang, H. Zhou and C. Chen, *High Perform. Polym.*, 2017, **29**, 922-930.

30) N. Sun, Z. Zhou, D. Chao, X. Chu, Y. Du, X. Zhao, D. Wang and C. Chen, *J. Polym. Sci., Part A: Polym. Chem.*, 2017, **55**, 213-222.

31) H.-M. Wang, S.-H. Hsiao, G.-S. Liou and C.-H. Sun, *J. Polym. Sci., Part A: Polym. Chem.*, 2010, **48**, 4775-4789.

32) M. Wałęsa-Chorab and W. G. Skene, *Sol. Energy Mater. Sol. Cells*, 2019, **200**, 109977.

33) M.-H. Tremblay, T. Skalski, Y. Gautier, G. Pianezzola and W. G. Skene, *J. Phys. Chem.*, 2016, **120**, 9081-9087.

34) Vasu, K. A. Nirmala, D. Chopra, S. Mohan and J. Saravanan, *Acta Crystallogr. E*, 2004, **60**, o756-o757.

35) S. Alley, J. F. Gallagher, P. T. M. Kenny and A. J. Lough, *Acta Crystallogr. E*, 2005, **61**, m201-m203.

36) A. Mukhtar, M. N. Tahir, M. A. Khan, A. Q. Ather and M. N. Khan, *Acta Crystallogr. E*, 2012, **68**, o2042.

37) W. T. A. Harrison, H. S. Yathirajan, B. V. Ashalatha, K. K. Vijaya Raj and B. Narayana, *Acta Crystallogr. E*, 2006, **62**, o3732-o3734.

38) Y. Gautier, T. Maris and W. G. Skene, *Acta Crystallography Section E*, 2019, submitted.

39) L. Vacareanu, T. Ivan and M. Grigoras, *High Perform. Polym.*, 2012, **24**, 717-729.

40) M. Mulholland, D. Navarathne, S. Khedri and W. G. Skene, *New J. Chem.*, 2014, **38**, 1668-1674.

41) S. Dapperheld, E. Steckhan, K.-H. G. Brinkhaus and T. Esch, *Chem. Ber.*, 1991, **124**, 2557-2567.

42) P. Blanchard, C. Malacrida, C. Cabanetos, J. Roncali and S. Ludwigs, *Polym. Int.*, 2019, **68**, 589-606.

43) *Colorimetry — Part 5: CIE 1976 L*u*v* colour space and u', v' uniform chromaticity scale diagram*, International Organization for Standardization: CIE International Commission on Illumination, 2016.

44) T. Yanai, D. P. Tew and N. C. Handy, *Chem. Phys. Lett.*, 2004, **393**, 51-57.

45) M. J. Frisch, G. W. Trucks, H. B. Schlegel, G. E. Scuseria, M. A. Robb, J. R. Cheeseman, G. Scalmani, V. Barone, G. A. Petersson, H. Nakatsuji, M. C. X. Li, A. V. Marenich, J. Bloino,

B. G. Janesko, R. Gomperts, B. Mennucci, H. P. Hratchian, J. V. Ortiz, A. F. Izmaylov, J. L. Sonnenberg, D. Williams-Young, F. Ding, F. Lipparini, F. Egidi, J. Goings, B. Peng, A. Petrone, T. Henderson, D. Ranasinghe, V. G. Zakrzewski, J. Gao, N. Rega, G. Zheng, W. Liang, M. Hada, M. Ehara, K. Toyota, R. Fukuda, J. Hasegawa, M. Ishida, T. Nakajima, Y. Honda, O. Kitao, H. Nakai, T. Vreven, K. Throssell, J. J. A. Montgomery, J. E. Peralta, F. Ogliaro, M. J. Bearpark, J. J. Heyd, E. N. Brothers, K. N. Kudin, V. N. Staroverov, T. A. Keith, R. Kobayashi, J. Normand, K. Raghavachari, A. P. Rendell, J. C. Burant, S. S. Iyengar, J. Tomasi, M. Cossi, J. M. Millam, M. Klene, C. Adamo, R. Cammi, J. W. Ochterski, R. L. Martin, K. Morokuma, O. Farkas, J. B. Foresman and D. J. Fox, *Journal*, 2016.

46) P. J. Stephens, F. J. Devlin, C. F. Chabalowski and M. J. Frisch, *J. Phys. Chem.*, 1994, **98**, 11623-11627.

47) S. H. Vosko, L. Wilk and M. Nusair, *Can. J. Phys.*, 1980, **58**, 1200-1211.

48) A. D. Becke, *Phys. Rev. A*, 1988, **38**, 3098-3100.

49) M. E. Casida, in *Recent Advances in Density Functional Methods*, ed. D. P. Chong, World Scientific, Singapore, 1995, vol. 1, pp. 155-192.

50) R. L. Martin, *J. Chem. Phys.*, 2003, **118**, 4775-477

SUPPORTING INFORMATION I
ELECTROCHEMICAL AND SPECTROSCOPIC DATA

Extending the duty cycle of azomethine electrochromes by structural modification

Yohan Gautier and W. G. Skene

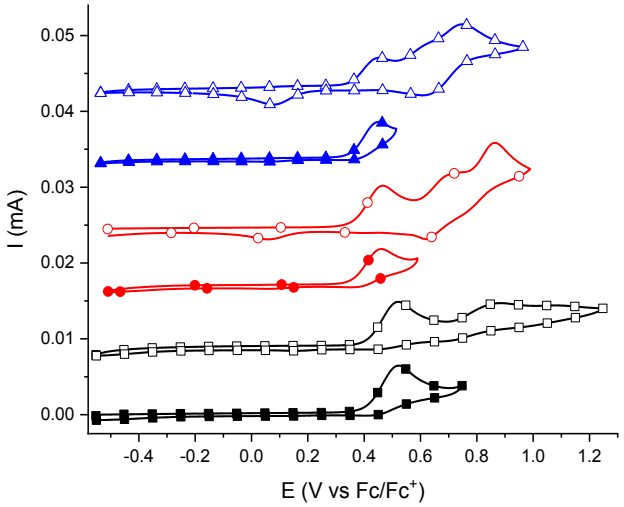

Figure S1-8Anodic cyclic voltammograms of the dyads **1** (squares), **2** (circles), and **3** (triangles) measured in degassed and anhydrous dichloromethane at 100 mV/s with 0.1 M $TBAPF_6$.

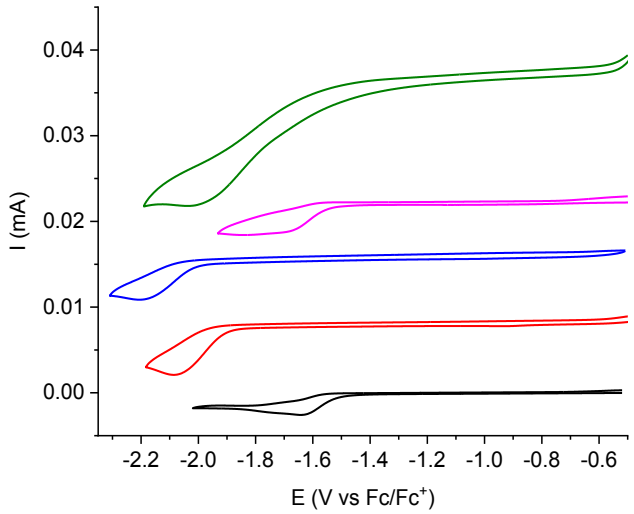

Figure S1-9 Cathodic cyclic voltammograms of **1A** (black),[1] **1C** (red), **1D** (blue). **3A** (pink), **3D** (green) measured in 0.1 M $TBAPF_6$ in degassed and anhydrous dichloromethane at 100 mV/s.

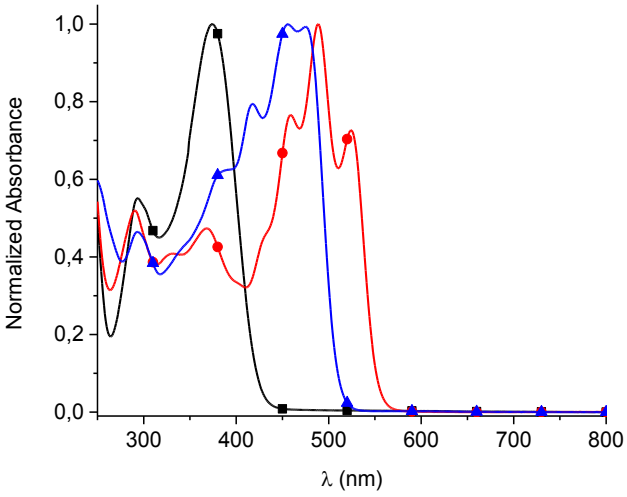

Figure S1-10 Absorption spectra of **2** (squares), **2A** (circles), **2D** (triangles) measured in dichloromethane.

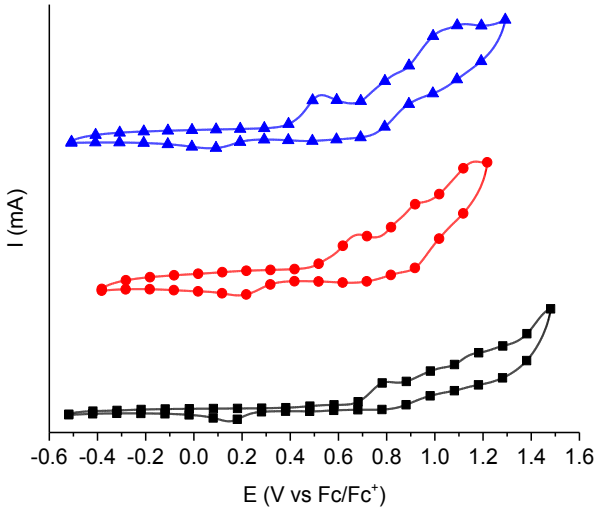

Figure S1-11 Anodic cyclic voltammograms of the **1A** (■),[1] **1C** (●), and **1D** (▲) measured in degassed and anhydrous dichloromethane at 100 mV/s with 10^{-3} M ferrocene as an internal reference and with 0.1 M $TBAPF_6$ between -0.5 and ca 1.2 V vs. Fc/Fc^+.

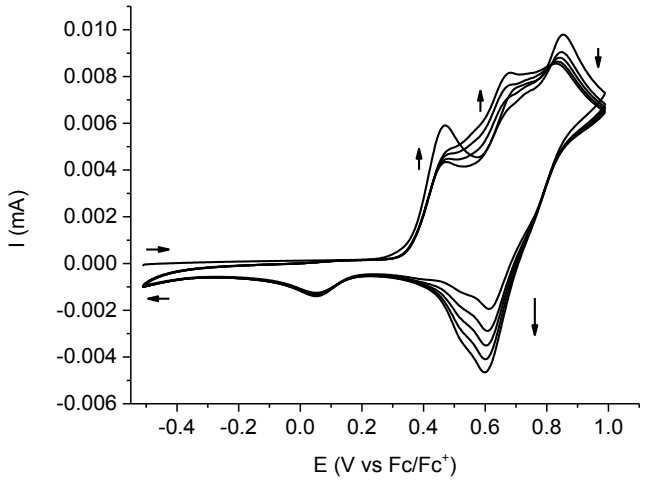

Figure S1-12 Multiple anodic cyclic voltammograms of **2** measured in 0.1 M $TBAPF_6$ in degassed and anhydrous dichloromethane at 100 mV/s.

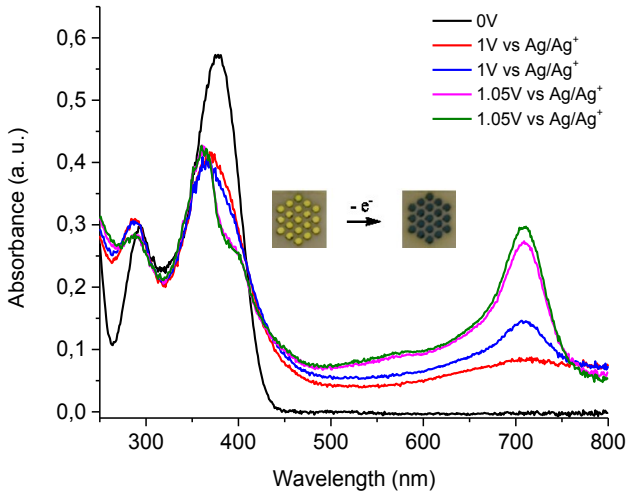

Figure S1-13 Change in absorption spectra of **3** with applied potential measured between 60 and 90 sec after the applying the potential in degassed and anhydrous dichloromethane. Inset: Photographs of the honeycomb gold electrode of the neutral (left) and electrochemically oxidized (right) states.

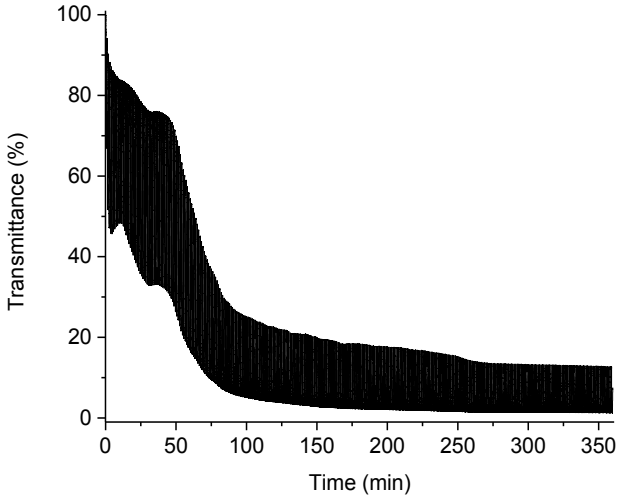

Figure S1-14 Uncorrected change in percent transmittance of **3** when switching the applied potential between 0.8 V and -0.2 V at 30 second intervals monitored at 705 nm during for 6 hours.

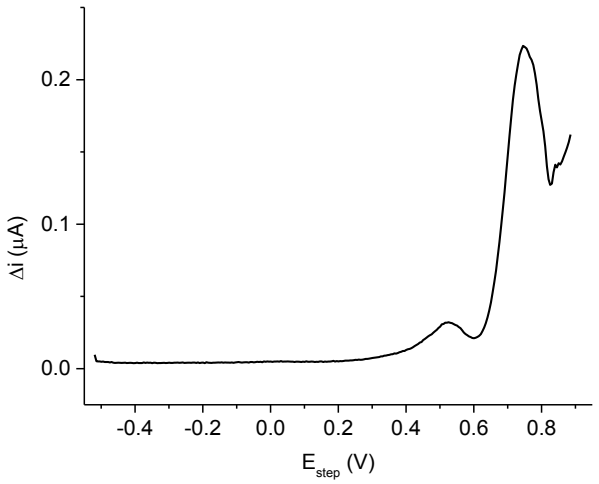

Figure S1-15 Differential pulse voltammogram of **1A** measured in degassed and anhydrous dichloromethane with 0.1 M $TBAPF_6$.

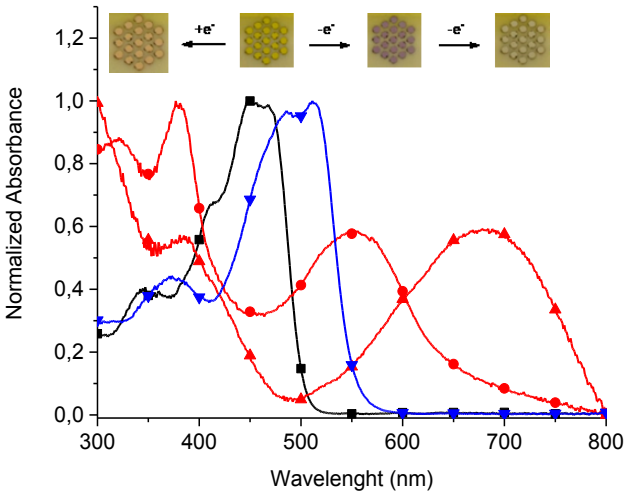

Figure S1-16 Absorption spectra of the neutral (■), electrochemically oxidized (●, ▲), and electrochemically reduced (▼) states of **1C** with applied potentials of 1.05, 1.3, and -1.8 V vs Ag^{o}, respectively. Inset: Photographs of the honeycomb gold electrode of the reduced, neutral, first oxidized, and second oxidized (from left to right) states.

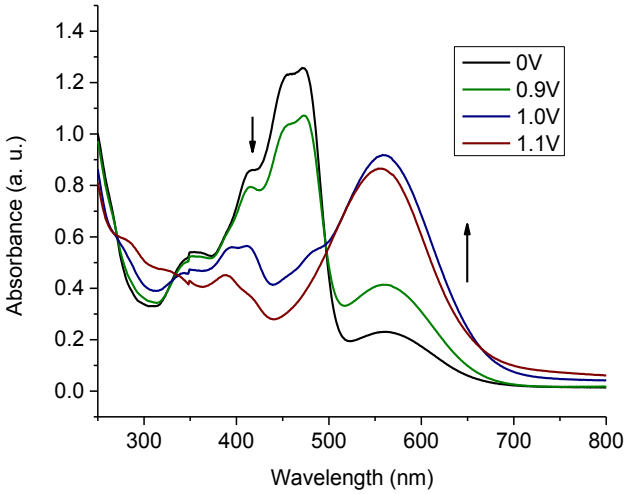

Figure S1-17 Change in absorption spectra of **1D** with applied positive potential measured in anhydrous and degassed dichloromethane with 0.1 M $TBAPF_6$ at 100 mV/s.

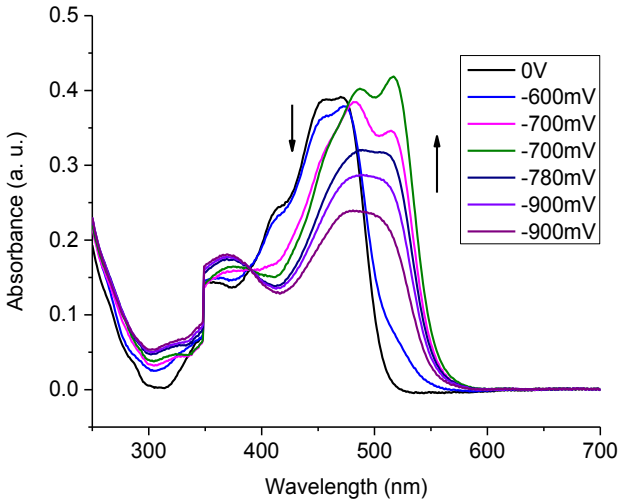

Figure S1-18 Change in absorption spectra of **1D** with applied negative potential measured in anhydrous and degassed dichloromethane with 0.1 M $TBAPF_6$ at 100 mV/s.

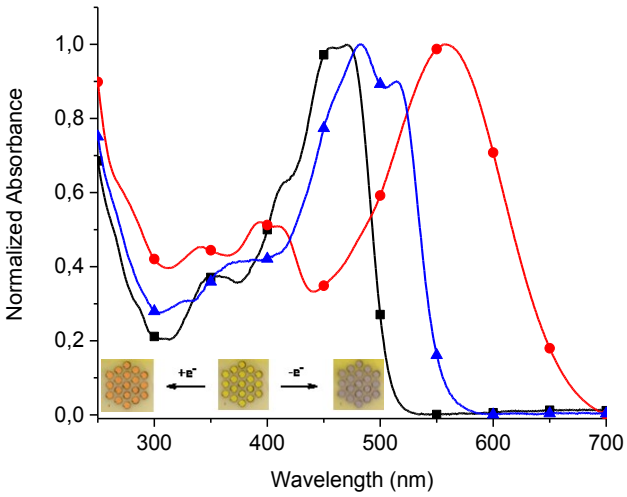

Figure S1-19 Absorption spectra of the neutral (■), electrochemically oxidized (●), and electrochemically reduced (▲) states of **1D**. Inset: Photographs of the honeycomb gold electrode of the reduced, neutral, and oxidized (from left to right) states.

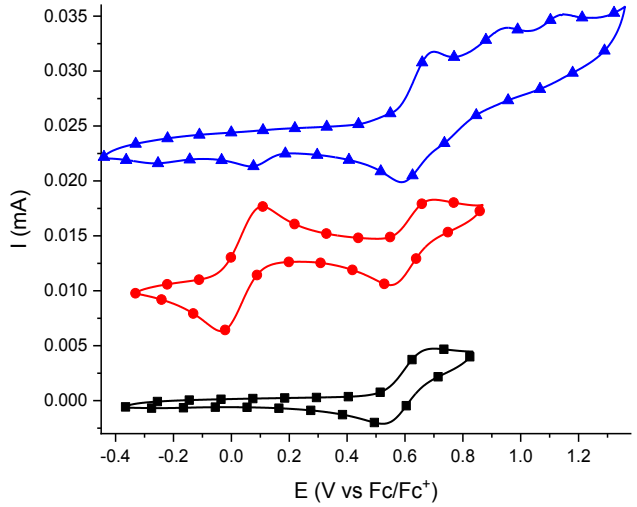

Figure S1-20 Anodic cyclic voltammograms of **3A** measured in degassed and anhydrous dichloromethane with 0.1 M $TBAPF_6$ at 100 mV/s without (black squares and blue triangles) and with 10^{-3} M ferrocene (red circles).

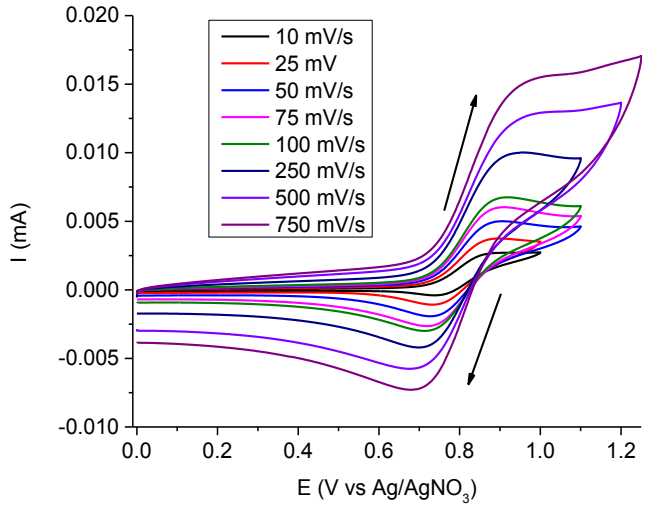

Figure S1-21 Anodic cyclic voltammograms of **3A** measured at different scan speeds (10 to 750 mV/s) in 0.1 M $TBAPF_6$ in in degassed and anhydrous dichloromethane.

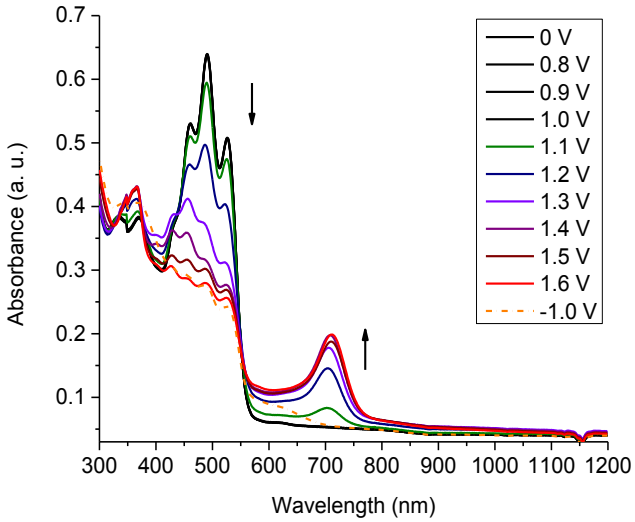

Figure S1-22 Change in absorption spectra of **3A** with applied positive potential.

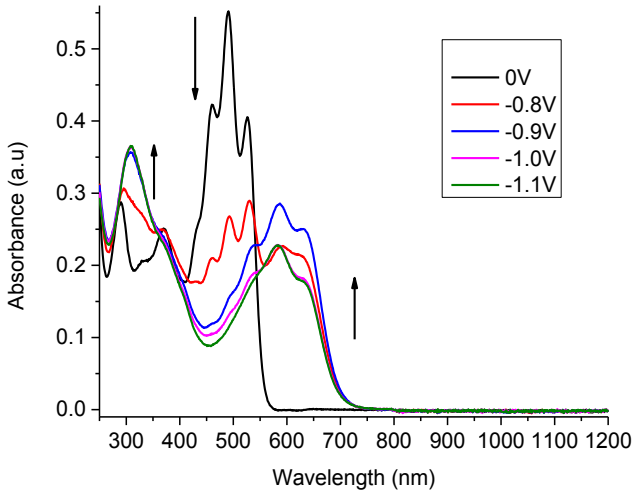

Figure S1-23 Change in absorption spectra of **3A** with applied negative potential.

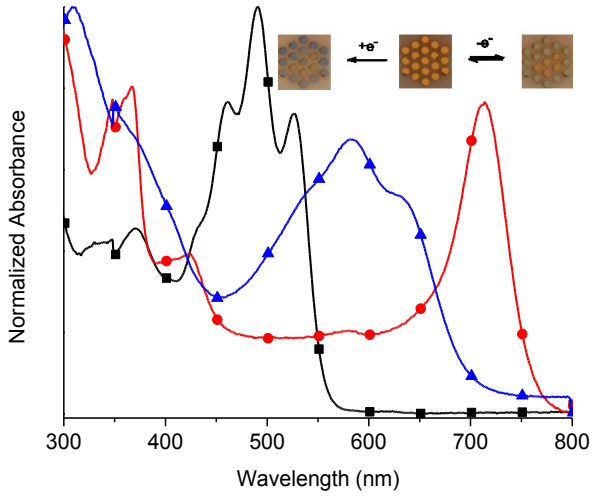

Figure S1-24 Absorption spectra of the neutral (■), electrochemically oxidized (●), and electrochemically reduced (▲) states of **3A**. Inset: Photographs of the honeycomb gold electrode of the electrochemically reduced (left), neutral (middle), and electrochemically oxidized (right) states.

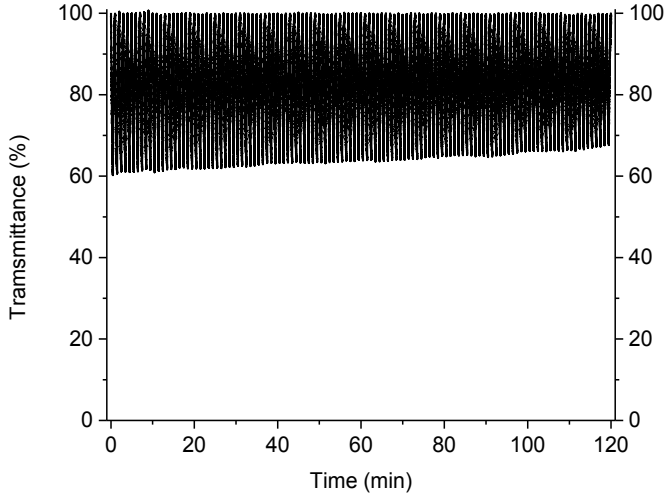

Figure S1-25 Change in percent transmittance of **3A** monitored at 708 nm with switching the applied potential between 1.15 and -0.1 V vs. Ag^{o} at 30 sec intervals over a 2 hour time range corrected for baseline drift over time at 100% transmittance.

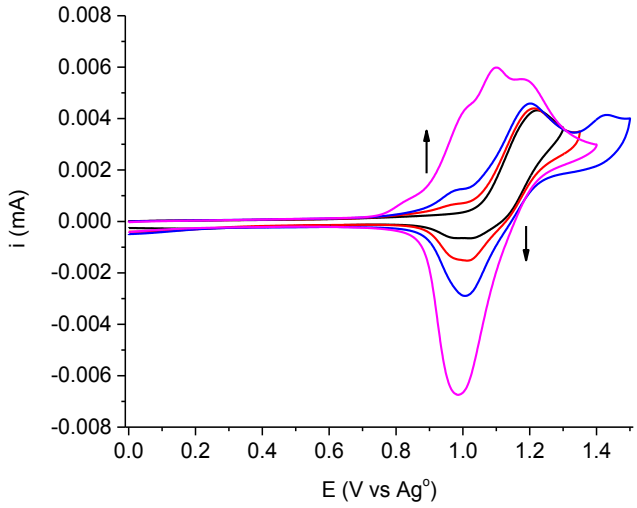

Figure S1-26 Multiple anodic cyclic voltammograms of **2A** measured in 0.1 M $TBAPF_6$ in degassed and anhydrous dichloromethane at 100 mV/s.

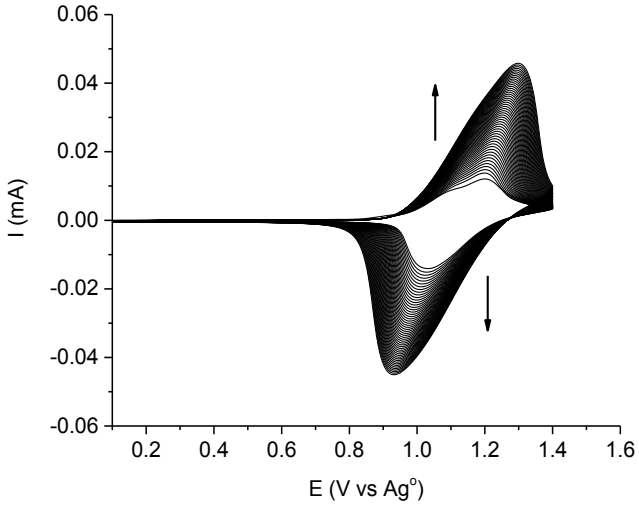

Figure S1-27 Multiple (50) anodic cyclic voltammograms of **2A** leading to its electropolymerization measured in 0.1 M $TBAPF_6$ in in degassed and anhydrous dichloromethane at 100 mV/s.

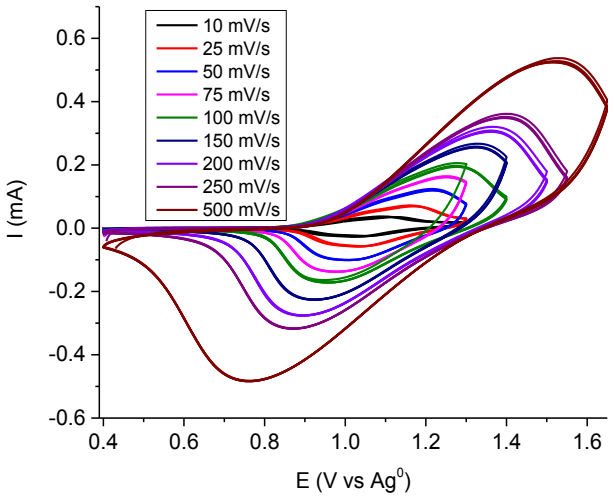

Figure S1-28 Cyclic voltammograms of the resulting electropolymerized film of **2A** on an ITO electrode measured at different scan speeds in 0.1 M $TBAPF_6$ in degassed and anhydrous dichloromethane.

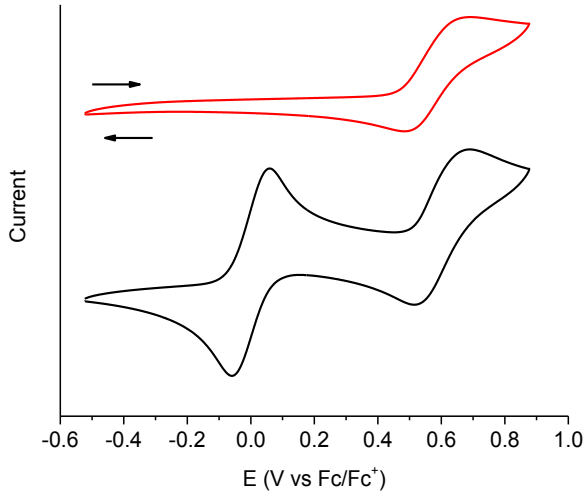

Figure S1-29 Anodic cyclic voltammogram of **3B** measured in 0.1 M $TBAPF_6$ in degassed and anhydrous dichloromethane at 100 mV/s without (red) and with 10^{-3} M ferrocene.

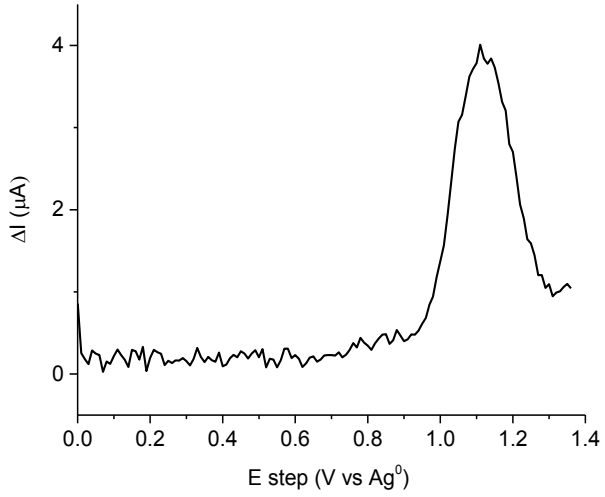

Figure S1-30 Anodic square wave voltammogram of **3B** measured in dichloromethane with 0.1 M $TBAPF_6$.

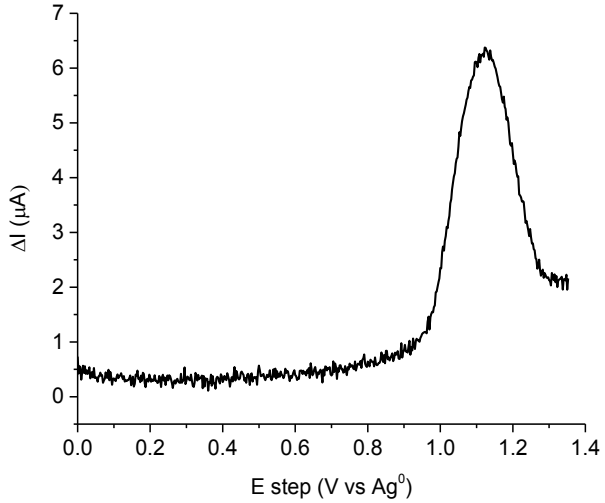

Figure S1-31 Anodic differential pulse voltammogram of **3B** measured in dichloromethane with 0.1 M $TBAPF_6$.

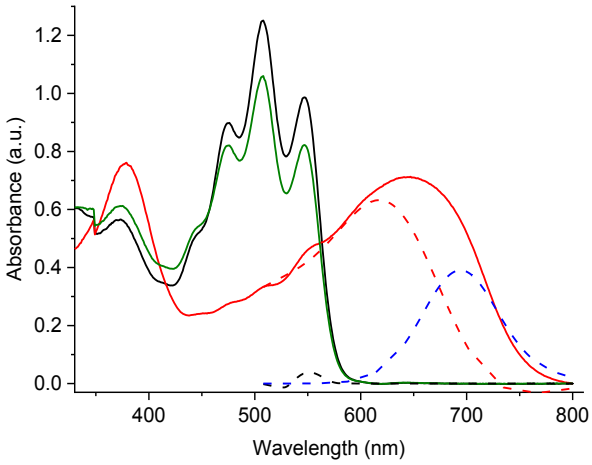

Figure S1-32 Absorption spectra of **3B** with applied potential: 0 V (—), after 15 min. at 1.1 V (—), and return to 0 V (—). Dotted lines are the mathematical deconvolution of the oxidized state at 1.1 V into the corresponding three spectral components: neutral (—), oxidized core (—), and oxidized end groups (—).

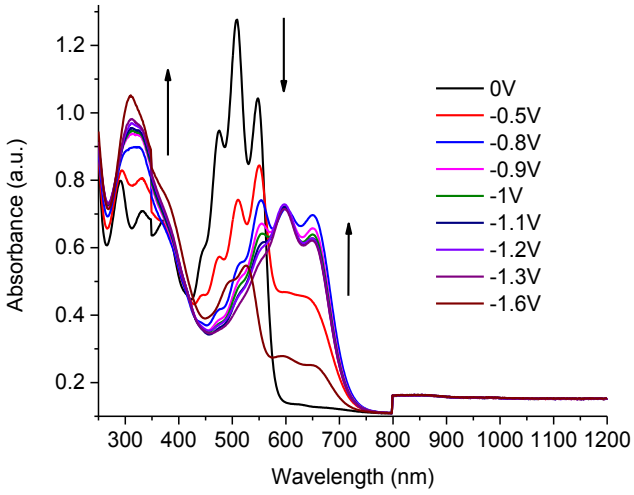

Figure S1-33 Change in absorption spectra of **3B** with applied negative potential.

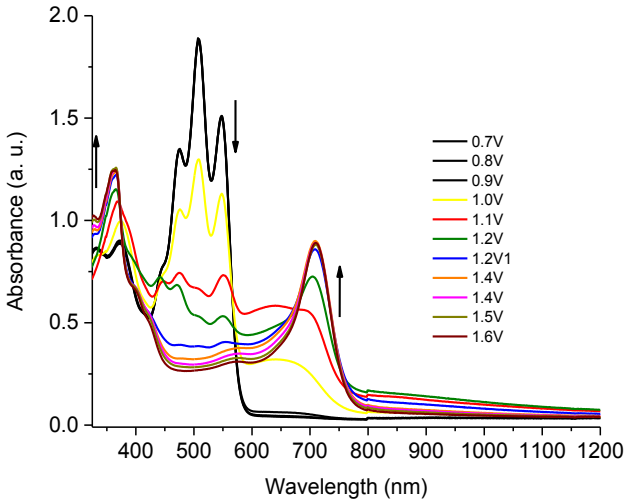

Figure S1-34 Change in absorption spectra of **3B** with applied positive potential.

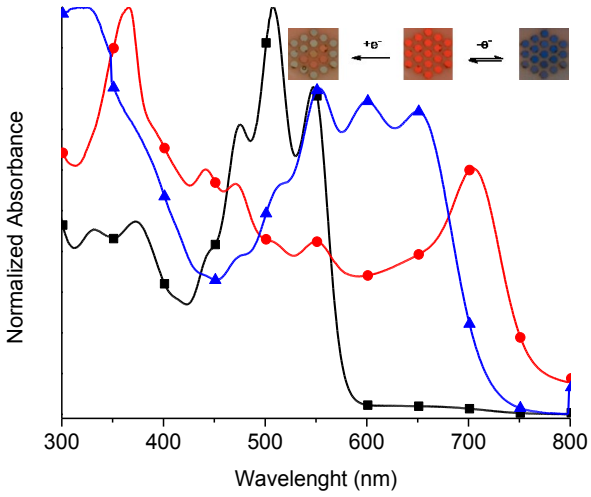

Figure S1-35 Absorption spectra of the neutral (■), electrochemically oxidized (●), and electrochemically reduced (▲) states of **3B**. Inset: Photographs of the honeycomb gold electrode of the electrochemically reduced (left), neutral (middle), and electrochemically oxidized (right) states.

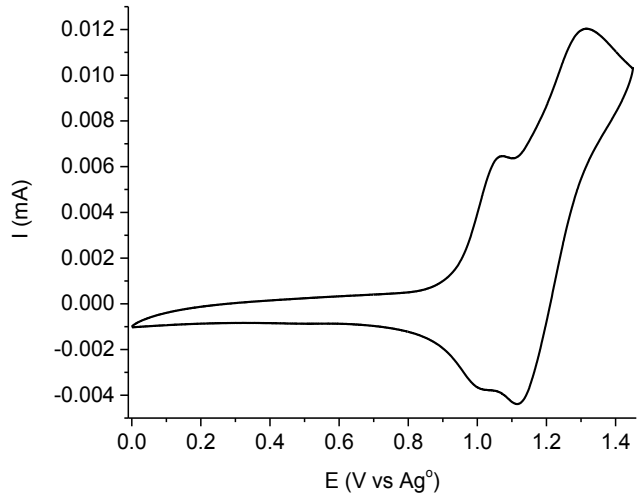

Figure S1-36 Anodic cyclic voltammogram of **2D** measured in 0.1 M $TBAPF_6$ in degassed and anhydrous dichloromethane at 100 mV/s.

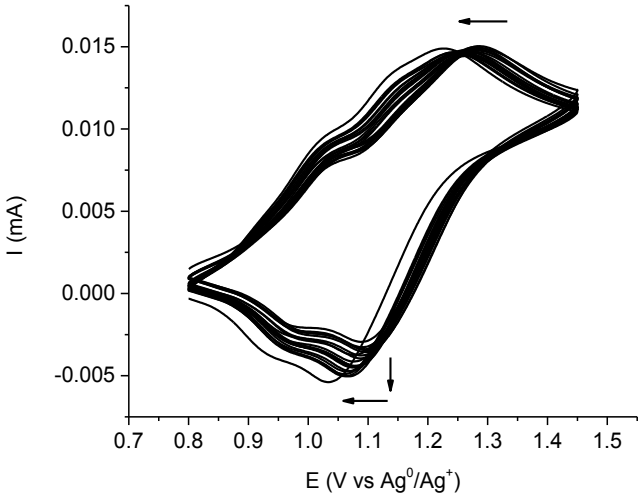

Figure S1-37 Multiple (20) anodic cyclic voltammogram of **2D** measured in 0.1 M $TBAPF_6$ in degassed and anhydrous dichloromethane at 100 mV/s leading to its electropolymerization.

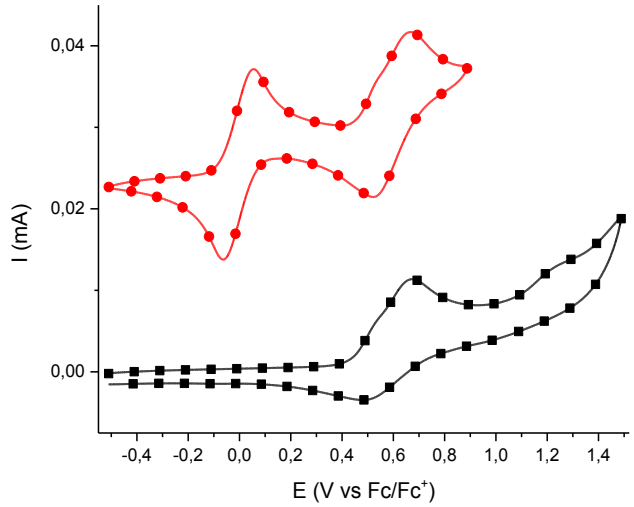

Figure S1-38 Anodic cyclic voltammograms of **3D** measured in 0.1 M $TBAPF_6$ in degassed and anhydrous dichloromethane at 100 mV/s with 10^{-3} M ferrocene as internal reference (red circles).

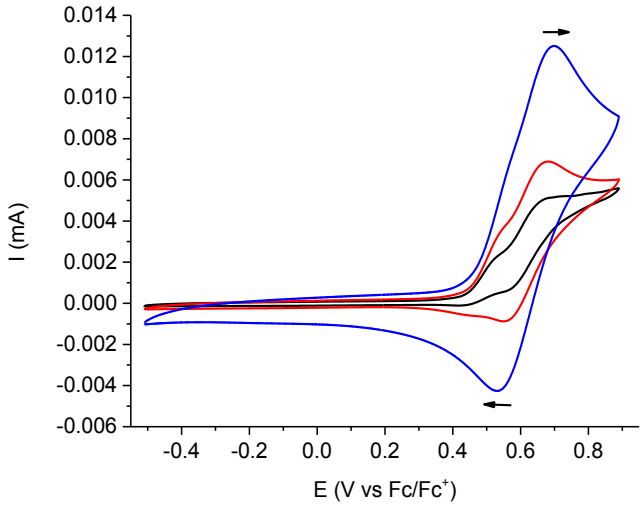

Figure S1-39 Anodic cyclic voltammograms of **3D** at different scan rates: 10mV/s (━), 25 mV/s (━) and 100 mV/s (━), measured in 0.1 M $TBAPF_6$ in degassed and anhydrous dichloromethane.

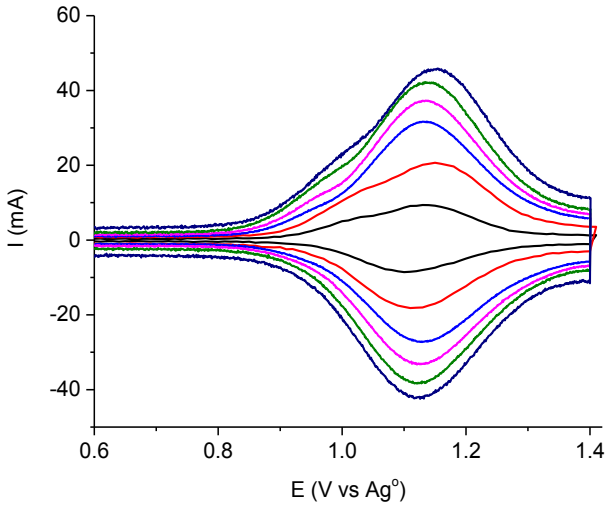

Figure S1-40 Squarewave voltammograms of **3D** contingent on different scan parameters.

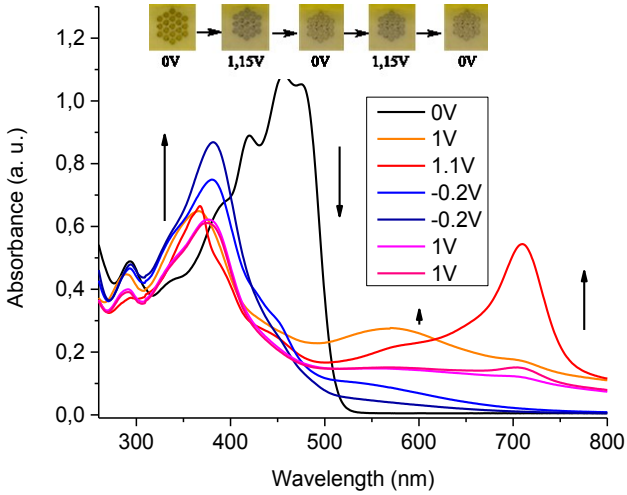

Figure S1-41 Change in absorption spectra of **3D** with switching the applied potential. Inset: Photographs of the honeycomb gold electrode showing the change in color of **3D** contingent on applied potential.

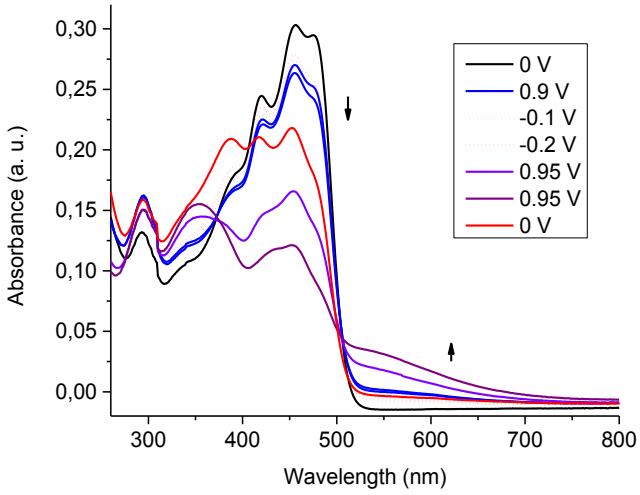

Figure S1-42 Change in absorption spectra of **3D** with switching the applied potential up to 1 V max.

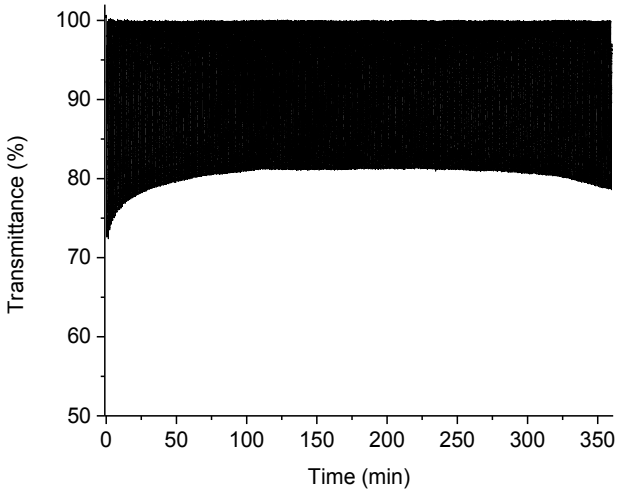

Figure S1-43 Change in percent transmittance of **3D** monitored at 709 nm with applied potentials switched between 1.1 V and -0.3 V vs Ag^{o} at 30 sec intervals over 6 hours corrected for the baseline drift overtime at 100% transmittance.

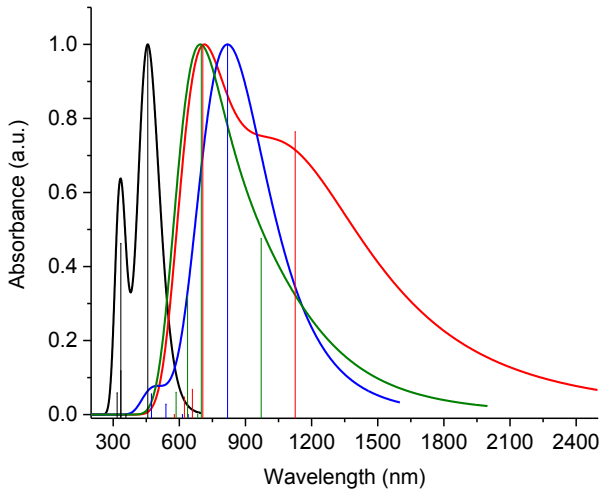

Figure S1-44 Calculated absorption spectra of **2B** via TD-DFT with CAM-B3LYP/6-311+g(d,p) in dichloromethane as the continuum solvent of the neutral singlet (—), radical cation (—), dication (—), and triplet dication (—). The vertical lines are the discrete calculated transitions for the given multiplicity and charge.

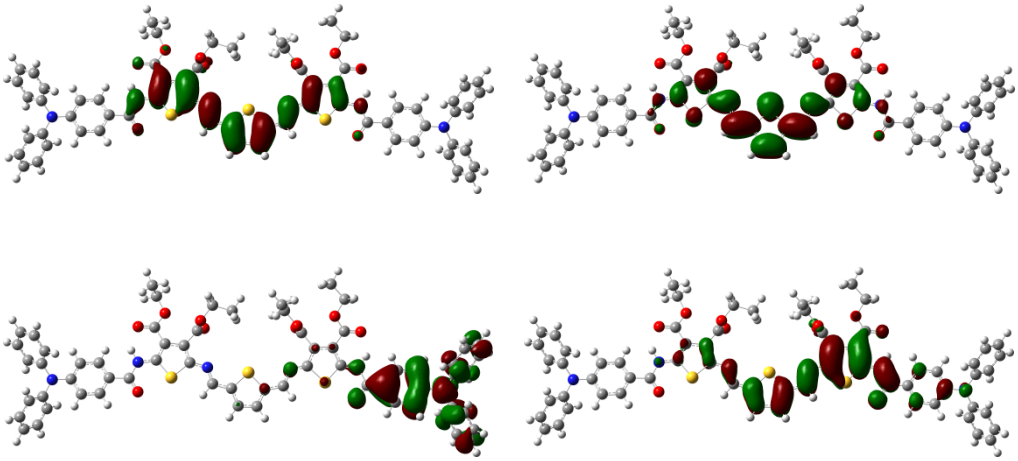

Figure S1-45 Calculated NTOs of the α–HOMO (top left), β–HOMO (bottom left), α–LUMO (top right), and β–LUMO (bottom right) Frontier orbitals of the radical cation of **2A** that are principally involved in the excitation transition at 706 nm.

References

S1) M. Mulholland, D. Navarathne, S. Khedri and W. G. Skene, *New J. Chem.*, 2014, **38**, 1668-1674.

SUPPORTING INFORMATION II
NMR SPECTRA

Extending the duty cycle of azomethine electrochromes by structural modification

Yohan Gautier and W. G. Skene

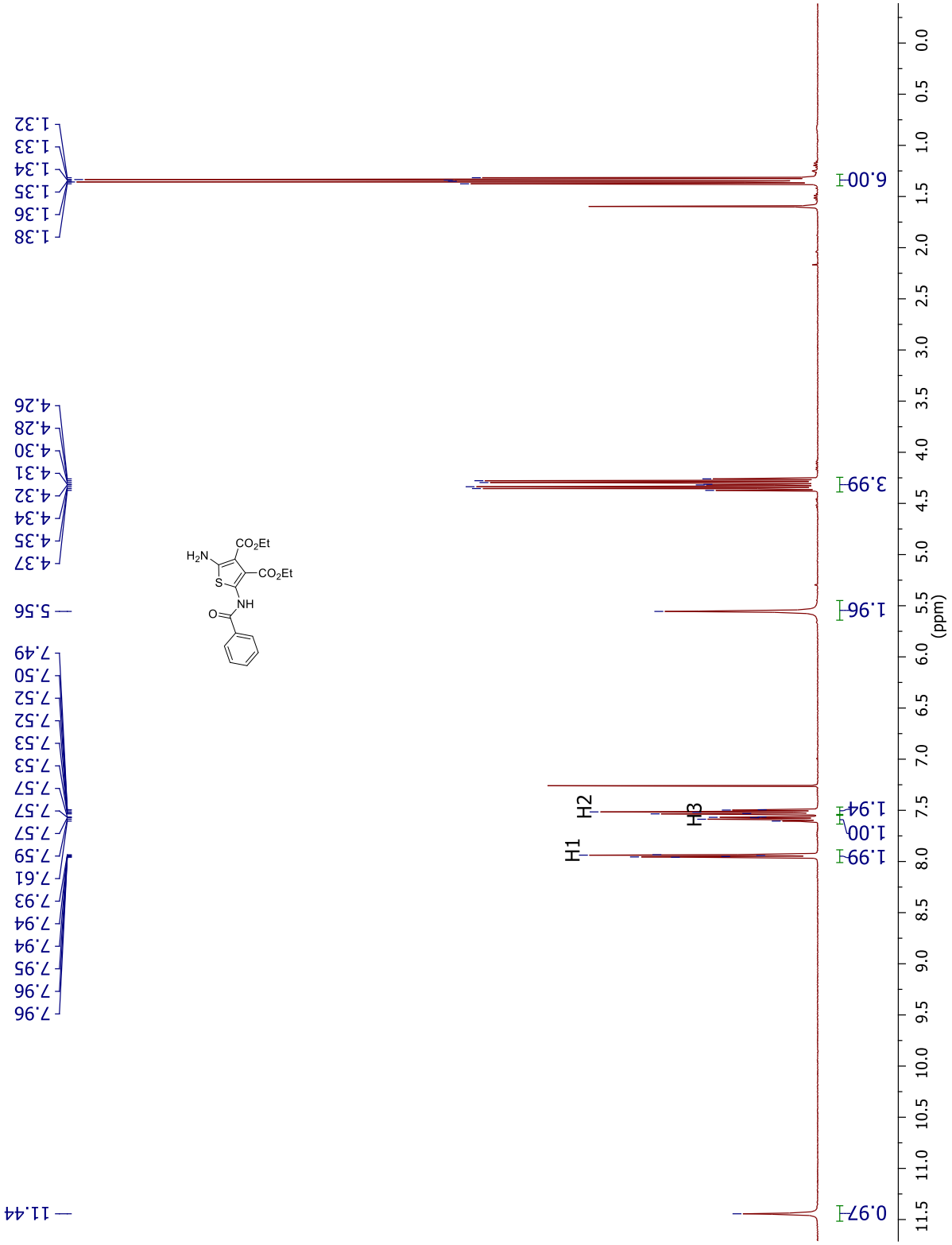

Figure S1-46. ^{1}H NMR spectrum of **1** in deuterated chloroform.

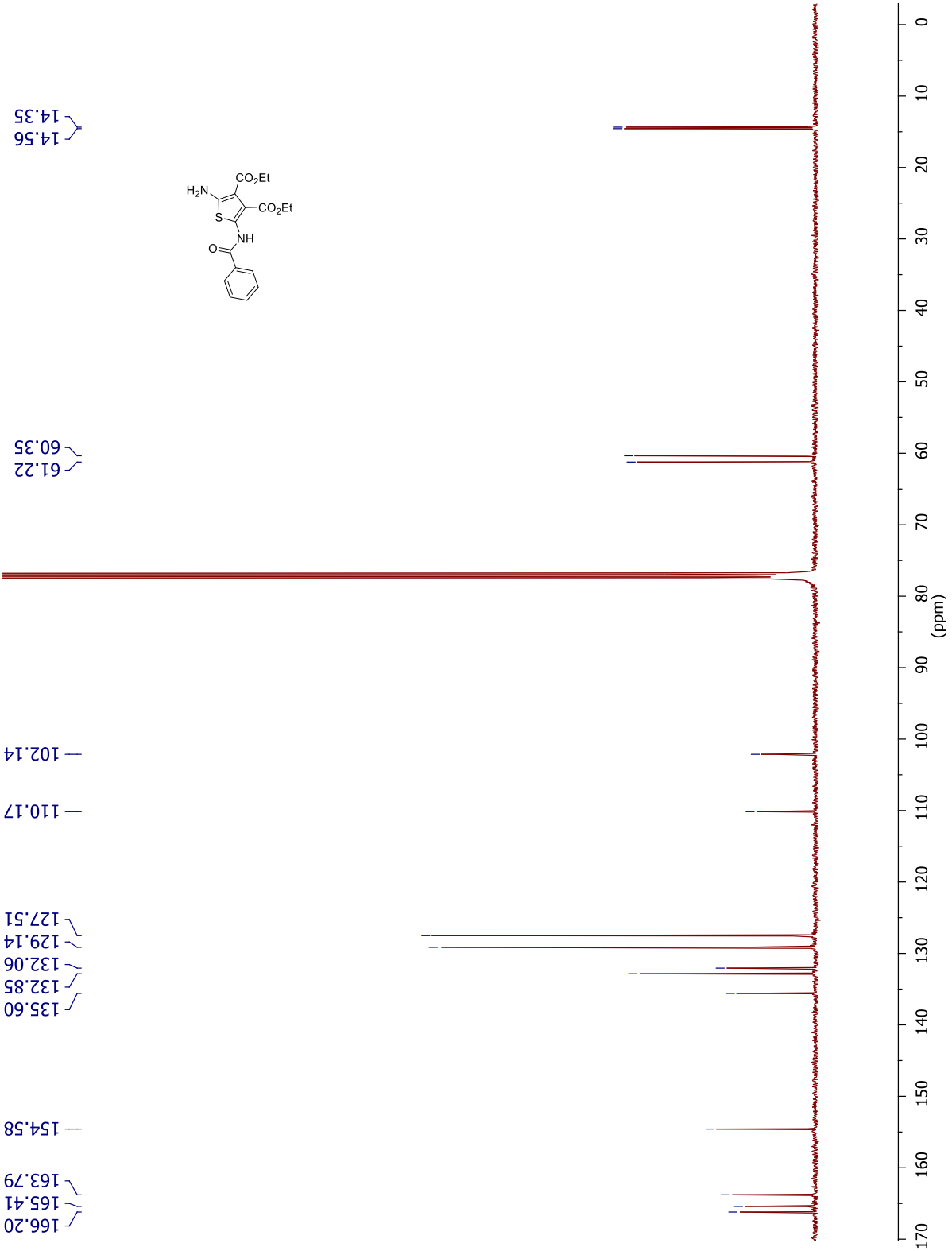

Figure S1-47. ^{13}C NMR spectrum of **1** in deuterated chloroform.

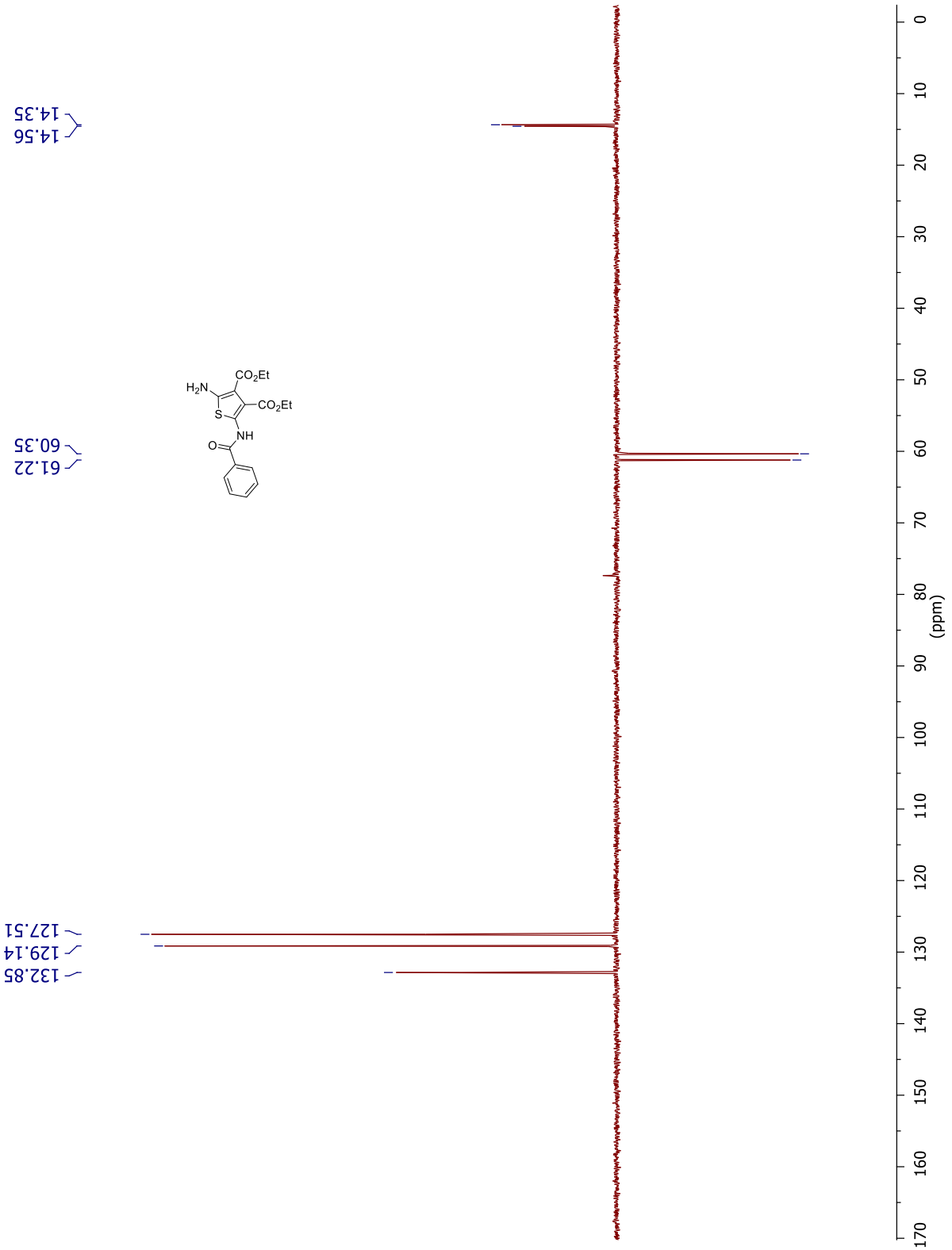

Figure S1-48. DEPT-135 NMR spectrum of **1** in deuterated chloroform.

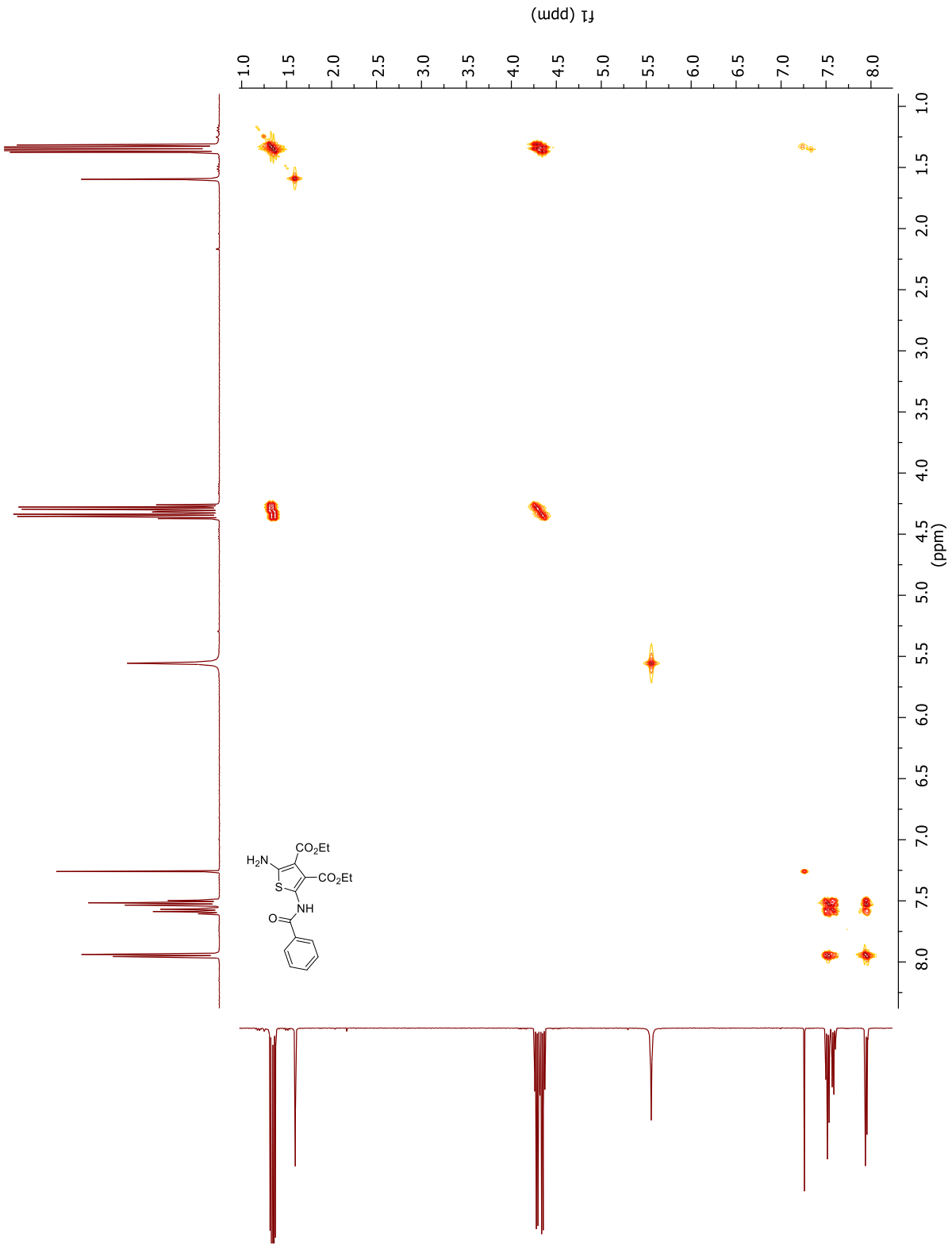

Figure S1-49. COSY ^{1}H-^{1}H correlation NMR spectrum of **1** in deuterated chloroform.

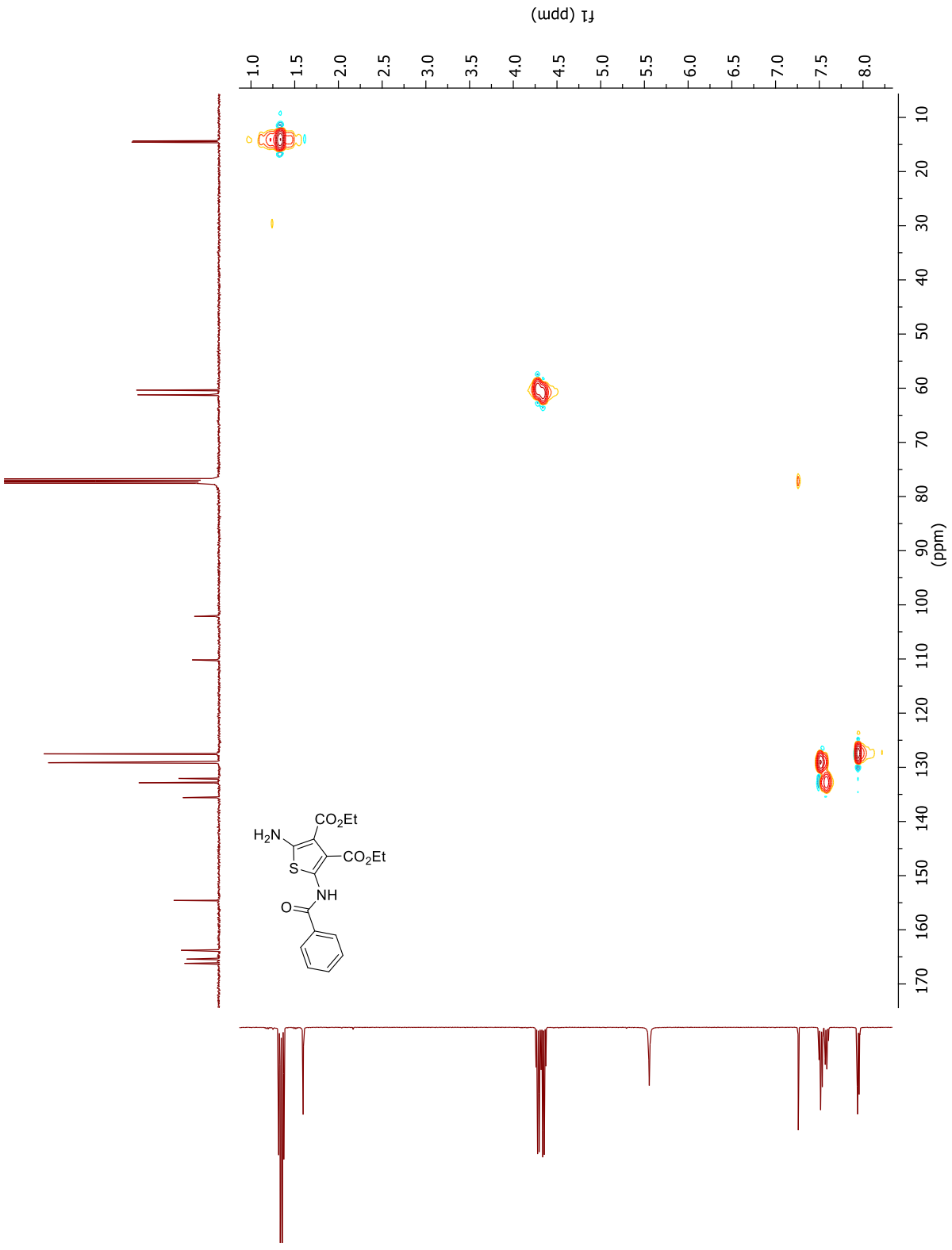

Figure S1-50. HSQC ^{13}C- ^{1}H correlation NMR spectrum of **1** in deuterated chloroform.

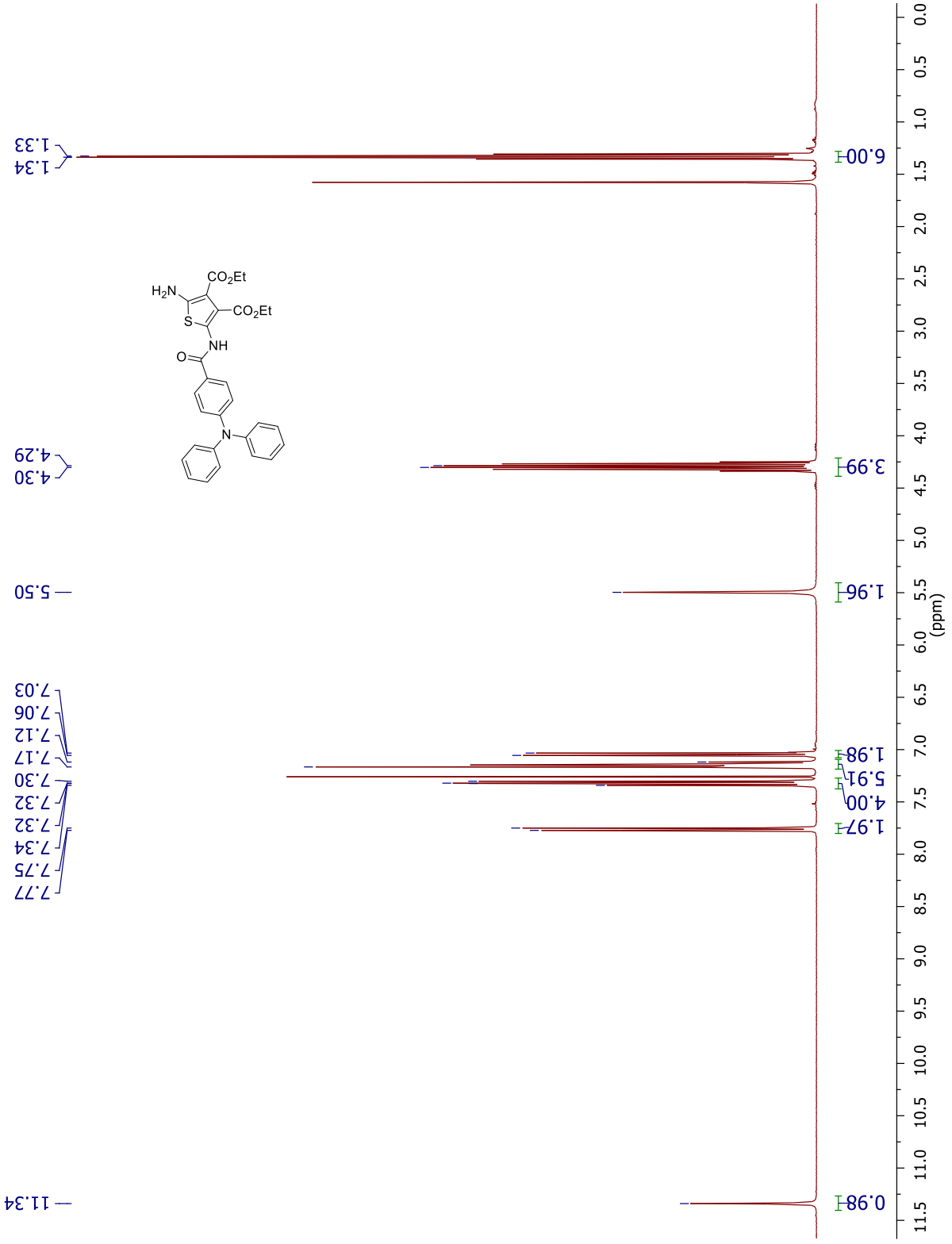

Figure S1-51. ^{1}H NMR spectrum of **2** in deuterated chloroform.

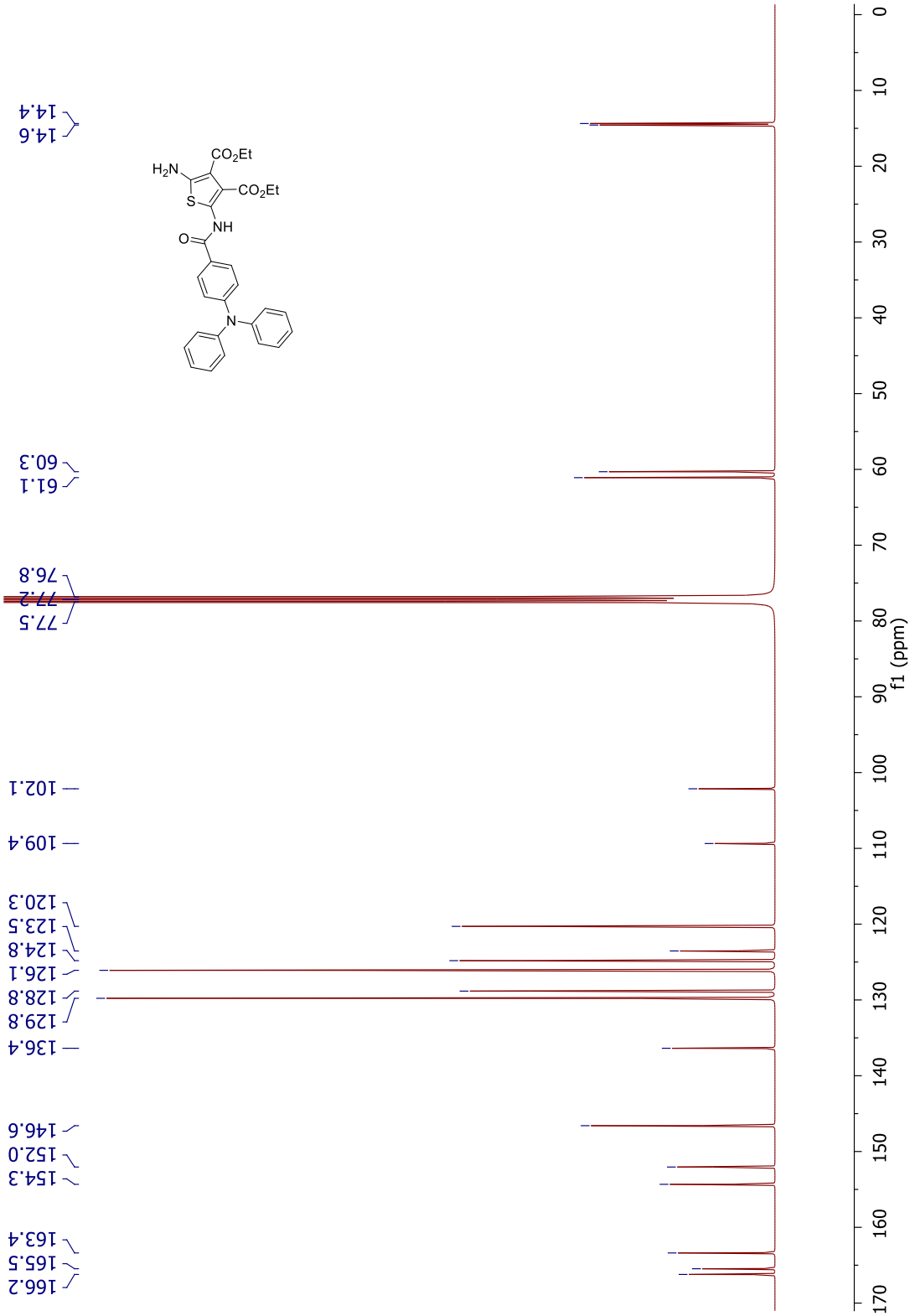

Figure S1-52. ^{13}C NMR spectrum of **2** in deuterated chloroform.

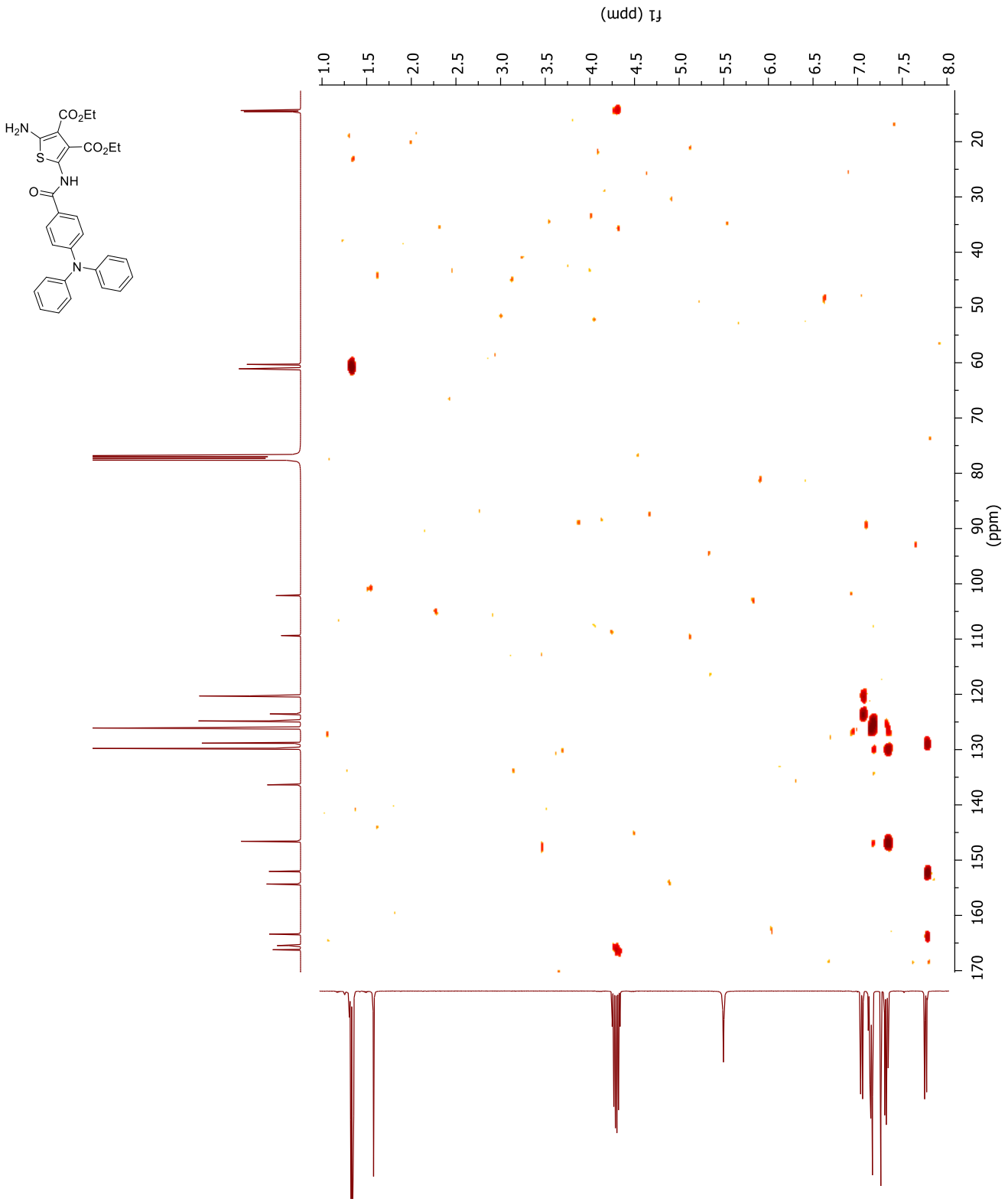

Figure S1-53. HMBC ^{13}C-^{1}H correlation NMR spectrum of **2** in deuterated chloroform.

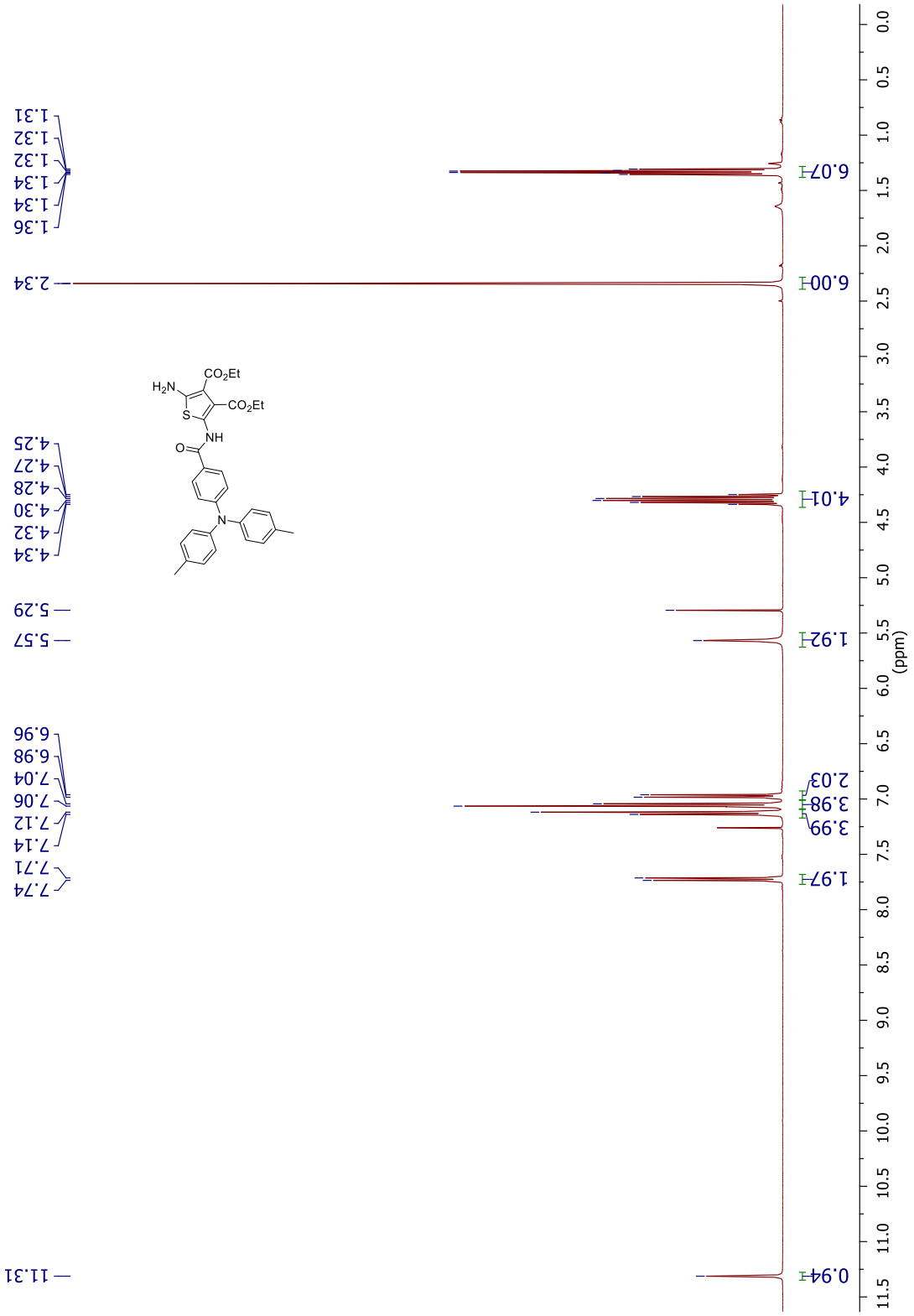

Figure S1-54. ^{1}H NMR spectrum of **3** in deuterated chloroform.

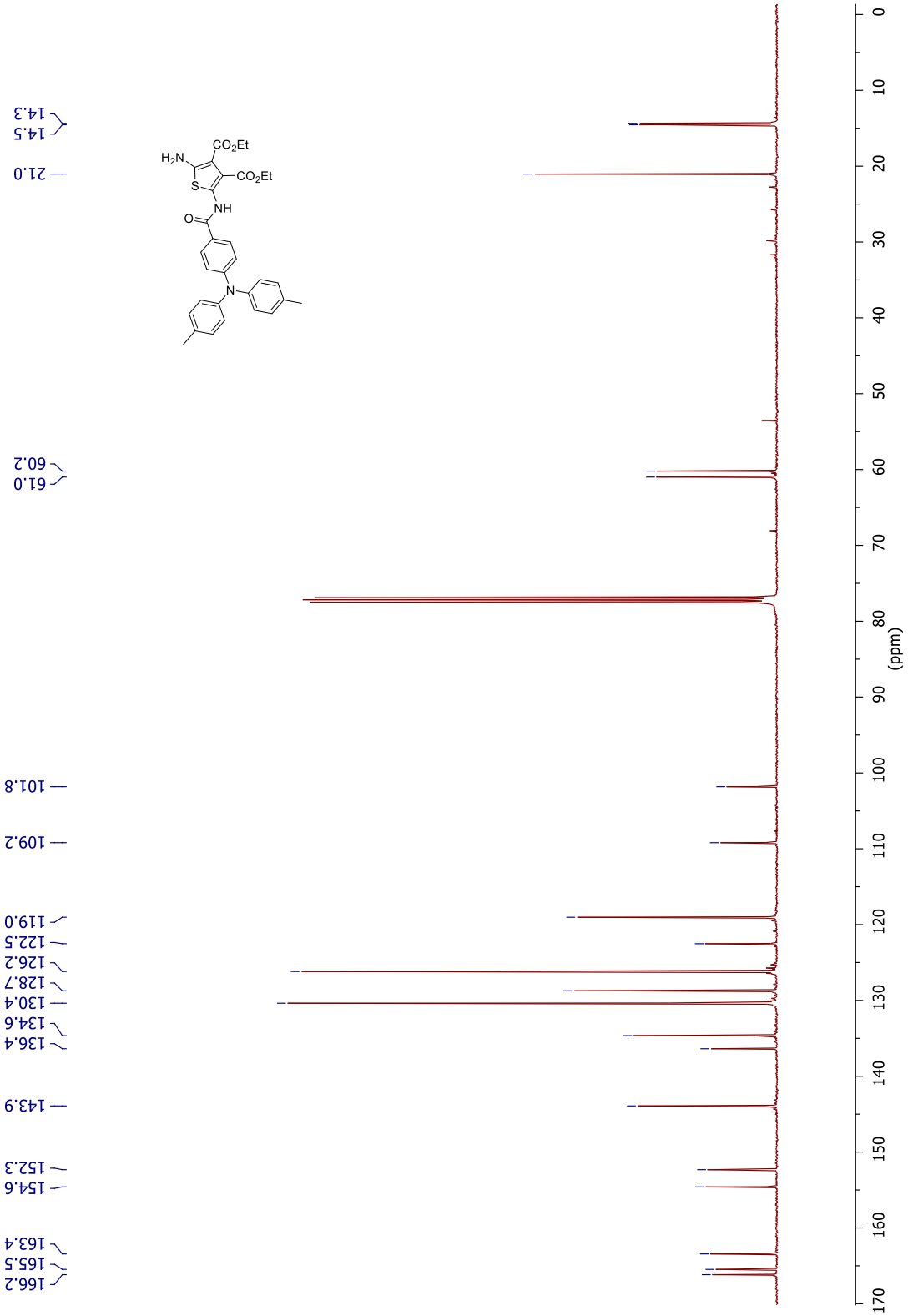

Figure S1-55. ^{13}C NMR spectrum of **3** in deuterated chloroform.

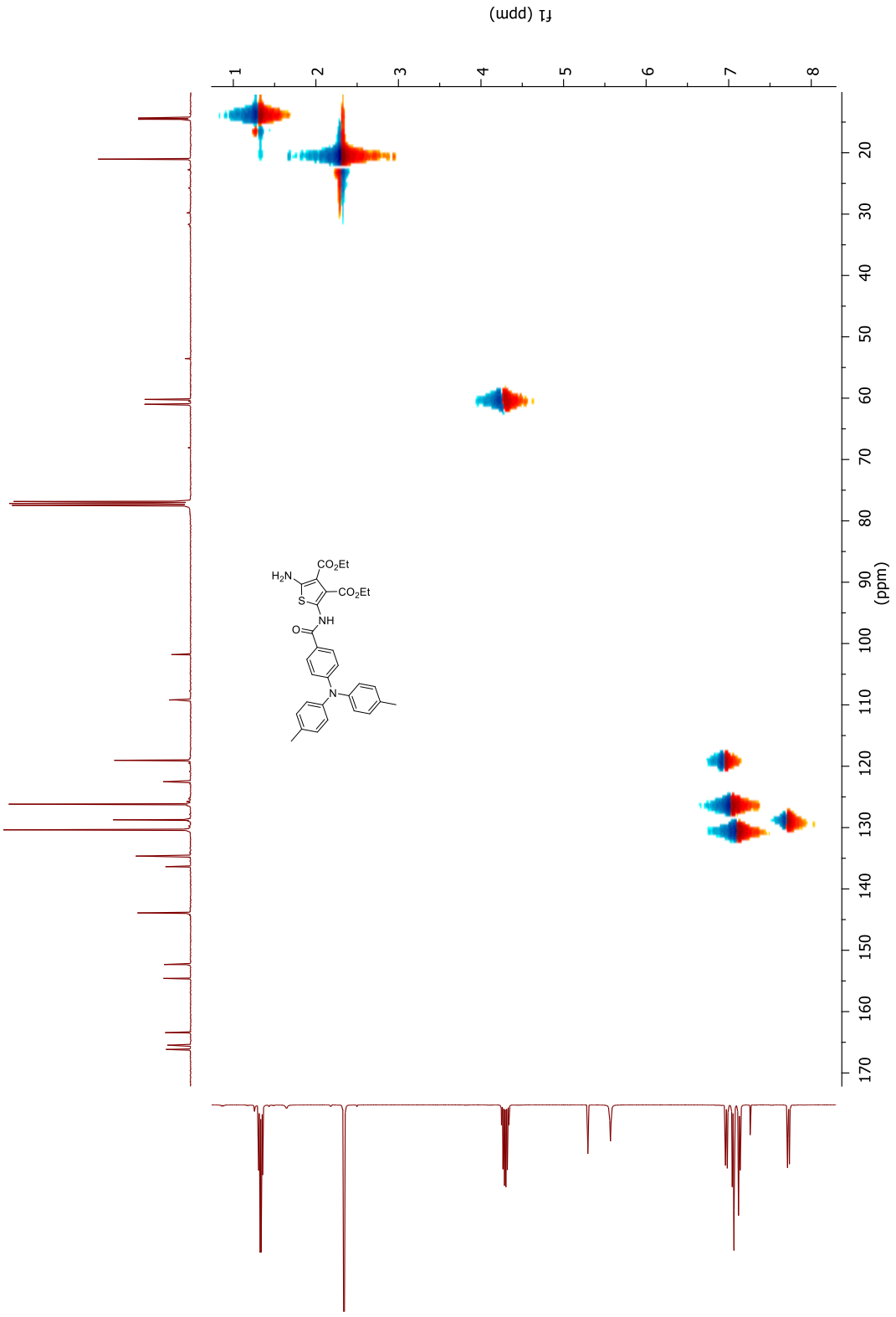

Figure S1-56. HSQC ^{13}C-^{1}H correlation NMR spectrum of **3** in deuterated chloroform.

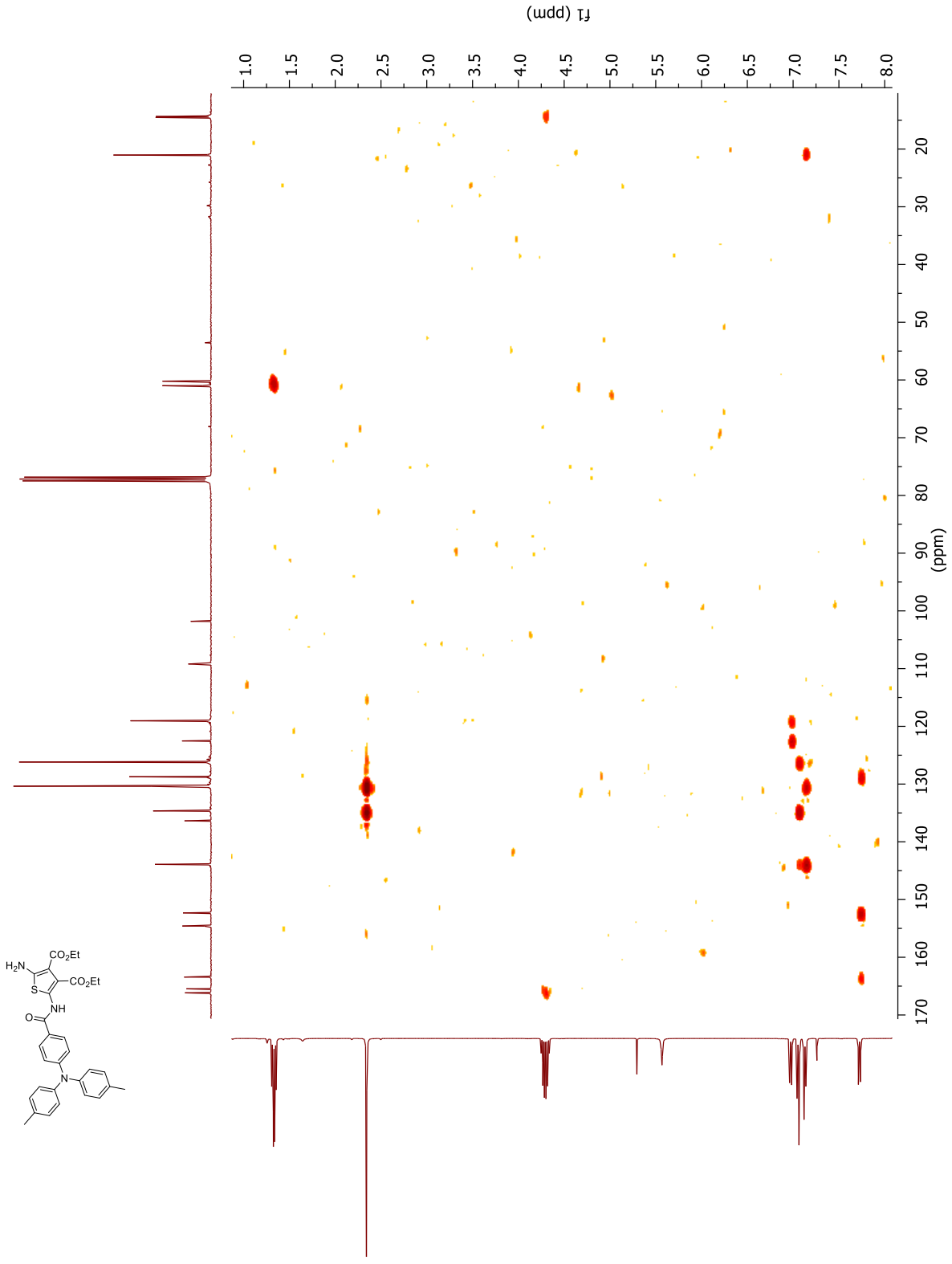

Figure S1-57. HMBC ^{13}C-^{1}H correlation NMR spectrum of **3** in deuterated chloroform.

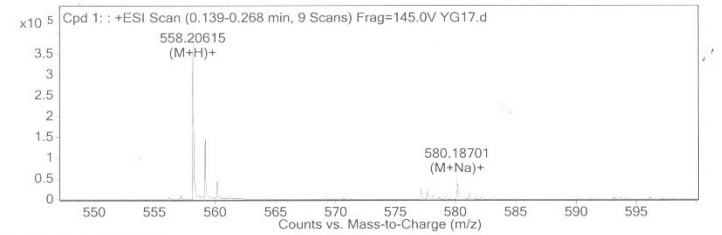

MS Spectrum Peak List

Ion	Ion Formula	Abund	*Expe. m/z*	*Calc. m/z*	Diff(ppm)
(M+H)+	C31H32N3O5S	404993.5	558.20615	558.20572	0.78
(M+Na)+	C31H31N3NaO5S	54122	580.18701	580.18766	-1.12

Figure S1-58. High resolution mass spectrum of **3**.

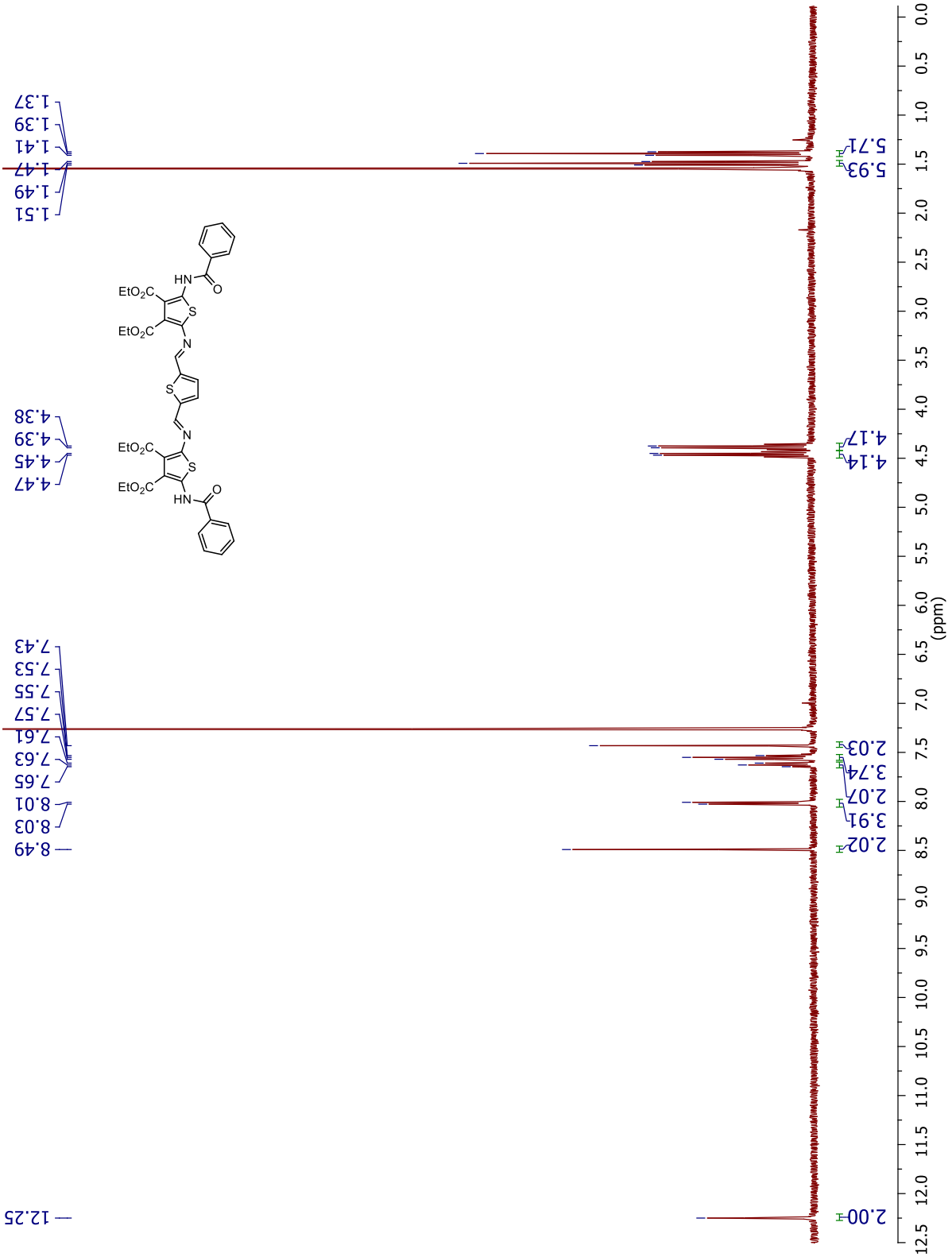

Figure S1-59. ^{1}H NMR spectrum of **1A** in deuterated chloroform.

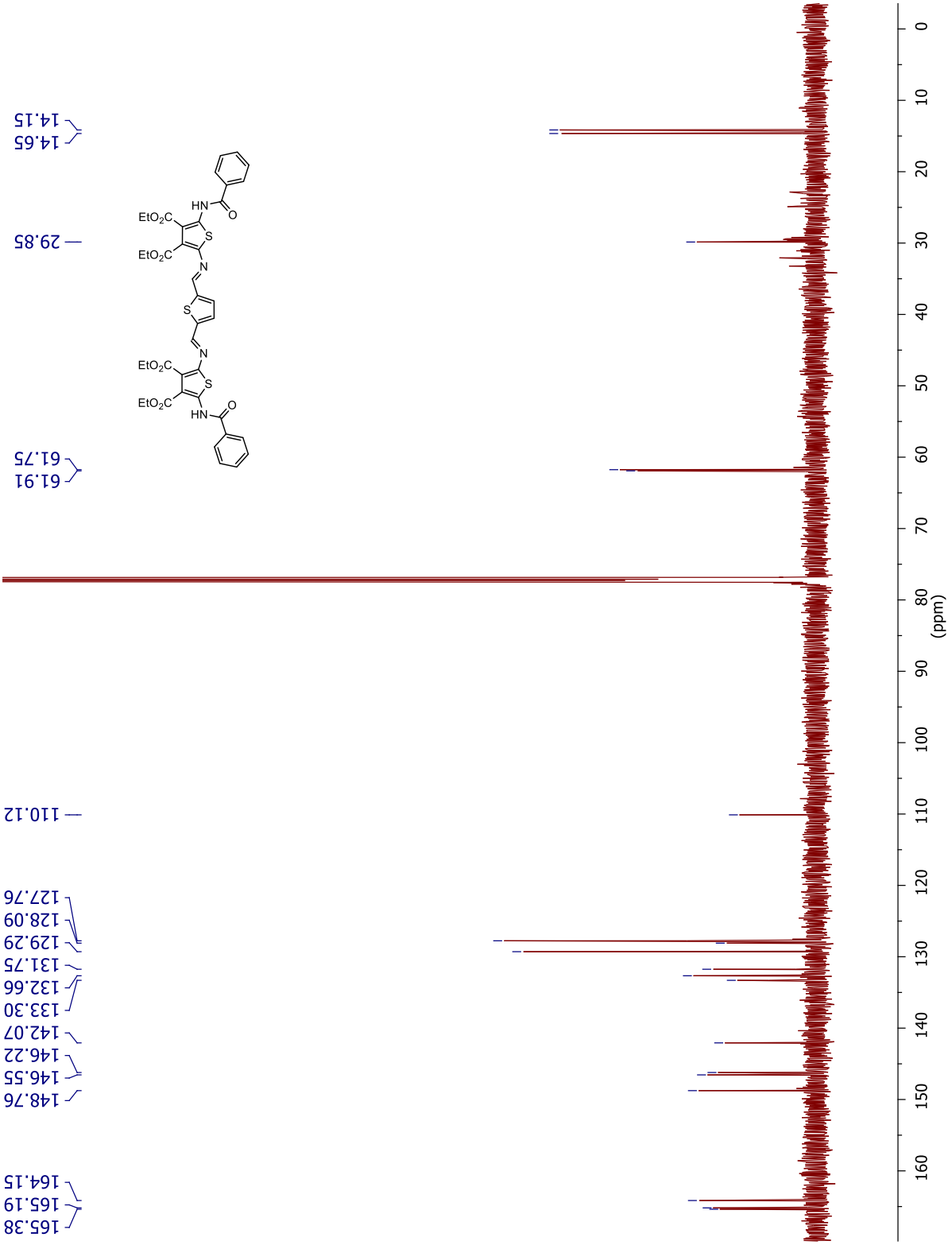

Figure S1-60. ^{13}C NMR spectrum of **1A** in deuterated chloroform.

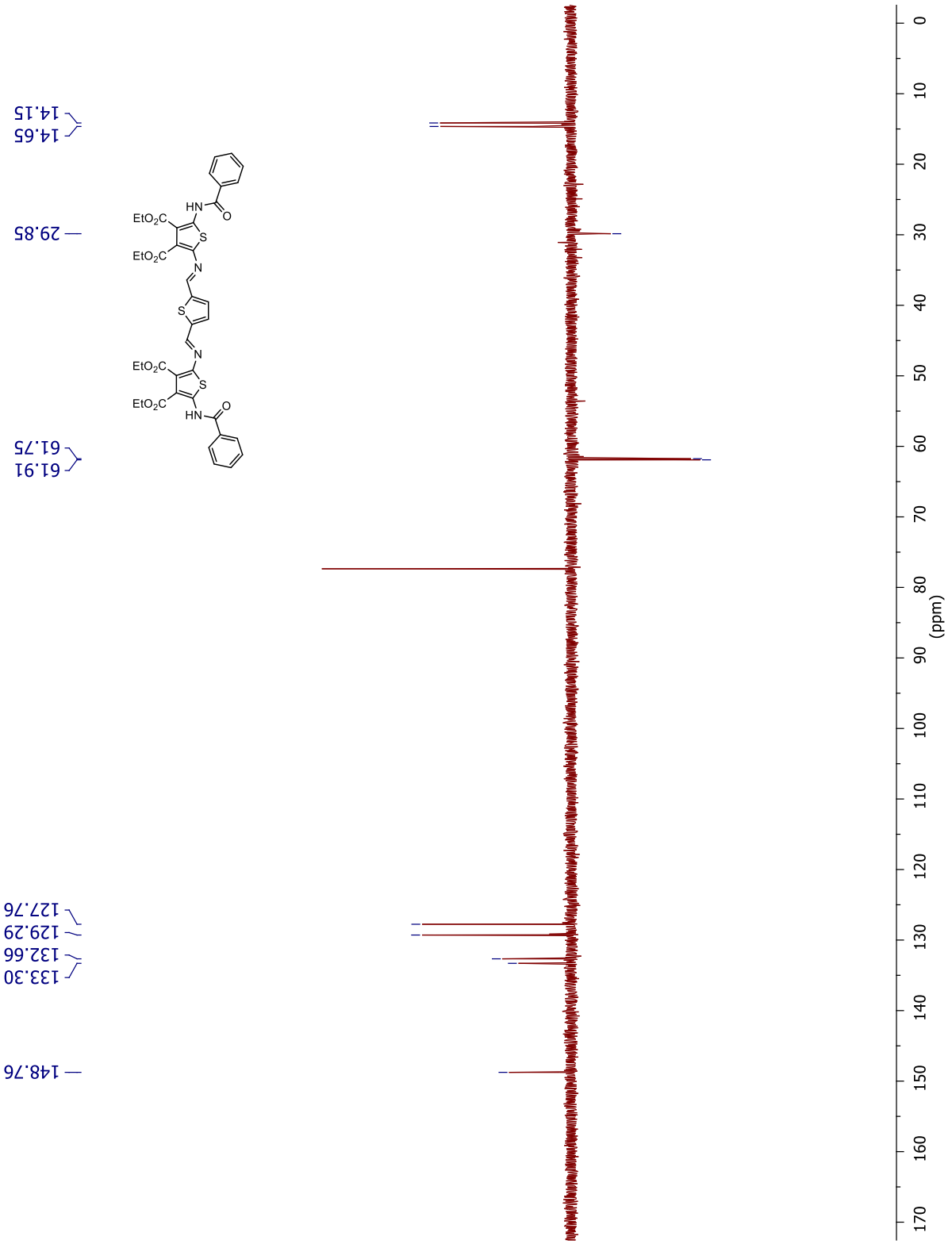

Figure S1-61. DEPT-135 NMR spectrum of **1A** in deuterated chloroform.

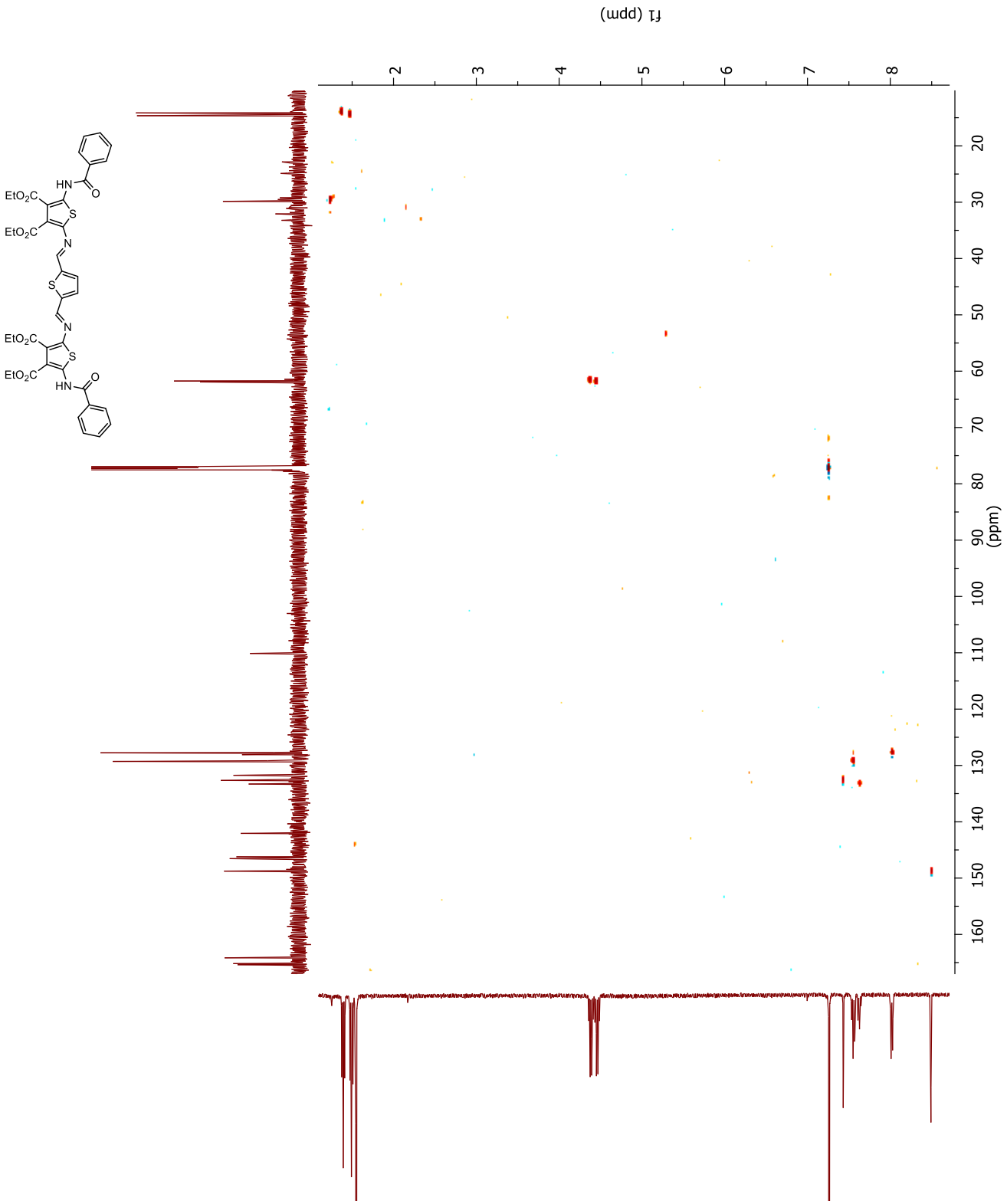

Figure S1-62. HSQC ^{13}C-^{1}H correlation NMR spectrum of **1A** in deuterated chloroform.

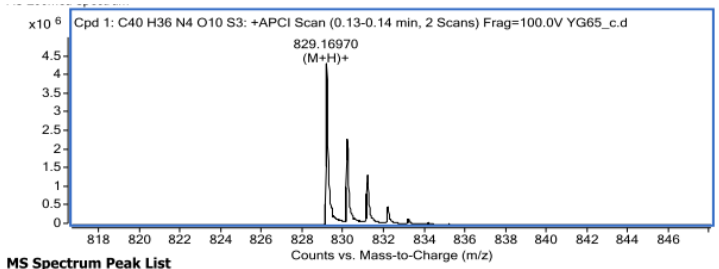

MS Spectrum Peak List

Ion	Ion Formula	Abund	*Expe. m/z*	*Calc. m/z*	Diff(ppm)
(M+H)+	C40H37N4O10S3	4313631.2	829.1697	829.16663	3.7

Figure S1-63. High resolution mass spectrum of **1A**.

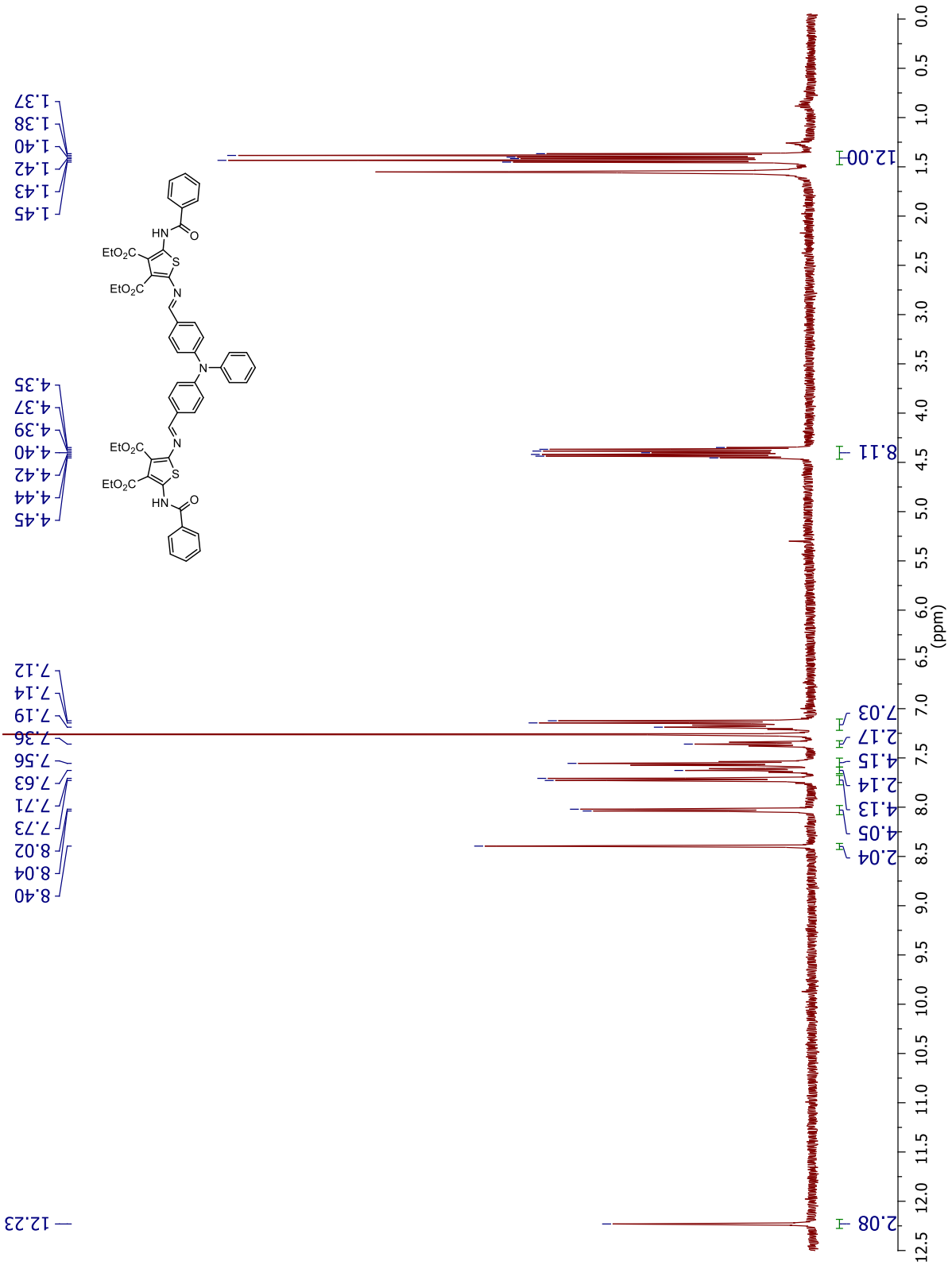

Figure S1-64. ^{1}H NMR spectrum of **1C** in deuterated chloroform.

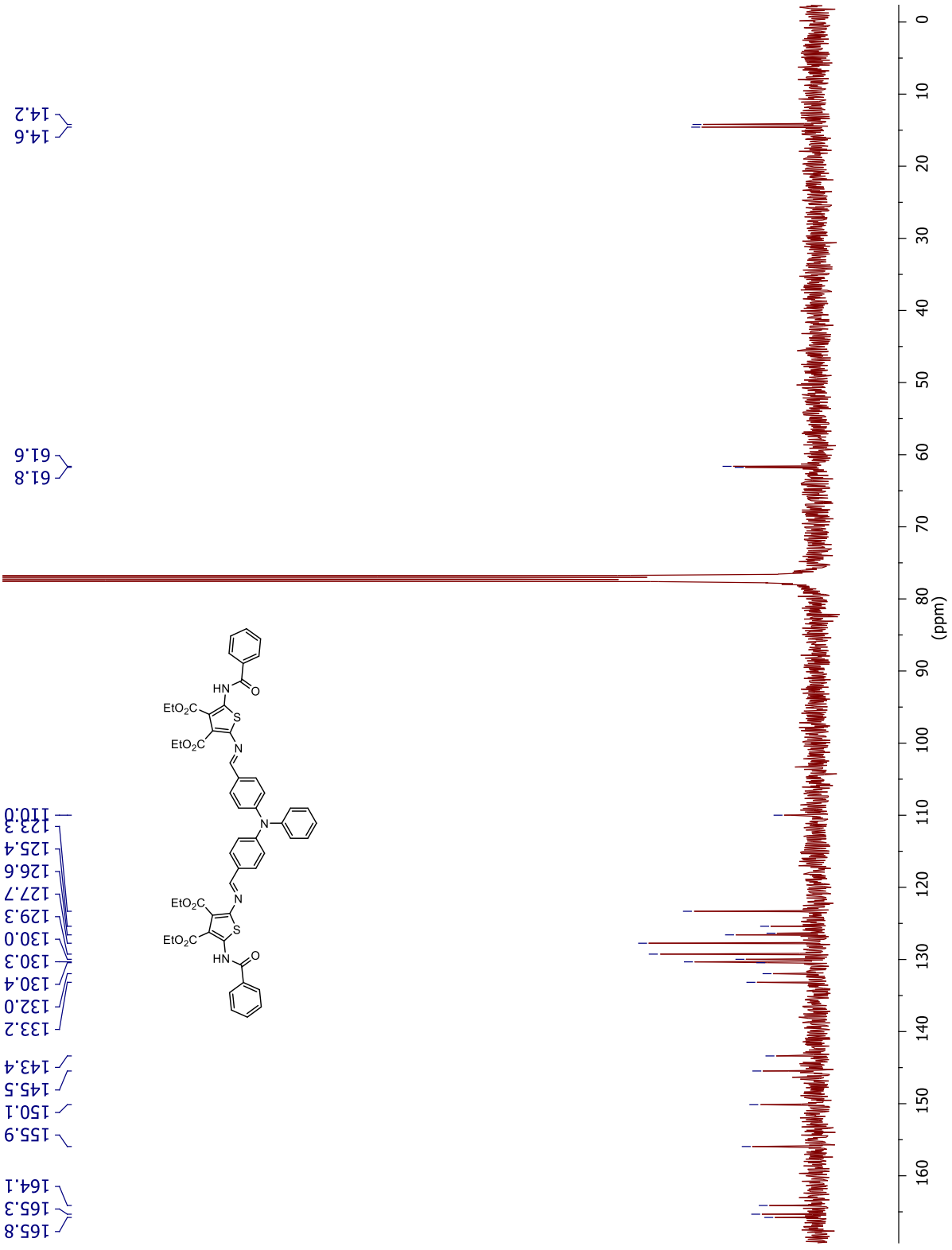

Figure S1-65. ^{13}C NMR spectrum of **1C** in deuterated chloroform.

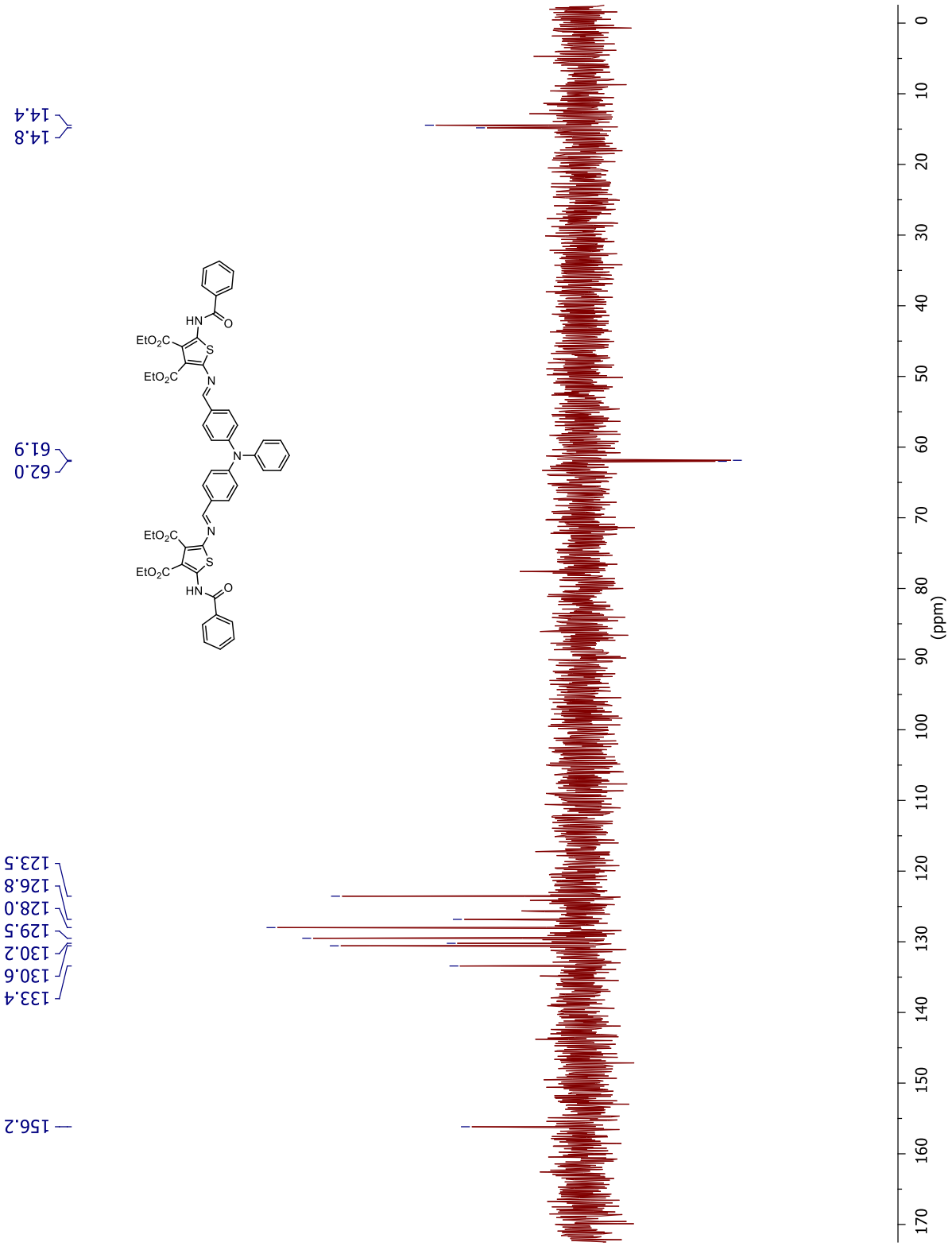

Figure S1-66. DEPT-135 NMR spectrum of **1C** in deuterated chloroform.

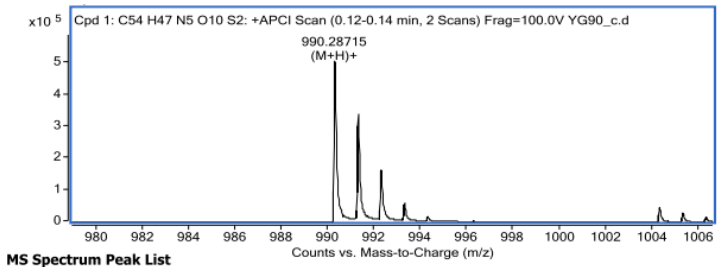

MS Spectrum Peak List

Ion	Ion Formula	Abund	*Expe. m/z*	*Calc. m/z*	Diff(ppm)
(M+H)+	C54H48N5O10S2	516216.84	990.28715	990.28371	3.47

Figure S1-67. High resolution mass spectrum of **1C**.

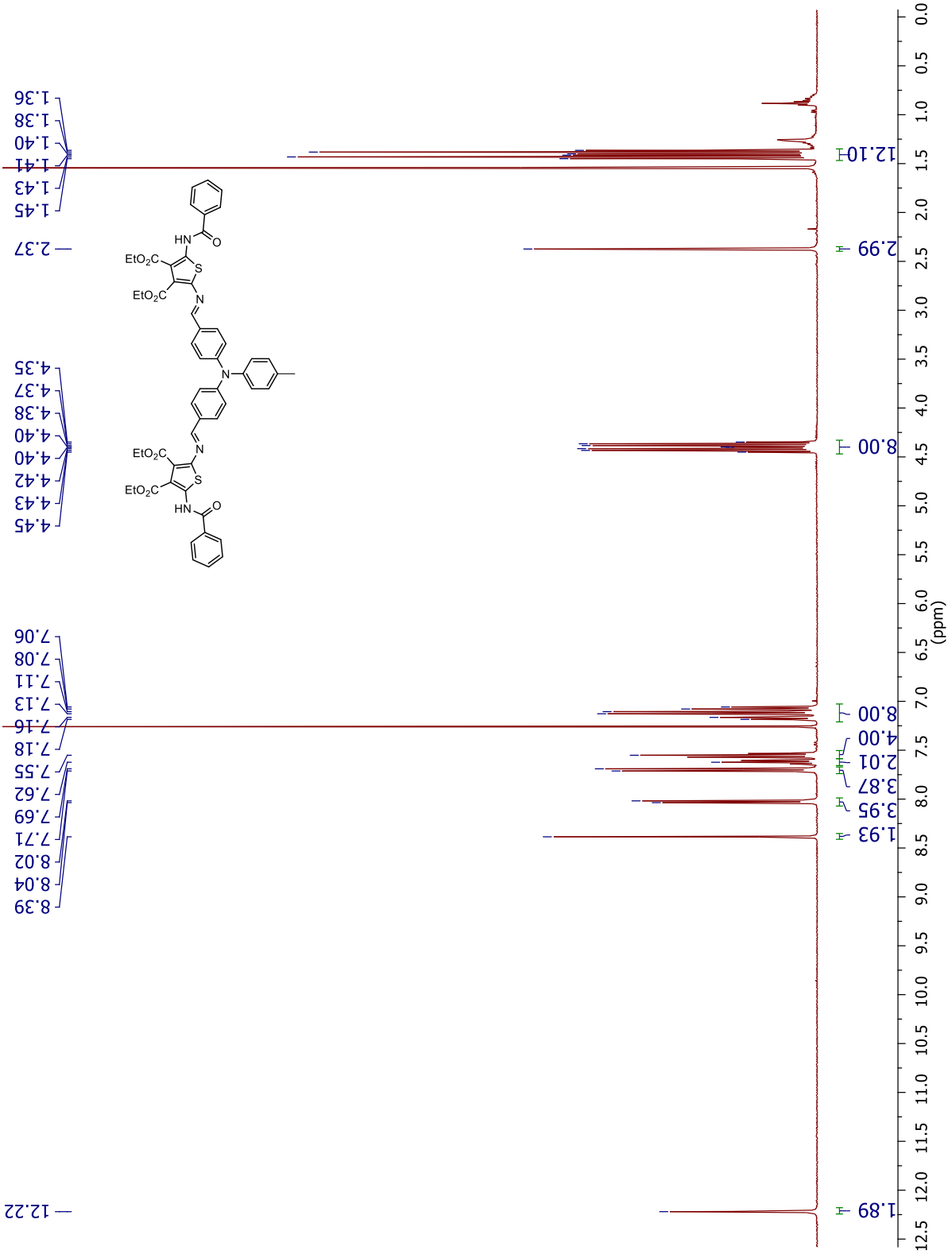

Figure S1-68. ^{1}H NMR spectrum of **1D** in deuterated chloroform.

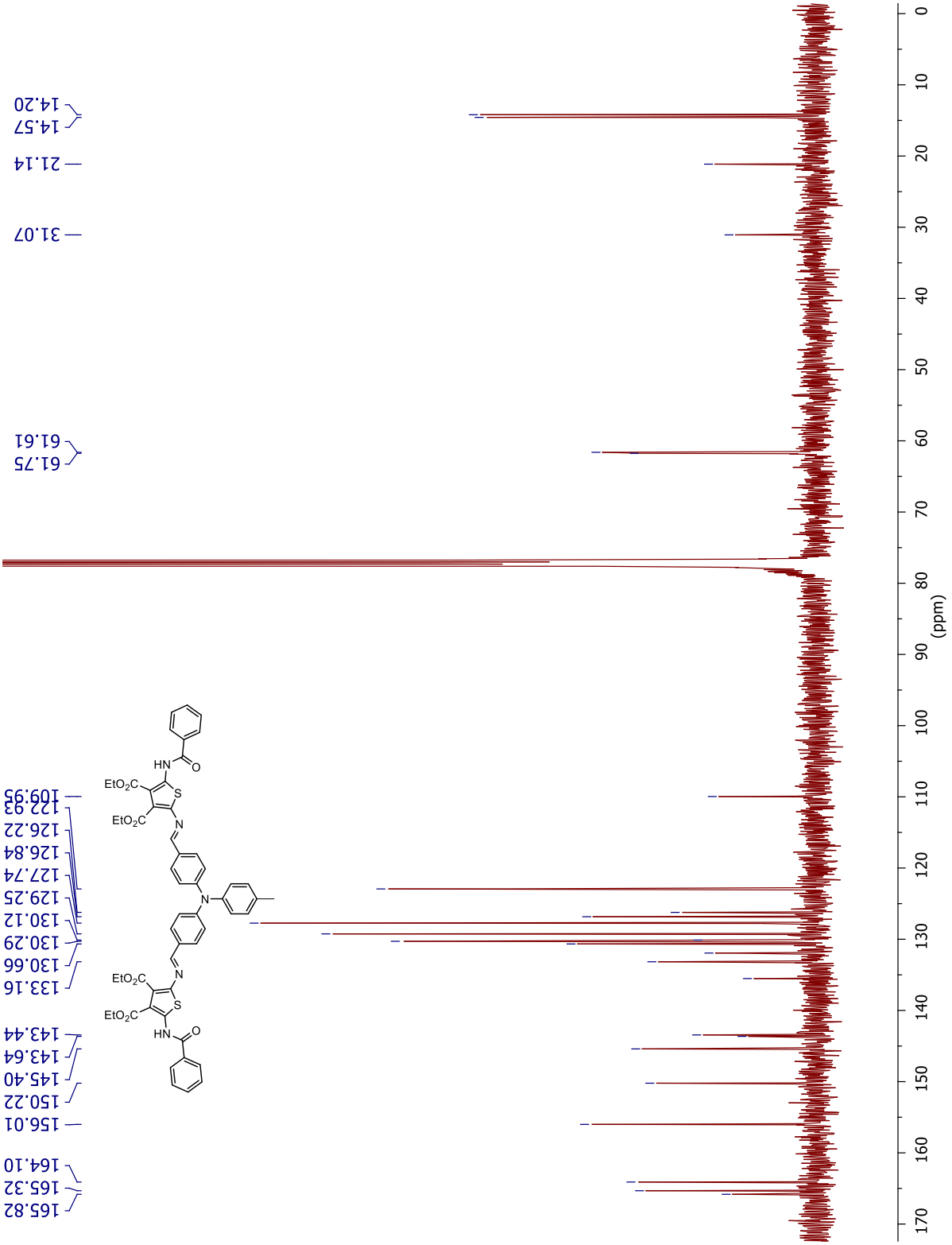

Figure S1-69. ^{13}C NMR spectrum of **1D** in deuterated chloroform.

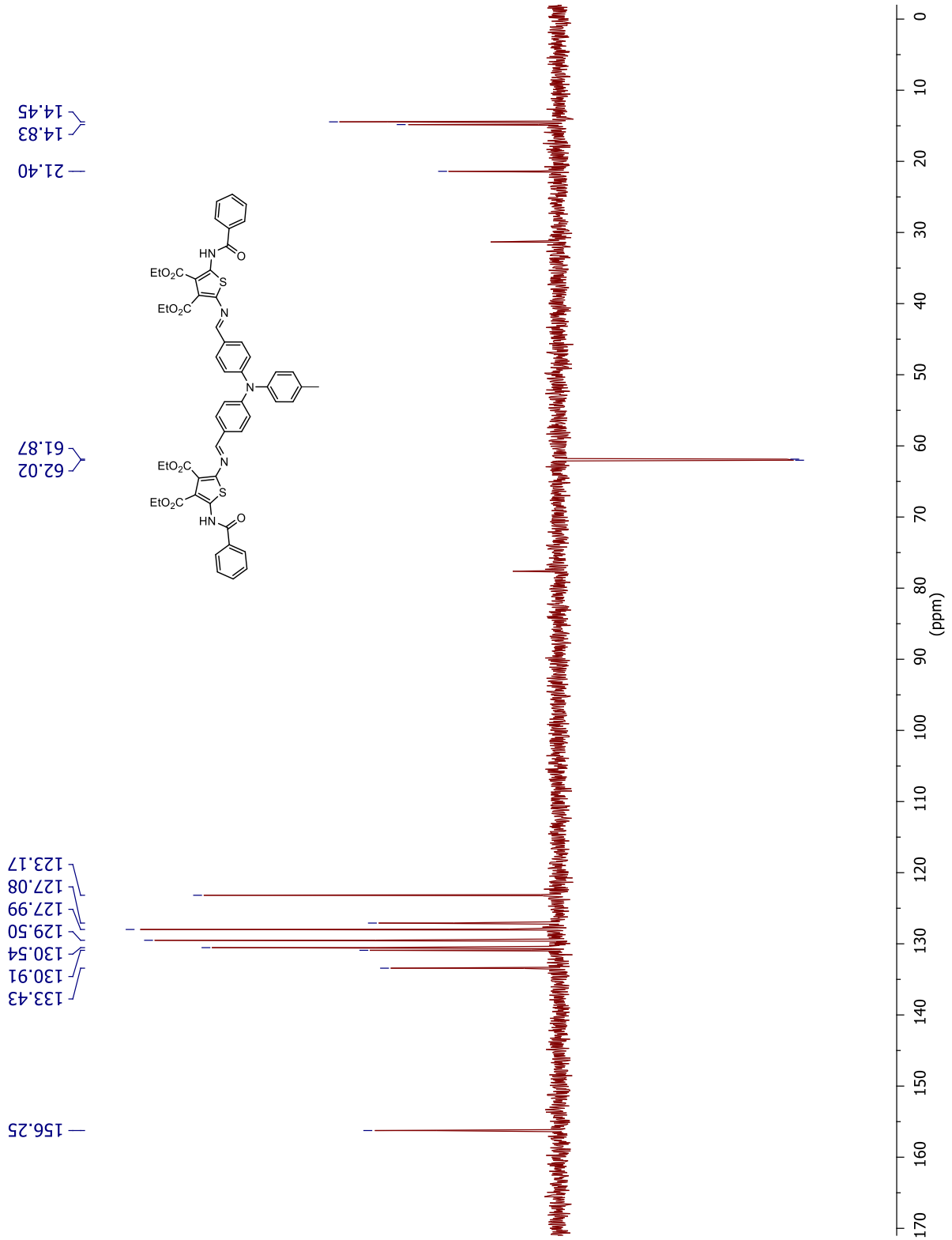

Figure S1-70. DEPT-135 NMR spectrum of **1D** in deuterated chloroform.

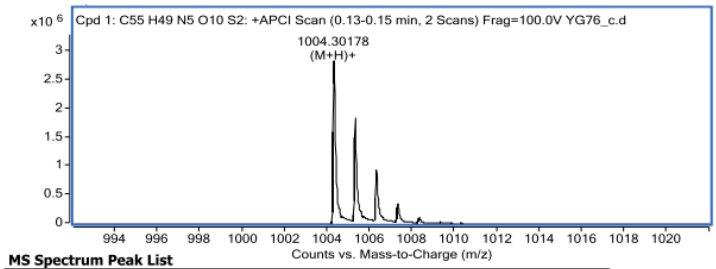

MS Spectrum Peak List

Ion	Ion Formula	Abund	*Expe. m/z*	*Calc. m/z*	Diff(ppm)
(M+H)+	C55H50N5O10S2	2839879.48	1004.30178	1004.29936	2.41

Figure S1-71. High resolution mass spectrum of **1D**.

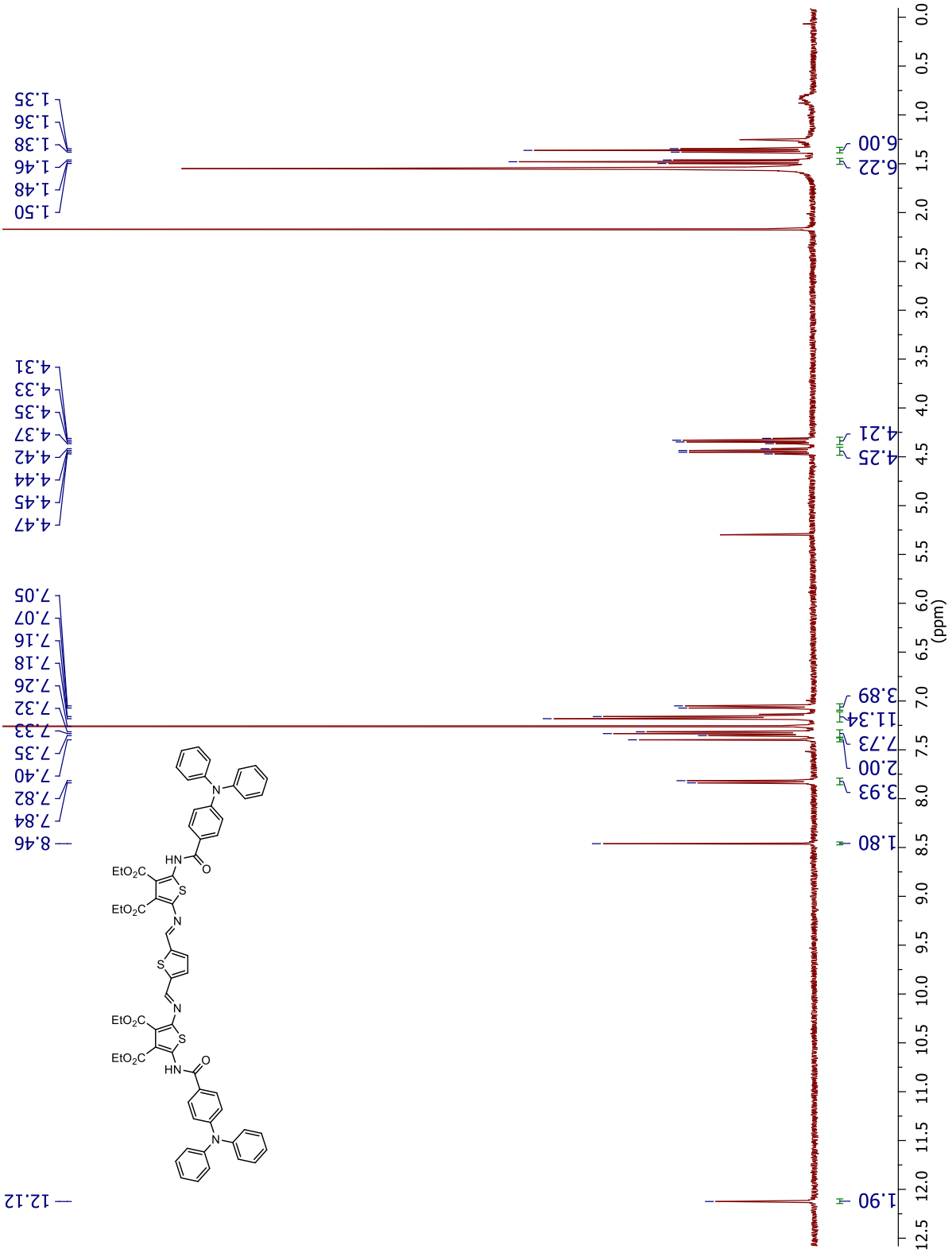

Figure S1-72. ^{1}H NMR spectrum of **2A** in deuterated chloroform.

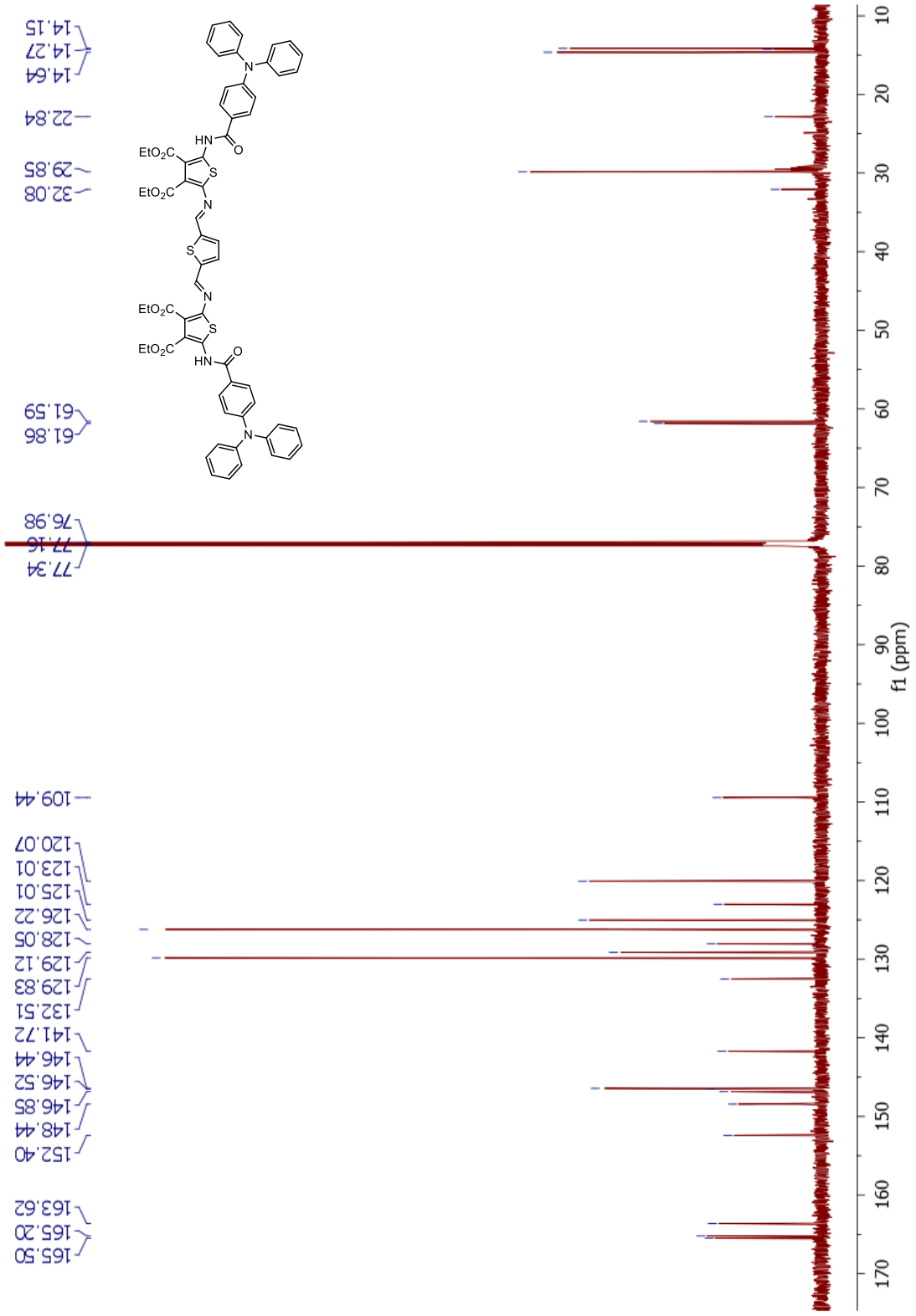

Figure S1-73. ^{13}C NMR spectrum of **2A** in deuterated chloroform.

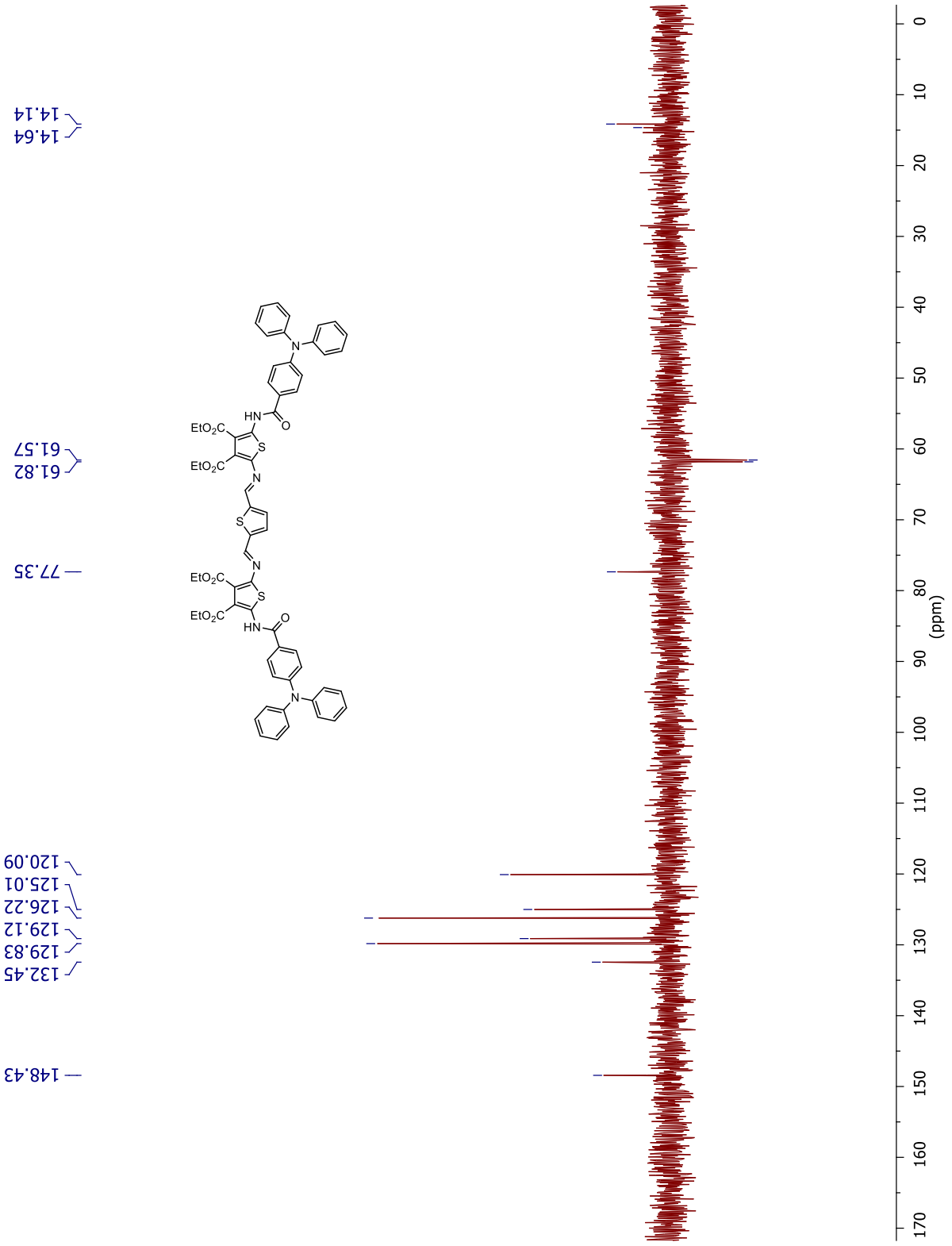

Figure S1-74. DEPT-135 NMR spectrum of **2A** in deuterated chloroform.

Figure S1-75. COSY ^{1}H-^{1}H correlation NMR spectrum of **2A** in deuterated chloroform.

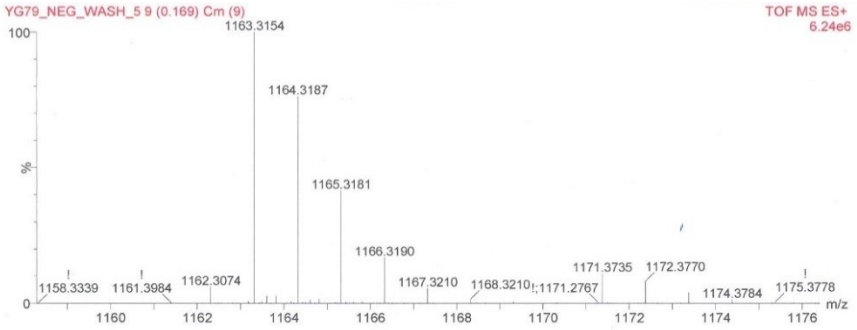

Ion	Ion Formula	Expe. m/z	Calc. m/z	Diff (ppm)
M+H	C64 H55 N6 O10 S3	1163.3154	1163.3142	1

Figure S1-76. High resolution mass spectrum of **2A**.

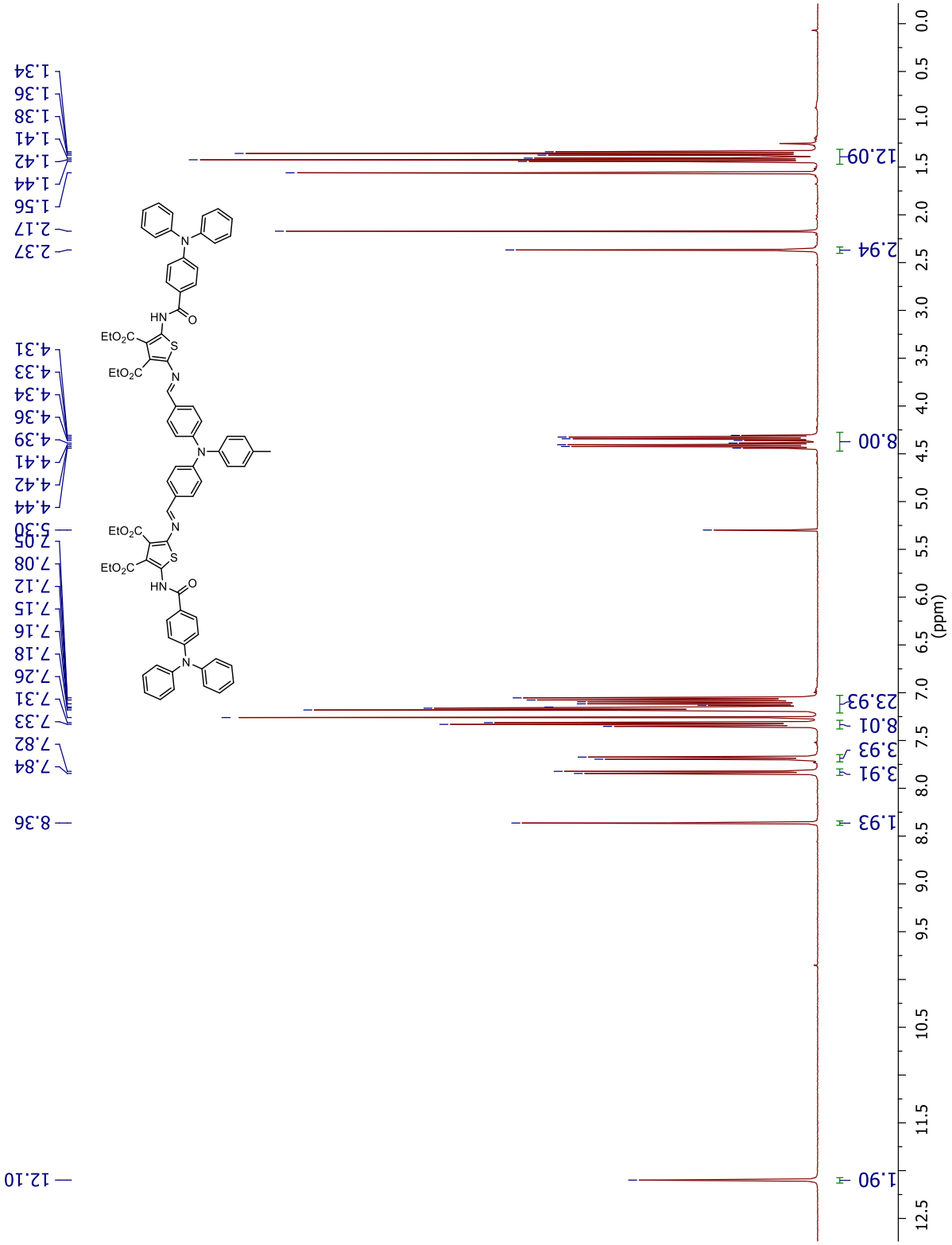

Figure S1-77. ^{1}H NMR spectrum of **2D** in deuterated chloroform.

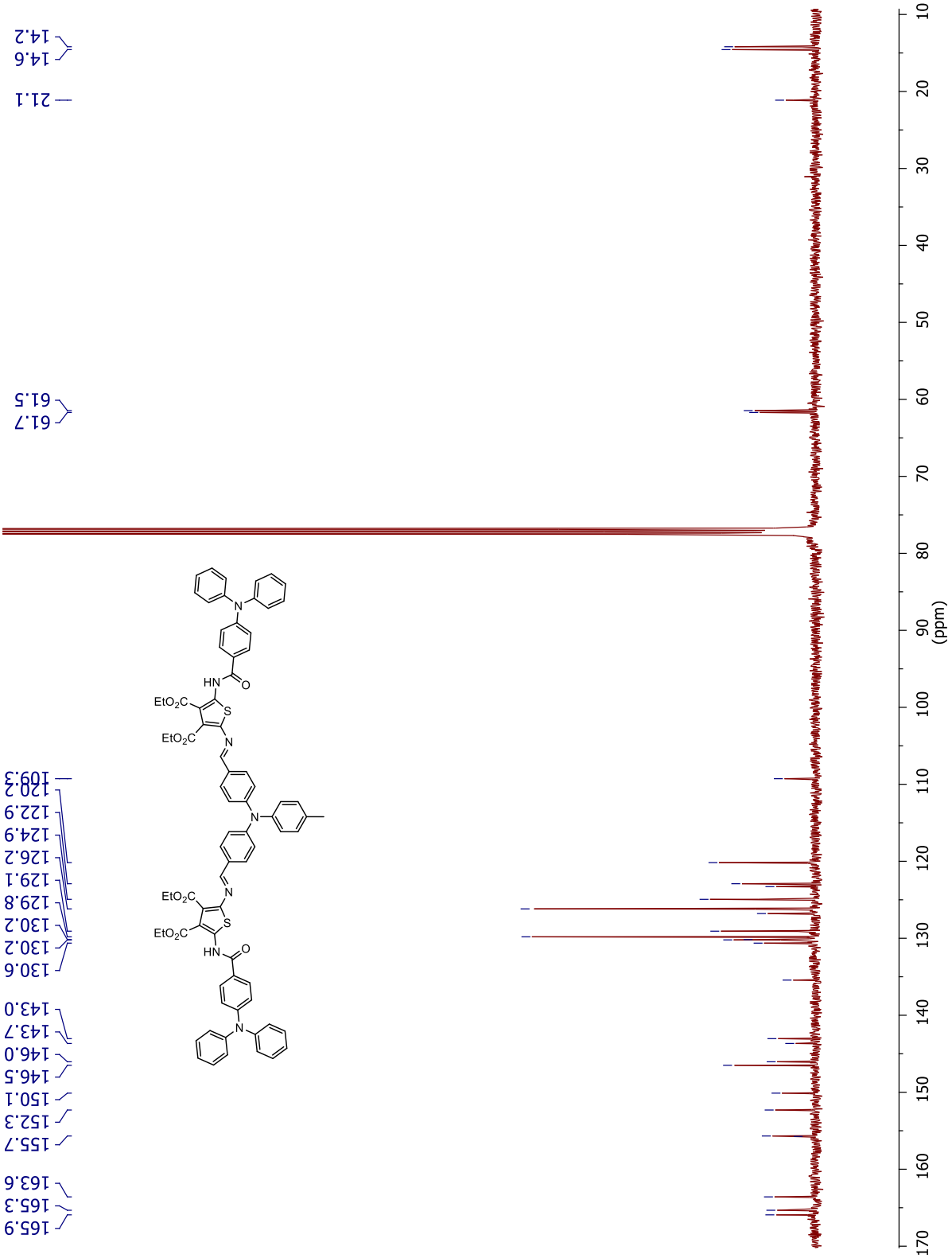

Figure S1-78. ^{13}C NMR spectrum of **2D** in deuterated chloroform.

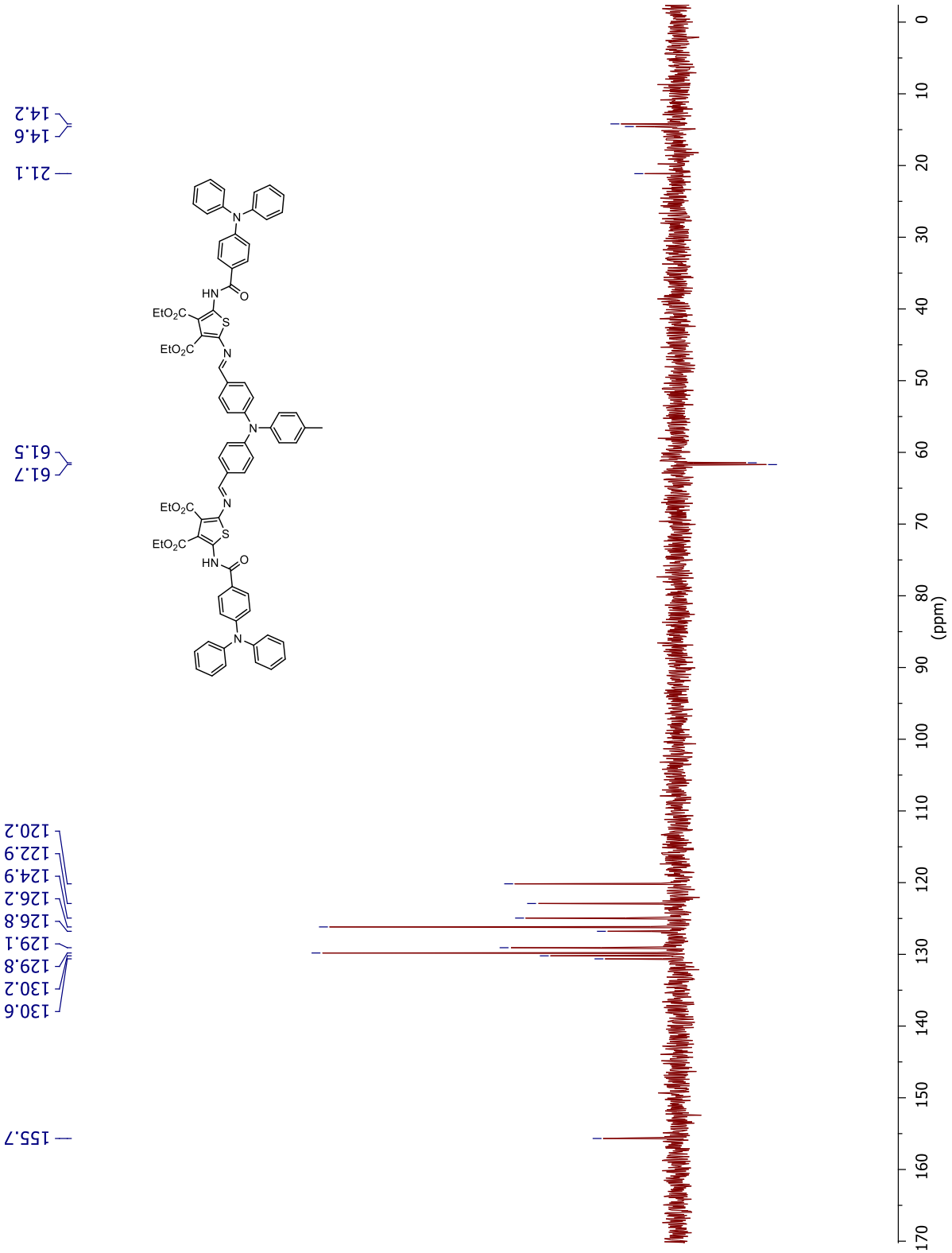

Figure S1-79. DEPT NMR spectrum of **2D** in deuterated chloroform.

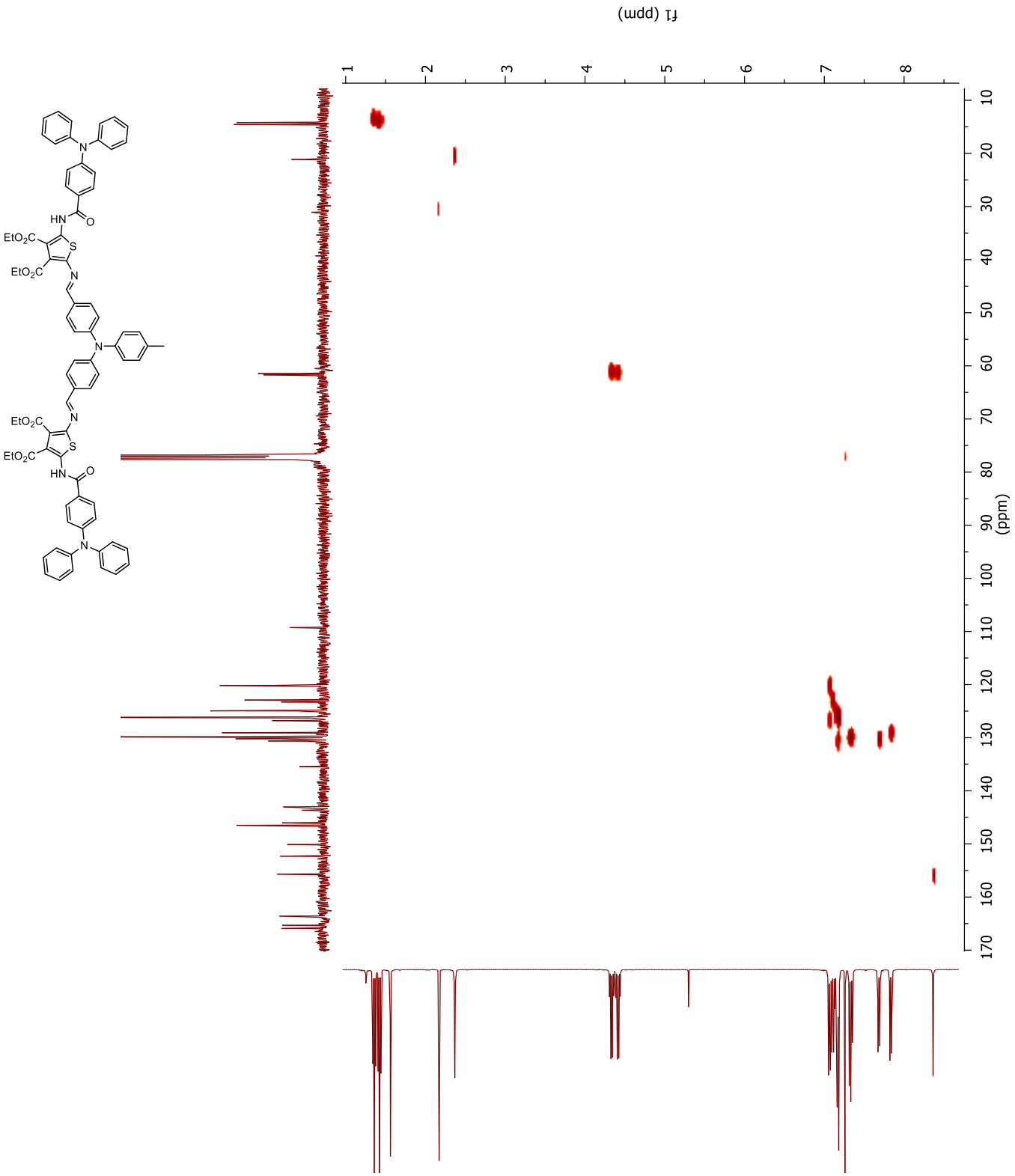

Figure S1-80. HSQC ^{13}C-^{1}H correlation NMR spectrum of **2D** in deuterated chloroform.

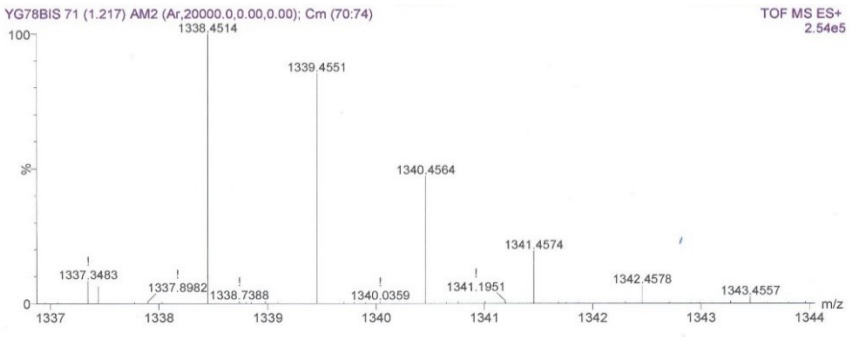

Ion	Ion Formula	Expe. m/z	Calc. m/z	Diff (ppm)
M+H	C79 H68 N7 O10 S2	1338.4514	1338.4469	3.4

Figure S1-81. High resolution mass spectrum of **2D**.

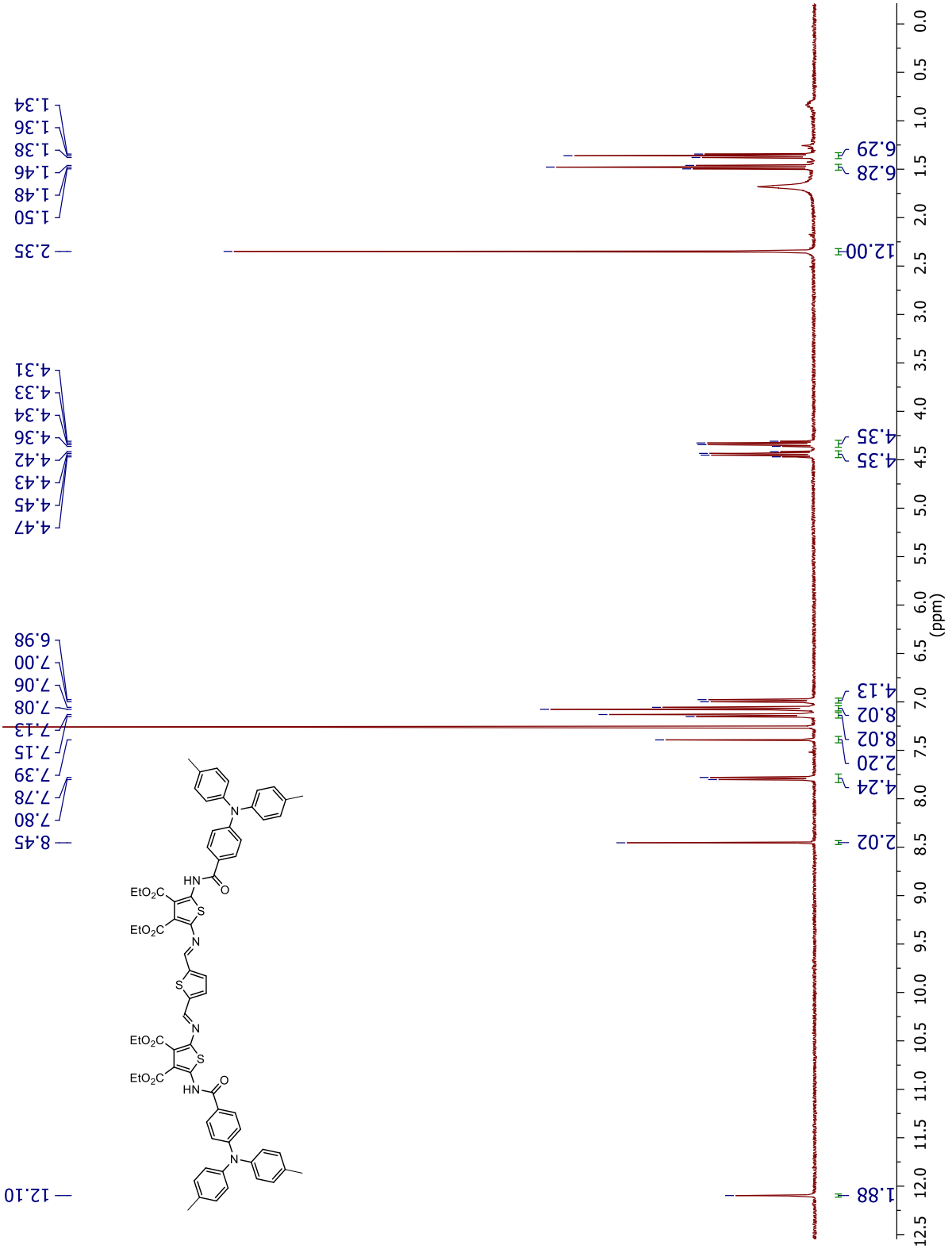

Figure S1-82. ^{1}H NMR spectrum of **3A** in deuterated chloroform.

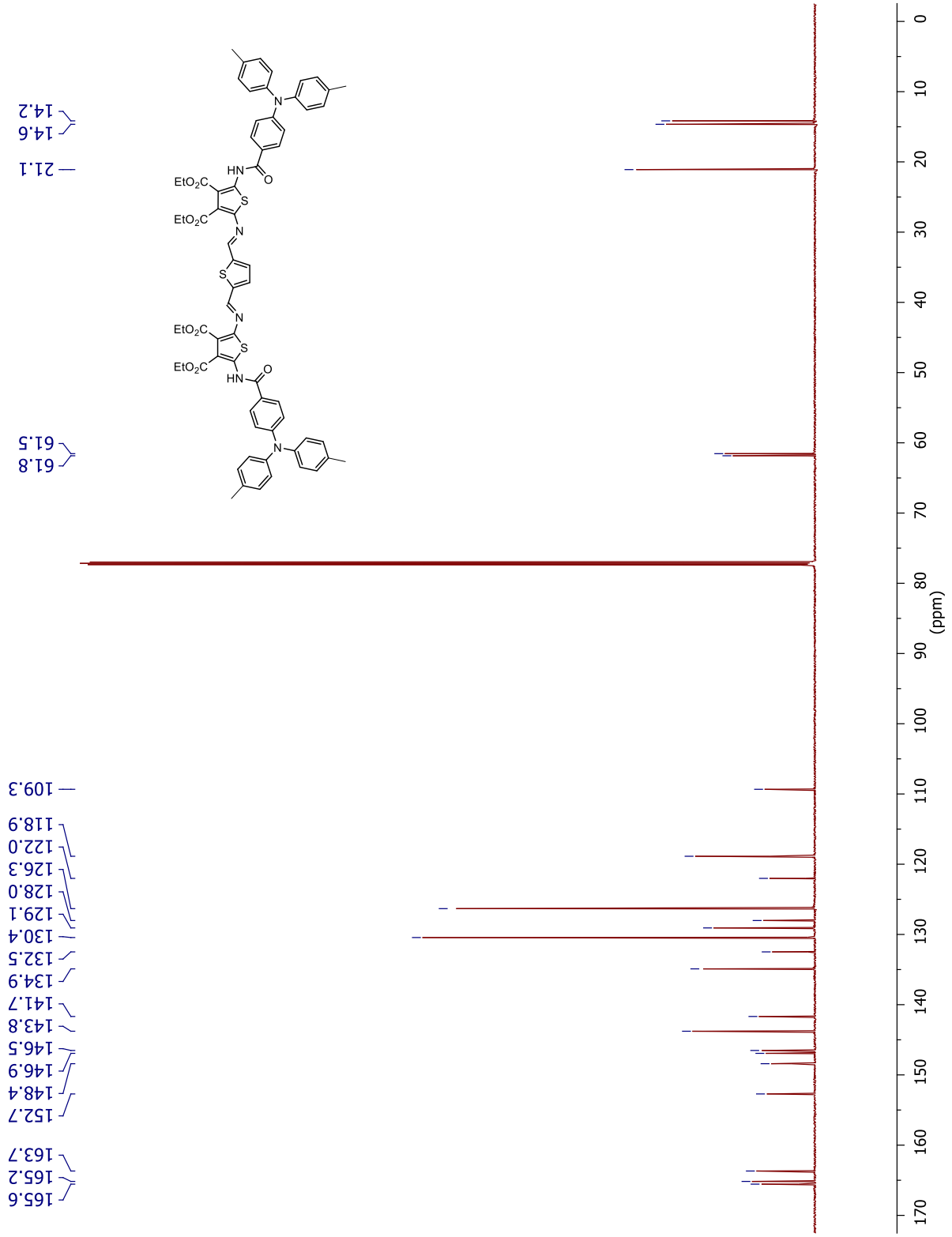

Figure S1-83. ^{13}C NMR spectrum of **3A** in deuterated chloroform.

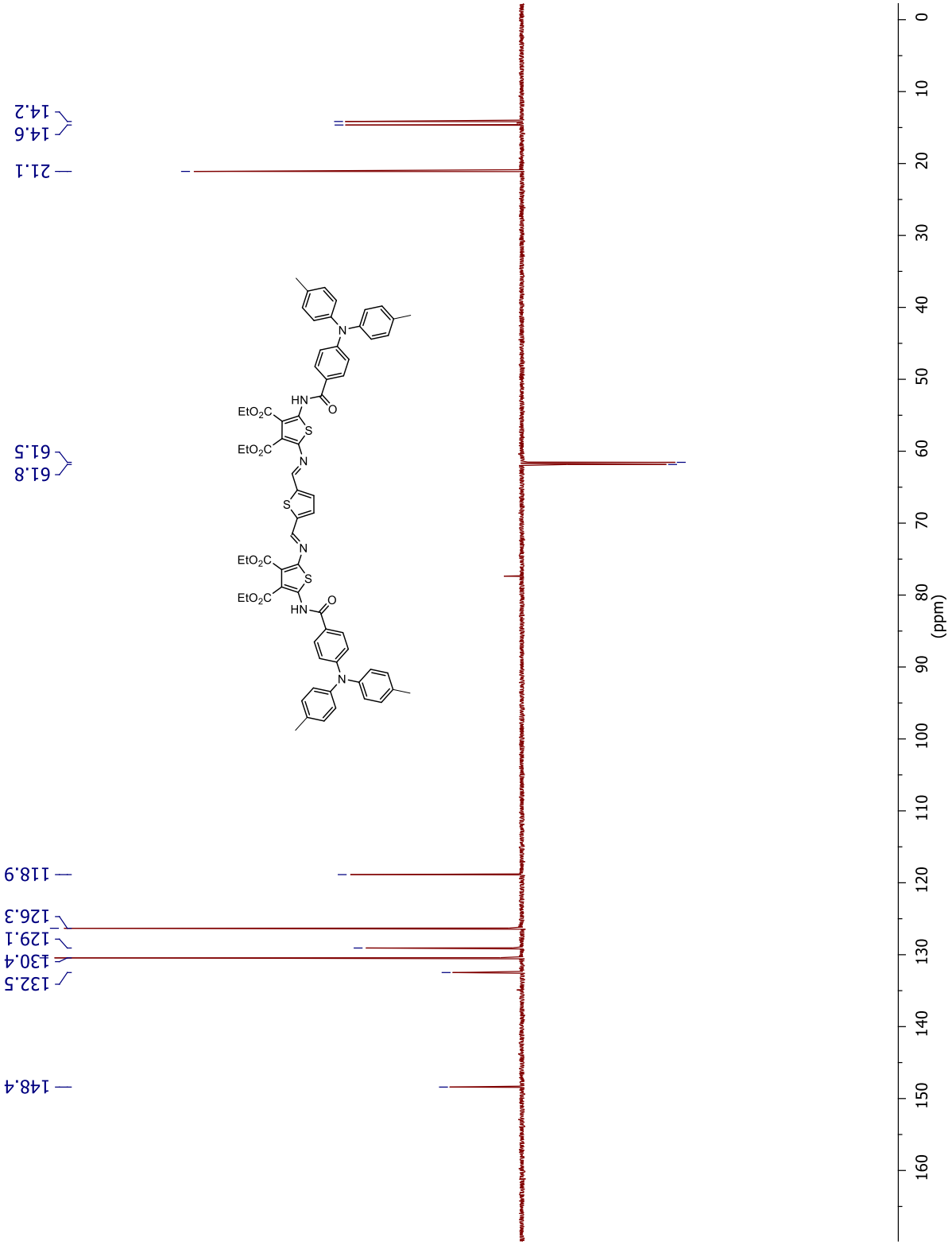

Figure S1-84. DEPT-135 NMR spectrum of **3A** in deuterated chloroform.

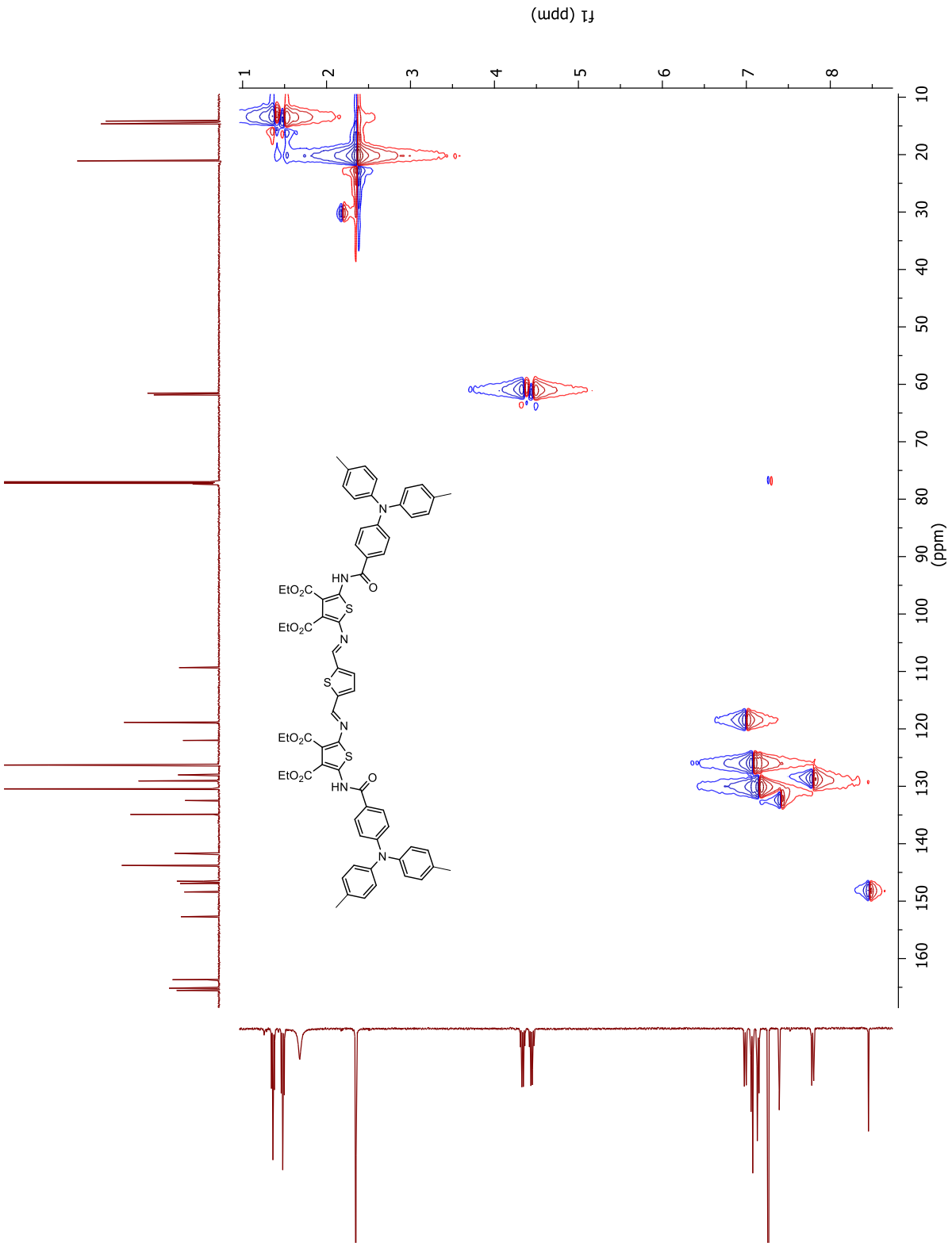

Figure S1-85. HSQC ^{13}C-^{1}H correlation NMR spectrum of **3A** in deuterated chloroform.

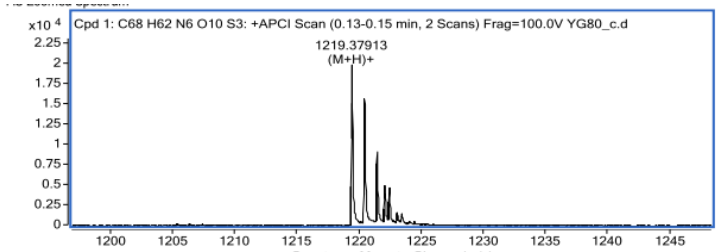

MS Spectrum Peak List

Ion	Ion Formula	Abund	*Expe. m/z*	*Calc. m/z*	Diff(ppm)
(M+H)+	C68H63N6O10S3	19947.73	1219.37913	1219.37623	2.38

Figure S1-86. High resolution mass spectrum of **3A**.

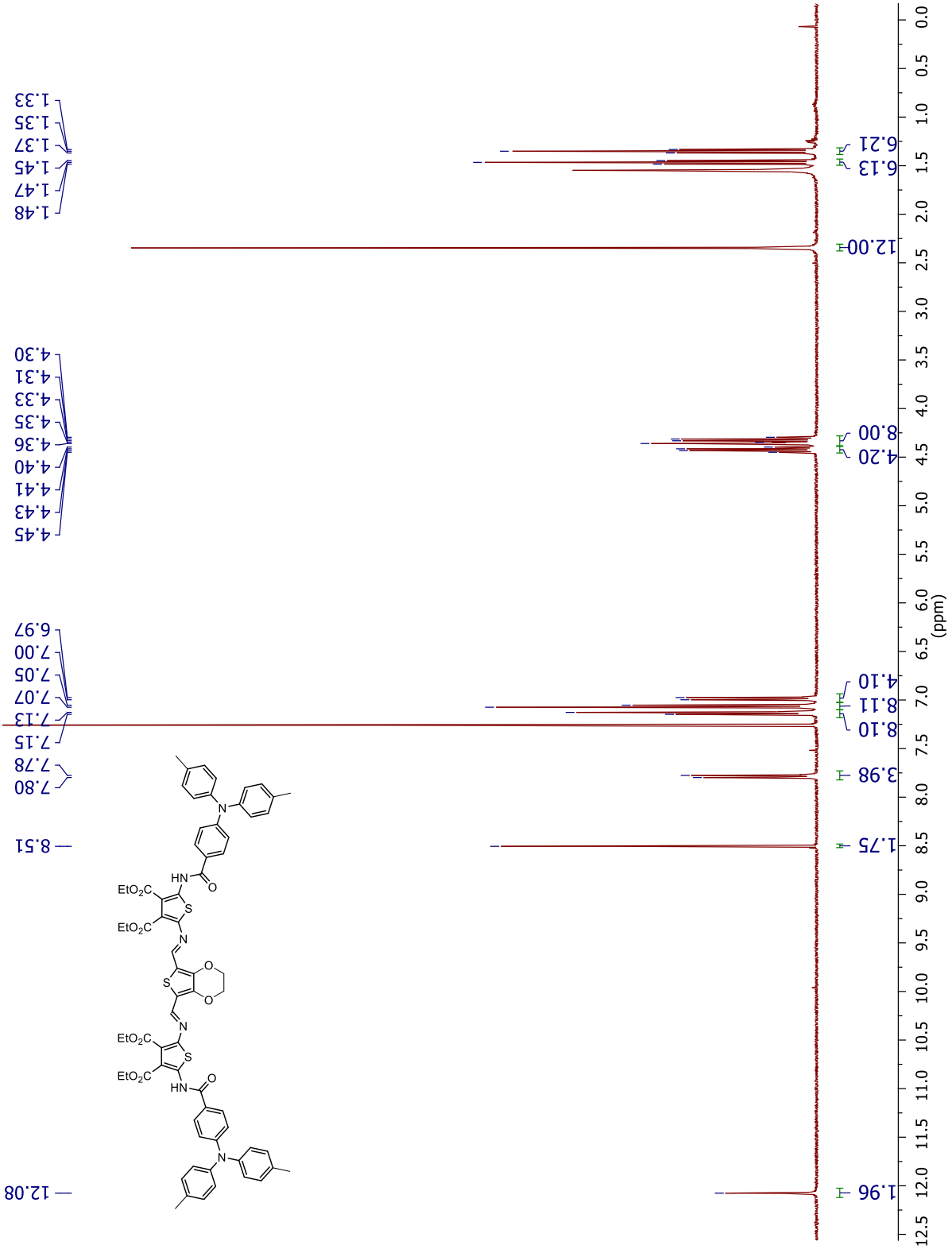

Figure S1-87. ^{1}H NMR spectrum of **3B** in deuterated chloroform.

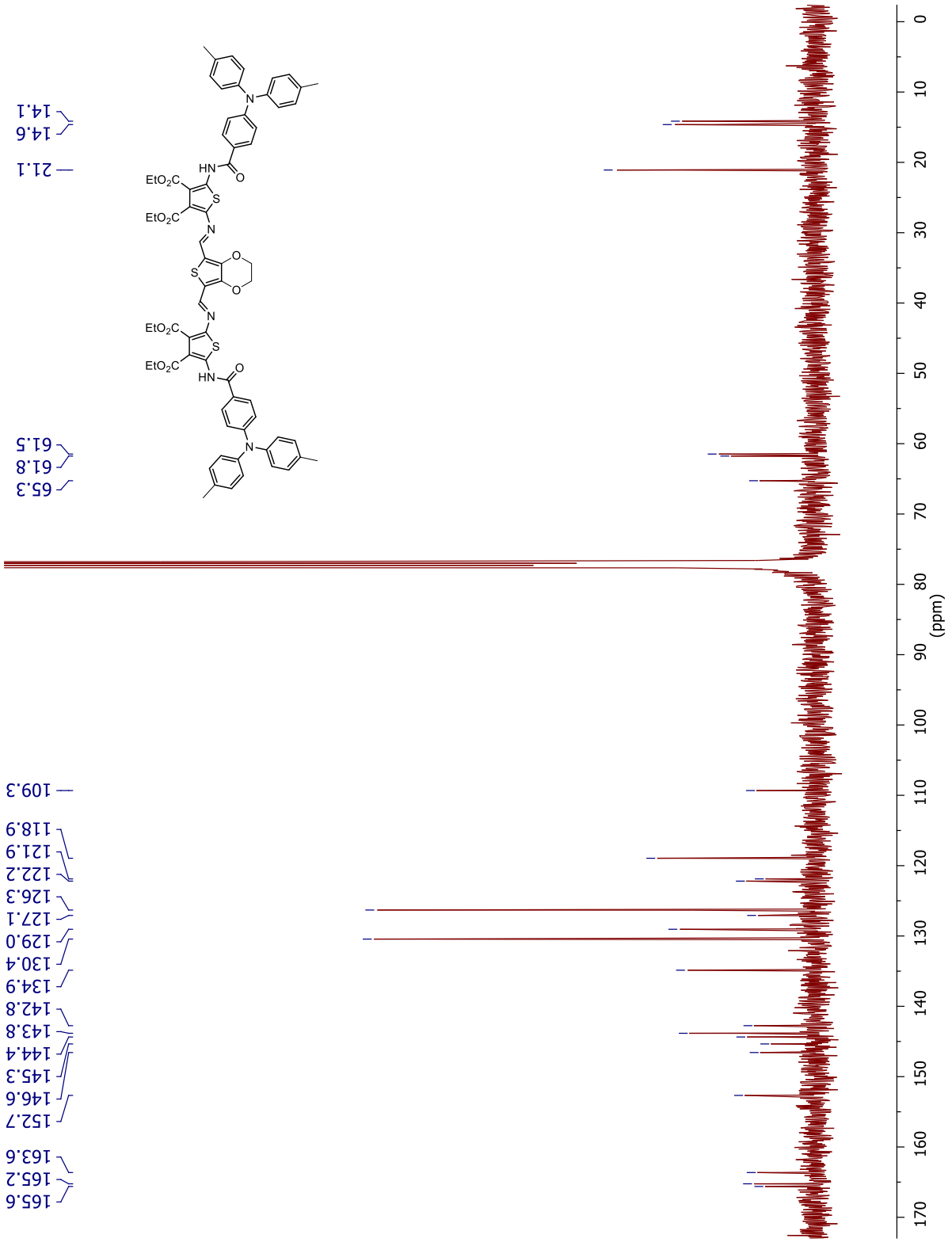

Figure S1-88. ^{13}C NMR spectrum of **3B** in deuterated chloroform.

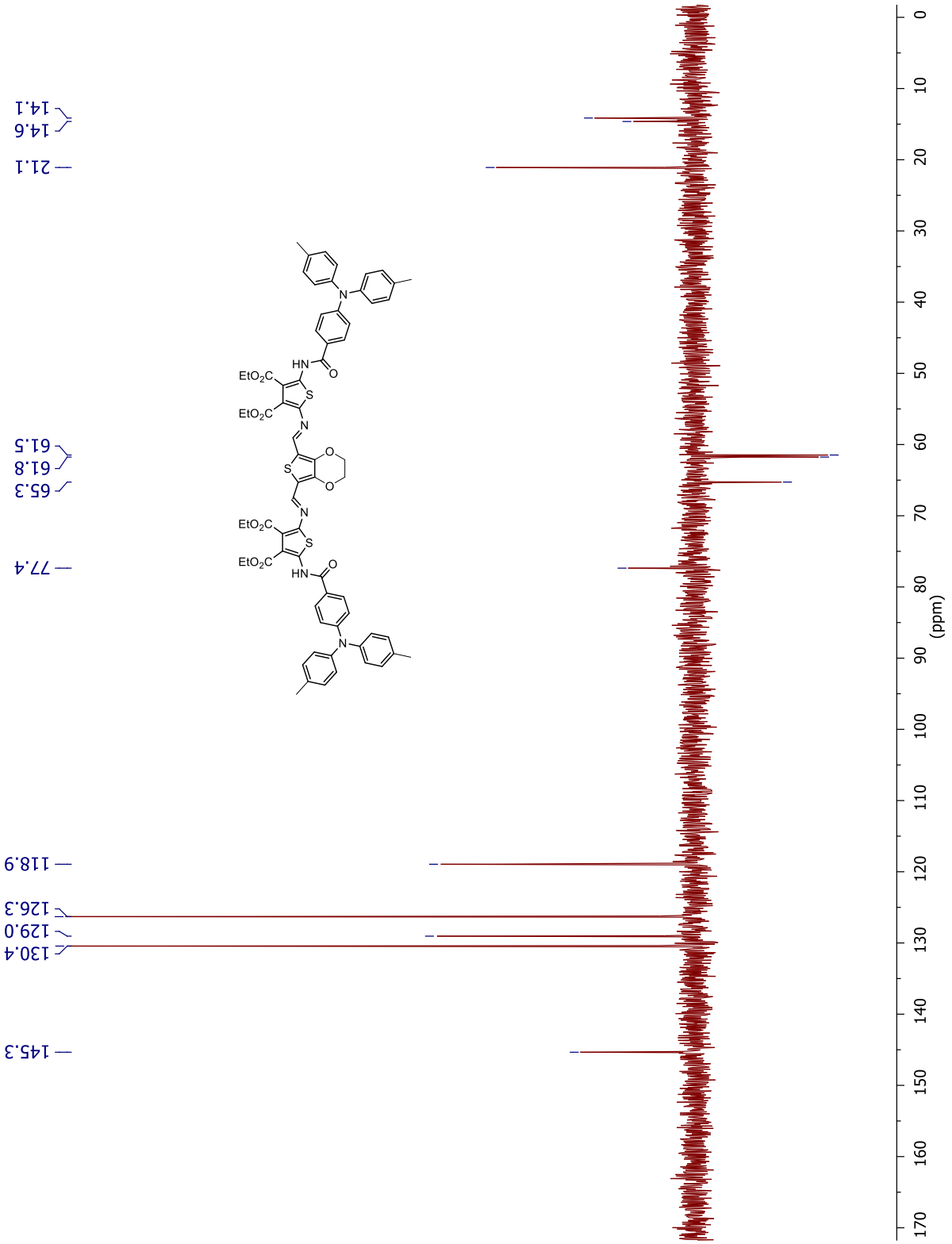

Figure S1-89. DEPT-135 NMR spectrum of **3B** in deuterated chloroform.

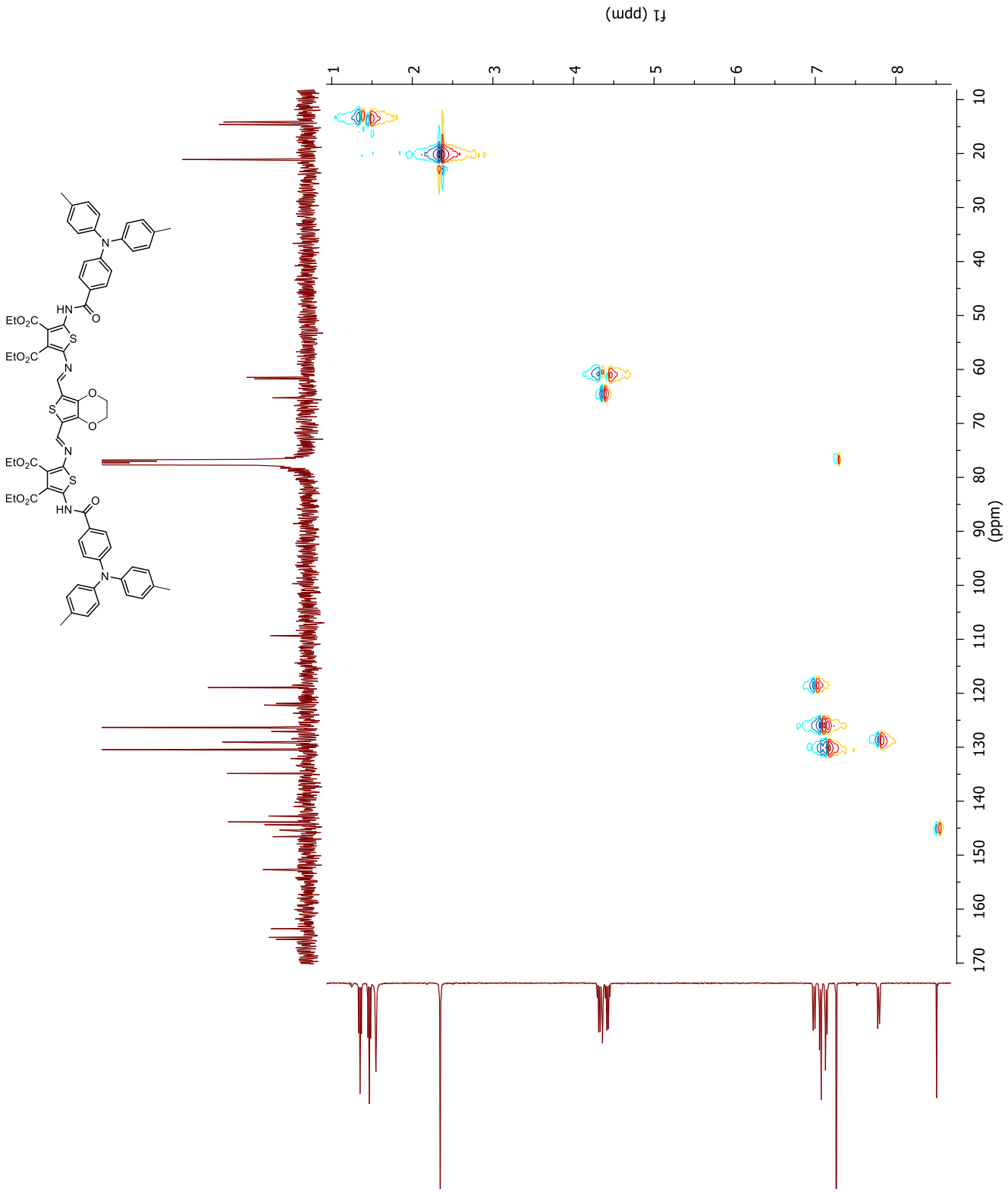

Figure S1-90. HSQC ^{13}C-^{1}H correlation NMR spectrum of **3B** in deuterated chloroform.

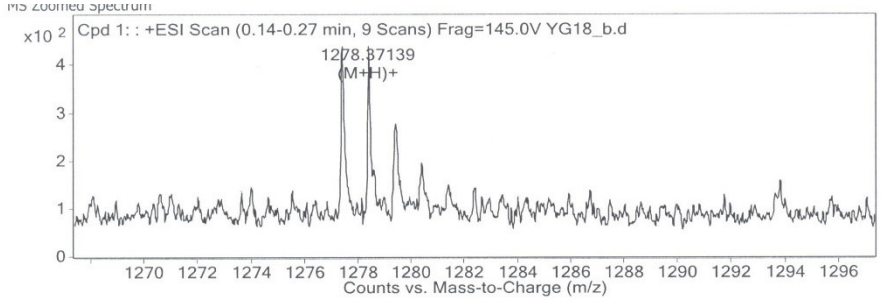

MS Spectrum Peak List

Ion	Ion Formula	Abund	*Expe. m/z*	*Calc. m/z*	Diff(ppm)
(M+H)+	C70H65N6O12S3	413.9	1277.3817	1277.38171	-0.01

Figure S1-91. High resolution mass spectrum of **3B**.

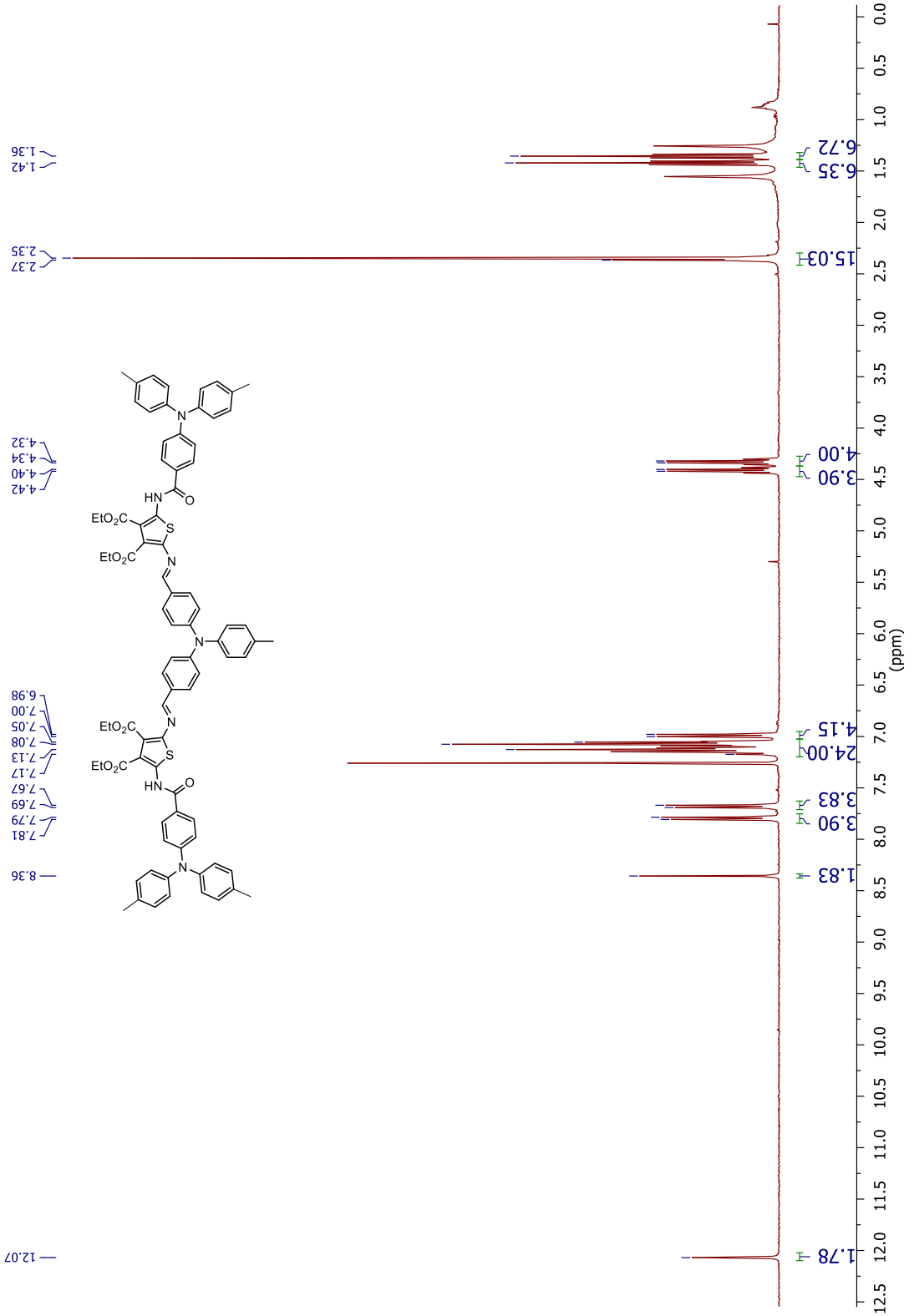

Figure S1-92. ^{1}H NMR spectrum of **3D** in deuterated chloroform.

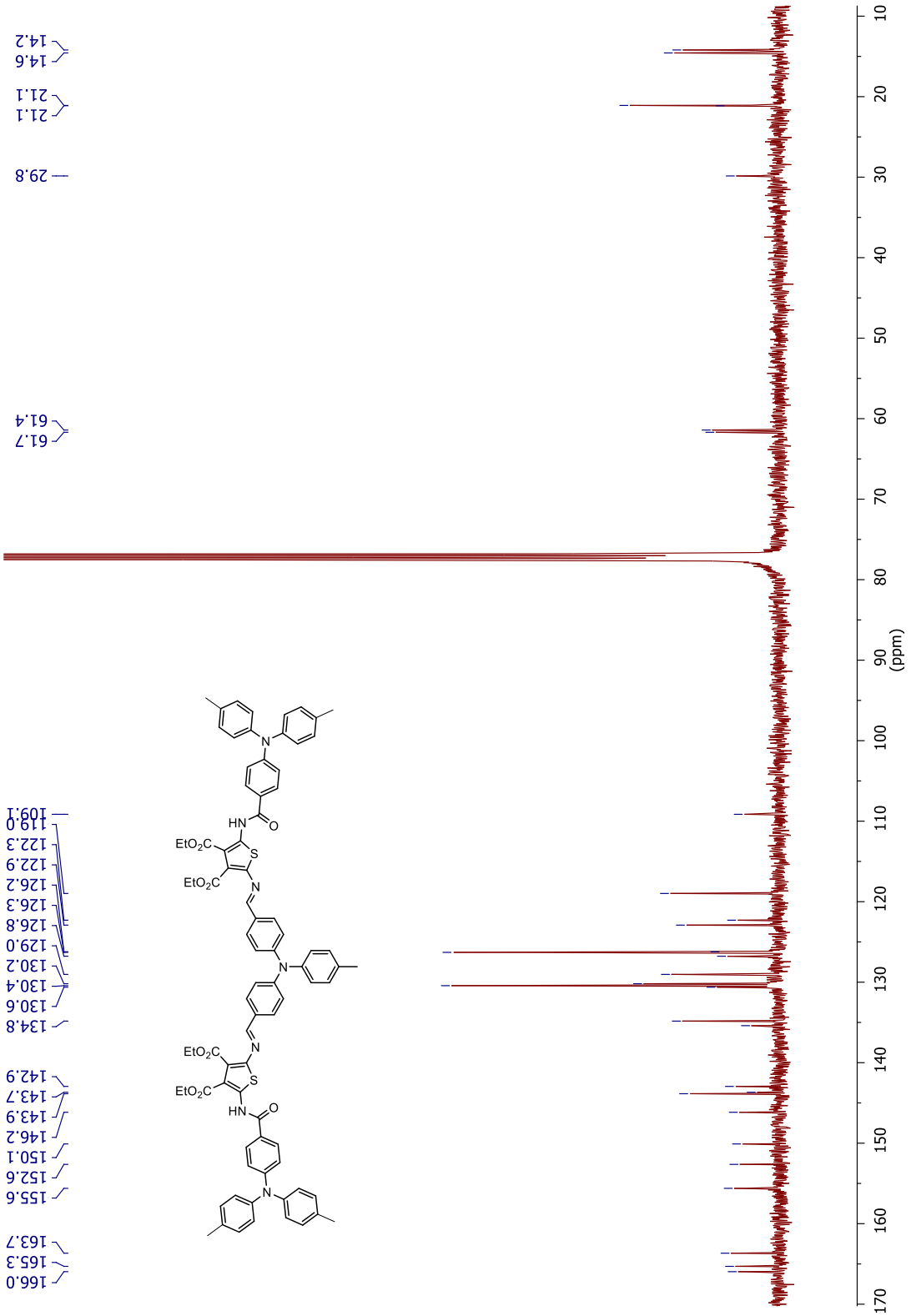

Figure S1-93. ^{13}C NMR spectrum of **3D** in deuterated chloroform.

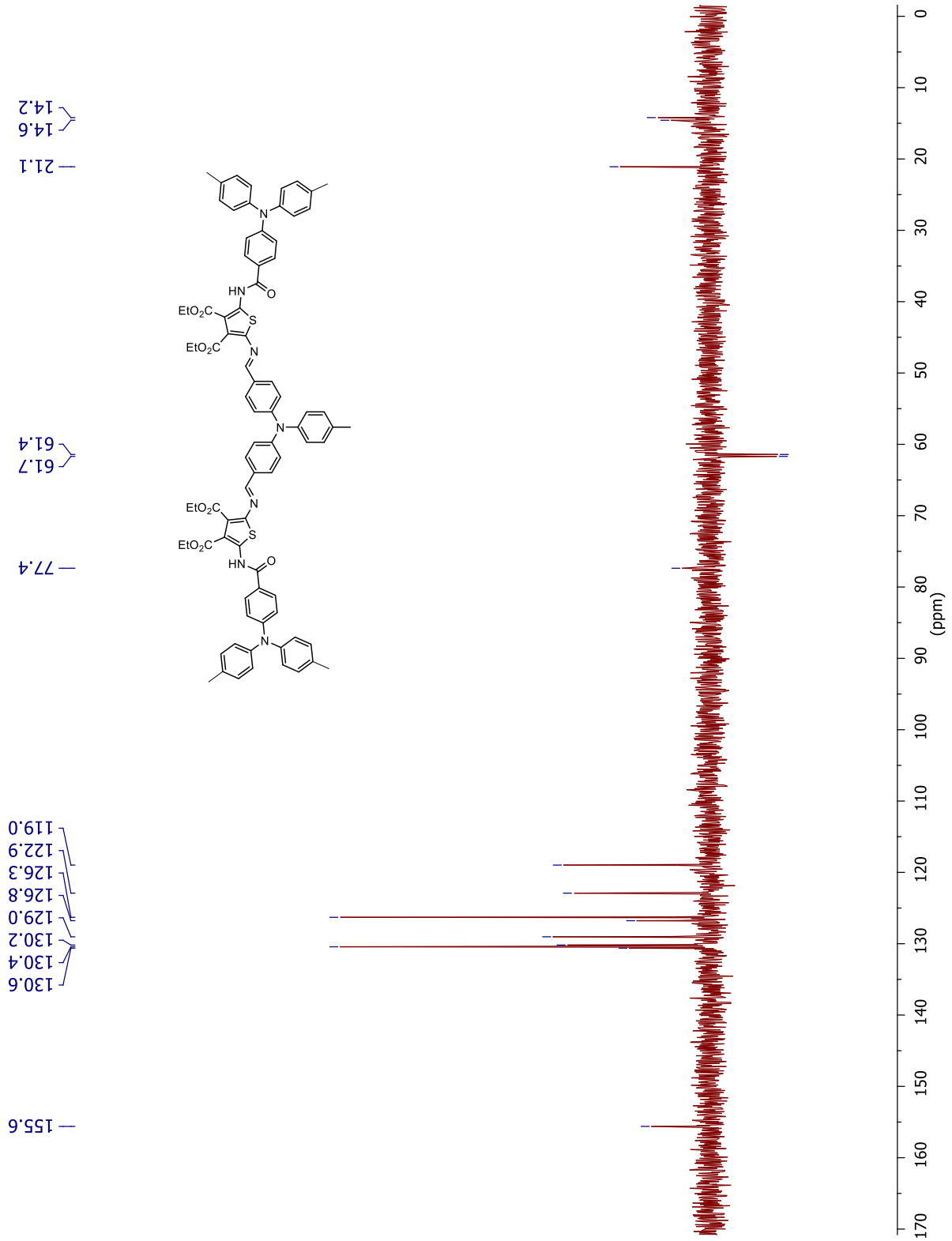

Figure S1-94. DEPT-135 NMR spectrum of **3D** in deuterated chloroform.

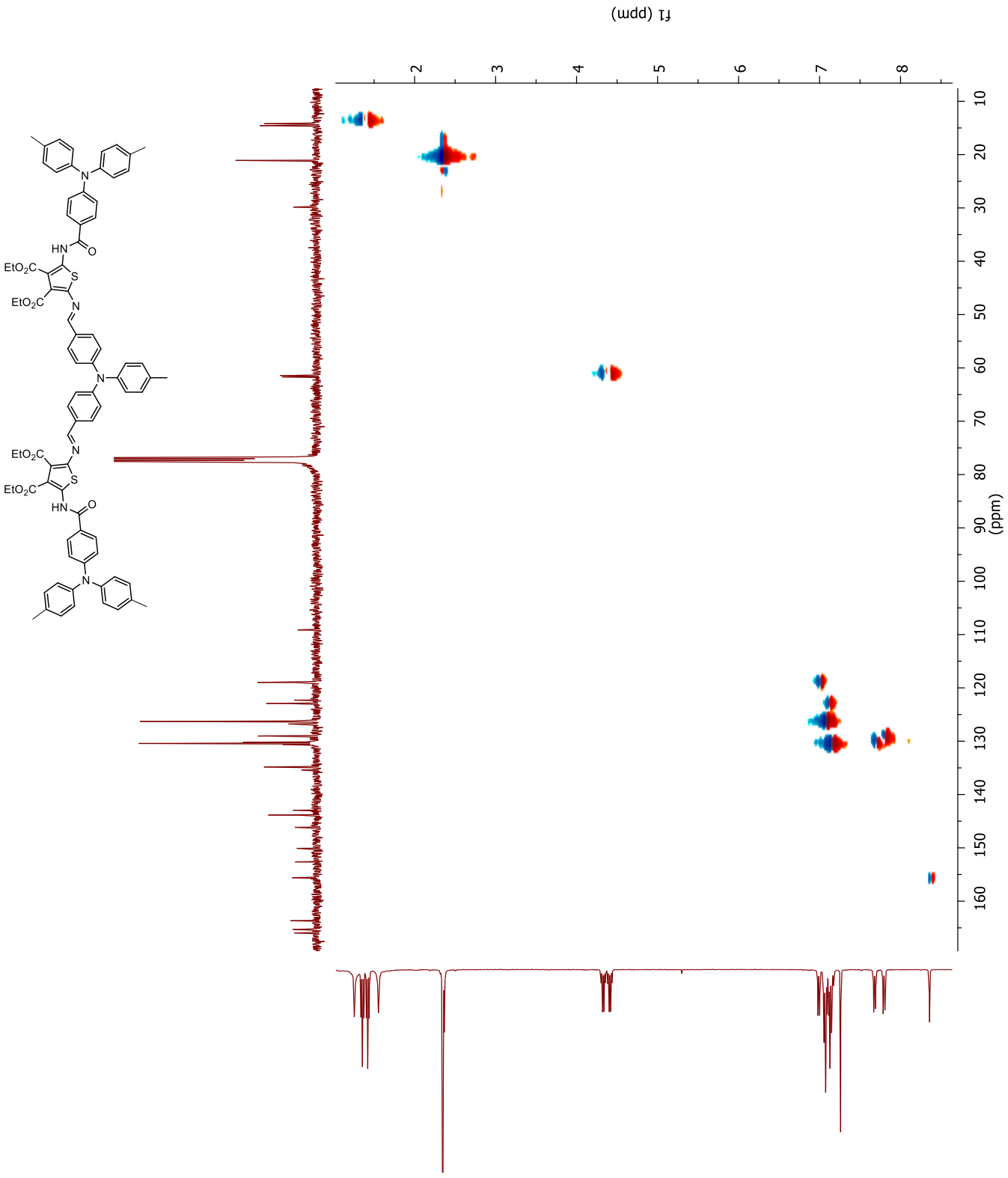

Figure S1-95. HSQC ^{13}C-^{1}H correlation NMR spectrum of **3D** in deuterated chloroform.

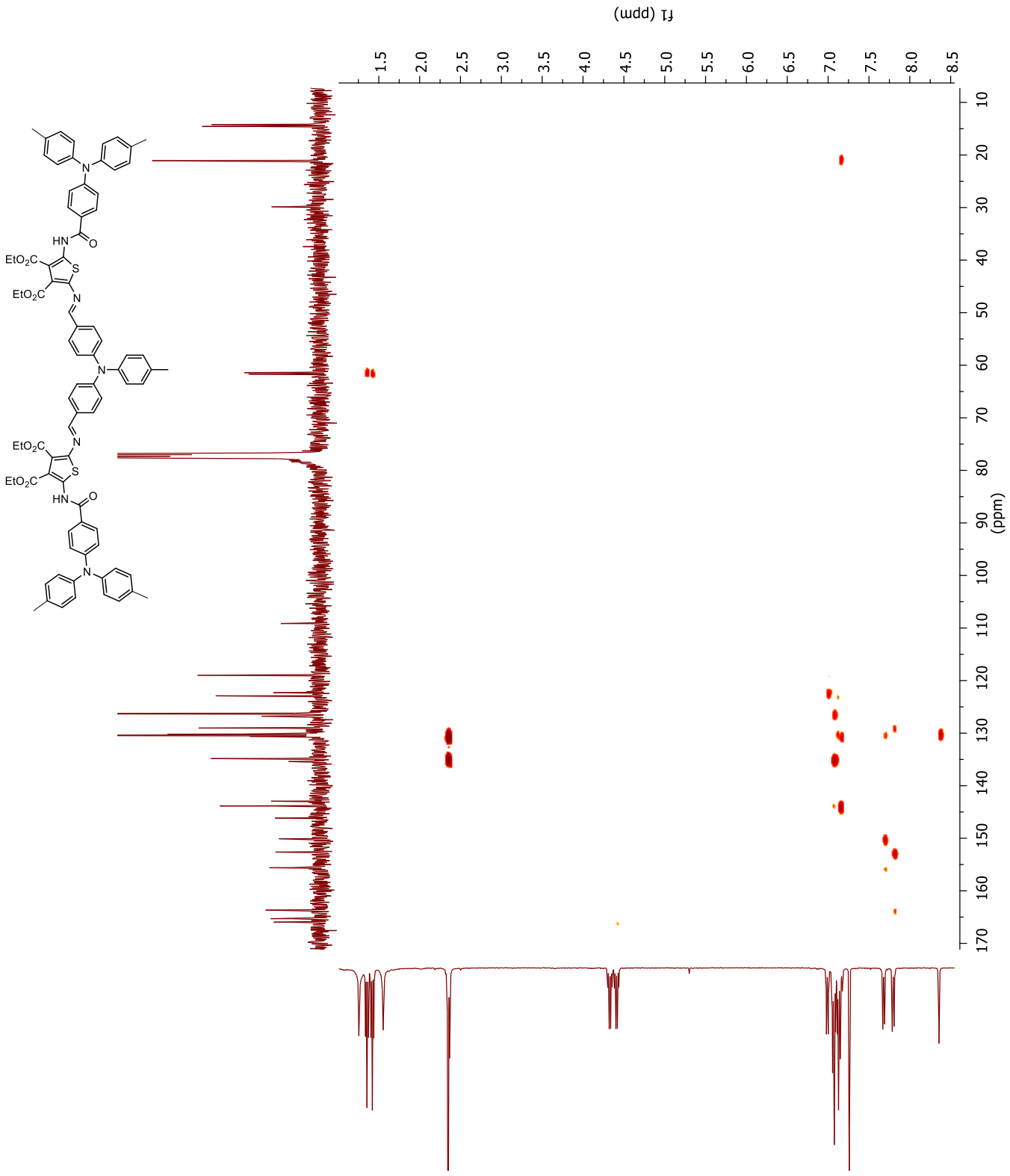

Figure S1-96. HMBC ^{13}C-^{1}H correlation NMR spectrum of **3D** in deuterated chloroform.

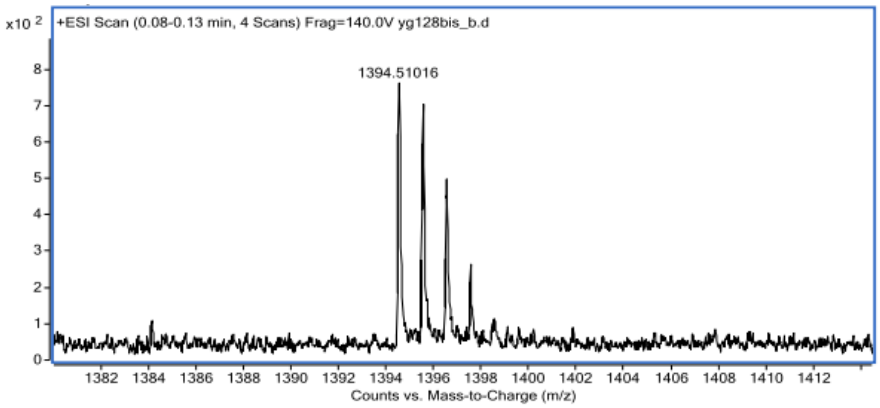

Ion	Ion Formula	Expe. m/z	Calc. m/z	Diff (ppm)
[M+H]+	C83 H76 N7 O10 S2	1394.51016	1394.50896	-0.86

Figure S1-97. High resolution mass spectrum of **3D**.

SUPPORTING INFORMATION III
THEORETICALLY CALCULATED GEOMETRY COORDINATES

Extending the duty cycle of azomethine electrochromes by structural modification

Yohan Gautier and W. G. Skene

Table 1-3 Atomic coordinates of the neutral singlet of **2B** calculated by CAM-B3LYP/6-311+g(d,p).

Atom	z	y	z
H	-3.04818	5.09506	1.16704
H	-3.06457	5.04934	-0.60857
H	-0.72171	4.98307	0.27372
H	-1.10573	3.48316	-0.58312
H	-1.10257	3.5179	1.19101
H	-8.05522	4.94877	-1.65615
H	-6.47439	5.75704	-1.63132
H	-7.99158	6.76417	0.07766
H	-6.62187	5.96608	0.86311
H	-8.21459	5.18138	0.83413
H	3.19639	5.17912	-0.05581
H	1.81688	4.07778	0.0483
H	3.38483	5.18357	2.45038
H	2.00127	4.07907	2.55415
H	1.77922	5.72328	1.93958
H	7.83333	5.10958	-1.53577
H	7.872	5.27414	0.22479
H	5.55321	6.16898	-1.58342
H	6.74085	7.24488	-0.83351
H	5.6054	6.34696	0.18207
H	-3.31106	-2.03585	0.03851
H	3.31371	-2.04348	0.09065
H	-10.71905	0.99146	-0.21818
H	-13.11592	0.77996	-0.14663
H	-8.80179	0.97311	-0.33669
H	13.11791	0.70693	-0.45362
H	10.71754	0.91304	-0.4989

H	10.32496	-3.20187	0.65125
H	12.76916	-3.41137	0.70414
H	8.81133	0.97795	-0.15649
C	-2.80139	4.4965	0.2922
C	-1.34572	4.08688	0.29229
O	-3.67314	3.34471	0.39608
O	-3.59962	3.02384	-1.82496
C	-3.99816	2.71779	-0.73023
C	-7.16937	5.14888	-1.05589
C	-7.51856	5.79784	0.26456
O	-6.45874	3.90329	-0.85336
O	-8.39235	2.78321	-0.65808
C	-7.17063	2.79802	-0.66318
C	2.72715	4.4045	0.55197
C	2.46096	4.87102	1.96107
O	3.63129	3.27818	0.62968
O	3.62718	3.10076	-1.60419
C	4.00254	2.72949	-0.52121
C	7.21538	5.17405	-0.63976
C	6.21207	6.29639	-0.72343
O	6.47619	3.93649	-0.50935
O	8.40205	2.80183	-0.39201
C	7.18022	2.81646	-0.39994
C	-2.64368	-1.17512	-0.05834
C	2.64924	-1.18233	-0.02109
S	0.00506	-0.28201	-0.15189
C	-1.24253	-1.48662	-0.0082
C	-0.71105	-2.74274	0.14192
C	0.70953	-2.74534	0.1492
C	1.24693	-1.49191	-0.00216

C	-10.31726	-1.12207	0.07542
C	-11.1337	0.00241	-0.06482
C	-12.50935	-0.10662	-0.02431
O	-8.14714	-2.0843	0.20946
C	-8.8371	-1.08917	0.0445
N	-8.24903	0.13264	-0.1839
N	-3.07039	0.02138	-0.20897
S	-5.71067	-0.86965	-0.03256
C	-6.90044	0.3675	-0.24098
C	-6.33988	1.61231	-0.46604
C	-4.90976	1.56081	-0.47089
C	-4.41301	0.31377	-0.25323
C	12.51415	-0.15283	-0.19808
C	11.13796	-0.04457	-0.21577
C	10.32561	-1.13923	0.08825
C	10.9447	-2.34855	0.40833
C	12.31835	-2.46543	0.43716
O	8.15678	-2.10489	0.22032
C	8.84553	-1.1045	0.08512
N	8.25741	0.12833	-0.07368
N	3.07948	0.01482	-0.15581
S	5.71939	-0.88244	0.00614
C	6.909	0.36557	-0.12574
C	6.34854	1.62059	-0.2858
C	4.91902	1.56687	-0.31017
C	4.42231	0.30908	-0.16552
C	13.13409	-1.36584	0.13323
C	-13.12522	-1.35187	0.16451
C	-10.93271	-2.36086	0.26278
H	-10.31	-3.2375	0.385

C	-12.3056	-2.48073	0.30866
H	-12.75248	-3.45284	0.46546
N	-14.5153	-1.4633	0.20881
N	14.52499	-1.47551	0.15755
C	-15.1668	-2.67587	-0.16006
C	-16.1304	-3.23067	0.67834
C	-14.86543	-3.30203	-1.36759
C	-16.78482	-4.39792	0.31097
H	-16.36669	-2.74285	1.61598
C	-15.51164	-4.47706	-1.72242
H	-14.12454	-2.86579	-2.02616
C	-16.4757	-5.02878	-0.88734
H	-17.53329	-4.82032	0.97065
H	-15.26921	-4.95594	-2.66354
H	-16.98388	-5.94249	-1.17004
C	-15.32561	-0.36812	0.62769
C	-15.05529	0.29476	1.82282
C	-16.41114	0.03096	-0.1478
C	-15.85484	1.3536	2.22753
H	-14.21826	-0.0221	2.43273
C	-17.21677	1.08097	0.26962
H	-16.62283	-0.48591	-1.07571
C	-16.94014	1.74971	1.45529
H	-15.63555	1.86237	3.1586
H	-18.05919	1.38278	-0.34115
H	-17.5671	2.57221	1.77696
C	15.16612	-2.72634	-0.07755
C	14.83459	-3.49236	-1.19302
C	16.14888	-3.18015	0.79853
C	15.47012	-4.70453	-1.41869

H	14.07852	-3.13557	-1.88151
C	16.79226	-4.3862	0.55933
H	16.40864	-2.58383	1.66449
C	16.45318	-5.15573	-0.54628
H	15.20404	-5.29246	-2.28895
H	17.55577	-4.72932	1.24718
H	16.9528	-6.09925	-0.72846
C	15.34551	-0.33988	0.41807
C	15.09995	0.47113	1.52398
C	16.41658	-0.04742	-0.42247
C	15.90922	1.56938	1.77507
H	14.2744	0.23828	2.18522
C	17.23214	1.04368	-0.15768
H	16.60926	-0.67906	-1.28089
C	16.98006	1.85923	0.93815
H	15.70903	2.19353	2.63774
H	18.06305	1.26153	-0.81794
H	17.61467	2.71332	1.14028
O	1.4333	-3.87648	0.28112
O	-1.44	-3.8695	0.28301
C	-0.66977	-5.0625	0.06046
C	0.6574	-4.98052	0.7764
H	1.24865	-5.8749	0.59348
H	0.51093	-4.8544	1.85219
H	-1.26492	-5.8864	0.44756
H	-0.52351	-5.19261	-1.01483

Table 1-4 Atomic coordinates of the radical cation of **2B** calculated by CAM-B3LYP/6-311+g(d,p).

atom	x	y	z
H	-3.11131	5.01668	1.43965
H	-2.96755	4.95584	-0.3301
H	-0.71416	4.92688	0.76411
H	-1.00127	3.41837	-0.11714
H	-1.15828	3.4617	1.65166
H	-7.83835	4.92359	-1.61754
H	-6.23788	5.69182	-1.57094
H	-7.75937	6.75096	0.10333
H	-6.42351	5.92646	0.91865
H	-8.03506	5.18129	0.86867
H	3.04926	5.06635	-0.11309
H	1.70776	3.96528	0.23134
H	3.50793	5.28726	2.34446
H	2.16662	4.17989	2.69557
H	1.84528	5.76293	1.97421
H	7.61558	5.03388	-1.72322
H	7.70054	5.27244	0.02932
H	5.31284	6.04435	-1.7468
H	6.49746	7.17475	-1.07815
H	5.41291	6.29847	0.00872
H	-3.28138	-2.17021	0.2919
H	3.29374	-2.16098	0.33778
H	-10.61641	1.02829	-0.19017
H	-13.01545	0.8698	-0.18856
H	-8.69642	0.97128	-0.32377
H	12.99512	0.79707	-0.52285
H	10.60026	0.95604	-0.49945
H	10.31886	-3.19167	0.5936
H	12.75989	-3.3533	0.57032

H	8.69096	0.98412	-0.21235
C	-2.77865	4.41521	0.5962
C	-1.32531	4.02249	0.73067
O	-3.64395	3.25211	0.63174
O	-3.36459	2.89513	-1.57019
C	-3.86389	2.61767	-0.51145
C	-6.95913	5.10822	-1.00299
C	-7.31386	5.77503	0.30643
O	-6.283	3.8443	-0.77768
O	-8.2438	2.76976	-0.60133
C	-7.024	2.76311	-0.58628
C	2.65906	4.34452	0.60439
C	2.54218	4.92314	1.99089
O	3.58819	3.23114	0.67403
O	3.42521	2.89886	-1.54199
C	3.87905	2.62664	-0.4628
C	7.02405	5.12829	-0.81272
C	5.99249	6.22163	-0.91239
O	6.31487	3.87523	-0.60966
O	8.25903	2.77383	-0.48023
C	7.04149	2.78574	-0.46335
C	-2.61204	-1.31674	0.17403
C	2.62064	-1.31323	0.20249
S	0.00732	-0.3861	0.04934
C	-1.22292	-1.60126	0.24275
C	-0.68371	-2.86851	0.44567
C	0.71103	-2.86862	0.45457
C	1.26005	-1.5918	0.24281
C	-10.26793	-1.10742	0.00554
C	-11.05579	0.0422	-0.09897

C	-12.43294	-0.03606	-0.09665
O	-8.11951	-2.11215	0.1726
C	-8.79332	-1.10716	0.0148
N	-8.16759	0.11422	-0.17011
N	-3.03128	-0.10863	-0.02265
S	-5.67674	-0.96103	0.04981
C	-6.82303	0.31027	-0.17605
C	-6.22311	1.55555	-0.36354
C	-4.81186	1.47374	-0.32127
C	-4.34447	0.19794	-0.10576
C	12.4177	-0.0797	-0.26686
C	11.04277	0.00002	-0.24665
C	10.25908	-1.11783	0.06058
C	10.91287	-2.32183	0.34496
C	12.28506	-2.41233	0.33121
O	8.1071	-2.10351	0.28089
C	8.79462	-1.11591	0.09945
N	8.16055	0.12125	-0.08218
N	3.06267	-0.08689	0.00813
S	5.68804	-0.97064	0.11801
C	6.83229	0.30569	-0.09128
C	6.2273	1.57153	-0.27365
C	4.84074	1.49533	-0.25002
C	4.35404	0.19441	-0.04734
C	13.07409	-1.2886	0.02397
C	-13.08249	-1.27545	0.01352
C	-10.91593	-2.34007	0.11707
H	-10.31698	-3.23641	0.21225
C	-12.2905	-2.43007	0.12124
H	-12.76198	-3.39807	0.21837

N	-14.47101	-1.35601	0.01766
N	14.45617	-1.36985	0.00773
C	-15.14285	-2.5502	-0.38008
C	-16.11817	-3.10471	0.44396
C	-14.85036	-3.15231	-1.60143
C	-16.79342	-4.25088	0.04869
H	-16.34755	-2.63324	1.39166
C	-15.51792	-4.30634	-1.98476
H	-14.10053	-2.71387	-2.24842
C	-16.49339	-4.85886	-1.16363
H	-17.55153	-4.67424	0.69654
H	-15.28345	-4.76754	-2.93662
H	-17.01836	-5.75579	-1.46853
C	-15.27246	-0.24691	0.42267
C	-15.0505	0.37355	1.64958
C	-16.30149	0.20284	-0.39967
C	-15.84257	1.44313	2.04069
H	-14.25782	0.01507	2.29479
C	-17.10022	1.26392	0.00304
H	-16.47517	-0.28332	-1.35179
C	-16.87162	1.89104	1.22119
H	-15.66263	1.91932	2.99703
H	-17.8994	1.60624	-0.64332
H	-17.49337	2.72164	1.53195
C	15.12561	-2.62296	-0.14731
C	14.84187	-3.4438	-1.23529
C	16.08931	-3.0112	0.77813
C	15.50812	-4.65137	-1.38522
H	14.10075	-3.13326	-1.9616
C	16.76263	-4.21386	0.61577

H	16.31124	-2.36767	1.62055
C	16.47184	-5.03972	-0.46254
H	15.28186	-5.28477	-2.23444
H	17.51232	-4.50863	1.34005
H	16.99581	-5.97958	-0.58553
C	15.27009	-0.20277	0.14339
C	15.11772	0.63802	1.24237
C	16.24115	0.07851	-0.81242
C	15.92273	1.76021	1.37371
H	14.37005	0.40908	1.9919
C	17.05285	1.19515	-0.66918
H	16.36009	-0.58091	-1.66336
C	16.89397	2.04166	0.42055
H	15.79873	2.40961	2.2319
H	17.8074	1.407	-1.41703
H	17.52614	2.9144	0.52888
O	1.44557	-3.96047	0.6448
O	-1.41911	-3.97976	0.60949
C	-0.64722	-5.17839	0.40505
C	0.67785	-5.08838	1.12518
H	1.28476	-5.9692	0.93269
H	0.53553	-4.96618	2.20024
H	-1.24161	-5.99714	0.80242
H	-0.50124	-5.31908	-0.66807

Table 1-5 Atomic coordinates of the singlet dication of **2B** calculated by CAM-B3LYP/6-311+g(d,p).

atom	x	y	z
H	-3.11135	5.0169	1.43876
H	-2.96769	4.95585	-0.331
H	-0.71424	4.92712	0.76307
H	-1.00135	3.41848	-0.11797
H	-1.15824	3.46203	1.65083
H	-7.8384	4.92341	-1.61823
H	-6.23796	5.69168	-1.57157
H	-7.75959	6.75087	0.10254
H	-6.42375	5.92646	0.918
H	-8.03529	5.18125	0.86795
H	3.0493	5.06648	-0.11291
H	1.70782	3.96545	0.23167
H	3.50821	5.28747	2.34458
H	2.16694	4.18012	2.69586
H	1.84553	5.76313	1.97448
H	7.61555	5.03403	-1.72309
H	7.70052	5.27259	0.02944
H	5.31279	6.04447	-1.74663
H	6.4974	7.17489	-1.07801
H	5.41289	6.2986	0.00888
H	-3.28136	-2.17016	0.2918
H	3.29376	-2.16085	0.33787
H	-10.61642	1.02823	-0.18978
H	-13.01547	0.86971	-0.18809
H	-8.69644	0.97118	-0.32406
H	12.99517	0.79711	-0.52247
H	10.60033	0.95616	-0.49908

H	10.31877	-3.19168	0.59344
H	12.7598	-3.35339	0.57017
H	8.69098	0.98422	-0.21227
C	-2.77871	4.41534	0.59535
C	-1.32535	4.0227	0.72978
O	-3.64396	3.2522	0.6311
O	-3.36475	2.89501	-1.57082
C	-3.86394	2.61763	-0.51201
C	-6.95922	5.1081	-1.00363
C	-7.31406	5.77498	0.30573
O	-6.28308	3.84421	-0.77821
O	-8.24386	2.76963	-0.60188
C	-7.02406	2.76301	-0.58678
C	2.65916	4.34468	0.60462
C	2.54243	4.92335	1.99111
O	3.58828	3.23129	0.67421
O	3.42518	2.899	-1.54181
C	3.87907	2.62679	-0.46264
C	7.02403	5.12843	-0.81259
C	5.99246	6.22177	-0.91224
O	6.31487	3.87537	-0.60952
O	8.25904	2.77398	-0.48017
C	7.0415	2.78588	-0.46325
C	-2.61203	-1.31669	0.17392
C	2.62066	-1.3131	0.20254
S	0.00733	-0.38601	0.0493
C	-1.2229	-1.60118	0.24269
C	-0.68368	-2.86842	0.44566
C	0.71105	-2.86851	0.4546
C	1.26007	-1.59169	0.24283

C	-10.26792	-1.1075	0.00557
C	-11.05579	0.04213	-0.09873
C	-12.43294	-0.03616	-0.09635
O	-8.11948	-2.11219	0.17264
C	-8.79331	-1.10722	0.01478
N	-8.1676	0.11415	-0.17028
N	-3.03128	-0.1086	-0.02284
S	-5.67672	-0.96104	0.04967
C	-6.82304	0.31022	-0.17628
C	-6.22314	1.55549	-0.36393
C	-4.81189	1.47371	-0.32166
C	-4.34448	0.19795	-0.10599
C	12.41773	-0.07967	-0.2666
C	11.04279	0.00009	-0.24641
C	10.25907	-1.11778	0.06067
C	10.91282	-2.32184	0.34491
C	12.285	-2.41237	0.33118
O	8.10706	-2.10342	0.28091
C	8.7946	-1.11583	0.09952
N	8.16056	0.12135	-0.08209
N	3.06269	-0.08676	0.0082
S	5.68805	-0.97051	0.11811
C	6.83231	0.30581	-0.09119
C	6.22732	1.57166	-0.27354
C	4.84076	1.49547	-0.24989
C	4.35405	0.19454	-0.04724
C	13.07407	-1.28863	0.02408
C	-13.08247	-1.27557	0.01366
C	-10.91589	-2.34018	0.11696
H	-10.31692	-3.23652	0.21198

C	-12.29046	-2.4302	0.12118
H	-12.76192	-3.39821	0.21819
N	-14.47099	-1.35614	0.01788
N	14.45615	-1.36992	0.00786
C	-15.14286	-2.55025	-0.38003
C	-16.11814	-3.10489	0.44397
C	-14.85043	-3.15217	-1.6015
C	-16.79342	-4.25099	0.04854
H	-16.34747	-2.63358	1.39175
C	-15.51802	-4.30613	-1.98498
H	-14.10064	-2.71363	-2.24845
C	-16.49346	-4.85878	-1.16389
H	-17.5515	-4.67446	0.69636
H	-15.2836	-4.76717	-2.93693
H	-17.01845	-5.75565	-1.46891
C	-15.27241	-0.2471	0.42313
C	-15.05034	0.37316	1.65011
C	-16.3015	0.20279	-0.39906
C	-15.84237	1.44269	2.04146
H	-14.25761	0.01458	2.2952
C	-17.1002	1.2638	0.00389
H	-16.47527	-0.28322	-1.35124
C	-16.87149	1.89073	1.22212
H	-15.66234	1.91872	2.99786
H	-17.89943	1.60623	-0.64235
H	-17.49321	2.72128	1.53306
C	15.12555	-2.62303	-0.14737
C	14.84176	-3.44371	-1.23546
C	16.08926	-3.01142	0.77799
C	15.50798	-4.65128	-1.38558

H	14.10064	-3.13305	-1.96171
C	16.76255	-4.21407	0.61545
H	16.31122	-2.36801	1.62049
C	16.47172	-5.03977	-0.46297
H	15.28169	-5.28455	-2.23488
H	17.51225	-4.50896	1.33968
H	16.99567	-5.97963	-0.5861
C	15.27011	-0.20288	0.14364
C	15.11777	0.63778	1.24272
C	16.24115	0.07849	-0.81215
C	15.92282	1.75994	1.37418
H	14.37012	0.40877	1.99224
C	17.05288	1.19509	-0.66881
H	16.36006	-0.58083	-1.66318
C	16.89404	2.04148	0.42103
H	15.79885	2.40924	2.23245
H	17.80741	1.40702	-1.41664
H	17.52623	2.91419	0.52945
O	1.44561	-3.96035	0.64486
O	-1.41907	-3.97968	0.60947
C	-0.64716	-5.17829	0.40506
C	0.67789	-5.08826	1.12525
H	1.28482	-5.96908	0.9328
H	0.53552	-4.96603	2.2003
H	-1.24155	-5.99705	0.80243
H	-0.50114	-5.319	-0.66805

Table 1-6 Atomic coordinates of the triplet dication of **2B** calculated by CAM-B3LYP/6-311+g(d,p).

atom	x	y	z
H	-3.12657	4.97232	1.60399
H	-2.96427	4.91442	-0.16434
H	-0.72265	4.86154	0.95791
H	-1.0134	3.36013	0.06569
H	-1.19146	3.39657	1.83233
H	-7.8472	4.87708	-1.53132
H	-6.25347	5.65455	-1.43352
H	-7.83076	6.70001	0.19686
H	-6.51532	5.88099	1.04937
H	-8.1202	5.12647	0.94935
H	3.03208	5.04686	-0.41251
H	1.69632	3.98222	0.05066
H	3.55661	5.44958	2.01004
H	2.21008	4.39262	2.47724
H	1.89228	5.91902	1.64038
H	7.54154	4.89536	-2.11948
H	7.6985	5.26356	-0.39408
H	5.24109	5.91385	-2.12338
H	6.45722	7.08379	-1.59448
H	5.41735	6.30143	-0.39813
H	-3.28531	-2.18961	0.47823
H	3.29765	-2.15046	0.46876
H	-10.60899	0.98788	0.41818
H	-13.03918	0.85824	0.31684
H	-8.71578	0.92522	-0.2718
H	12.97308	0.8032	-0.5895
H	10.58082	0.96011	-0.53491
H	10.32353	-3.14842	0.70989
H	12.76302	-3.30783	0.65205

H	8.66821	0.98125	-0.30248
C	-2.79013	4.37006	0.76259
C	-1.34205	3.96349	0.9123
O	-3.66477	3.21358	0.78612
O	-3.38039	2.87186	-1.4173
C	-3.88148	2.58548	-0.36168
C	-6.98848	5.06555	-0.88953
C	-7.38606	5.72606	0.41057
O	-6.31169	3.80442	-0.64728
O	-8.26844	2.71538	-0.52563
C	-7.04857	2.71879	-0.47974
C	2.65732	4.38614	0.36905
C	2.57832	5.07284	1.70804
O	3.58618	3.27761	0.50395
O	3.37975	2.77463	-1.6767
C	3.85467	2.58915	-0.5886
C	6.98828	5.06147	-1.19528
C	5.95628	6.1498	-1.33448
O	6.28523	3.82898	-0.87116
O	8.23121	2.73448	-0.71209
C	7.01524	2.75394	-0.66313
C	-2.62085	-1.33282	0.35064
C	2.61976	-1.30842	0.32014
S	-0.00202	-0.39827	0.1888
C	-1.22016	-1.6162	0.41968
C	-0.67845	-2.8708	0.64236
C	0.72308	-2.86408	0.63818
C	1.2609	-1.59165	0.39244
C	-10.30517	-1.12809	0.05946
C	-11.06903	0.02516	0.23719

C	-12.44822	-0.03955	0.19746
O	-8.17438	-2.15972	0.27145
C	-8.81038	-1.13654	0.10179
N	-8.19218	0.0717	-0.07485
N	-3.03933	-0.13601	0.14212
S	-5.69002	-0.98912	0.19259
C	-6.83684	0.2748	-0.05701
C	-6.24499	1.51511	-0.2407
C	-4.82737	1.43854	-0.1791
C	-4.36319	0.17137	0.04738
C	12.40148	-0.06514	-0.29502
C	11.02751	0.01284	-0.25773
C	10.25034	-1.09513	0.10119
C	10.91162	-2.28736	0.42006
C	12.28271	-2.37668	0.38716
O	8.10409	-2.0671	0.41858
C	8.78976	-1.09591	0.16211
N	8.14472	0.12828	-0.09522
N	3.05601	-0.08933	0.0744
S	5.68493	-0.95858	0.21906
C	6.82049	0.30343	-0.0982
C	6.20557	1.55625	-0.36235
C	4.82531	1.47927	-0.30911
C	4.34523	0.18947	-0.00968
C	13.06529	-1.26285	0.02758
C	-13.07258	-1.26694	-0.03357
C	-10.93927	-2.35242	-0.14898
H	-10.33755	-3.24426	-0.25853
C	-12.31518	-2.42832	-0.20753
H	-12.80607	-3.38048	-0.35712

N	-14.48323	-1.33437	-0.09214
N	14.44486	-1.34295	-0.00782
C	-15.10059	-2.12506	-1.07225
C	-16.26979	-2.83484	-0.7597
C	-14.54316	-2.20382	-2.35732
C	-16.86865	-3.61376	-1.72916
H	-16.67158	-2.79922	0.2438
C	-15.16215	-2.97836	-3.31687
H	-13.65749	-1.63213	-2.59953
C	-16.32158	-3.68555	-3.00732
H	-17.75884	-4.17889	-1.48594
H	-14.74734	-3.02489	-4.31525
H	-16.79836	-4.29562	-3.76396
C	-15.25493	-0.60803	0.82738
C	-14.82369	-0.48627	2.15659
C	-16.45042	-0.00468	0.40949
C	-15.59234	0.22588	3.05449
H	-13.91618	-0.97889	2.47846
C	-17.20057	0.71333	1.31898
H	-16.75701	-0.07248	-0.62546
C	-16.77798	0.82823	2.6404
H	-15.27432	0.30413	4.08583
H	-18.11294	1.19701	0.99561
H	-17.37316	1.38936	3.34953
C	15.11528	-2.6017	-0.11183
C	14.8289	-3.4667	-1.16404
C	16.08177	-2.94942	0.82634
C	15.49598	-4.67889	-1.26555
H	14.08556	-3.18669	-1.90045
C	16.75554	-4.15741	0.71246

H	16.30548	-2.27065	1.64014
C	16.46234	-5.02746	-0.32987
H	15.26837	-5.34736	-2.08705
H	17.50768	-4.42133	1.446
H	16.98693	-5.97115	-0.41508
C	15.2602	-0.16982	0.05519
C	15.13674	0.71574	1.12189
C	16.20348	0.07082	-0.93845
C	15.94352	1.84268	1.18374
H	14.41064	0.51741	1.9008
C	17.01694	1.19295	-0.86494
H	16.29998	-0.62408	-1.7636
C	16.88711	2.08406	0.1926
H	15.84292	2.52732	2.01723
H	17.75022	1.37368	-1.64152
H	17.52091	2.96065	0.24665
O	1.46184	-3.94835	0.83977
O	-1.40263	-3.9868	0.8361
C	-0.62575	-5.18091	0.62707
C	0.70563	-5.0799	1.33289
H	1.31716	-5.95686	1.13757
H	0.57473	-4.95337	2.40879
H	-1.20985	-6.00219	1.03441
H	-0.49012	-5.32585	-0.44705

Table 1-7 Atomic coordinates of the radical cation of **2A** calculated by CAM-B3LYP/6-311+g(d,p).

atom	x	y	z
H	-3.09736	4.91067	1.01358

H	-2.95672	4.68088	-0.74246
H	-0.69999	4.77337	0.33439
H	-0.98024	3.18098	-0.38494
H	-1.13027	3.40468	1.37115
H	-7.81925	4.56133	-1.95451
H	-6.21181	5.31377	-2.01343
H	-7.68685	6.53854	-0.41255
H	-6.3401	5.77913	0.44711
H	-7.95837	5.04944	0.50096
H	2.96677	4.77642	0.3431
H	1.64387	3.60992	0.49337
H	3.28177	4.7473	2.83357
H	1.96077	3.57249	2.9873
H	1.62671	5.21383	2.41863
H	7.55126	4.92186	-1.28226
H	7.69106	5.00149	0.48171
H	5.24832	5.9212	-1.14309
H	6.4489	6.99028	-0.40597
H	5.39968	6.00985	0.62521
H	-3.28206	-2.4002	0.3633
H	3.29602	-2.42114	0.44087
H	-10.59336	0.69442	-0.63813
H	-12.99429	0.53774	-0.65029
H	-8.68595	0.74448	-0.30538
H	12.97536	0.61384	-0.46296
H	10.58174	0.75443	-0.40474
H	10.34031	-3.44321	0.49821
H	12.78042	-3.58619	0.43821
H	8.67601	0.76254	-0.09364
C	-2.76226	4.23303	0.23099

C	-1.30537	3.86655	0.39802
O	-3.61897	3.0729	0.38002
O	-3.34225	2.51376	-1.77923
C	-3.8413	2.33446	-0.69916
C	-6.92492	4.79224	-1.37865
C	-7.24503	5.58103	-0.12942
O	-6.25493	3.54787	-1.05197
O	-8.22086	2.51085	-0.7507
C	-7.00093	2.494	-0.75298
C	2.56034	3.973	0.95763
C	2.34966	4.39684	2.38799
O	3.5205	2.88251	0.96281
O	3.43879	2.73543	-1.27847
C	3.86011	2.38388	-0.20956
C	6.98908	4.93171	-0.34878
C	5.95156	6.02315	-0.31573
O	6.28951	3.66031	-0.23742
O	8.23796	2.55789	-0.24958
C	7.02207	2.56816	-0.20183
C	-2.60515	-1.5553	0.22036
C	2.62114	-1.57379	0.30577
S	0.01617	-0.65502	0.11752
C	-1.2098	-1.85833	0.29971
C	-0.67853	-3.129	0.51887
C	0.70363	-3.13374	0.53553
C	1.25373	-1.8611	0.33463
C	-10.26028	-1.31066	0.12718
C	-11.04051	-0.22945	-0.29118
C	-12.41766	-0.30943	-0.30641
O	-8.11594	-2.2925	0.42651

C	-8.78566	-1.30614	0.16462
N	-8.15822	-0.10493	-0.11214
N	-3.01572	-0.3577	-0.01485
S	-5.66895	-1.17345	0.16367
C	-6.81095	0.08388	-0.14727
C	-6.20606	1.30436	-0.43712
C	-4.79149	1.21497	-0.40473
C	-4.33264	-0.04149	-0.10061
C	12.40715	-0.27799	-0.24134
C	11.03297	-0.20922	-0.20144
C	10.25983	-1.34636	0.06262
C	10.92538	-2.55849	0.28306
C	12.29683	-2.63856	0.24868
O	8.11428	-2.35081	0.26216
C	8.80001	-1.35716	0.11848
N	8.15292	-0.11077	0.00135
N	3.06534	-0.34909	0.13132
S	5.69498	-1.23212	0.17318
C	6.82979	0.06051	0.01917
C	6.21348	1.33764	-0.0881
C	4.8348	1.25224	-0.05978
C	4.35612	-0.06529	0.07962
C	13.07563	-1.49531	-0.01519
C	-13.07428	-1.48013	0.1035
C	-10.91501	-2.47729	0.52908
H	-10.3218	-3.31862	0.86298
C	-12.28976	-2.56617	0.52374
H	-12.76729	-3.47792	0.85462
N	-14.46315	-1.56202	0.09186
N	14.45522	-1.56609	-0.05147

C	-15.12655	-2.82098	-0.01018
C	-16.12513	-3.15506	0.90036
C	-14.80147	-3.71006	-1.03175
C	-16.79102	-4.36752	0.78872
H	-16.37965	-2.46114	1.69202
C	-15.46002	-4.92703	-1.12969
H	-14.03316	-3.44483	-1.74759
C	-16.45862	-5.25996	-0.22247
H	-17.56731	-4.61805	1.50167
H	-15.2	-5.61219	-1.92761
H	-16.9763	-6.20768	-0.30525
C	-15.27185	-0.38994	0.17916
C	-15.07436	0.52944	1.20654
C	-16.28423	-0.17418	-0.75159
C	-15.8739	1.65992	1.29072
H	-14.2948	0.35502	1.93793
C	-17.09077	0.95095	-0.65395
H	-16.43906	-0.89178	-1.5479
C	-16.88655	1.87427	0.3635
H	-15.71282	2.3693	2.09359
H	-17.87676	1.10947	-1.38249
H	-17.51431	2.75391	0.43565
C	15.13298	-2.81031	-0.24634
C	14.85777	-3.59455	-1.36278
C	16.0957	-3.22298	0.66906
C	15.53254	-4.79195	-1.55164
H	14.11691	-3.26374	-2.0804
C	16.77712	-4.41526	0.46831
H	16.31052	-2.60688	1.53353
C	16.49533	-5.20521	-0.63891

H	15.31348	-5.39746	-2.42275
H	17.52619	-4.73003	1.18472
H	17.02587	-6.13692	-0.79206
C	15.26502	-0.3969	0.09973
C	15.13791	0.40522	1.23006
C	16.20644	-0.07763	-0.87327
C	15.93902	1.52843	1.37612
H	14.41317	0.14564	1.99205
C	17.01434	1.0399	-0.71588
H	16.30572	-0.70799	-1.74841
C	16.88068	1.8484	0.40563
H	15.83532	2.14816	2.25855
H	17.74612	1.28211	-1.47696
H	17.50996	2.72176	0.52517
H	1.3155	-4.01264	0.68615
H	-1.29918	-4.0036	0.65447

Table 1-8 Atomic coordinates of the triplet dication of **2A** calculated by CAM-B3LYP/6-311+g(d,p).

atom	x	y	z
H	-3.12105	4.93478	0.74121
H	-2.97651	4.62279	-1.0017
H	-0.72194	4.76927	0.07306
H	-0.9984	3.14379	-0.56919
H	-1.1521	3.45174	1.1738
H	-7.8499	4.43598	-2.20799
H	-6.24531	5.19241	-2.29157
H	-7.73297	6.4783	-0.75067
H	-6.38678	5.76241	0.14575

H	-8.002	5.02821	0.22451
H	2.95358	4.78432	0.12046
H	1.6392	3.61174	0.29658
H	3.24692	4.83419	2.61477
H	1.93242	3.65554	2.79178
H	1.59306	5.27633	2.1695
H	7.56241	4.80076	-1.602
H	7.62858	5.05866	0.14941
H	5.24525	5.77661	-1.65551
H	6.40805	6.93199	-0.99102
H	5.32755	6.05342	0.09758
H	-3.28889	-2.40325	0.40474
H	3.29477	-2.41878	0.49102
H	-10.60617	0.8431	0.06703
H	-13.03277	0.69398	0.0771
H	-8.69968	0.69561	-0.43448
H	12.97089	0.62101	-0.40275
H	10.57841	0.75752	-0.37337
H	10.3361	-3.41772	0.63492
H	12.77592	-3.55624	0.60362
H	8.66468	0.76459	-0.12615
C	-2.78325	4.22161	-0.00792
C	-1.32621	3.86575	0.17922
O	-3.6384	3.06794	0.19396
O	-3.36326	2.4129	-1.93833
C	-3.85925	2.28015	-0.85015
C	-6.9597	4.69628	-1.6384
C	-7.28842	5.53571	-0.42521
O	-6.28566	3.46935	-1.25459
O	-8.24619	2.4335	-0.91836

C	-7.02526	2.42647	-0.91509
C	2.54838	3.99739	0.75675
C	2.32167	4.46384	2.17122
O	3.51833	2.91617	0.8045
O	3.40579	2.64541	-1.42462
C	3.84377	2.35703	-0.34402
C	6.96232	4.89803	-0.69769
C	5.91532	5.97387	-0.8179
O	6.26889	3.63464	-0.48742
O	8.22263	2.54647	-0.38122
C	7.0065	2.55482	-0.35581
C	-2.61385	-1.56078	0.23674
C	2.61923	-1.5764	0.32966
S	0.01181	-0.66762	0.11513
C	-1.21207	-1.8653	0.32982
C	-0.68511	-3.12543	0.5841
C	0.70221	-3.12971	0.60307
C	1.24889	-1.86643	0.36746
C	-10.29475	-1.30142	0.17512
C	-11.06121	-0.13728	0.11957
C	-12.44044	-0.20868	0.13772
O	-8.16125	-2.30591	0.46384
C	-8.79862	-1.30869	0.18029
N	-8.17884	-0.13691	-0.15804
N	-3.02227	-0.37696	-0.03678
S	-5.67846	-1.18402	0.17305
C	-6.82151	0.05268	-0.19897
C	-6.22471	1.25475	-0.54457
C	-4.80521	1.17185	-0.50373
C	-4.347	-0.06359	-0.13943

C	12.40247	-0.26649	-0.16528
C	11.02842	-0.20046	-0.14252
C	10.25458	-1.33281	0.14277
C	10.92124	-2.53745	0.40252
C	12.29239	-2.61512	0.38427
O	8.10926	-2.33348	0.36208
C	8.797	-1.34736	0.18434
N	8.14419	-0.10596	0.00702
N	3.06053	-0.35911	0.11484
S	5.69326	-1.23145	0.21377
C	6.82392	0.05778	0.00557
C	6.2011	1.32879	-0.1704
C	4.82608	1.2391	-0.14315
C	4.35216	-0.07508	0.05726
C	13.07199	-1.47646	0.09908
C	-13.0646	-1.45647	0.20074
C	-10.92848	-2.54133	0.25102
H	-10.32404	-3.43557	0.31557
C	-12.30478	-2.62808	0.25538
H	-12.79285	-3.59025	0.33176
N	-14.47533	-1.53349	0.21434
N	14.44999	-1.54429	0.07946
C	-15.12844	-2.52355	-0.53254
C	-16.28411	-3.13333	-0.02045
C	-14.62164	-2.90129	-1.78566
C	-16.9197	-4.10943	-0.7607
H	-16.64592	-2.86589	0.9631
C	-15.27666	-3.87137	-2.51596
H	-13.74707	-2.40779	-2.18753
C	-16.4228	-4.47848	-2.00777

H	-17.79933	-4.59589	-0.36005
H	-14.90104	-4.1503	-3.49172
H	-16.9284	-5.24245	-2.58461
C	-15.21391	-0.61806	0.98186
C	-14.73727	-0.22052	2.23929
C	-16.42147	-0.10786	0.48426
C	-15.47488	0.67183	2.99062
H	-13.81922	-0.64018	2.62809
C	-17.14006	0.7929	1.24486
H	-16.76281	-0.39176	-0.50216
C	-16.67324	1.18187	2.49718
H	-15.12167	0.96482	3.97061
H	-18.06236	1.20429	0.85624
H	-17.24374	1.88536	3.09015
C	15.13471	-2.79364	-0.05391
C	14.88721	-3.61812	-1.14738
C	16.07626	-3.16936	0.89837
C	15.56882	-4.8196	-1.2767
H	14.16285	-3.3154	-1.89367
C	16.76449	-4.36629	0.75733
H	16.2694	-2.52123	1.74435
C	16.51042	-5.19649	-0.32692
H	15.37197	-5.45703	-2.13015
H	17.4973	-4.65274	1.50185
H	17.04646	-6.13152	-0.43361
C	15.25657	-0.36736	0.18966
C	15.1307	0.46983	1.29415
C	16.19329	-0.07754	-0.79669
C	15.92933	1.59926	1.40123
H	14.40945	0.23252	2.06667

C	16.99835	1.04686	-0.67841
H	16.29138	-0.73587	-1.65112
C	16.86635	1.89029	0.41728
H	15.82736	2.2467	2.26373
H	17.72687	1.26658	-1.44935
H	17.49374	2.76862	0.50649
H	1.31344	-4.00457	0.77819
H	-1.30511	-3.99678	0.74233

Table 1-9 Atomic coordinates of the neutral singlet of **1B** calculated by CAM-B3LYP/6-311+g(d,p).

atom	x	y	z
H	-3.39618	4.77003	0.8824
H	-3.20408	4.5019	-0.86329
H	-0.97301	4.6529	0.27819
H	-1.21286	3.04352	-0.41579
H	-1.41978	3.30011	1.32735
H	-8.15385	4.18023	-2.02131
H	-6.58176	5.00053	-2.11409
H	-8.08305	6.17814	-0.50258
H	-6.69082	5.48734	0.34257
H	-8.2743	4.68855	0.43085
H	3.57759	3.91463	3.13286
H	3.27438	4.38512	1.44684
H	1.59173	2.3899	3.06555
H	1.27799	2.86991	1.38647
H	1.12092	4.05412	2.69112
H	8.19623	4.40817	1.15632
H	6.62877	5.2431	1.14187
H	6.68786	5.31023	-1.36299

H	8.26944	4.50272	-1.34701
H	8.09671	6.12807	-0.67224
H	-3.31262	-2.57415	0.07356
H	3.30192	-2.57433	0.13176
H	-10.6694	0.40111	0.46672
H	-13.1026	0.19744	0.53569
H	-8.84023	0.33842	-0.35217
H	13.02899	0.13388	-1.19257
H	10.60239	0.34115	-0.99622
H	10.3061	-3.84787	-0.11992
H	12.76873	-4.05277	-0.31714
H	8.83424	0.35546	-0.02398
C	-3.02855	4.0799	0.12523
C	-1.57122	3.74144	0.34128
O	-3.86415	2.90702	0.28024
O	-3.55401	2.3361	-1.86936
C	-4.05281	2.14198	-0.79034
C	-7.26081	4.4545	-1.46251
C	-7.59537	5.24381	-0.21694
O	-6.53316	3.24566	-1.13436
O	-8.44957	2.13242	-0.78944
C	-7.22878	2.1625	-0.80975
C	3.14774	3.59482	2.18544
C	1.69735	3.19637	2.33812
O	3.95996	2.46239	1.79221
O	3.52038	2.82473	-0.38067
C	4.07097	2.20405	0.49194
C	7.29271	4.5916	0.57736
C	7.60328	5.16087	-0.78853
O	6.55474	3.34965	0.46926

O	8.4605	2.18508	0.26361
C	7.2407	2.22432	0.30904
C	-2.65231	-1.70385	0.02476
C	2.64198	-1.70241	0.12464
S	-0.00443	-0.79336	0.042
C	-1.25018	-2.00706	0.09557
C	-0.71725	-3.26914	0.17636
C	0.7029	-3.26989	0.19577
C	1.23866	-2.0082	0.12795
C	-10.3271	-1.72309	0.22677
C	-11.11515	-0.58136	0.36899
C	-12.497	-0.69239	0.41757
O	-8.14703	-2.66827	0.38824
C	-8.83756	-1.6844	0.18103
N	-8.27062	-0.47319	-0.11987
N	-3.08967	-0.5087	-0.10386
S	-5.71695	-1.42153	0.11174
C	-6.92282	-0.2198	-0.1862
C	-6.38037	1.01347	-0.49475
C	-4.94953	0.98566	-0.48204
C	-4.43593	-0.23684	-0.17912
C	12.43806	-0.73956	-0.94675
C	11.06097	-0.62518	-0.82493
C	10.29129	-1.74712	-0.51903
C	10.91428	-2.98195	-0.34656
C	12.29062	-3.09171	-0.46072
O	8.10996	-2.7019	-0.46555
C	8.8071	-1.70413	-0.38733
N	8.25421	-0.47067	-0.15899
N	3.08085	-0.50088	0.1176

S	5.69478	-1.43101	-0.16763
C	6.91167	-0.21107	-0.03469
C	6.38283	1.04538	0.19319
C	4.95316	1.02032	0.25306
C	4.42747	-0.22294	0.08489
C	13.05454	-1.97006	-0.76075
C	-13.09998	-1.93977	0.3211
C	-10.93757	-2.97333	0.1432
H	-10.31583	-3.85336	0.04305
C	-12.31823	-3.08068	0.18408
H	-12.78582	-4.05471	0.11018
O	1.42799	-4.40552	0.26147
O	-1.44479	-4.40359	0.23776
C	-0.67028	-5.57817	-0.05707
C	0.65034	-5.54196	0.67441
H	-14.17948	-2.0229	0.35653
H	14.1304	-2.05562	-0.8539
H	1.24535	-6.42087	0.43696
H	0.49435	-5.48856	1.7549
H	-1.26702	-6.42686	0.26918
H	-0.51466	-5.63595	-1.13732

Table 1-10 Atomic coordinates of the radical cation of **1B** calculated by CAM-B3LYP/6-311+g(d,p).

atom	x	y	z
H	-3.3985	4.69575	1.22311
H	-3.03199	4.47133	-0.50083
H	-0.92761	4.61841	0.86444
H	-1.07422	3.02819	0.10448

H	-1.4585	3.23196	1.82607
H	-7.82479	4.29801	-1.99939
H	-6.21874	5.05598	-2.02395
H	-7.72381	6.26029	-0.43451
H	-6.38823	5.49552	0.43815
H	-8.00528	4.76099	0.45901
H	3.61175	3.96187	3.16268
H	3.05758	4.2963	1.5076
H	1.76572	2.29598	3.44911
H	1.20255	2.6314	1.79895
H	1.11177	3.88821	3.03917
H	8.02246	4.51172	0.83794
H	6.42869	5.29405	0.9095
H	6.30204	5.26591	-1.59435
H	7.90918	4.51134	-1.66747
H	7.72825	6.15413	-1.04114
H	-3.2886	-2.66805	0.29559
H	3.27793	-2.6818	0.47887
H	-10.57391	0.49096	0.16401
H	-13.00994	0.35208	0.07414
H	-8.69621	0.42533	-0.53569
H	12.77598	0.28083	-1.71782
H	10.37333	0.42552	-1.31645
H	10.28121	-3.75451	-0.32805
H	12.72128	-3.89094	-0.73778
H	8.67335	0.4403	-0.25538
C	-2.94797	4.02898	0.49062
C	-1.51612	3.69893	0.84187
O	-3.78183	2.84288	0.53538
O	-3.26573	2.31474	-1.58841

C	-3.86744	2.11155	-0.56669
C	-6.94118	4.52668	-1.40652
C	-7.28357	5.30119	-0.15446
O	-6.27273	3.28093	-1.079
O	-8.23649	2.21995	-0.85645
C	-7.01769	2.21849	-0.81668
C	3.08794	3.55237	2.30167
C	1.7095	3.05411	2.66656
O	3.93091	2.45117	1.86667
O	3.30764	2.69197	-0.2849
C	3.94594	2.15367	0.57869
C	7.07471	4.64752	0.32031
C	7.26195	5.16799	-1.08559
O	6.37243	3.3728	0.31358
O	8.28464	2.24623	-0.00973
C	7.07678	2.27302	0.13821
C	-2.6197	-1.80781	0.24057
C	2.60975	-1.82038	0.43297
S	0.00274	-0.87094	0.29958
C	-1.23279	-2.09335	0.364
C	-0.70342	-3.37286	0.50235
C	0.69096	-3.37984	0.54668
C	1.24784	-2.09239	0.44131
C	-10.27109	-1.62974	-0.15847
C	-11.03634	-0.47315	-0.00913
C	-12.42056	-0.54762	-0.05008
O	-8.12546	-2.63552	0.08351
C	-8.78496	-1.63098	-0.11104
N	-8.16482	-0.41562	-0.31209
N	-3.03467	-0.5985	0.05096

S	-5.67634	-1.46077	0.04631
C	-6.81859	-0.20797	-0.27465
C	-6.22011	1.0309	-0.4895
C	-4.81078	0.96337	-0.37895
C	-4.34597	-0.29933	-0.09481
C	12.23476	-0.60266	-1.4041
C	10.87156	-0.52414	-1.16468
C	10.16772	-1.66267	-0.7704
C	10.83934	-2.87697	-0.6269
C	12.20217	-2.94854	-0.85873
O	8.02736	-2.66406	-0.46882
C	8.70912	-1.66152	-0.51261
N	8.11797	-0.41647	-0.30022
N	3.06193	-0.58307	0.37842
S	5.64055	-1.49173	-0.05295
C	6.80449	-0.21827	-0.08274
C	6.24083	1.0571	0.13778
C	4.86425	0.99593	0.31813
C	4.34829	-0.30798	0.24616
C	12.90085	-1.81123	-1.24723
C	-13.04713	-1.77182	-0.24407
C	-10.90583	-2.85774	-0.34017
H	-10.30203	-3.74944	-0.44619
C	-12.28823	-2.92723	-0.38886
H	-12.77528	-3.88265	-0.53893
O	1.41728	-4.48409	0.67636
O	-1.44499	-4.48983	0.56832
C	-0.67128	-5.67248	0.29004
C	0.63558	-5.64426	1.04745
H	-14.12843	-1.82583	-0.27887

H	13.96667	-1.86772	-1.4317
H	1.24601	-6.50907	0.80118
H	0.46746	-5.60536	2.12489
H	-1.27692	-6.5171	0.60838
H	-0.50004	-5.72985	-0.78706

Table 1-11 . Atomic coordinates of the triplet dication of **1B** calculated by CAM-B3LYP/6-311+g(d,p).

atom	x	y	z
H	-2.54195	4.53921	-0.44199
H	-2.53262	3.92601	-2.10989
H	-0.22299	3.89894	-1.12744
H	-0.76711	2.25387	-1.47881
H	-0.79159	2.86423	0.18886
H	-7.69521	3.96673	-2.95881
H	-6.06137	4.59411	-3.26909
H	-7.36536	6.21072	-1.87931
H	-5.99644	5.57075	-0.96086
H	-7.63965	4.96511	-0.65633
H	3.1641	2.55477	4.45664
H	2.84582	3.54842	3.01843
H	1.3115	1.003	3.80041
H	0.9771	2.00118	2.36933
H	0.7106	2.65548	3.99036
H	7.916	4.04318	2.45018
H	6.31935	4.68674	2.89316
H	6.02655	5.56488	0.56231
H	7.63662	4.94975	0.12769
H	7.47355	6.24415	1.31923

H	-3.30378	-2.79924	-0.21991
H	3.26853	-2.79797	0.54235
H	-10.36496	0.99032	0.27557
H	-12.78356	1.03954	0.55731
H	-8.57097	0.63495	-0.47313
H	12.68529	0.92109	-1.32325
H	10.30059	0.92442	-0.83646
H	10.11184	-3.28199	-1.7192
H	12.53926	-3.26924	-2.2118
H	8.53751	0.63887	-0.03385
C	-2.34393	3.6726	-1.06824
C	-0.94988	3.13063	-0.85701
O	-3.34673	2.70287	-0.6462
O	-3.32823	1.671	-2.64901
C	-3.72753	1.79733	-1.52342
C	-6.75518	4.26579	-2.49936
C	-6.94816	5.30979	-1.42557
O	-6.11887	3.07139	-1.95308
O	-8.0901	2.22261	-1.29675
C	-6.88033	2.16041	-1.39427
C	2.76992	2.54898	3.44328
C	1.35838	2.01298	3.39074
O	3.68466	1.67553	2.71981
O	3.24711	2.68694	0.75488
C	3.81687	1.86765	1.42233
C	6.93489	4.32552	2.07323
C	7.01954	5.32497	0.94433
O	6.24991	3.11126	1.64174
O	8.14276	2.24577	0.80211
C	6.95026	2.18612	1.02858

C	-2.61639	-1.9517	-0.17745
C	2.58557	-1.95399	0.42445
S	-0.01045	-1.03144	0.08683
C	-1.24881	-2.25442	0.01793
C	-0.73667	-3.53319	0.14575
C	0.67746	-3.53542	0.31149
C	1.20836	-2.25928	0.29291
C	-10.19509	-1.14378	0.64263
C	-10.88048	0.06402	0.49681
C	-12.25531	0.10098	0.66457
O	-8.08004	-2.22237	0.84343
C	-8.73313	-1.26517	0.49609
N	-8.065	-0.17669	-0.10495
N	-3.01632	-0.72411	-0.33567
S	-5.64674	-1.34745	0.22116
C	-6.74788	-0.11126	-0.27871
C	-6.10015	1.00642	-0.88748
C	-4.73366	0.85416	-0.92559
C	-4.29899	-0.37798	-0.38644
C	12.12555	-0.00165	-1.4047
C	10.76919	-0.00904	-1.12215
C	10.04257	-1.1963	-1.2329
C	10.68632	-2.36922	-1.63314
C	12.04192	-2.35701	-1.908
O	7.90161	-2.24172	-1.23282
C	8.59609	-1.28851	-0.96197
N	7.99614	-0.17939	-0.32925
N	3.00318	-0.72549	0.43617
S	5.55403	-1.34814	-0.38187
C	6.70307	-0.10483	-0.02363

C	6.12302	1.02153	0.63319
C	4.76879	0.86917	0.82547
C	4.2829	-0.373	0.35934
C	12.76216	-1.17316	-1.79388
C	-12.95048	-1.06124	0.97317
C	-10.89774	-2.307	0.96371
H	-10.35454	-3.23554	1.07936
C	-12.27118	-2.26518	1.12289
H	-12.81434	-3.16998	1.36402
O	1.3813	-4.65172	0.46159
O	-1.45871	-4.647	0.11402
C	-0.66624	-5.84249	-0.08375
C	0.57046	-5.80835	0.7782
H	-14.02558	-1.0281	1.09989
H	13.8232	-1.16304	-2.0109
H	1.19657	-6.67526	0.58559
H	0.31807	-5.76474	1.83894
H	-1.30583	-6.67576	0.19422
H	-0.41342	-5.90925	-1.14324

Table 1-12. Atomic coordinates of the neutral singlet of **2** calculated by CAM-B3LYP/6-311+g(d,p).

atom	x	y	z
H	7.26786	2.81321	-0.82633
H	8.25926	1.5259	-0.11017
H	7.3637	1.65173	-3.04414
H	8.37474	0.37783	-2.3314
H	8.98847	2.03234	-2.45677
H	3.621	3.68698	0.75731

H	5.14253	3.60176	1.66937
H	3.90204	2.71342	3.6562
H	2.37742	2.82176	2.75232
H	3.26926	4.29164	3.16816
H	-2.82485	1.56144	0.52971
H	-0.52456	0.82142	0.55996
H	-1.74736	-3.0876	-0.70837
H	-4.08413	-2.33699	-0.74779
H	-4.05233	1.63177	-2.12262
H	-4.62412	3.99462	-2.53816
H	-6.20222	5.17748	-1.03638
H	-7.19343	3.9723	0.8896
H	-6.59823	1.61542	1.31642
H	-5.1717	-1.64039	1.87126
H	-7.03468	-3.21014	2.25737
H	-8.97049	-3.2511	0.70956
H	-9.01648	-1.71108	-1.23216
H	-7.138	-0.16015	-1.62888
H	1.24998	0.18591	-0.09834
C	7.5453	1.7626	-0.89769
C	8.09718	1.43029	-2.26684
O	6.31579	1.05207	-0.64141
O	7.46966	-0.724	0.09905
C	6.40058	-0.17016	-0.11205
C	4.14525	3.17815	1.56457
C	3.37471	3.24798	2.86436
O	4.38413	1.80746	1.17192
O	2.39107	1.72018	0.15335
C	3.45621	1.19658	0.44697
C	-2.59676	0.54448	0.24157

C	-1.28426	0.11473	0.24758
C	-0.95593	-1.19823	-0.09491
C	-1.99111	-2.0682	-0.43849
C	-3.30413	-1.64576	-0.45918
C	-4.73314	2.15044	-1.459
C	-5.05762	3.47925	-1.68943
C	-5.94511	4.14197	-0.85021
C	-6.50204	3.46507	0.22738
C	-6.16902	2.14032	0.4719
C	-6.01181	-1.66473	1.18819
C	-7.06161	-2.54588	1.40187
C	-8.14888	-2.56692	0.53669
C	-8.17501	-1.70171	-0.54975
C	-7.12033	-0.82907	-0.7773
C	-6.03218	-0.80536	0.09165
C	-5.28243	1.47473	-0.37121
C	-3.63404	-0.32658	-0.11796
N	-4.96174	0.10778	-0.1316
O	0.67393	-2.92918	-0.15392
C	0.42669	-1.73121	-0.09865
N	1.43909	-0.81103	-0.05112
N	6.04001	-3.08611	0.05553
S	3.37786	-2.75029	-0.0661
C	2.7857	-1.10627	-0.02105
C	3.79378	-0.19098	0.11031
C	5.10865	-0.80862	0.10341
C	5.02908	-2.18132	0.04326
H	6.97271	-2.69274	0.02914
H	5.90335	-3.98243	-0.38477

Table 1-13 Atomic coordinates of the radical cation of **2** calculated by CAM-B3LYP/6-311+g(d,p).

atom	x	y	z
H	7.3067	2.7695	-0.84767
H	8.25045	1.50766	-0.02566
H	7.55323	1.53926	-3.01819
H	8.52267	0.29306	-2.20218
H	9.13338	1.94602	-2.33662
H	3.69793	3.70195	0.70581
H	5.26115	3.60656	1.54636
H	4.1015	2.78459	3.61088
H	2.53497	2.90439	2.78005
H	3.47393	4.36294	3.11905
H	-2.79367	1.64468	0.18245
H	-0.5103	0.9156	0.21952
H	-1.78145	-3.15208	-0.36503
H	-4.10926	-2.40893	-0.39908
H	-4.28499	1.54481	-2.27603
H	-4.89193	3.89983	-2.71268
H	-6.25881	5.15452	-1.07116
H	-7.00882	4.03904	1.00958
H	-6.38113	1.68912	1.4504
H	-5.3116	-1.42548	2.02004
H	-7.2033	-2.96269	2.42577
H	-9.00918	-3.17976	0.74397
H	-8.90602	-1.85474	-1.34635
H	-7.00022	-0.33415	-1.75596
H	1.28477	0.20887	0.02692
C	7.59935	1.72224	-0.87095
C	8.23443	1.34451	-2.18866

O	6.34588	1.00876	-0.67565
O	7.40681	-0.75574	0.21744
C	6.391	-0.17462	-0.10591
C	4.25026	3.20787	1.50263
C	3.54504	3.31143	2.83448
O	4.44477	1.81415	1.12779
O	2.42043	1.71726	0.16978
C	3.49006	1.21482	0.45679
C	-2.58131	0.59339	0.05267
C	-1.27467	0.16295	0.06863
C	-0.95795	-1.19359	-0.07813
C	-2.01193	-2.1021	-0.23988
C	-3.32029	-1.68415	-0.25851
C	-4.87284	2.09938	-1.55486
C	-5.21637	3.42169	-1.7964
C	-5.98594	4.12448	-0.87734
C	-6.40792	3.49833	0.28853
C	-6.05641	2.1796	0.54099
C	-6.09709	-1.53091	1.28166
C	-7.16124	-2.39245	1.50572
C	-8.17585	-2.51182	0.56388
C	-8.11882	-1.76732	-0.60739
C	-7.0501	-0.91357	-0.84225
C	-6.03611	-0.79494	0.10222
C	-5.28637	1.47785	-0.38043
C	-3.64021	-0.31974	-0.11269
N	-4.95167	0.10929	-0.13045
O	0.68747	-2.90889	-0.13835
C	0.3985	-1.72816	-0.06995
N	1.45263	-0.79776	0.01884

N	5.9577	-3.06125	-0.08713
S	3.29236	-2.78171	-0.10886
C	2.74578	-1.13298	0.02414
C	3.8035	-0.20276	0.13926
C	5.05476	-0.80586	0.03562
C	4.95132	-2.21943	-0.04853
H	6.89901	-2.68823	0.01347
H	5.82422	-4.0601	-0.16493

Table 1-14 Atomic coordinates of the triplet dication of **2** calculated by CAM-B3LYP/6-311+g(d,p).

atom	x	y	z
H	7.25599	2.85182	-0.5824
H	8.19051	1.54991	0.18667
H	7.57569	1.75764	-2.8169
H	8.53758	0.47416	-2.05008
H	9.13166	2.13805	-2.06807
H	3.59259	3.63541	0.98657
H	5.17133	3.50171	1.7925
H	4.05746	2.52666	3.8153
H	2.47423	2.68768	3.02371
H	3.40742	4.12831	3.44436
H	-2.87557	1.45914	0.79098
H	-0.56074	0.70281	0.76226
H	-1.7688	-2.96436	-1.12896
H	-4.1183	-2.19461	-1.0995
H	-3.79711	1.50101	-2.08265
H	-4.3159	3.8228	-2.72324
H	-6.07729	5.07874	-1.52096
H	-7.31978	4.01187	0.3343
H	-6.80053	1.69427	0.99654

H	-4.8004	-1.70246	1.77689
H	-6.59823	-3.23987	2.46364
H	-8.80329	-3.15139	1.3434
H	-9.20891	-1.52617	-0.47862
H	-7.4146	0.00689	-1.18817
H	1.24514	0.19239	0.00024
C	7.56182	1.81125	-0.66224
C	8.2362	1.51975	-1.98195
O	6.30954	1.07489	-0.54689
O	7.35854	-0.73581	0.26534
C	6.35096	-0.1401	-0.05365
C	4.1638	3.09617	1.73946
C	3.48192	3.09953	3.08707
O	4.36783	1.73223	1.26668
O	2.33955	1.67255	0.31392
C	3.42014	1.17062	0.55991
C	-2.62863	0.50193	0.35235
C	-1.31849	0.06397	0.32784
C	-1.00727	-1.18438	-0.21034
C	-2.02206	-1.99985	-0.71061
C	-3.33405	-1.57418	-0.68739
C	-4.55214	2.05999	-1.54652
C	-4.85273	3.35679	-1.90749
C	-5.85136	4.05914	-1.23575
C	-6.55787	3.45767	-0.19787
C	-6.27921	2.15705	0.16968
C	-5.75873	-1.68029	1.27603
C	-6.77135	-2.5326	1.66314
C	-8.01526	-2.47504	1.03758
C	-8.24848	-1.55505	0.01892

C	-7.2511	-0.68646	-0.37445
C	-5.99794	-0.74517	0.25631
C	-5.27188	1.45117	-0.50661
C	-3.63487	-0.31782	-0.1582
N	-4.97931	0.13155	-0.13689
O	0.63004	-2.89115	-0.46441
C	0.37639	-1.72426	-0.26345
N	1.41231	-0.81345	-0.07816
N	5.94692	-3.02073	-0.27751
S	3.27919	-2.76485	-0.3554
C	2.71666	-1.14264	-0.08223
C	3.75644	-0.21487	0.13224
C	5.01531	-0.79268	0.00114
C	4.92992	-2.19809	-0.20381
H	6.88017	-2.6447	-0.11852
H	5.83225	-4.01292	-0.43664

Table 1-15 Excitation energies and oscillator strengths (f) of the neutral singlet of **2B**. Total energy E(TD-HF/TD-DFT)= -4973.7019 Hartrees.

Excited state transition 457 nm (2.7128 eV) f=2.1716

From orbital	(#)	To orbital	(#)	f
HOMO-3	316	LUMO+1	321	0.10899
HOMO-2	317	LUMO	320	-0.25878
HOMO	319	LUMO	320	0.62034

Excited state transition 357.63 nm (3.4668 eV) f=0.0069

From orbital	(#)	To orbital	(#)	f
HOMO-3	316	LUMO	320	0.40558
HOMO-2	317	LUMO+3	323	0.11164
HOMO-1	318	LUMO	320	-0.28202
HOMO-1	318	LUMO+2	322	-0.20964

HOMO	319	LUMO+1	321	0.38421

Excited state transition 334.85 nm (3.7027 eV) f=0.2628

From orbital	(#)	To orbital	(#)	f
HOMO-4	315	LUMO	320	0.58974
HOMO-3	316	LUMO	320	-0.21806
HOMO-1	318	LUMO+2	322	-0.12074
HOMO	319	LUMO+1	321	0.16129

Excited state transition 334.57 nm (3.7058 eV) f=1.0076

From orbital	(#)	To orbital	(#)	f
HOMO-4	315	LUMO	320	-0.1441
HOMO-2	317	LUMO	320	-0.23924
HOMO-2	317	LUMO+2	322	-0.17223
HOMO-2	317	LUMO+6	326	-0.12584
HOMO-1	318	LUMO+1	321	0.37823
HOMO-1	318	LUMO+3	323	0.14093
HOMO	319	LUMO+2	322	-0.37798

Excited state transition 318.03 nm (3.8985 eV) f=0.1342

From orbital	(#)	To orbital	(#)	f
HOMO-4	315	LUMO	320	0.26256
HOMO-3	316	LUMO	320	0.36075
HOMO-2	317	LUMO+1	321	-0.29193
HOMO-2	317	LUMO+7	327	-0.10254
HOMO-1	318	LUMO+2	322	0.31492
HOMO-1	318	LUMO+6	326	0.11413
HOMO	319	LUMO+1	321	-0.1006
HOMO	319	LUMO+3	323	-0.19499

Table 1-16 Excitation energies and oscillator strengths (f) of the radical cation of **2B**. Total energy E(TD-HF/TD-DFT)= -4973.55739 Hartrees.

Excited state transition 1125.61 nm (1.1015 eV) f=0.9470

From orbital	(#)	To orbital	(#)	f
HOMO-2	317A	LUMO	320A	-0.14939
HOMO-8	310B	LUMO	319B	0.16914
HOMO-8	310B	LUMO+1	320B	-0.10161
HOMO-2	316B	LUMO	319B	0.81036
HOMO-2	316B	LUMO+1	320B	0.21727
HOMO-1	317B	LUMO	319B	-0.25234
HOMO	318B	LUMO	319B	-0.35759
LUMO	319B	HOMO-2	316B	0.11688

Excited state transition 706.72 nm (1.7544 eV) f=1.2344

From orbital	(#)	To orbital	(#)	f
HOMO-16	303A	LUMO	320A	-0.14835
HOMO-3	316A	LUMO	320A	-0.13087
HOMO-3	316A	LUMO+1	321A	-0.15059
HOMO-3	316A	LUMO+3	323A	0.14149
HOMO-2	317A	LUMO	320A	0.6785
HOMO-1	318A	LUMO	320A	0.30784
HOMO	319A	LUMO	320A	-0.39014
HOMO-3	315B	LUMO	319B	-0.1616
HOMO-2	316B	LUMO+1	320B	-0.1027
HOMO-1	317B	LUMO	319B	-0.18327
HOMO	318B	LUMO	319B	-0.11311

Excited state transition 659.34 nm (1.8804 eV) f=0.0984

From orbital	(#)	To orbital	(#)	f
HOMO-4	315A	LUMO	320A	-0.13695
HOMO-3	316A	LUMO	320A	0.14828

HOMO-9	310B	LUMO	319B	0.17824
HOMO-5	314B	LUMO	319B	0.19572
HOMO-3	315B	LUMO	319B	0.70214
HOMO-3	315B	LUMO+1	320B	0.13476
HOMO-2	316B	LUMO	319B	-0.13529
HOMO-2	316B	LUMO	320B	-0.11985
HOMO-1	317B	LUMO	319B	-0.50991
HOMO-1	317B	LUMO+1	320B	0.123

Excited state transition 623.18 nm (1.9896 eV) f=0.0731

From orbital	(#)	To orbital	(#)	f
HOMO-4	315A	LUMO	320A	-0.11992
HOMO-2	317A	LUMO	320A	0.15188
HOMO-1	318A	LUMO	320A	0.10789
HOMO-5	313B	LUMO	319B	0.11438
HOMO-3	315B	LUMO	319B	0.49359
HOMO-3	315B	LUMO+1	320B	0.11552
HOMO-2	316B	LUMO	319B	0.22777
HOMO-1	317B	LUMO	319B	0.70521
HOMO-1	317B	LUMO+1	320B	-0.12019
HOMO-1	317B	LUMO+2	321B	-0.10036
HOMO	318B	LUMO	319B	-0.13236

Excited state transition 577.79 nm (2.1458 eV) f=0.0153

From orbital	(#)	To orbital	(#)	f
HOMO-3	316A	LUMO	320A	0.3746
HOMO-2	317A	LUMO+1	321A	-0.14461
HOMO-2	317A	LUMO+3	323A	0.11659
HOMO-1	318A	LUMO	320A	-0.11979
HOMO-11	307B	LUMO	319B	-0.12113

HOMO-8	310B	LUMO	319B	0.35849
HOMO-3	315B	LUMO	319B	-0.12586
HOMO-2	316B	LUMO	319B	0.30558
HOMO-2	316B	LUMO+1	320B	-0.3529
HOMO-1	317B	LUMO	319B	0.10837
HOMO	318B	LUMO	319B	0.47969
HOMO	318B	LUMO+1	320B	0.20685

Table 1-17 Excitation energies and oscillator strengths (f) of the dication of **2B**. Total energy E(TD-HF/TD-DFT)= -4973.319834 Hartrees.

Excited state transition 819.02 nm (1.5138 eV) f=2.9175

From orbital	(#)	To orbital	(#)	f
HOMO-2	316	LUMO	319	0.50142
HOMO	318	LUMO	319	0.47281

Excited state transition 640.08 nm (1.937 eV) f=0.0032

From orbital	(#)	To orbital	(#)	f
HOMO-1	317	LUMO	319	0.67793
HOMO	318	LUMO+1	320	0.15721

Excited state transition 614.01 nm (2.0192 eV) f=0.0032

From orbital	(#)	To orbital	(#)	f
HOMO-2	316	LUMO	319	-0.47799
HOMO-1	317	LUMO+1	320	0.14068
HOMO	318	LUMO	319	0.48101

Excited state transition 539.27 nm (2.2991 eV) f=0.0853

From orbital	(#)	To orbital	(#)	f
HOMO-7	311	LUMO	319	0.67174
HOMO-7	311	LUMO+2	321	-0.10058

Excited state transition 473.51 nm (2.6184 eV) f=0.1662

From orbital	(#)	To orbital	(#)	f
HOMO-2	316	LUMO+1	320	0.5623
HOMO	318	LUMO+1	320	0.40218

Table 1-18 Excitation energies and oscillator strengths of the triplet dication of **2B**. Total energy E(TD-HF/TD-DFT)= -4973.33810045 Hartrees.

Excited State transition 700 nm (1.7712 eV) f=1.2467

From orbital	#	To orbital	#	
HOMO-11	308A	LUMO	320A	-0.10404
HOMO-2	317A	LUMO	320A	-0.10297
HOMO-2	317A	LUMO+1	321A	0.12431
HOMO-2	317A	LUMO+3	323A	-0.12254
HOMO-1	318A	LUMO	320A	0.6059
HOMO	319A	LUMO	320A	-0.28515
HOMO-5	312B	LUMO+1	319B	-0.12816
HOMO	317B	LUMO	318B	-0.12356
HOMO	317B	LUMO+1	319B	-0.57718
HOMO	317B	LUMO+2	320B	-0.15545

Excited State transition 683.58 nm (1.8138 eV) f=0.0377

From orbital	#	To orbital	#	
HOMO-4	315A	LUMO	320A	0.15482
HOMO-2	317A	LUMO	320A	0.20044
HOMO-1	318A	LUMO	320A	-0.25595
HOMO	319A	LUMO	320A	0.17988
HOMO-2	315B	LUMO	318B	0.14273
HOMO-2	315B	LUMO+1	319B	0.69685
HOMO-2	315B	LUMO+2	320B	-0.20554
HOMO-1	316B	LUMO+1	319B	0.20178
HOMO	317B	LUMO+1	319B	-0.38874

Excited State transition 637.42 nm (1.9451 eV) f=0.4263

From orbital	#	To orbital	#	
HOMO-4	315A	LUMO	320A	0.13786
HOMO-1	318A	LUMO	320A	0.32357

HOMO	319A	LUMO	320A	-0.20752
HOMO-6	311B	LUMO+1	319B	-0.15984
HOMO-2	315B	LUMO	318B	0.10888
HOMO-2	315B	LUMO+1	319B	0.50989
HOMO-2	315B	LUMO+2	320B	-0.12665
HOMO-1	316B	LUMO+1	319B	-0.29609
HOMO	317B	LUMO	318B	0.12411
HOMO	317B	LUMO+1	319B	0.53184

Excited State transition 585.61 nm (2.1172 eV) f=0.1107

From orbital	#	To orbital	#	
HOMO-2	317A	LUMO	320A	0.11017
HOMO-11	306B	LUMO	318B	0.45930
HOMO-10	307B	LUMO	318B	0.40774
HOMO-9	308B	LUMO	318B	-0.38153
HOMO-6	311B	LUMO	318B	-0.11617
HOMO-5	312B	LUMO	318B	-0.14228
HOMO-1	316B	LUMO	318B	0.48292
HOMO-1	316B	LUMO+1	319B	-0.19651
HOMO-1	316B	LUMO+2	320B	-0.12900
HOMO-1	316B	LUMO+3	321B	0.10132
HOMO	317B	LUMO	318B	0.16929

SUPPORTING INFORMATION IV
X-RAY CRYSTALLOGRAPHIC DATA

Extending the duty cycle of azomethine electrochromes by structural modification

Yohan Gautier and W. G. Skene

Table 1-19 Crystal data and structure refinement for **1C**.

Empirical formula	$C_{55}H_{49}N_5O_{10}S_2$ + 2x $CHCl_3$ (solvent)
Formula weight	1003.29 (1284.24 with solvent)
Temperature/K	100
Crystal system	Monoclinic
Space group	C2/c
a/Å	15.4323(7)
b/Å	18.1725(9)
c/Å	21.3004(10)
α/°	90
β/°	94.768(2)
γ/°	90
Volume/Å^3	5952.9(5)
Z	4
ρ_{calc}g/cm^3	1.387
μ/mm^{-1}	2.504
F(000)	2568.0
Crystal size/mm^3	0.17 × 0.12 × 0.06
Radiation	GaKα (λ = 1.34139)
Collection 2Θ range for data /°	6.55 to 121.53
Index ranges	-19 ≤ h ≤ 20, -22 ≤ k ≤ 23, -27 ≤ l ≤ 25
Reflections collected	39504
Independent reflections	6837 [R_{int} = 0.0531, R_{sigma} = 0.0370]
Data/restraints/parameters	6837/84/402
Goodness-of-fit on F^2	1.069
Final R indexes [I>=2σ (I)]	R_1 = 0.0469, wR_2 = 0.1323
Final R indexes [all data]	R_1 = 0.0572, wR_2 = 0.1395
Largest diff. peak/hole / e Å^{-3}	0.45/-0.28

Table 1-20 Fractional atomic coordinates ($\times 10^4$) and equivalent isotropic displacement parameters ($Å^2 \times 10^3$) for **1C**.

Atom	*x*	*y*	*z*	U(eq)
S1	6181.3(3)	2054.1(2)	4445.0(2)	38.76(13)
O1	4488.9(9)	2112.7(8)	4724.8(7)	53.7(4)
O2	8757.2(9)	611.9(8)	4395.8(6)	53.6(4)
O3	8794.1(8)	1079.4(7)	5374.3(6)	43.6(3)
O4	6126.3(9)	-16.9(7)	5657.6(6)	45.9(3)
O5	7546.0(8)	-101.9(7)	5500.6(6)	44.7(3)
N1	10000	4486.5(12)	2500	42.7(5)
N2	7875.2(9)	2225.3(8)	4111.5(6)	37.3(3)
N3	5244.8(9)	1142.6(9)	5143.8(7)	40.6(3)
C1	10000	6799.4(19)	2500	77.8(11)
C2	9804.3(18)	6408.0(13)	3030.6(11)	64.7(6)
C3	9810.8(14)	5652.7(11)	3035.8(9)	47.8(4)
C4	10000	5262.5(14)	2500	42.9(6)
C5	9411.0(12)	4085.1(10)	2846.1(8)	39.3(4)
C6	9701.4(11)	3457.6(10)	3177.2(8)	38.5(4)
C7	9139.1(11)	3056.0(10)	3510.3(8)	37.5(4)
C8	8266.9(11)	3268.8(10)	3516.6(7)	37.8(4)
C9	7984.4(12)	3900.0(10)	3193.1(8)	40.9(4)
C10	8548.4(12)	4309.8(10)	2858.4(8)	42.2(4)
C11	7656.4(11)	2836.2(10)	3850.3(8)	38.3(4)
C12	7282.8(11)	1817.0(10)	4419.3(8)	36.7(4)
C13	7493.4(11)	1194.4(10)	4748.1(7)	36.5(4)
C14	6771.1(11)	882.8(10)	5036.8(7)	36.8(4)
C15	6026.9(11)	1295.4(10)	4904.7(7)	37.4(4)
C16	4525.1(11)	1581.0(11)	5077.0(8)	43.8(4)
C17	3813.0(11)	1384.1(12)	5478.4(8)	44.7(4)
C18	3777.7(12)	718.3(12)	5798.0(8)	45.8(4)

C19	3106.3(13)	586.4(14)	6176.1(9)	55.2(5)
C20	2485.5(16)	1107.5(16)	6239.9(12)	72.5(7)
C21	2511.8(17)	1770.5(18)	5928.3(13)	79.9(8)
C22	3179.7(14)	1910.1(14)	5540.9(11)	60.9(6)
C23	8408.6(11)	915.9(10)	4807.1(8)	40.0(4)
C24	9691.5(13)	840.1(15)	5497.8(11)	62.4(6)
C25	9962(2)	1030(2)	6153.9(17)	116.4(15)
C26	6770.1(12)	220.3(10)	5426.5(8)	40.1(4)
C27	7611.3(15)	-762.5(12)	5887.9(9)	53.2(5)
C28	8513(2)	-1052.1(17)	5850.8(15)	84.0(9)
C29	10000	7639(2)	2500	147(3)
Cl1A	7394(2)	1237.3(11)	2682.5(8)	77.0(6)
Cl2A	9192(2)	1599.9(14)	2560.1(11)	117.3(13)
Cl3A	8669(3)	108.6(19)	2685(2)	80.9(9)
C1A	8466(5)	1024(4)	2908(4)	67.6(19)
Cl1B	7030.0(13)	1220.6(11)	2869.6(13)	73.7(6)
Cl3B	8569(3)	370.5(19)	2661.6(16)	73.4(8)
Cl2B	8437(2)	1930.3(10)	2353.2(8)	100.5(10)
C1B	8156(5)	1244(4)	2874(4)	67.9(19)

U_{eq} is defined as 1/3 of the trace of the orthogonalised U_{IJ} tensor.

Table 1-21 Anisotropic displacement parameters ($Å^2 \times 10^3$) for **1C**.

Atom	U_{11}	U_{22}	U_{33}	U_{23}	U_{13}	U_{12}
S1	34.5(2)	47.3(3)	35.3(2)	4.96(16)	8.32(16)	-1.16(17)
O1	40.1(7)	69.6(9)	52.8(8)	19.0(7)	12.2(6)	2.9(6)
O2	59.6(8)	62.1(9)	41.6(7)	-5.4(6)	18.4(6)	16.8(7)
O3	35.1(6)	52.2(8)	44.0(7)	-7.8(5)	6.0(5)	7.1(5)
O4	54.2(7)	47.7(7)	37.7(6)	2.4(5)	14.8(5)	-3.8(6)
O5	48.7(7)	48.2(7)	37.5(6)	6.7(5)	6.0(5)	2.9(6)
N1	51.2(12)	40.1(11)	39.7(11)	0	20.9(9)	0
N2	37.2(7)	45.3(8)	30.6(7)	-0.4(6)	9.9(5)	-1.9(6)
N3	37.8(7)	48.2(9)	37.1(7)	4.0(6)	10.9(6)	-5.0(6)
C1	131(4)	40.6(17)	61(2)	0	2(2)	0
C2	95.8(18)	48.8(12)	48.7(11)	-10.6(9)	0.1(11)	7.0(12)
C3	60.5(11)	46.9(11)	36.4(9)	-1.5(8)	5.8(8)	3.7(9)
C4	52.0(14)	41.3(14)	36.0(12)	0	7.2(10)	0
C5	46.2(9)	43.2(9)	30.8(8)	-2.5(7)	15.5(7)	-0.7(7)
C6	38.3(8)	45.5(10)	33.2(8)	-1.9(7)	12.4(6)	1.3(7)
C7	39.8(8)	42.3(9)	31.7(8)	0.4(6)	10.4(6)	2.0(7)
C8	40.1(8)	43.6(9)	31.1(8)	-2.3(7)	12.8(6)	0.2(7)
C9	40.8(9)	48.5(10)	35.0(8)	-0.2(7)	12.7(7)	5.1(7)
C10	50.6(10)	44.3(10)	33.4(8)	2.3(7)	14.0(7)	6.4(8)
C11	38.1(8)	46.2(10)	32.1(8)	-1.8(7)	12.6(6)	1.6(7)
C12	35.0(8)	43.9(9)	32.3(8)	-1.7(7)	9.9(6)	-1.0(7)
C13	37.4(8)	42.9(9)	30.3(7)	-3.7(6)	9.5(6)	-0.5(7)
C14	39.4(8)	42.3(9)	29.7(7)	-2.0(6)	8.7(6)	-1.5(7)
C15	38.6(8)	44.2(9)	30.5(7)	-0.7(7)	9.2(6)	-5.8(7)
C16	36.9(8)	58.9(11)	36.3(8)	3.2(8)	7.5(7)	-4.5(8)
C17	37.1(9)	64.8(12)	32.7(8)	2.4(8)	6.6(7)	-4.4(8)
C18	43.6(9)	59.8(12)	34.9(8)	-1.9(8)	7.5(7)	-9.7(8)
C19	50.0(11)	77.6(15)	39.1(9)	6.8(9)	10.8(8)	-14.7(10)
C20	52.3(12)	107(2)	62.5(14)	23.1(13)	28.1(11)	2.7(13)
C21	58.6(14)	111(2)	75.2(16)	26.4(16)	34.0(12)	25.8(14)
C22	46.9(11)	83.3(16)	54.9(12)	19.1(11)	17.6(9)	12.3(10)
C23	42.2(9)	41.5(9)	37.7(8)	0.6(7)	12.6(7)	3.0(7)
C24	37.4(10)	81.0(16)	68.9(14)	-8.5(12)	5.0(9)	17.5(10)
C25	73.3(18)	162(4)	106(2)	-50(2)	-43.3(17)	52(2)
C26	48.1(9)	43.9(10)	29.2(8)	-3.8(7)	9.2(7)	-3.3(7)
C27	69.0(13)	50.1(11)	40.5(10)	9.6(8)	4.5(9)	3.8(10)
C28	84.6(18)	82.3(19)	86.1(19)	34.0(15)	12.5(15)	26.9(15)
C29	303(10)	44(2)	98(4)	0	32(5)	0
Cl1A	98.0(18)	77.9(9)	53.0(8)	-17.5(7)	-6.4(8)	5.5(10)
Cl2A	166(3)	91.4(15)	104.5(14)	-50.5(12)	70.6(16)	-70.5(17)

Cl3A	82.4(17)	82.4(19)	78.0(11)	13.0(14)	7.7(10)	-16.9(14)
C1A	83(4)	80(4)	42(3)	-19(3)	17(3)	-24(3)
Cl1B	60.7(10)	69.0(8)	88.8(14)	-28.5(9)	-8.9(8)	1.0(7)
Cl3B	78.6(10)	90(2)	51.8(9)	-7.6(12)	10.1(7)	11.0(15)
Cl2B	159(3)	74.8(10)	73.0(10)	-22.6(7)	38.9(11)	-30.3(12)
C1B	71(4)	85(4)	49(3)	-22(3)	14(3)	-8(3)

The Anisotropic displacement factor exponent takes the form: $-2\pi^2[h^2a^{*2}U_{11}+2hka^*b^*U_{12}+\ldots]$

Table 1-22 Bond lengths for **1C**.

Atom	Atom	Length/Å	Atom	Atom	Length/Å
S1	C12	1.7588(17)	C7	C8	1.402(2)
S1	C15	1.7191(17)	C8	C9	1.390(3)
O1	C16	1.222(2)	C8	C11	1.457(2)
O2	C23	1.200(2)	C9	C10	1.387(2)
O3	C23	1.335(2)	C12	C13	1.356(2)
O3	C24	1.455(2)	C13	C14	1.434(2)
O4	C26	1.223(2)	C13	C23	1.496(2)
O5	C26	1.330(2)	C14	C15	1.381(2)
O5	C27	1.455(2)	C14	C26	1.462(2)
N1	C4	1.410(3)	C16	C17	1.491(2)
N1	C5[1]	1.4187(19)	C17	C18	1.392(3)
N1	C5	1.4188(19)	C17	C22	1.381(3)
N2	C11	1.275(2)	C18	C19	1.385(3)
N2	C12	1.384(2)	C19	C20	1.362(3)
N3	C15	1.377(2)	C20	C21	1.378(4)
N3	C16	1.365(2)	C21	C22	1.396(3)
C1	C2	1.390(3)	C24	C25	1.466(4)
C1	C2[1]	1.390(3)	C27	C28	1.496(3)
C1	C29	1.526(5)	Cl1A	C1A	1.729(8)
C2	C3	1.373(3)	Cl2A	C1A	1.742(7)
C3	C4	1.395(2)	Cl3A	C1A	1.765(7)
C5	C6	1.395(3)	Cl1B	C1B	1.738(7)
C5	C10	1.395(2)	Cl3B	C1B	1.783(8)
C6	C7	1.375(2)	Cl2B	C1B	1.747(8)

[1]2-X,+Y,1/2-Z

Table 1-23 Bond angles for **1C**.Table 1-24. Hydrogen bonds for **1C**.

D	H	A	d(D-H)/Å	d(H-A)/Å	d(D-A)/Å	D-H-A/°
N3	H3	O4	0.88	2.03	2.691(2)	131.0
C3	H3A	O4[1]	0.95	2.54	3.441(2)	158.9
C10	H10	Cl1B[2]	0.95	2.94	3.877(3)	169.0
C28	H28B	Cl2B[3]	0.98	2.80	3.587(3)	138.2
C1A	H1A	O2	1.00	2.32	3.252(9)	154.6
C1B	H1B	N2	1.00	2.50	3.241(8)	130.8

[1]3/2-X,1/2-Y,1-Z; [2]3/2-X,1/2+Y,1/2-Z; [3]+X,-Y,1/2+Z

Table 1-25 Torsion Angles for **1C**.

A	B	C	D	Angle/°	A	B	C	D	Angle/°
S1	C12	C13	C14	-0.14(19)	C12	C13	C14	C15	0.4(2)
S1	C12	C13	C23	-177.46(13)	C12	C13	C14	C26	-179.48(16)
O1	C16	C17	C18	168.71(19)	C12	C13	C23	O2	-75.1(3)
O1	C16	C17	C22	-13.2(3)	C12	C13	C23	O3	102.46(18)
N1	C5	C6	C7	-179.31(15)	C13	C14	C15	S1	-0.45(19)
N1	C5	C10	C9	179.03(15)	C13	C14	C15	N3	-177.04(15)
N2	C12	C13	C14	178.53(15)	C13	C14	C26	O4	-179.76(16)
N2	C12	C13	C23	1.2(3)	C13	C14	C26	O5	-0.2(2)
N3	C16	C17	C18	-13.7(3)	C14	C13	C23	O2	108.0(2)
N3	C16	C17	C22	164.39(19)	C14	C13	C23	O3	-74.5(2)
C1	C2	C3	C4	-1.2(3)	C15	S1	C12	N2	-178.75(15)
C2[1]	C1	C2	C3	0.60(17)	C15	S1	C12	C13	-0.10(13)
C2	C3	C4	N1	-179.41(17)	C15	N3	C16	O1	9.3(3)
C2	C3	C4	C3[1]	0.59(17)	C15	N3	C16	C17	-168.33(16)
C4	N1	C5	C6	-139.14(12)	C15	C14	C26	O4	0.4(3)
C4	N1	C5	C10	40.91(18)	C15	C14	C26	O5	179.98(15)
C5	N1	C4	C3[1]	-145.92(13)	C16	N3	C15	S1	-3.6(2)
C5	N1	C4	C3	34.08(13)	C16	N3	C15	C14	172.71(17)
C5[1]	N1	C4	C3[1]	34.08(13)	C16	C17	C18	C19	178.15(18)

C5[1]	N1	C4	C3	-145.92(13)	C16	C17	C22	C21	-177.7(2)
C5[1]	N1	C5	C6	40.86(12)	C17	C18	C19	C20	-0.5(3)
C5[1]	N1	C5	C10	-139.09(18)	C18	C17	C22	C21	0.4(3)
C5	C6	C7	C8	0.5(3)	C18	C19	C20	C21	0.3(4)
C6	C5	C10	C9	-0.9(3)	C19	C20	C21	C22	0.2(5)
C6	C7	C8	C9	-1.4(3)	C20	C21	C22	C17	-0.6(4)
C6	C7	C8	C11	177.99(16)	C22	C17	C18	C19	0.1(3)
C7	C8	C9	C10	1.1(3)	C23	O3	C24	C25	-176.2(3)
C7	C8	C11	N2	-4.8(3)	C23	C13	C14	C15	177.52(16)
C8	C9	C10	C5	0.0(3)	C23	C13	C14	C26	-2.3(3)
C9	C8	C11	N2	174.58(16)	C24	O3	C23	O2	-2.5(3)
C10	C5	C6	C7	0.6(3)	C24	O3	C23	C13	179.98(17)
C11	N2	C12	S1	3.9(2)	C26	O5	C27	C28	175.13(19)
C11	N2	C12	C13	-174.57(16)	C26	C14	C15	S1	179.41(13)
C11	C8	C9	C10	-178.29(16)	C26	C14	C15	N3	2.8(3)
C12	S1	C15	N3	176.95(15)	C27	O5	C26	O4	-1.1(3)
C12	S1	C15	C14	0.32(14)	C27	O5	C26	C14	179.35(15)
C12	N2	C11	C8	-179.13(15)	C29	C1	C2	C3	-179.40(17)

[1]2-X,+Y,1/2-Z

Table 1-26 Hydrogen atom coordinates (Å×10^4) and isotropic displacement parameters (Å^2×10^3) for **1C**.

Atom	***x***	***y***	***z***	**U(eq)**
H3	5205.93	730.2	5356.2	49
H2	9663.62	6667.41	3395.77	78
H3A	9686.03	5394.72	3405.59	57
H6	10290.34	3306.93	3172.57	46
H7	9343.13	2631.77	3737.59	45
H9	7396.8	4052.92	3201.2	49
H10	8348.53	4740.61	2638.95	51
H11	7081.01	3013.73	3873.78	46
H18	4212.57	355.43	5756.97	55
H19	3078.69	130.57	6391.88	66
H20	2029.43	1012.83	6502.21	87
H21	2076.97	2131.38	5976.85	96

H22	3198.56	2364.26	5321.58	73
H24A	10066.93	1091.72	5209.77	75
H24B	9736.85	302.42	5433.41	75
H25A	9943.38	1565.96	6205.84	175
H25B	10555.18	853.98	6262.32	175
H25C	9566.41	798.8	6432.17	175
H27A	7176.65	-1131.82	5726.72	64
H27B	7508.8	-643.78	6329.25	64
H28A	8603.72	-1168.33	5411.78	126
H28B	8591.01	-1498.53	6107.46	126
H28C	8935.27	-679.33	6008.91	126
H29A	10151.48	7818.7	2089.36	221
H29B	9420.77	7818.7	2580.28	221
H29C	10427.75	7818.71	2830.36	221
H1A	8567.13	1067.13	3376.03	81
H1B	8408.28	1372.63	3308.19	81

Table 1-27 Atomic Occupancy for **1C**.

Atom	***Occupancy***	**Atom**	***Occupancy***		**Atom**	***Occupancy***
H29A	0.5	H29B	0.5	H29C		0.5
Cl1A	0.503(4)	Cl2A	0.503(4)	Cl3A		0.503(4)
C1A	0.503(4)	H1A	0.503(4)	Cl1B		0.497(4)
Cl3B	0.497(4)	Cl2B	0.497(4)	C1B		0.497(4)
H1B	0.497(4)					

Chapitre 2

Résumé

Cet article est un rapport de structure cristallographique du composé **1C**. Il décrit les caractéristiques spatiales des cristaux obtenus, la position des différents éléments au sein du réseau cristallin, les longueurs de liaison, les caractéristiques de la maille cristalline, ainsi que l'arrangement entre elles des molécules au sein du cristal. Il permet aussi de décrire la configuration spatiale des différents plans et unités aromatiques entre eux, ainsi que les interactions intra et inter-moléculaires des molécules cristallisées dans ces conditions particulières. Des calculs théoriques de DFT (Théorie de la fonctionnelle de la Densité) permettent, de plus, de comparer les similarités des géométries observées et calculées.

Ma contribution à ces travaux a été la synthèse du composé reporté, l'obtention de cristaux appropriés à la diffraction des rayons X, et une participation au montage du cristal sur le diffractomètre ainsi qu'à la résolution de la structure à partir des données collectées. Celle-ci a été majoritairement finalisée par Thierry Maris, du Laboratoire de diffraction des rayons X de l'UdeM.

Crystal structure and DFT calculation of tetraethyl 5,5'-(((1*E*,1'*E*)-thiophene-2,5-diylbis(methanylylidene))bis(azanylylidene))bis(2-(4-(di-p-tolylamino)benzamido)thiophene-3,4-dicarboxylate)

Yohan Gautier, Thierry Maris and W. G. Skene*

Département de chimie, Université de Montréal, CP 6128, Centre-ville Montreal, QC, H3C 3J7, Canada

Submitted to *Acta Crystallographica, Section E*

Received July 18th 2019 (correction process)

Abstract and keywords

In the title compound, $C_{40}H_{36}N_4O_{10}S_3$, the imine bonds adopt the *E*-isomer. Two S(6) motifs form from two sets of intramolecular N-H···O bonds involving the N atom of the amides and the esters. The two terminal thiophenes are twisted by 28.9(3) and 31.3(3)^o with respect to the central thiophene to which they are connected by an azomethine bond. The corresponding angles are 6.3^o and 6.9^o for the optimized structure calculated by DFT-B3LYP.

Keywords

Crystal structure, Intramolecular hydrogen bonding, DFT calculation

Chemical context

Imines are important bonds for all aspects of chemistry. For example, they are forming well-defined structures such as covalent organic frameworks.(Segura *et al.*, 2016) Their reversible formation is also key for self-healing materials.(Li *et al.*, 2017) They additionally can be used in conjugated functional materials.(Janica *et al.*, 2018) This is in part due to their intrinsic electron withdrawing character where alternating p-n type materials are possible when electronic rich precursors are used for their preparation. Such materials have found uses in a wide gamut of applications that range from sensors(Wang *et al.*, 2018) to organic electronics (Gawlinska *et al.*, 2017).

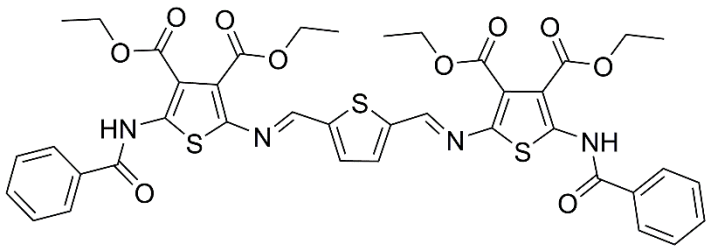

Properties suitable for active materials in organic electronic are possible with imines prepared from 2,5-diamino thiophenes and heterocyclic aldehydes. These derivatives are conjugated, resulting absorptions in the visible spectrum (Bolduc *et al.*, 2013). This aspect is interesting for electrochromic applications, especially since their colors can be visibly switched with applied electrochemical potentials. Towards tailoring the optical and electrochemical properties, the bisamide (I) was prepared and crystalized. The X-ray crystal structure is important for confirming the identity of the compound. Of importance is the geometry of the imine bond, which is not be absolutely assigned by ^{1}H NMR. It can only be confirmed by the X-ray structure. The structure therefore provides important structural information to the field, especially in light that no amide derivatives of **I** have been reported.

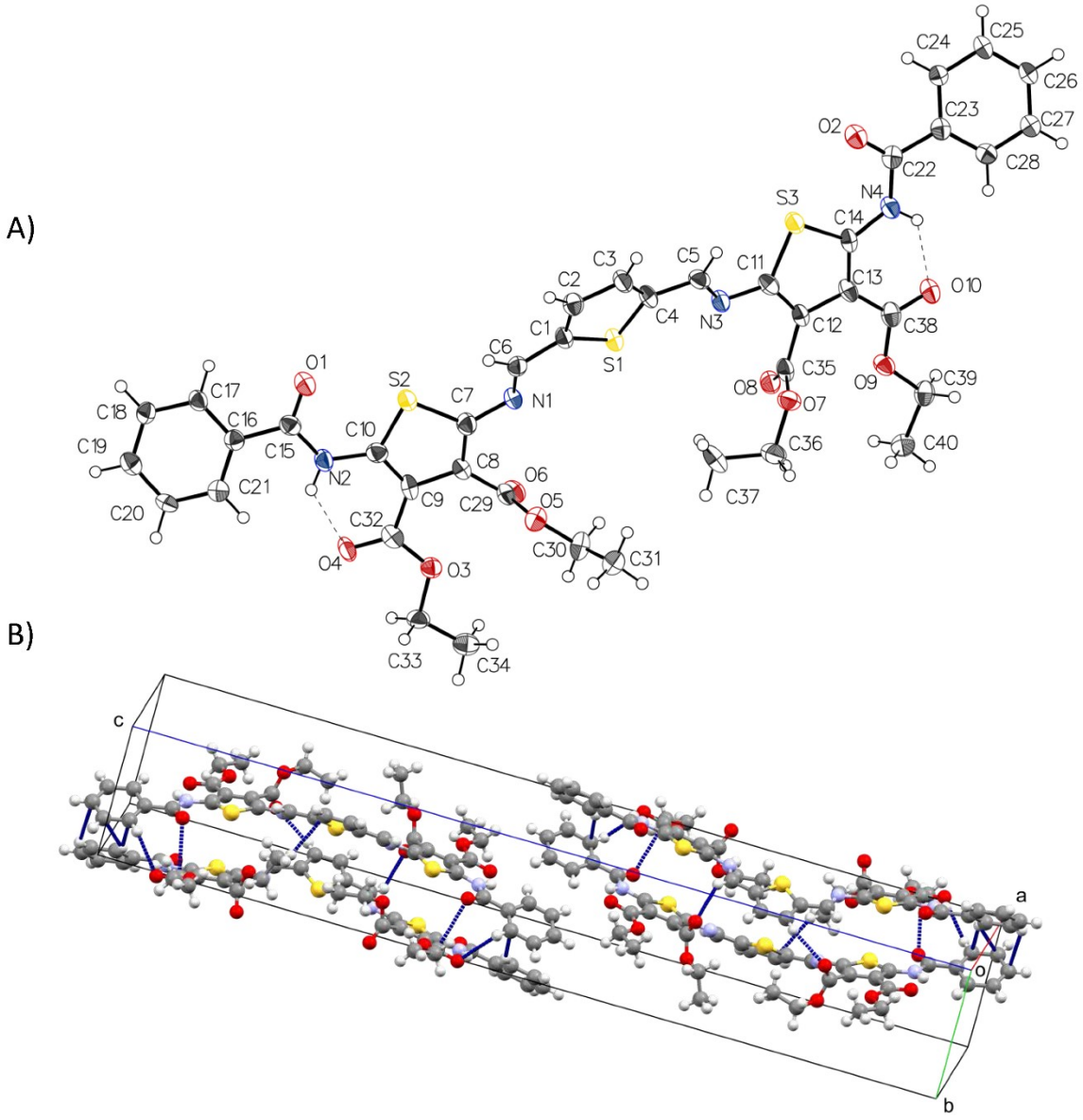

Figure 2-1 A) The atom-numbering diagram of **I**. C, N, O and S atoms are shown as displacement ellipsoids at the 50% probability level and H atoms are shown as spheres of arbitrary radius. B) Crystal lattice of **I** showing the intermolecular contacts (blue lines).

Structural commentary

The resolved structure is represented inFigure 2-1. A salient feature of the structure is the *anti* orientation of the thiophenes that is adopted. The structure of **I** can also be confirmed,

notably the two amides and to the two azomethine bonds. The double bond of the heteroatoms is confirmed by their short bond lengths; 1.277(10) Å. This is in contrast to the corresponding single =N—thiophene single bond whose average distance was calculated to be 1.397(8). Most importantly, the absolute configuration of the isomer of the two azomethines can be assigned by the structure. Both heteroatomic bonds adopt the thermodynamically *E* configuration. While this is not surprising, the overall configuration adopted by the triad is the atypical. Similar compounds thiophene triads consisting of terminal amines instead phenylamides are uniquely coplanar. In fact, the planes described by the terminal thiophenes and the central thiophene are twisted by less than 10^{o} (Bourgeaux & Skene, 2007). In contrast, the plane defined by the central thiophene in **I** is twisted by 28.9(3) and 31.3(3)^{o} relative to the planes of the two flanking thiophenes and two azomethines bonds. This twisting from coplanarity of the external thiophenes is evident when visualizing the title compound along the *c*-axis as in Figure 2-2A.

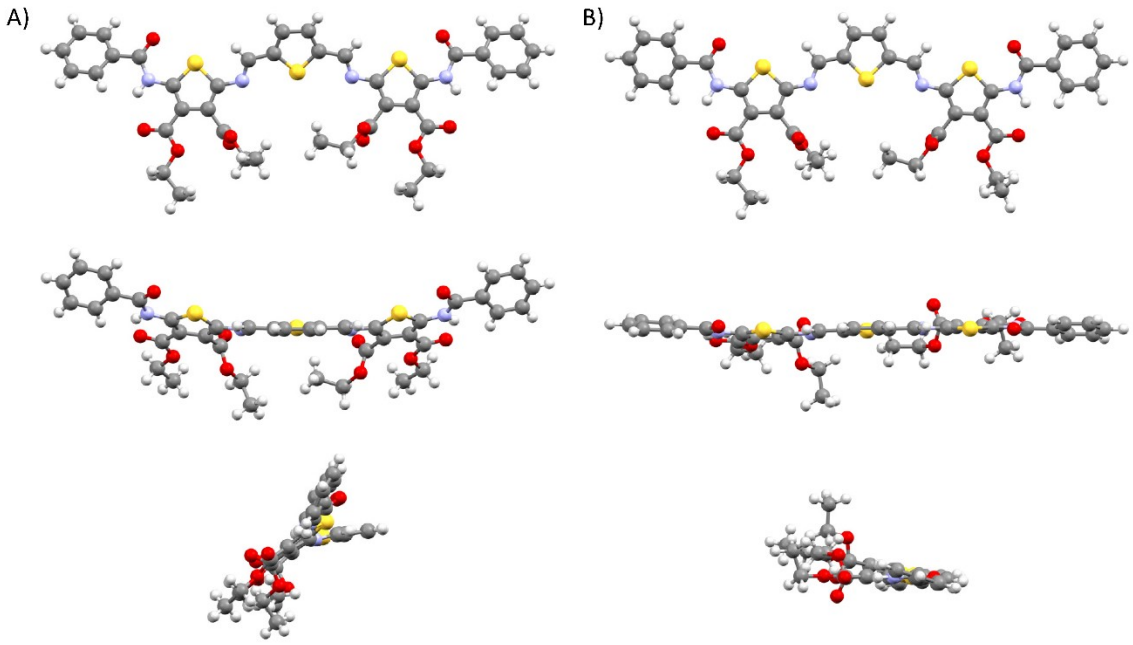

Figure 2-2 Top-down (top), side-on (middles), and *c*-axis views of the resolved X-ray crystallographic structure (A) and optimized geometry by DFT-B3LYP calculations with 6-31+g(d,p) basis set (B) **I**.

Supramolecular features

I undergoes intramolecular hydrogen bonding between the amide nitrogen donor and the ester carbonyl. These bonds are illustrated in Figure 2-1A, with the corresponding distances listed in Table 2-2. The intramolecular hydrogen bond is typical of 2-amino-3-ester thiophene (Dufresne & Skene, 2010). The distortion from planarity observed for **I** is in part owing to the multiple contacts it forms in the solid state. For example, two sets of two nearly anti-parallel superimposable molecules in the crystal lattice undergo multiple intermolecular contacts. These are illustrated by the dotted lines in Figure 2-1A and tabulated in Table 2-2. These collective contributions result in organized stacked sheets when they pack.

DFT Calculations

The optimized geometry of **I** was calculated by DFT-B3LYP (Becke, 1992, 1993, Lee *et al.*, 1988, Vosko *et al.*, 1980, Stephens *et al.*, 1994) using with the 6-311+G(d,p) basis set. The lowest energy geometry of **I** has an anti-parallel orientation of the three thiophenes, similar to the crystal structure. In contrast, the planes of the three thiophenes are nearly coplanar. Indeed, the flanking thiophenes are twisted by only 6.3^{o} and 6.9^{o}, relative to the central thiophene. The N=CH bonds were calculated to be 1.29 Å, about 0.01 Å shorter than the experimental value. Similarly, the =N—thiophene bond length is 1.37 Å, being 0.03 Å shorter than in the crystal state. Given the similar geometry and configuration of both the calculated and crystallographic data of **I**, insight about the physical properties can be had from the theoretical values. The absorbance spectrum and the corresponding molecular orbitasl were therefore calculated by time-dependent DFT using dichloromethane as the continuum solvent. The principle transition calculated was from the HOMO to the LUMO+1 orbitals. The resulting spectrum is illustrated in Figure 2-3, where the theoretical spectrum is red-shifted by 74 nm from the corresponding experimentally measured spectrum.(Mulholland *et al.*, 2014) The calculated absorption maximum was 556 nm. The orbitals involved in the absorption are also found in Figure 2-3.

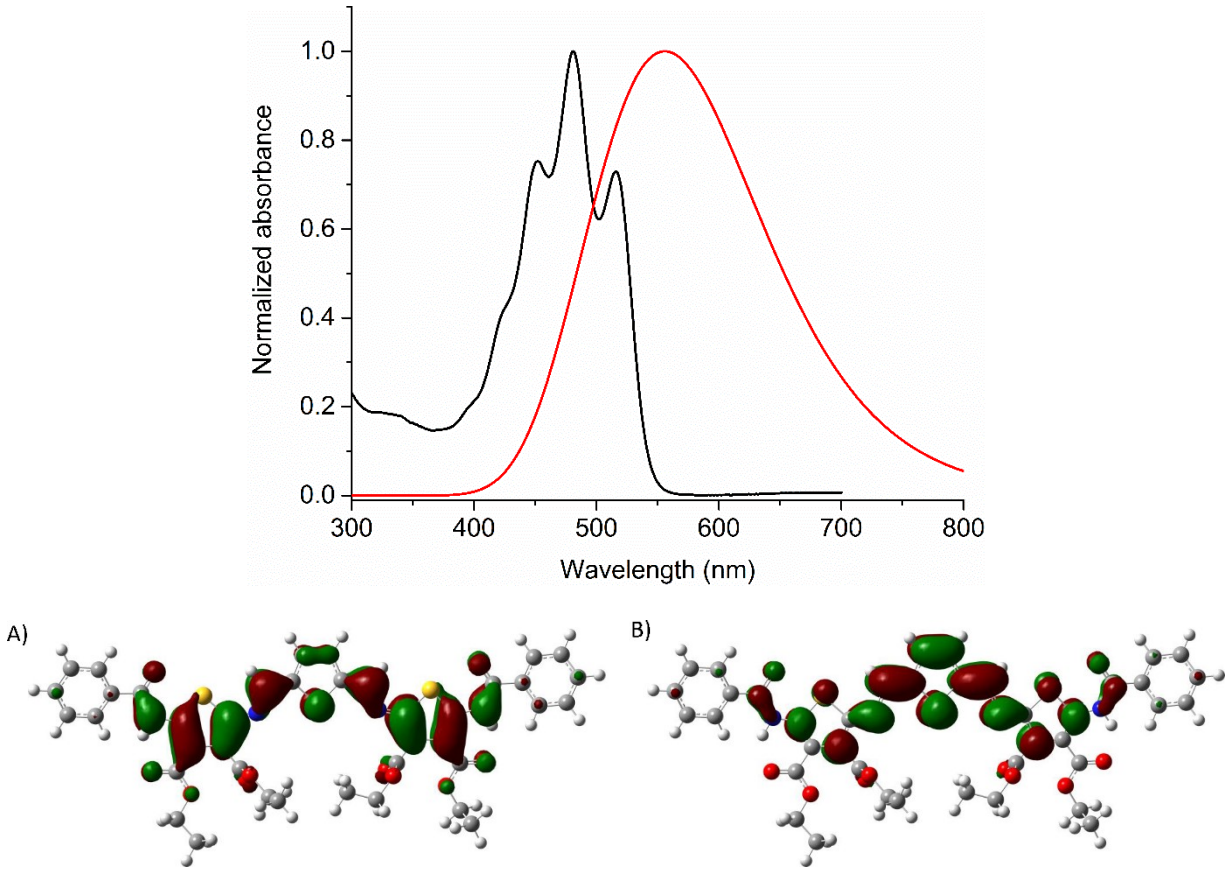

Figure 2-3 Experimental (black) and calculated (red) absorption spectra of I in dichloromethane (top). HOMO (A) and LUMO (B) Frontier orbitals of **I** (bottom) calculated by DFT-B3LP.

Database survey

No exact structure of **I** was found in the Cambridge Structural Database (5.40 November 2018). In fact, no compounds in the database were identified with a 2-phenylamide-3-ethylester thiophene similar to the external segment of **I**. In contrast, when the 3-position of the thiophene is substituted with the electron accepting nitrile, fifteen structures were found with a phenylamide. A comparison can be done between **I** and its reported counterparts. Of interest are the C10-N2, N2-C15, C15-C16 bonds lengths. For **I**, the respective average bond lengths are 1.396(9), 1.365(8), and 1.502(8) Å. There is some variability in the corresponding lengths for the reported structures with the average lengths being 1.38, 1.36, and 1.49 Å, respectively. The complete set of distances, the minimum and maximum values, and the standard deviations of the reported compounds are summaried in Table 2-3. The bond lengths of **I** are consistent with

the similar structures. Of interest is the torsion angle involving C10-N2-C15-C16. The angle describes the coplanarity of the amide bond with its adjacent thiophene. In the case of **I**, the angles are 1.0(11) and 3.33(11)^{o}, whereas the corresponding values for the reported structures vary between 0.4 and 6.8^{o}. Another salient feature is the coplanarity of the thiophene and phenyl aromatics. This is derived from the angle between the planes described by the phenyl and thiophene aromatics. For **I**, these angles are 30.1(4) and 32.4(3)^{o}. There is also a large variability in the corresponding angles for the literature values, ranging from 2.5 to 43.2^{o}.

Synthesis and crystallization

Crystals suitable for X-ray crystallography of **I** were obtained by the slow evaporation of deuterated chloroform. The preparation of the title compound is reported elsewhere (Mulholland *et al.*, 2014). Gaussian 16 Revision B.01 was used for calculating the optimized geometry of **I** ((Frisch *et al.*, 2016)).

Refinement

Crystal data, data collection and structure refinement details are summarized in Table 1.

Table 2-1 Experimental details

Crystal data	
Chemical formula	$C_{40}H_{36}N_4O_{10}S_3$
M_r	828.91
Crystal system, space group	Monoclinic, $P2_1/n$
Temperature (K)	105
a, b, c (Å)	10.9842 (4), 7.3930 (3), 46.5544 (17)
β (°)	91.634 (2)
V (Å^3)	3779.0 (2)
Z	4
Radiation type	Ga $K\alpha$, λ = 1.34139 Å
μ (mm^{-1})	1.53
Crystal size (mm)	0.24 × 0.02 × 0.02
Data collection	
Diffractometer	Bruker Venture Metaljet
Absorption correction	Multi-scan TWINABS-2012/1 (Bruker,2012) was used for absorption correction.

Final HKLF 4 output contains 95714 reflections, Rint = 0.1943 (21222 with I > 3sig(I), Rint = 0.1091)

T_{min}, T_{max}	0.548, 0.751
No. of measured, independent and observed [$I > 2\sigma(I)$] reflections	7850, 7850, 5045
R_{int}	?
$(\sin\theta/\lambda)_{max}$ (Å^{-1})	0.626
Refinement	
$R[F^2 > 2\sigma(F^2)]$, $wR(F^2)$, S	0.093, 0.238, 1.04
No. of reflections	7850
No. of parameters	519
H-atom treatment	H-atom parameters constrained
$\Delta\rho_{max}$, $\Delta\rho_{min}$ (e Å^{-3})	0.47, −0.83

Computer programs: *APEX* 2 (2013) Bruker AXS Inc., Madison, WI 53719-1173., *SAINT* (2013) V8.34A; Integration Software for Single Crystal Data. Bruker AXS Inc., ShelXT (Sheldrick, 2015), XL (Sheldrick, 2008), *OLEX2* (Dolomanov *et al.*, 2009), *Mercury* (Macrae *et al.*, 2008), and *PLATON* for Windows Taskbar v1.19 (Spek, 2009), *OLEX2* (Dolomanov *et al.*, 2009) and *publCIF* (Westrip, 2010).

Table 2-2 Hydrogen-bond geometry (Å, º) for (yohan1)

D—H···*A*	*D*—H	H···*A*	*D*···*A*	*D*—H···*A*
N2—H2···O4	0.88	2.08	2.733 (7)	129.9
N4—H4···O10	0.88	2.07	2.729 (7)	131.5
C2—H2A···O8^{i}	0.95	2.52	3.314 (8)	140.8
C5—H5···O6^{i}	0.95	2.60	3.394 (8)	140.7
C34—H34A···O1^{ii}	0.98	2.60	3.383 (9)	137.0
C40—H40C···O2^{ii}	0.98	2.52	3.314 (9)	138.4

Symmetry codes: (i) −x+1/2, y−1/2, −z+3/2; (ii) x+1, y, z.

Table 2-3 Comparison of selected bond lengths and angles of the title compound and literature counter parts.

Refcode	dN2-C10 (Å)"dN2-C15 (Å)	dN2-C15 (Å)	dC15-C16 (Å)	TorsionO1-C15-N2-C10 (o)	Anglethiophene-phenyl (o)
KABDUO	1.381	1.359	1.487	4.41	8.13
LOYDIM	1.391	1.355	1.482	0.03	4.74
TAPXEO	1.385	1.368	1.482	2.85	9.70
TEKFEX	1.38	1.364	1.494	0.44	23.72
TEKFIB	1.369	1.361	1.483	3.80	6.38
TEKFOH	1.385	1.359	1.499	0.23	39.02
TEKFUN	1.373	1.354	1.494	0.60	2.53
TEKFUN	1.382	1.36	1.484	2.45	6.01
VESHIN	1.375	1.365	1.486	0.27	17.75
VESHOT	1.379	1.367	1.486	3.90	7.17
VESHUZ	1.378	1.38	1.516	7.52	36.43
VESJAH	1.371	1.363	1.498	5.12	41.74
VESJEL	1.378	1.357	1.491	6.80	22.71
VESJIP	1.381	1.353	1.493	3.72	40.45
VESJIP	1.396	1.36	1.497	4.28	43.16
WOJBII	1.378	1.369	1.494	1.21	7.11
Average	1.380	1.362	1.492	3.00	19.8
esd	0.007	0.007	0.009	2.40	15.5
min	1.369	1.353	1.482	0.03	2.5
max	1.396	1.380	1.516	7.52	43.2

Acknowledgements

Both NSERC Canada and the Canada Foundation for Innovation are acknowledged for Discovery and infrastructure grants that enabled this work. Compute Canada (www.computecanada.ca) and their partners, Compute Ontario (computeontario.ca) and

WestGrid (www.westgrid.ca), are also thanked for access to both computational resources and software for theoretical calculations.

Funding information

Funding for this research was provided by: Natural Sciences and Engineering Research Council of Canada (grant No. Discovery to W. G. Skene); Canada Foundation for Innovation ; Quebec Centre for Advanced Materials .

References

Becke, A. D. (1992). *J. Chem. Phys.* **96**, 2155-2160.

Becke, A. D. (1993). *J. Chem. Phys.* **98**, 5648-5652.

Bolduc, A., Mallet, C. & Skene, W. G. (2013). *Sci. China Chem.* **51**, 3-23.

Bourgeaux, M. & Skene, W. G. (2007). *J. Org. Chem.* **72**, 8882-8892.

Dufresne, S. & Skene, W. G. (2010). *Acta Cryst.* **E66**, o3221.

Frisch, M. J., Trucks, G. W., Schlegel, H. B., Scuseria, G. E., Robb, M. A., Cheeseman, J. R., Scalmani, G., Barone, V., Petersson, G. A., Nakatsuji, H., X. Li, M. C., Marenich, A. V., Bloino, J., Janesko, B. G., Gomperts, R., Mennucci, B., Hratchian, H. P., Ortiz, J. V., Izmaylov, A. F., Sonnenberg, J. L., Williams-Young, D., Ding, F., Lipparini, F., Egidi, F., Goings, J., Peng, B., Petrone, A., Henderson, T., Ranasinghe, D., Zakrzewski, V. G., Gao, J., Rega, N., Zheng, G., Liang, W., Hada, M., Ehara, M., Toyota, K., Fukuda, R., Hasegawa, J., Ishida, M., Nakajima, T., Honda, Y., Kitao, O., Nakai, H., Vreven, T., Throssell, K., J. A. Montgomery, J., Peralta, J. E., Ogliaro, F., Bearpark, M. J., Heyd, J. J., Brothers, E. N., Kudin, K. N., Staroverov, V. N., Keith, T. A., Kobayashi, R., Normand, J., Raghavachari, K., Rendell, A. P., Burant, J. C., Iyengar, S. S., Tomasi, J., Cossi, M., Millam, J. M., Klene, M., Adamo, C., Cammi, R., Ochterski, J. W., Martin, R. L., Morokuma, K., Farkas, O., Foresman, J. B. & Fox, D. J. (2016). *Gaussian 16, Revision B.01.*

Gawlinska, K., Iwan, A., Starowicz, Z., Kulesza-Matlak, G., Stan-Glowinska, K., Janusz, M., Lipinski, M., Boharewicz, B., Tazbir, I. & Sikora, A. (2017). *Opto-Electron. Rev.* **25**, 274-284.

Janica, I., Patroniak, V., Samorì, P. & Ciesielski, A. (2018). *Chemistry – An Asian Journal* **13**, 465-481.

Lee, C., Yang, W. & Parr, R. G. (1988). *Phys. Rev. B* **37**, 785-789.

Li, J., Geng, L., Wang, G., Chu, H. & Wei, H. (2017). *Chem. Mater.* **29**, 8932-8952.

Mulholland, M., Navarathne, D., Khedri, S. & Skene, W. G. (2014). *New J. Chem.* **38**, 1668-1674.

Segura, J. L., Mancheno, M. J. & Zamora, F. (2016). *Chem. Soc. Rev.* **45**, 5635-5671.

Stephens, P. J., Devlin, F. J., Chabalowski, C. F. & Frisch, M. J. (1994). *J. Phys. Chem.* **98**, 11623-11627.

Vosko, S. H., Wilk, L. & Nusair, M. (1980). *Can. J. Phys.* **58**, 1200-1211.

Wang, L., Wu, S., Tang, H., Meier, H. & Cao, D. (2018). *Sens. Actuators, B* **273**, 1085-1090.

Supporting information

Crystal structure and DFT calculation of tetra-ethyl 5,5'-(((1*E*,1'*E*)-thio-phene-2,5-diylbis(methanylyl-idene))bis-(aza-nylyl-idene))bis-(2-(4-(di-*p*-tolyl-amino)-benzamido)-thio-phene-3,4-di-carboxyl-ate)

Yohan Gautier, Thierry Maris and W. G. Skene*

Computing details

Data collection: *APEX* 2 (2013) Bruker AXS Inc., Madison, WI 53719-1173.; cell refinement: *SAINT* (2013) V8.34A; Integration Software for Single Crystal Data. Bruker AXS Inc., Madison, WI 53719-1173.; data reduction: *SAINT* (2013) V8.34A; Integration Software for Single Crystal Data. Bruker AXS Inc., Madison, WI 53719-1173.; program(s) used to solve structure: ShelXT (Sheldrick, 2015); program(s) used to refine structure: XL (Sheldrick, 2008); molecular graphics: *OLEX2* (Dolomanov *et al.*, 2009), *Mercury* (Macrae *et al.*, 2008), and *PLATON* for Windows Taskbar v1.19 (Spek, 2009); software used to prepare material for publication: *OLEX2* (Dolomanov *et al.*, 2009) and *publCIF* (Westrip, 2010).

(yohan1)

Crystal data

$C_{40}H_{36}N_4O_{10}S_3$	$F(000) = 1728$
$M_r = 828.91$	$D_x = 1.457$ Mg m^{-3}
Monoclinic, $P2_1/n$	Ga $K\alpha$ radiation, $\lambda = 1.34139$ Å
$a = 10.9842$ (4) Å	Cell parameters from 9749 reflections
$b = 7.3930$ (3) Å	$\theta = 3.3–56.9°$
$c = 46.5544$ (17) Å	$\mu = 1.53$ mm^{-1}
$\beta = 91.634$ (2)°	$T = 105$ K
$V = 3779.0$ (2) Å^3	Needle, orange

$Z = 4$	0.24 × 0.02 × 0.02 mm

Data collection

Bruker Venture Metaljet diffractometer	7850 measured reflections
Radiation source: Metal Jet, Gallium Liquid Metal Jet Source	7850 independent reflections
Helios MX Mirror Optics monochromator	5045 reflections with $I > 2\sigma(I)$
Detector resolution: 10.24 pixels mm^{-1}	$\theta_{max} = 57.1°$, $\theta_{min} = 1.7°$
ω and ϕ scans	$h = -13 \rightarrow 13$
Absorption correction: multi-scan TWINABS-2012/1 (Bruker,2012) was used for absorption correction. Final HKLF 4 output contains 95714 reflections, Rint = 0.1943 (21222 with I > 3sig(I), Rint = 0.1091)	$k = 0 \rightarrow 9$
$T_{min} = 0.548$, $T_{max} = 0.751$	$l = 0 \rightarrow 58$

Refinement

Refinement on F^2	Primary atom site location: dual
Least-squares matrix: full	Hydrogen site location: inferred from neighbouring sites
$R[F^2 > 2\sigma(F^2)] = 0.093$	H-atom parameters constrained
$wR(F^2) = 0.238$	$w = 1/[\sigma^2(F_o^2) + (0.1146P)^2 + 6.4459P]$ where $P = (F_o^2 + 2F_c^2)/3$
$S = 1.04$	$(\Delta/\sigma)_{max} = 0.001$
7850 reflections	$\Delta\rangle_{max} = 0.47$ e Å^{-3}
519 parameters	$\Delta\rangle_{min} = -0.83$ e Å^{-3}
0 restraints	

Special details

Experimental. X-ray crystallographic data for I were collected from a single crystal sample, which was mounted on a loop fiber. Data were collected using a Bruker Venture diffractometer equipped with a Photon 100 CMOS Detector, a Helios MX optics and a Kappa goniometer. The crystal-to-detector distance was 4.0 cm, and the data collection was carried out in 1024 x 1024 pixel mode.
Geometry. All esds (except the esd in the dihedral angle between two l.s. planes) are estimated using the full covariance matrix. The cell esds are taken into account individually in the estimation of esds in distances, angles and torsion angles; correlations between esds in cell parameters are only used when they are defined by crystal symmetry. An approximate (isotropic) treatment of cell esds is used for estimating esds involving l.s. planes.

Refinement. Refined as a 2-component twin.

Fractional atomic coordinates and isotropic or equivalent isotropic displacement parameters (Å²) for (yohan1)

	x	*y*	*z*	U_{iso}*/U_{eq}
S1	0.22757 (16)	0.4037 (3)	0.74926 (3)	0.0307 (4)
S2	0.18344 (15)	0.4820 (3)	0.62928 (3)	0.0311 (4)
S3	0.16348 (16)	0.4865 (3)	0.86829 (3)	0.0311 (4)
O1	0.0635 (4)	0.5675 (7)	0.57910 (9)	0.0361 (12)
O2	0.0503 (4)	0.5791 (7)	0.91827 (10)	0.0380 (12)
O3	0.6177 (4)	0.4319 (7)	0.61168 (9)	0.0318 (12)
O4	0.5145 (4)	0.5230 (7)	0.57166 (9)	0.0357 (12)
O5	0.5487 (4)	0.2850 (7)	0.67322 (10)	0.0374 (12)
O6	0.5801 (4)	0.5849 (7)	0.67239 (10)	0.0358 (12)
O7	0.5082 (4)	0.2400 (7)	0.82911 (10)	0.0344 (12)
O8	0.5643 (4)	0.5348 (7)	0.82829 (9)	0.0339 (12)
O9	0.5992 (4)	0.4214 (7)	0.89003 (9)	0.0314 (11)
O10	0.5001 (4)	0.5115 (7)	0.92946 (9)	0.0355 (12)
N1	0.2704 (5)	0.4189 (8)	0.68505 (11)	0.0280 (12)
N2	0.2667 (5)	0.5353 (8)	0.57513 (11)	0.0319 (14)
H2	0.327378	0.533856	0.563192	0.038*
N3	0.2512 (5)	0.4142 (8)	0.81336 (11)	0.0296 (13)
N4	0.2529 (5)	0.5387 (8)	0.92335 (11)	0.0306 (14)
H4	0.315590	0.540893	0.935550	0.037*
C1	0.1351 (6)	0.3301 (9)	0.72121 (13)	0.0287 (16)
C2	0.0281 (6)	0.2542 (10)	0.73046 (14)	0.0316 (16)
H2A	-0.034717	0.209097	0.717982	0.038*
C3	0.0237 (6)	0.2519 (10)	0.76097 (14)	0.0345 (17)
H3	-0.041567	0.201608	0.771291	0.041*
C4	0.1240 (6)	0.3301 (10)	0.77369 (13)	0.0312 (16)
C5	0.1471 (6)	0.3548 (9)	0.80451 (14)	0.0310 (16)
H5	0.085803	0.327256	0.817809	0.037*
C6	0.1666 (7)	0.3574 (9)	0.69159 (13)	0.0296 (16)
H6	0.108645	0.329021	0.676723	0.035*
C7	0.2960 (6)	0.4479 (10)	0.65623 (14)	0.0320 (17)
C8	0.4110 (6)	0.4580 (9)	0.64596 (13)	0.0279 (16)

C9	0.4107 (7)	0.4868 (10)	0.61534 (13)	0.0328 (17)
C10	0.2944 (6)	0.5057 (10)	0.60432 (14)	0.0311 (16)
C11	0.2742 (6)	0.4430 (9)	0.84273 (13)	0.0285 (16)
C12	0.3886 (6)	0.4425 (9)	0.85442 (13)	0.0272 (15)
C13	0.3924 (6)	0.4756 (10)	0.88501 (13)	0.0306 (17)
C14	0.2761 (6)	0.5016 (10)	0.89474 (13)	0.0286 (15)
C15	0.1525 (6)	0.5661 (10)	0.56387 (14)	0.0309 (16)
C16	0.1446 (6)	0.6057 (10)	0.53226 (13)	0.0287 (15)
C17	0.0428 (6)	0.7000 (10)	0.52164 (13)	0.0295 (16)
H17	-0.018975	0.737192	0.534244	0.035*
C18	0.0324 (6)	0.7390 (9)	0.49234 (14)	0.0305 (16)
H18	-0.035389	0.805801	0.484960	0.037*
C19	0.1210 (7)	0.6803 (10)	0.47414 (14)	0.0350 (17)
H19	0.112708	0.705155	0.454162	0.042*
C20	0.2219 (6)	0.5857 (10)	0.48449 (14)	0.0312 (16)
H20	0.282538	0.546312	0.471761	0.037*
C21	0.2331 (6)	0.5493 (10)	0.51357 (14)	0.0312 (16)
H21	0.302205	0.484868	0.520837	0.037*
C22	0.1406 (6)	0.5719 (10)	0.93402 (14)	0.0308 (16)
C23	0.1380 (6)	0.6089 (10)	0.96574 (13)	0.0288 (15)
C24	0.0370 (6)	0.7005 (10)	0.97593 (13)	0.0302 (16)
H24	-0.026842	0.737438	0.963030	0.036*
C25	0.0304 (7)	0.7380 (10)	1.00556 (13)	0.0335 (17)
H25	-0.037664	0.800960	1.012761	0.040*
C26	0.1235 (6)	0.6826 (10)	1.02395 (14)	0.0312 (16)
H26	0.119729	0.709683	1.043850	0.037*
C27	0.2217 (6)	0.5887 (10)	1.01397 (14)	0.0315 (16)
H27	0.284888	0.550267	1.026917	0.038*
C28	0.2280 (6)	0.5501 (10)	0.98465 (13)	0.0323 (17)
H28	0.294835	0.482956	0.977753	0.039*
C29	0.5228 (7)	0.4548 (10)	0.66525 (14)	0.0319 (17)
C30	0.6583 (7)	0.2652 (11)	0.69173 (16)	0.0408 (18)
H30A	0.656514	0.352186	0.707884	0.049*
H30B	0.732251	0.288199	0.680638	0.049*
C31	0.6585 (7)	0.0743 (11)	0.70287 (16)	0.0431 (19)
H31A	0.653208	-0.010171	0.686664	0.065*

H31B	0.588530	0.056555	0.715155	0.065*
H31C	0.733987	0.052165	0.714054	0.065*
C32	0.5167 (6)	0.4832 (10)	0.59742 (14)	0.0310 (16)
C33	0.7270 (6)	0.4120 (11)	0.59527 (14)	0.0332 (17)
H33A	0.740083	0.521814	0.583579	0.040*
H33B	0.718801	0.307078	0.582158	0.040*
C34	0.8326 (6)	0.3843 (11)	0.61587 (16)	0.0411 (19)
H34A	0.907005	0.366058	0.605100	0.062*
H34B	0.817735	0.277601	0.627761	0.062*
H34C	0.842207	0.490987	0.628213	0.062*
C35	0.4991 (6)	0.4142 (11)	0.83605 (13)	0.0320 (16)
C36	0.6075 (7)	0.1938 (11)	0.81035 (15)	0.042 (2)
H36A	0.626647	0.063440	0.812345	0.051*
H36B	0.681165	0.263228	0.816227	0.051*
C37	0.5738 (8)	0.2358 (11)	0.77896 (14)	0.046 (2)
H37A	0.639064	0.194214	0.766656	0.069*
H37B	0.562871	0.366601	0.776600	0.069*
H37C	0.497799	0.173625	0.773513	0.069*
C38	0.4996 (6)	0.4715 (10)	0.90365 (14)	0.0334 (17)
C39	0.7122 (6)	0.4102 (11)	0.90652 (14)	0.0344 (17)
H39A	0.710998	0.305394	0.919741	0.041*
H39B	0.725214	0.521567	0.918014	0.041*
C40	0.8117 (6)	0.3885 (11)	0.88527 (15)	0.0371 (18)
H40A	0.813304	0.494651	0.872688	0.056*
H40B	0.796355	0.279765	0.873674	0.056*
H40C	0.890310	0.376772	0.895598	0.056*

Atomic displacement parameters (Å²) for (yohan1)

	U^{11}	U^{22}	U^{33}	U^{12}	U^{13}	U^{23}
S1	0.0357 (10)	0.0351 (10)	0.0214 (7)	-0.0022 (9)	0.0008 (7)	0.0005 (7)
S2	0.0340 (9)	0.0371 (11)	0.0225 (8)	0.0001 (9)	0.0015 (7)	0.0005 (7)
S3	0.0337 (9)	0.0371 (11)	0.0224 (8)	-0.0004 (8)	0.0015 (7)	-0.0013 (7)
O1	0.039 (3)	0.042 (3)	0.027 (2)	-0.006 (2)	0.003 (2)	-0.002 (2)
O2	0.041 (3)	0.042 (3)	0.031 (3)	-0.005 (3)	0.002 (2)	-0.002 (2)
O3	0.026 (3)	0.039 (3)	0.030 (2)	-0.002 (2)	0.003 (2)	0.001 (2)
O4	0.040 (3)	0.049 (3)	0.018 (2)	-0.004 (2)	0.003 (2)	0.002 (2)

O5	0.035 (3)	0.038 (3)	0.039 (3)	0.000 (2)	-0.003 (2)	0.005 (2)
O6	0.037 (3)	0.038 (3)	0.032 (3)	-0.006 (3)	0.003 (2)	-0.003 (2)
O7	0.036 (3)	0.033 (3)	0.034 (3)	0.004 (2)	0.007 (2)	-0.002 (2)
O8	0.034 (3)	0.040 (3)	0.027 (2)	-0.002 (2)	0.000 (2)	0.001 (2)
O9	0.026 (2)	0.042 (3)	0.026 (2)	-0.007 (2)	0.0038 (19)	-0.004 (2)
O10	0.040 (3)	0.043 (3)	0.023 (2)	-0.006 (2)	0.000 (2)	-0.001 (2)
N1	0.033 (3)	0.030 (3)	0.021 (3)	-0.003 (3)	0.003 (2)	0.003 (2)
N2	0.033 (3)	0.042 (4)	0.021 (3)	-0.003 (3)	-0.002 (2)	-0.002 (2)
N3	0.027 (3)	0.041 (4)	0.021 (3)	-0.006 (3)	0.000 (2)	0.000 (3)
N4	0.032 (3)	0.037 (4)	0.024 (3)	-0.004 (3)	0.003 (2)	0.001 (2)
C1	0.035 (4)	0.031 (4)	0.020 (3)	0.000 (3)	0.001 (3)	-0.001 (3)
C2	0.033 (4)	0.033 (4)	0.029 (3)	-0.004 (3)	-0.003 (3)	-0.002 (3)
C3	0.034 (4)	0.047 (5)	0.023 (3)	-0.003 (4)	0.004 (3)	0.001 (3)
C4	0.038 (4)	0.034 (4)	0.022 (3)	-0.005 (3)	0.008 (3)	0.006 (3)
C5	0.030 (4)	0.033 (4)	0.030 (3)	0.000 (3)	0.009 (3)	0.002 (3)
C6	0.034 (4)	0.027 (4)	0.027 (3)	0.005 (3)	-0.001 (3)	-0.001 (3)
C7	0.034 (4)	0.035 (5)	0.027 (3)	-0.001 (3)	-0.002 (3)	-0.002 (3)
C8	0.033 (4)	0.029 (4)	0.022 (3)	-0.002 (3)	0.003 (3)	-0.001 (3)
C9	0.044 (4)	0.035 (4)	0.019 (3)	-0.005 (4)	-0.001 (3)	0.003 (3)
C10	0.035 (4)	0.027 (4)	0.031 (3)	0.003 (3)	0.004 (3)	-0.002 (3)
C11	0.034 (4)	0.026 (4)	0.025 (3)	-0.007 (3)	0.006 (3)	-0.004 (3)
C12	0.037 (4)	0.026 (4)	0.018 (3)	-0.002 (3)	0.001 (3)	-0.001 (3)
C13	0.036 (4)	0.034 (4)	0.023 (3)	-0.009 (3)	0.006 (3)	0.003 (3)
C14	0.041 (4)	0.026 (4)	0.019 (3)	-0.004 (3)	-0.003 (3)	0.001 (3)
C15	0.035 (4)	0.027 (4)	0.030 (3)	0.001 (3)	0.004 (3)	-0.005 (3)
C16	0.032 (4)	0.027 (4)	0.027 (3)	-0.001 (3)	0.000 (3)	-0.002 (3)
C17	0.029 (4)	0.037 (4)	0.022 (3)	-0.003 (3)	-0.001 (3)	-0.004 (3)
C18	0.031 (4)	0.032 (4)	0.028 (3)	0.000 (3)	-0.005 (3)	0.000 (3)
C19	0.045 (5)	0.032 (4)	0.029 (4)	-0.003 (3)	0.006 (3)	0.001 (3)
C20	0.029 (4)	0.036 (4)	0.029 (3)	-0.001 (3)	0.010 (3)	-0.005 (3)
C21	0.031 (4)	0.030 (4)	0.032 (4)	-0.002 (3)	0.000 (3)	-0.001 (3)
C22	0.031 (4)	0.030 (4)	0.032 (4)	-0.005 (3)	-0.002 (3)	0.001 (3)
C23	0.029 (4)	0.030 (4)	0.028 (3)	-0.007 (3)	0.001 (3)	0.002 (3)
C24	0.030 (4)	0.035 (4)	0.025 (3)	0.001 (3)	0.001 (3)	0.000 (3)
C25	0.040 (4)	0.039 (5)	0.022 (3)	-0.003 (4)	0.003 (3)	0.000 (3)
C26	0.037 (4)	0.035 (4)	0.022 (3)	-0.002 (3)	0.005 (3)	0.001 (3)

C27	0.034 (4)	0.033 (4)	0.028 (3)	-0.002 (3)	0.002 (3)	-0.001 (3)
C28	0.034 (4)	0.033 (4)	0.030 (3)	0.001 (3)	0.002 (3)	-0.002 (3)
C29	0.037 (4)	0.036 (5)	0.023 (3)	0.000 (3)	0.007 (3)	0.006 (3)
C30	0.044 (4)	0.041 (5)	0.037 (4)	-0.004 (4)	-0.012 (3)	0.007 (3)
C31	0.039 (4)	0.049 (5)	0.041 (4)	0.006 (4)	-0.003 (3)	0.005 (4)
C32	0.036 (4)	0.027 (4)	0.029 (3)	-0.011 (3)	0.003 (3)	-0.004 (3)
C33	0.026 (4)	0.038 (5)	0.036 (4)	0.002 (3)	0.009 (3)	0.002 (3)
C34	0.034 (4)	0.044 (5)	0.046 (4)	-0.003 (4)	0.008 (4)	0.000 (4)
C35	0.041 (4)	0.036 (4)	0.019 (3)	-0.001 (4)	-0.004 (3)	-0.002 (3)
C36	0.041 (4)	0.047 (5)	0.040 (4)	0.006 (4)	0.013 (3)	-0.001 (4)
C37	0.065 (5)	0.048 (5)	0.026 (4)	-0.010 (4)	0.013 (4)	-0.006 (3)
C38	0.039 (4)	0.032 (5)	0.029 (4)	-0.007 (3)	0.000 (3)	0.005 (3)
C39	0.036 (4)	0.035 (4)	0.032 (4)	-0.006 (4)	-0.007 (3)	0.000 (3)
C40	0.023 (4)	0.048 (5)	0.041 (4)	-0.008 (4)	0.000 (3)	0.002 (4)

Geometric parameters (Å, º) for (yohan1)

S1—C1	1.720 (7)	C15—C16	1.500 (9)
S1—C4	1.720 (6)	C16—C17	1.396 (9)
S2—C7	1.754 (7)	C16—C21	1.387 (9)
S2—C10	1.717 (7)	C17—H17	0.9500
S3—C11	1.756 (7)	C17—C18	1.396 (9)
S3—C14	1.724 (7)	C18—H18	0.9500
O1—C15	1.224 (8)	C18—C19	1.378 (9)
O2—C22	1.218 (8)	C19—H19	0.9500
O3—C32	1.332 (8)	C19—C20	1.385 (10)
O3—C33	1.449 (7)	C20—H20	0.9500
O4—C32	1.234 (8)	C20—C21	1.383 (9)
O5—C29	1.337 (8)	C21—H21	0.9500
O5—C30	1.467 (8)	C22—C23	1.503 (9)
O6—C29	1.192 (9)	C23—C24	1.394 (9)
O7—C35	1.333 (9)	C23—C28	1.375 (9)
O7—C36	1.457 (8)	C24—H24	0.9500
O8—C35	1.205 (8)	C24—C25	1.411 (9)
O9—C38	1.332 (8)	C25—H25	0.9500
O9—C39	1.444 (8)	C25—C26	1.377 (9)
O10—C38	1.237 (8)	C26—H26	0.9500

N1—C6	1.273 (9)	C26—C27	1.375 (10)
N1—C7	1.395 (8)	C27—H27	0.9500
N2—H2	0.8800	C27—C28	1.398 (9)
N2—C10	1.401 (8)	C28—H28	0.9500
N2—C15	1.365 (9)	C30—H30A	0.9900
N3—C5	1.281 (9)	C30—H30B	0.9900
N3—C11	1.400 (8)	C30—C31	1.503 (10)
N4—H4	0.8800	C31—H31A	0.9800
N4—C14	1.391 (8)	C31—H31B	0.9800
N4—C22	1.365 (9)	C31—H31C	0.9800
C1—C2	1.382 (10)	C33—H33A	0.9900
C1—C6	1.445 (8)	C33—H33B	0.9900
C2—H2A	0.9500	C33—C34	1.498 (10)
C2—C3	1.422 (9)	C34—H34A	0.9800
C3—H3	0.9500	C34—H34B	0.9800
C3—C4	1.365 (10)	C34—H34C	0.9800
C4—C5	1.461 (9)	C36—H36A	0.9900
C5—H5	0.9500	C36—H36B	0.9900
C6—H6	0.9500	C36—C37	1.529 (10)
C7—C8	1.365 (9)	C37—H37A	0.9800
C8—C9	1.441 (8)	C37—H37B	0.9800
C8—C29	1.501 (9)	C37—H37C	0.9800
C9—C10	1.370 (10)	C39—H39A	0.9900
C9—C32	1.451 (9)	C39—H39B	0.9900
C11—C12	1.355 (10)	C39—C40	1.503 (9)
C12—C13	1.444 (8)	C40—H40A	0.9800
C12—C35	1.519 (9)	C40—H40B	0.9800
C13—C14	1.381 (9)	C40—H40C	0.9800
C13—C38	1.443 (10)		
C4—S1—C1	90.8 (3)	N4—C22—C23	115.7 (6)
C10—S2—C7	90.0 (3)	C24—C23—C22	117.4 (6)
C14—S3—C11	89.9 (3)	C28—C23—C22	122.5 (6)
C32—O3—C33	117.2 (5)	C28—C23—C24	120.0 (6)
C29—O5—C30	114.9 (6)	C23—C24—H24	120.3
C35—O7—C36	115.8 (6)	C23—C24—C25	119.4 (6)

C38—O9—C39	117.9 (5)	C25—C24—H24	120.3
C6—N1—C7	119.4 (6)	C24—C25—H25	120.3
C10—N2—H2	117.6	C26—C25—C24	119.5 (7)
C15—N2—H2	117.6	C26—C25—H25	120.3
C15—N2—C10	124.8 (6)	C25—C26—H26	119.5
C5—N3—C11	120.1 (6)	C27—C26—C25	121.1 (6)
C14—N4—H4	117.4	C27—C26—H26	119.5
C22—N4—H4	117.4	C26—C27—H27	120.2
C22—N4—C14	125.2 (6)	C26—C27—C28	119.6 (7)
C2—C1—S1	112.4 (5)	C28—C27—H27	120.2
C2—C1—C6	125.6 (6)	C23—C28—C27	120.4 (7)
C6—C1—S1	121.9 (5)	C23—C28—H28	119.8
C1—C2—H2A	124.1	C27—C28—H28	119.8
C1—C2—C3	111.7 (6)	O5—C29—C8	110.2 (6)
C3—C2—H2A	124.1	O6—C29—O5	125.0 (7)
C2—C3—H3	123.9	O6—C29—C8	124.8 (7)
C4—C3—C2	112.2 (6)	O5—C30—H30A	110.4
C4—C3—H3	123.9	O5—C30—H30B	110.4
C3—C4—S1	112.8 (5)	O5—C30—C31	106.8 (6)
C3—C4—C5	126.5 (6)	H30A—C30—H30B	108.6
C5—C4—S1	120.7 (5)	C31—C30—H30A	110.4
N3—C5—C4	119.1 (6)	C31—C30—H30B	110.4
N3—C5—H5	120.4	C30—C31—H31A	109.5
C4—C5—H5	120.4	C30—C31—H31B	109.5
N1—C6—C1	121.2 (6)	C30—C31—H31C	109.5
N1—C6—H6	119.4	H31A—C31—H31B	109.5
C1—C6—H6	119.4	H31A—C31—H31C	109.5
N1—C7—S2	123.5 (5)	H31B—C31—H31C	109.5
C8—C7—S2	112.4 (5)	O3—C32—C9	112.9 (5)
C8—C7—N1	124.0 (6)	O4—C32—O3	123.0 (6)
C7—C8—C9	112.3 (6)	O4—C32—C9	124.1 (6)
C7—C8—C29	122.6 (6)	O3—C33—H33A	110.0
C9—C8—C29	124.9 (6)	O3—C33—H33B	110.0
C8—C9—C32	125.9 (6)	O3—C33—C34	108.3 (5)
C10—C9—C8	111.1 (6)	H33A—C33—H33B	108.4
C10—C9—C32	122.8 (6)	C34—C33—H33A	110.0

N2—C10—S2	122.3 (5)	C34—C33—H33B	110.0
C9—C10—S2	114.1 (5)	C33—C34—H34A	109.5
C9—C10—N2	123.6 (6)	C33—C34—H34B	109.5
N3—C11—S3	125.5 (5)	C33—C34—H34C	109.5
C12—C11—S3	112.4 (5)	H34A—C34—H34B	109.5
C12—C11—N3	122.1 (6)	H34A—C34—H34C	109.5
C11—C12—C13	113.3 (6)	H34B—C34—H34C	109.5
C11—C12—C35	121.4 (5)	O7—C35—C12	109.7 (6)
C13—C12—C35	125.3 (6)	O8—C35—O7	126.3 (6)
C14—C13—C12	110.2 (6)	O8—C35—C12	123.9 (7)
C14—C13—C38	123.5 (6)	O7—C36—H36A	109.4
C38—C13—C12	126.1 (6)	O7—C36—H36B	109.4
N4—C14—S3	123.4 (5)	O7—C36—C37	111.1 (6)
C13—C14—S3	114.1 (5)	H36A—C36—H36B	108.0
C13—C14—N4	122.5 (6)	C37—C36—H36A	109.4
O1—C15—N2	121.3 (6)	C37—C36—H36B	109.4
O1—C15—C16	122.8 (6)	C36—C37—H37A	109.5
N2—C15—C16	115.9 (6)	C36—C37—H37B	109.5
C17—C16—C15	117.9 (6)	C36—C37—H37C	109.5
C21—C16—C15	122.3 (6)	H37A—C37—H37B	109.5
C21—C16—C17	119.8 (6)	H37A—C37—H37C	109.5
C16—C17—H17	120.3	H37B—C37—H37C	109.5
C18—C17—C16	119.4 (6)	O9—C38—C13	112.7 (6)
C18—C17—H17	120.3	O10—C38—O9	123.2 (6)
C17—C18—H18	120.1	O10—C38—C13	124.0 (7)
C19—C18—C17	119.8 (7)	O9—C39—H39A	110.4
C19—C18—H18	120.1	O9—C39—H39B	110.4
C18—C19—H19	119.4	O9—C39—C40	106.7 (5)
C18—C19—C20	121.1 (6)	H39A—C39—H39B	108.6
C20—C19—H19	119.4	C40—C39—H39A	110.4
C19—C20—H20	120.4	C40—C39—H39B	110.4
C21—C20—C19	119.2 (6)	C39—C40—H40A	109.5
C21—C20—H20	120.4	C39—C40—H40B	109.5
C16—C21—H21	119.6	C39—C40—H40C	109.5
C20—C21—C16	120.7 (7)	H40A—C40—H40B	109.5
C20—C21—H21	119.6	H40A—C40—H40C	109.5

O2—C22—N4	121.2 (6)	H40B—C40—H40C	109.5
O2—C22—C23	123.1 (6)		
S1—C1—C2—C3	-1.7 (8)	C11—C12—C13—C38	175.7 (7)
S1—C1—C6—N1	8.0 (10)	C11—C12—C35—O7	-76.0 (8)
S1—C4—C5—N3	-7.5 (10)	C11—C12—C35—O8	101.3 (8)
S2—C7—C8—C9	-2.4 (8)	C12—C13—C14—S3	0.2 (8)
S2—C7—C8—C29	172.8 (6)	C12—C13—C14—N4	-179.1 (6)
S3—C11—C12—C13	0.7 (8)	C12—C13—C38—O9	-4.1 (11)
S3—C11—C12—C35	-177.8 (5)	C12—C13—C38—O10	175.4 (7)
O1—C15—C16—C17	20.1 (10)	C13—C12—C35—O7	105.7 (8)
O1—C15—C16—C21	-158.7 (7)	C13—C12—C35—O8	-77.0 (10)
O2—C22—C23—C24	-17.5 (11)	C14—S3—C11—N3	-179.5 (6)
O2—C22—C23—C28	160.0 (7)	C14—S3—C11—C12	-0.4 (6)
N1—C7—C8—C9	179.4 (7)	C14—N4—C22—O2	-3.3 (11)
N1—C7—C8—C29	-5.4 (11)	C14—N4—C22—C23	-180.0 (6)
N2—C15—C16—C17	-157.3 (7)	C14—C13—C38—O9	171.8 (7)
N2—C15—C16—C21	24.0 (10)	C14—C13—C38—O10	-8.8 (12)
N3—C11—C12—C13	179.8 (6)	C15—N2—C10—S2	6.8 (11)
N3—C11—C12—C35	1.3 (11)	C15—N2—C10—C9	-175.6 (7)
N4—C22—C23—C24	159.1 (7)	C15—C16—C17—C18	-179.9 (7)
N4—C22—C23—C28	-23.4 (10)	C15—C16—C21—C20	178.9 (7)
C1—S1—C4—C3	0.4 (6)	C16—C17—C18—C19	1.7 (11)
C1—S1—C4—C5	-179.2 (6)	C17—C16—C21—C20	0.2 (11)
C1—C2—C3—C4	2.0 (10)	C17—C18—C19—C20	-1.2 (11)
C2—C1—C6—N1	-175.9 (7)	C18—C19—C20—C21	0.3 (11)
C2—C3—C4—S1	-1.4 (9)	C19—C20—C21—C16	0.3 (11)
C2—C3—C4—C5	178.2 (7)	C21—C16—C17—C18	-1.1 (11)
C3—C4—C5—N3	173.0 (7)	C22—N4—C14—S3	-1.7 (11)

C4—S1—C1—C2	0.8 (6)	C22—N4—C14—C13	177.5 (7)
C4—S1—C1—C6	177.4 (6)	C22—C23—C24—C25	179.9 (6)
C5—N3—C11—S3	-24.9 (10)	C22—C23—C28—C27	179.7 (7)
C5—N3—C11—C12	156.1 (7)	C23—C24—C25—C26	-0.4 (11)
C6—N1—C7—S2	23.2 (10)	C24—C23—C28—C27	-2.9 (11)
C6—N1—C7—C8	-158.7 (7)	C24—C25—C26—C27	-1.1 (11)
C6—C1—C2—C3	-178.1 (7)	C25—C26—C27—C28	0.6 (11)
C7—S2—C10—N2	178.6 (6)	C26—C27—C28—C23	1.4 (11)
C7—S2—C10—C9	0.8 (7)	C28—C23—C24—C25	2.3 (11)
C7—N1—C6—C1	-178.3 (6)	C29—O5—C30—C31	169.3 (6)
C7—C8—C9—C10	3.0 (9)	C29—C8—C9—C10	-172.1 (7)
C7—C8—C9—C32	-172.5 (7)	C29—C8—C9—C32	12.4 (12)
C7—C8—C29—O5	79.6 (8)	C30—O5—C29—O6	-1.1 (9)
C7—C8—C29—O6	-100.5 (9)	C30—O5—C29—C8	178.8 (5)
C8—C9—C10—S2	-2.2 (9)	C32—O3—C33—C34	170.8 (6)
C8—C9—C10—N2	180.0 (7)	C32—C9—C10—S2	173.4 (6)
C8—C9—C32—O3	6.2 (11)	C32—C9—C10—N2	-4.4 (12)
C8—C9—C32—O4	-173.8 (7)	C33—O3—C32—O4	-4.0 (11)
C9—C8—C29—O5	-105.8 (8)	C33—O3—C32—C9	175.9 (6)
C9—C8—C29—O6	74.2 (10)	C35—O7—C36—C37	-80.5 (8)
C10—S2—C7—N1	179.2 (6)	C35—C12—C13—C14	177.8 (7)
C10—S2—C7—C8	1.0 (6)	C35—C12—C13—C38	-5.9 (12)
C10—N2—C15—O1	-1.0 (11)	C36—O7—C35—O8	0.1 (10)
C10—N2—C15—C16	176.4 (7)	C36—O7—C35—C12	177.4 (5)
C10—C9—C32—O3	-168.7 (7)	C38—O9—C39—C40	-168.9 (6)
C10—C9—C32—O4	11.2 (13)	C38—C13—C14—S3	-176.2 (6)
C11—S3—C14—N4	179.4 (6)	C38—C13—C14—N4	4.5 (12)
C11—S3—C14—C13	0.1 (6)	C39—O9—C38—O10	1.2 (11)
C11—N3—C5—C4	178.5 (6)	C39—O9—C38—C13	-179.3 (6)
C11—C12—C13—	-0.6 (9)		

C14			

Hydrogen-bond geometry (Å, º) for (yohan1)

D—H···*A*	*D*—H	H···*A*	*D*···*A*	*D*—H···*A*
N2—H2···O4	0.88	2.08	2.733 (7)	130
N4—H4···O10	0.88	2.07	2.729 (7)	132
C2—H2*A*···O8^{i}	0.95	2.52	3.314 (8)	141
C5—H5···O6^{i}	0.95	2.60	3.394 (8)	141
C34—H34*A*···O1^{ii}	0.98	2.60	3.383 (9)	137
C40—H40*C*···O2^{ii}	0.98	2.52	3.314 (9)	138

Symmetry codes: (i) -*x*+1/2, *y*-1/2, -*z*+3/2; (ii) *x*+1, *y*, *z*.

Comparison of selected bond lengths and angles of the title compound and literature counter parts.

Refcode	dN2-C10 (Å)"dN2-C15 (Å)	dN2-C15 (Å)	dC15-C16 (Å)	TorsionO1-C15-N2-C10 (o)	Anglethiophene-phenyl (o)
KABDUO	1.381	1.359	1.487	4.41	8.13
LOYDIM	1.391	1.355	1.482	0.03	4.74
TAPXEO	1.385	1.368	1.482	2.85	9.70
TEKFEX	1.38	1.364	1.494	0.44	23.72
TEKFIB	1.369	1.361	1.483	3.80	6.38
TEKFOH	1.385	1.359	1.499	0.23	39.02
TEKFUN	1.373	1.354	1.494	0.60	2.53
TEKFUN	1.382	1.36	1.484	2.45	6.01
VESHIN	1.375	1.365	1.486	0.27	17.75
VESHOT	1.379	1.367	1.486	3.90	7.17
VESHUZ	1.378	1.38	1.516	7.52	36.43
VESJAH	1.371	1.363	1.498	5.12	41.74
VESJEL	1.378	1.357	1.491	6.80	22.71
VESJIP	1.381	1.353	1.493	3.72	40.45
VESJIP	1.396	1.36	1.497	4.28	43.16
WOJBII	1.378	1.369	1.494	1.21	7.11
Average	1.380	1.362	1.492	3.00	19.8

esd	0.007	0.007	0.009	2.40	15.5
min	1.369	1.353	1.482	0.03	2.5
max	1.396	1.380	1.516	7.52	43.2

Conclusion

En conclusion, de nouvelles azométhines conjuguées électrochromes, en substituant les amines terminales de composés déjà précédemment bien étudié, par des amides, elles-mêmes substituées par des groupes aromatiques, démontrent une fois de plus qu'elles ont la capacité de présenter des changements d'absorbance dans le domaine du visible, tant à l'oxydation qu'à la réduction. Le choix de la TPA comme groupe de fin de chaine s'est révélé concluant, permettant de conserver une oxydation réversible accompagnée d'une modulation des couleurs en changeant les unités aromatiques du cœur. De plus, de pair avec la réversibilité, la résistance de ces nouveaux composés face au stress imposés par les essais de *switching* a été établie.

Si le choix des unités aromatiques et des groupements électro-actifs dans leur conception permettent de moduler et contrôler les propriétés spectroscopiques et le caractère réversible du processus anodique, des efforts restent à faire pour idéalement parvenir à un processus cathodique réversible, et conservant un changement de couleur. D'autres fonctions que les amides pourraient être étudiées pour fonctionnaliser les amines terminales, et l'exploration d'autres unités aromatiques aux extrémités, ainsi qu'au centre de ces oligomères pourraient alors offrir des perspectives intéressantes.

Un premier travail préliminaire, non présenté ici, a déjà été effectué dans ce sens. Les TPA terminales ont été remplacées par des anthraquinones, avec le thiophène au centre. Le trimère en résultant n'a jamais pu être caractérisé, la molécule étant totalement insoluble dans tous les solvants essayés. L'introduction de groupements solubilisants (chaines alkyles par exemple) sur le squelette de la molécule pourrait permettre de l'étudier plus en profondeur. De même, une mono-azométhine intermédiaire, composée d'une unité anthraquinone et d'une unité de DAT séparées par une amide, le DAT étant connecté via l'azométhine à une TPA di-méthylée, a elle donné des résultats plus probants, avec à la fois des processus anodiques et cathodiques réversibles, mais une absence de changement de couleur notable lors du processus cathodique. Une poursuite dans ce sens pourrait se voir couronnée de succés.

Enfin, même si peu mentionné dans le corps du mémoire, des essais de dispositifs électrochromiques ont été effectués, mais sont limités par les contraintes engendrées par l'utilisation de molécules électrochromes de relatives faibles masses molaires. Celles-ci ont

tendance à se solubiliser dans les gels électrolytiques utilisés, qui sont souvent plus adaptés à l'utilisation de polymères, et la réalisation de dispositifs concluants les intégrant est encore la plupart du temps un challenge. Etant une des étapes les plus significatives dans l'étude de matériaux conjugués, il serait intéressant de se pencher sur cette problématique pour pleinement démontrer le potentiel des azométhines conjuguées comme matériaux électrochromes.